Universität Bremen

Max-Planck-Institute for Marine Microbiology

# In situ quantification of biogeochemical processes at cold seeps

Dissertation

zur Erlangung des Doktorgrades

der Naturwissenschaften

-Dr. rer. nat.-

dem Fachbereich 5 (Geowissenschaften) der

Universität Bremen vorgelegt von

Anna Lichtschlag

Bremen, 2009

1. Gutachter: Prof. Dr. Bo Barker Jørgensen

2. Gutachter: Priv. Doz. Dr. Matthias Zabel

Weitere Prüfer:

Prof. Dr. Gerhard Bohrmann

Dr. Dirk de Beer

Tag des Promotionskolloquiums: 9. November 2009

**TABLE OF CONTENTS**

## SUMMARY

This thesis focuses on the interaction between microbiology and geochemistry, and the physical driving forces for the biogeochemical cycles in the near-surface sediments of cold seeps. Cold seeps are extraordinary players in the marine realm, harboring a large biodiversity, and characterized by intense biogeochemical reactions that are stimulated by the advective influx of reduced compounds into the oxidized upper sediment layer (Chapter 1). Cold seeps are difficult research objects as the sediments are highly gaseous, which makes undisturbed retrieval almost impossible, and in situ studies at these remote habitats are only possible since a few years. The results so far show that cold seeps are highly variable environments, both in space and time. The investigation of rates and pathways of methane, sulfate, and sulfide turnover at cold seeps is environmentally and ecologically relevant as methane is a powerful greenhouse gas and sulfide is toxic for most organisms, but also supports primary production through chemoautotrophic consumption. Due to the high rates of redox processes, chemoautotrophy is highly intense and the seeps are oases of high diverse life. They form ideal natural laboratories to study the link between diversity and energy supply. The main objectives of this thesis were to study the influence of transport on different biogeochemical processes and to determine which parameters control the chemoautotrophy-driven primary production at cold seeps. In particular, it was investigated how methane oxidation, sulfate reduction, and sulfide production are organized in cold seeps in oxic and in permanently anoxic environments, and what impact fluid flow has on these conversion processes. Furthermore, the pathways of sulfide oxidation in oxic and anoxic cold seep surface sediments were studied, and the areal primary production of the different microbial habitats was estimated. This was based on measuring the turnover of geochemically and biologically relevant components (i.e. oxygen, sulfate, nitrate, methane, and metal-oxides), the efflux of emanating products (i.e. sulfide and dissolved inorganic carbon), and the investigation of the distribution, physiology, and behavior of sulfide oxidizing bacteria in situ, ex situ and experimentally.

At the **Håkon Mosby Mud Volcano** (Chapter 2) geochemically controlled redox reactions and biological turnover were compared in the *Beggiatoa* habitat, at the gray mat site, and in the center of the mud volcano. All three habitats showed substantial small-scale variability in carbon fixation pathways and primary production was driven either directly through the biological use of methane or indirectly by chemoautotrophic oxidation of sulfide derived from anaerobic oxidation of methane (AOM). In the thiotrophic mat habitats fluxes of oxygen and nitrate were sufficient for a complete consumption of sulfide by the microbial thiotrophic community, and geochemical sulfide oxidation with iron-oxides was of minor importance. However, in the center of the Håkon Mosby Mud Volcano geochemical sulfide oxidation processes predominated and biomass production was largely limited to direct energy conservation from aerobic and anaerobic methane oxidation.

Similarly, at the coastal cold seep in **Eckernförde Bay** (Chapter 3) the actual importance of nitrate-storing *Beggiatoa* for the benthic sulfur cycle and their success in competing with chemical sulfide

oxidation were studied. At Eckernförde Bay a 2-10 cm thick suboxic zone without oxygen and sulfide was found. The highest biomass of *Beggiatoa* was detected within this zone, with the thiotrophs living on the oxidation of sulfide with internally stored nitrate. Despite their high abundance, *Beggiatoa*-mediated sulfide oxidation accounted only for a small fraction of the total sulfide removal in the sediment and most of the sulfide flux into the suboxic layer was removed by geochemical processes.

Spatial variations in fluid flow as well as methane and sulfide fluxes were investigated at the **Dvurechenskii mud volcano** (Chapter 4), an active mud volcano in the deep Black Sea. The aim of this study was to determine (i) if fluid flow, methane efflux and consumption decrease radially from the center of the mud volcano to the outer edge, (ii) if the methane consumption and sulfide production are controlled by fluid flow, and (iii) if the mud volcano is a significant source of methane and sulfide to the Black Sea hydrosphere. Our results showed that at the Dvurechenskii mud volcano fluid and mud flow have significant impacts on the efflux of methane and sulfide, as well as on the anaerobic oxidation of methane. Medium to low fluid upflow in the outer center of the mud volcano allowed high sulfate and methane consumption and reduced the methane emission to the water column by up to 70%. Instead a high fluid upflow of >1 m $yr^{-1}$ and extrusion of microbe-depleted subsurface muds, as found at the small summit north of the geographical center, was correlated with almost no microbial sulfide production and a high methane emission rate of >400 mmol $m^{-2}$ $d^{-1}$. Our results suggest that deep-water mud volcanoes have only a small contribution to the methane and sulfide inventory of the Black Sea, and that most methane is derived from the abundant gas vents in shallower areas on the Black Sea margin.

During pore fluid and solid phase analyses at the **Dvurechenskii mud volcano** (Chapter 5) we found that the surface sediments of the mud volcano form a unique oxidative environment. Advecting muds and fluids contain high concentrations of methane, but also reactive iron-minerals. In the presence of sulfate, methane was consumed by anaerobic methane oxidation in the near-surface sediments, and produced sulfide reacted at the surface of the AOM-zone with the iron-minerals. Thus, sulfur intermediates such as elemental sulfur, polysulfides, thiosulfate, and sulfite formed despite the permanently anoxic surrounding. The concentrations of these sulfur intermediates do not reach chemical equilibrium, either due to slow kinetics or because the fluid flow continuously transports them away from their site of production.

# ZUSAMMENFASSUNG

Gegenstand der vorliegenden Doktorarbeit ist die Untersuchung der Zusammenhänge zwischen mikrobiellen und geochemischen Prozessen, sowie der physikalischen Ursachen für die Abläufe biogeochemischer Prozesse in oberflächennahen Sedimenten von Cold Seeps („kalte Quellen“). Cold Seeps sind außergewöhnlich in der marinen Welt. Sie zeigen hohe Biodiversitäten und es kommt zu vielfältige biogeochemische Reaktionen durch den Einstrom reduzierter Stoffe in oxidierte, oberflächennahe Sedimente (Kapitel 1). Allerdings sind Untersuchungen an Cold Seeps nicht einfach: die Sedimente sind sehr gashaltig und eine Probenahme ohne Beeinträchtigung der Sedimente ist bislang fast nicht möglich. In situ Studien an solch schwer zugänglichen Orten werden erst seit wenigen Jahren durchgeführt. Die bisherigen Erkenntnisse zeigen, dass Cold Seeps sehr unterschiedlich sein können und auch temporären Veränderungen unterworfen sind.

Sowohl für ihr Umfeld als auch aus ökologischer Sicht ist es wichtig, den Grad und die genauen Umsatzwege für Methan, Sulfat und Sulfid an Cold Seeps zu kennen. Methan ist ein starkes Treibhausgas und Sulfid wirkt toxisch auf viele Organismen, ist aber auch ein wichtiges Substrat in der chemoautotrophen Primärproduktion. Eben durch diese chemoautotrophen Prozesse sind Cold Seeps Oasen für vielfältiges Leben. Weiterhin sind Cold Seeps „natürliche Labore“, in denen man den Zusammenhang zwischen Biodiversität und deren benötigten Energiezufuhr studieren kann. Das Ziel dieser Arbeit war es herauszufinden, welchen Einfluss physikalische Transportprozesse auf biogeochemische Prozesse haben, und welche Faktoren die chemoautotrophe Primärproduktion an Cold Seeps beeinflussen. Im Einzelnen wurde untersucht, wie Sulfatreduktion, Methanoxidation und Sulfidproduktion in Cold Seep Sedimenten in oxischem und anoxischem Umfeld aufgeteilt sind und inwieweit Fluidflüsse diese Prozesse beeinflussen. Des Weiteren wurde untersucht, wie die Sulfidoxidation in oberflächennahen Sedimenten abläuft und die Höhe der Primärproduktion in den verschiedenen mikrobiellen Habitaten wurde ermittelt. Hierfür wurde mit in situ und ex situ Techniken sowie mit Experimenten der Umsatz von geochemisch und biologisch relevanten Stoffen bestimmt. Relevant waren hierbei vor allem der Verbrauch von Sauerstoff, Sulfat, Nitrat, Methan und oxidierten Metallen sowie die Produktionsraten von Sulfid und anorganischem gelöstem Kohlenstoff. Des Weiteren wurden die Verteilung, die Physiologie und die Verhaltensweise von sulfidoxidierenden Bakterien untersucht.

Am **Håkon Mosby Schlammvulkan** (Kapitel 2) wurden die geochemischen Redoxprozesse und die biologischen Umsatzraten aus 3 Gebieten miteinander verglichen, wobei es sich um ein *Beggiatoa*-dominiertes Habitat, um ein Areal mit grauen mikrobiellen Matten und um das Zentrum des Schlammvulkans handelte. Die drei Habitate zeigten wesentliche Unterschiede im Kohlenstoffumsatz und die Primärproduktion wurde entweder direkt, durch den mikrobiellen Umsatz von Methan, oder indirekt, durch die chemoautotrophe Oxidation von Sulfid, welches während der anaeroben Methanoxidation (AOM) gebildet wurde, gesteuert. In den thiotrophen Matten waren die Sauerstoff-

und Nitratflüsse ausreichend für einen vollständigen biologischen Umsatz von Sulfid und geochemische Sulfidoxidation mit Eisen-Oxiden spielte keine Rolle. Im Gegensatz dazu wurde im Zentrum des Schlammvulkans Sulfid vor allem geochemisch umgesetzt und die Produktion von Biomasse war eingeschränkt auf direkte aerobe und anaerobe Methanoxidation.

Eine ähnliche Studie wurde in den methanhaltigen Küstensedimenten der **Eckernförder Bucht** durchgeführt (Kapitel 3), wobei auch hier die Bedeutung von nitratspeichernden *Beggiatoa* Spezies für den sedimentären Schwefelkreislauf, sowie ihre Fähigkeit, sich gegen die chemische Sulfidoxidation durchzusetzen, untersucht wurde. In den Sedimenten der Eckernförder Bucht ist eine 2-10 cm dicke suboxische Zone ohne Sauerstoff und Sulfid ausgebildet. Die höchste Biomasse an *Beggiatoa* wurde in dieser Zone gefunden, wobei die thiotrophen Bakterien hier von der Oxidation des Sulfids mit intern gespeichertem Nitrat leben. Obwohl sie in großer Zahl vorkamen, konsumierten *Beggiatoa* nur einen kleinen Teil des Sulfids. Der Großteil des Sulfids wurde durch geochemische Prozesse in der suboxischen Zone umgesetzt.

Räumliche Unterschiede im Fluidtransport, sowie im Methan- und Sulfid-Fluss wurden am **Dvurechenskii Schlammvulkan** untersucht (Kapitel 4), einem aktiven Schlammvulkan im tiefen Teil des Schwarzen Meeres (2060m). Das Hauptziel dieser Studie war es herauszufinden, ob die Stärke des Fluidtransports und das Ausströmen bzw. der Verbrauch von Methan vom Zentrum des Schlammvulkans nach außen hin gleichmäßig abnehmen. Des Weiteren wurde untersucht, ob Methanumsatz und Sulfidproduktion durch den Fluidfluss kontrolliert werden und ob der Schlammvulkan zum Methan- und Sulfidgehalt der Wassersäule des Schwarzen Meeres beiträgt. Unsere Resultate machen deutlich, dass am Dvurechenskii Schlammvulkan der Fluidfluss, aber auch das Ausfließen von Schlamm, einen starken Einfluss auf das Ausströmen von Methan und Sulfid, sowie auf die anaerobe Methanoxidation hat. Mittlerer bis geringer Fluidfluss, welcher im äußeren Zentrum des Schlammvulkans zu finden war, bewirkte hohe Sulfat- und Methanumsatzraten, wobei der Methanfluss in die Wassersäule um bis zu 70% reduziert wurde. Im Gegensatz dazu bewirkte ein Fluidfluss von mehr als 1 m $yr^{-1}$, sowie frischer, in Mikroben abgereicherter Schlamm an einer Anhöhe nördlich des geographischen Zentrums, dass so gut wie keine mikrobielle Sulfidproduktion stattfand und Methan mit einer Emissionsrate von mehr als 400 mmol $m^{-2}$ $d^{-1}$ ausströmte. Unsere Resultate zeigen, dass Tiefsee-Schlammvulkane nur wenig zum Methan- und Sulfidgehalt des Schwarzen Meeres beitragen. Der Großteil des Methans in der Wassersäule stammt von zahlreichen Gasquellen aus flacheren Regionen des Schwarzen Meeres.

Im Zuge der Porenwasser- und Festphasen-Untersuchungen am **Dvurechenskii Schlammvulkan** haben wir entdeckt, dass die oberflächennahen Sedimente des Schlammvulkans eine einzigartige, oxidative Umgebung bilden (Kapitel 5). Advektiv aufsteigender Schlamm und Fluide enthalten große Mengen an Methan, aber auch reaktive Eisenminerale. Sobald Methan und Sulfat in den oberflächennahen Sedimenten miteinander in Kontakt kommen, wird Methan mikrobiell unter anaeroben Bedingungen umgesetzt und das daraus entstehende Sulfid reagiert in der AOM-Zone mit

den reaktiven Eisenmineralen. Im Zuge dessen entstehen trotz der anoxischen Umgebung Schwefel-Intermediate, wie etwa Elementarschwefel, Polysulfid, Thiosulfat and Sulfit. Die Konzentrationen erreichen jedoch kein chemisches Gleichgewicht, entweder auf Grund der langsamen Kinetik, oder weil Fluidflüsse die Schwefel-Intermediate von ihrem Entstehungsort entfernen.

Chapter 1

# Cold seep systems-
# a general introduction

## 1. COLD SEEP SYSTEMS

This PhD thesis presents a study on the geochemical, biological, and physical parameters that drive the near-surface processes in marine cold seeps. Marine cold seeps are the outlets of channels that transport fluids and sediment from large depth to the seafloor, and bring them in contact with the marine realm. In cold seep surface sediments various biogeochemical reactions are stimulated by the injection of reduced compounds, like methane, ammonium, $Fe^{2+}$ or sulfide, into the thin sediment layer containing oxidized compounds. Also primary production, fixation of $CO_2$ in biomass, is driven by the conversion of the reduced compounds with oxygen, nitrate, and sulfate, and this biomass production facilitates life at an otherwise deserted seafloor. At these hot spots of 'dark energy' a characteristic faunal community develops that is nourished by these chemolithotrophic processes. These oases of life are important habitats for a large biodiversity. Cold and hot seeps might have been the refuges for life during 'snowball earth' events. Despite worldwide research, the knowledge about cold seeps is still limited as surveys are difficult, costly, and time-intensive. The results so far show that cold seeps are highly variable environments, both in space and time. This variability is reflected in the key biogeochemical seep processes - namely sulfate reduction, methane oxidation, methane release, and sulfide oxidation. The intensity of these processes varies between different cold seeps, but a high spatial variation develops also within one seep structure: usually a horizontal zonation is combined with a distinct vertical stratification of geochemical and microbial processes. Cold seep habitats and their rates of methane, sulfate and sulfide turnover might be environmentally and ecologically relevant: methane is a powerful greenhouse gas and sulfide is toxic for most organisms.

To define the environmental and the ecological relevance of cold seeps, we must determine the areal biogeochemical conversion rates at the sediment-water interface, which can be rather heterogeneous. Cold seeps can be seen as a natural reactor system. Essentially, when a reaction is possible, it will be limited either by the availability of reactants (transport limited) or by the presence of catalysts (kinetically limited). Thus, we need to assess whether the system is in thermodynamic disequilibrium, and whether microbial life can thrive on this disequilibrium, to finally understand the physico-chemical drivers of the system, including mass transfer phenomena. Whether energetically marginal microbial conversions occur can only be understood from thermodynamics. Examples are syntrophic reactions that occur only within narrow boundaries of reactant concentrations. A process used by bacteria must be able to drive ATP synthesis, thus needs a $\Delta G^0$ of at least -20 kJ per mole (Schink, 1997). Some reactions that are thermodynamically feasible are not found, they are probably beyond catalytical possibilities, e.g. methane or ammonium oxidation by Fe(III). Anaerobic oxidation of methane by sulfate (AOM) is arguably the most important reaction at cold seeps. Although energetically marginal and the pathway not understood, the main controls are well known: transport of methane and sulfate. Obviously these two compounds must be brought together to react, and the

distribution of AOM can largely be understood from the transport of methane from large depth to the sediment surface and penetration of the seawater-derived sulfate into the sediment. Simply speaking, the fluid upflow that characterizes cold seeps transports methane rapidly from large depth to the oxidized seawater, but hinders the entering of sulfate into the sediment. In this scenario, AOM can only occur where methane and sulfate transport are more or less balanced and AOM is transport-controlled. However, it must be noted that the organisms responsible for AOM have an extremely low growth rate, thus long colonization times. Thus areas where sediments are often disturbed may not be colonized by AOM microbes, and then AOM will be kinetically limited. AOM is not only a filter for methane, but also the main supplier of sulfide to the system. Sulfide oxidation at seeps is an important process driving chemosynthesis, thus responsible for the primary production and derived biodiversity.

In summary, cold seeps are highly valuable sites for research, forming unique natural laboratories to study which parameters control chemoautotrophic-driven biodiversity, and how transport processes control biogeochemical processes. A description of the functioning of cold seeps is only satisfactory in a multi-disciplinary approach, including geological, seismic, geochemical and microbiological processes. The following paragraphs will give an overview of marine cold seep sites (Section 1.1.), will explain how they function (Section 1.2.), and will introduce the characteristic chemosynthetic community thriving on cold seep discharges (Section 1.3.). Known geochemical and microbiological processes that are relevant in hydrocarbon- and sulfide-rich sediments are introduced in Section 1.4.. The mass transfer and exchange processes in cold seep sediments, their implications for the cold seep systems and how they are best determined is described in Sections 1.5.; interesting examples for measurements at cold seep sites are presented in Section 1.6..

### 1.1. Marine Cold Seeps

Marine cold seeps are visible at the sea bottom as geomorphological structures, formed from fluids (water, brine, gas, and oil) and sediments rising from the subsurface and piercing the seafloor. Submarine cold seeps are found in all water depths from coastal zones (e.g. Eckernförde Bay, Anderson et al., 1998) to deep sea trenches in several thousand meters depth (e.g. Japan Trench, Kobayashi et al., 1992). The sizes of the seep surface expressions range from centimeter to kilometer and are a function of the size of the conduits through which the mobilized fluids and sediments escape (Kopf, 2002). The largest cold seep structures are mud volcanoes of several kilometers diameter with several meters wide conduits at the seafloor (Kopf, 2002 and literature therein); the smallest features are only few centimeter wide, like the bubble-site on the northwestern Crimean shelf in the Black Sea (Fig. 1b), where single gas bubbles escape from the sediment. Depending on the geological setting, the driving force for the seep formation, the intensity of the fluid flow, and the nature of the discharge,

different types of cold seep surface phenomena can develop (Fig. 1), the most important being mud volcanoes, pockmarks, gas seeps and brine/oil pools.

*Mud volcanoes.*- Submarine mud volcanoes are large, topographically expressed seafloor edifices from which mud and fluids flow. The main driving forces for the formation of mud volcanoes are high pore-fluid pressure and buoyancy. As consequence of the high pore-fluid pressure the bulk density, shear strength and viscosity of the sediment is decreased, and the mud-fluid-mixture becomes semi-liquid and capable of plastic deformation. Buoyancy, produced e.g. from density inversion between undercompacted sediments or salt deposits and the overlying sediment layers, facilitates the diaphiric upward movement of the mud-fluid-mixture (Dimitrov, 2002; Judd and Hovland, 2007). Fast burial of fine-grained sediment with a high initial water content and in situ hydrocarbon generation leads to mud volcano formation at passive continental margins and abyssal parts of inland seas, like the Black Sea and the Caspian Sea. At active continental margins, particularly in plate collision zones or fold-thrust belts, pore-fluid pressure is built up by lateral tectonic compression (Milkov, 2000). Submarine mud volcanoes occur worldwide on shelves, continental and insular slopes, and abyssal parts of inland seas. The existence of $10^3$-$10^5$ deep-water mud volcanoes is estimated. Currently 27 regions with submarine mud volcano structures have been described (Milkov, 2000). Prominent research areas are the Black Sea (Sorokin Trough, abyssal plain), the Eastern Mediterranean, offshore Barbados, offshore Nigeria, and the Gulf of Mexico (summarized in Milkov, 2000; Dimitrov, 2002; Kopf, 2002). In addition to the submarine mud volcanoes, more than 900 terrestrial mud volcanoes are known from active areas of plate boundaries and zones of young orogenic structures, like the Alpine-Himalaya Belt, the Indonesian Arc, and the West Pacific Subduction Belt (Dimitrov, 2002). During the course of this thesis, work was done on the Håkon Mosby Mud Volcano (off the coast off Norway, Chapter 2, Fig. 1c, d), on the Dvurechenskii mud volcano in the Black Sea (Chapter 4, 5), and on the Amon Mud Volcano in the Nile Deep Sea Fan (Fig. 1d; Felden et al. in prep. (included as abstract); Grinth at al. in prep. (included as abstract); Grünke et al. in prep.).

*Pockmarks.*- Pockmarks are morphological indicators of focused fluid outbursts. On seismic profiles and underwater video observations they are visible as local depressions in soft, fine grained seafloor sediments - typically several tens of meters across and only few meters deep. The depression is formed by the eruption of liquids and gases, powerful enough to erode the covering sediment (Hovland and Sommerville, 1985; Judd and Hovland, 2007). The outburst is initiated by high pore-fluid pressure caused by the destabilization of subsurface methane hydrates, and by overpressurized fluids and gases often enriched in methane and higher hydrocarbons. No solid components, only fluids, are involved in pockmark formation, thus pockmarks are not elevated above the seafloor as are mud volcanoes. During the initial outburst of pockmark fluids a new conduit is created, and this channel facilitates subsequent fluid escape. Consequently, pockmark surveys only occasionally found strong

gas ebullitions. However, methane seepage can be inferred from the presence of methane-dependent fauna and bacterial mats, and large deposits of methane-derived authigenic carbonates (Hovland and Judd, 1988; Judd and Hovland, 2007).

Pockmarks are mostly found in areas where large amounts of hydrocarbons are generated in the sediment or methane hydrates and gas have accumulated in subsurface reservoirs. First described from offshore Nova Scotia (Canada) (King and MacLean, 1970), pockmarks have been found in various regions such as the North Sea (summarized in Judd and Hovland, 2007), the Eastern Mediterranean (Mascle et al., 2000; Bellaiche et al., 2001), and on the Equatorial African Margin (Ondreas et al., 2005). Work on pockmarks was done during this thesis on a structure in the Central Province of the Nile Deep Sea Fan (Grünke et al. in prep.) and on pockmarks at the Storegga Slide (Nyegga area) (unpublished data; Grünke et al. submitted (included as abstract)).

*Gas seeps.*- Gas seeps are spatially restricted cold seep sites with high fluid expulsion, oversaturated with methane so that continuous ebullition occurs in the exit channel. Sources for the fluids are ancient reservoirs, dissociated methane hydrates or accumulations of shallow gas (Judd et al., 2002). Focused cold fluid discharge is also known from accretionary wedges at convergent plate boundaries. Here hydrocarbon-rich fluids are formed by sediment compaction and mineral dehydration due to the rapid sediment burial, accompanied by microbial and thermogenic organic matter diagenesis. The geomorphological surface expressions of gas seeps are not as conspicuous as the large mud volcano cones and the pockmark depressions. Nevertheless, gas seeps easily can be recognized by the abundant seep fauna feeding on the cold seep discharges. Well-documented research areas for gas seeps are the Gulf of Mexico (Kennicutt et al., 1985), the Eel River Basin (Field and Kvenvolden, 1985), the Aleutian Subduction Zone (Suess et al., 1998), the slopes of the Black Sea (Ivanov et al., 1996), and the Cascadian Convergent Margin ('Hydrate Ridge', Suess et al., 1999). Fascinating phenomena associated with focused hydrocarbon seepage are the microbial reef structures found southwest of the Crimean Peninsula in the anoxic part of the Black Sea, which were also investigated during this thesis (Fig. 1a; unpublished data).

*Brine pools, higher hydrocarbon seeps, and asphalt flows.*- Very remarkable seep systems are formed when salt and higher hydrocarbons are brought to the surface. Due to the very strong salinity differences, brine acts as a separate heavy liquid phase. Pools, lakes, and even brine rivers are found at the seafloor, and pockmark and mud volcano craters are brine-filled (Fig. 1g) as reported from the Gulf of Mexico and the Eastern Mediterranean (MacDonald et al., 1990; Woodside and Volgin, 1996). These brine pools and lakes can be several hundred meters in diameter, have a salinity of 120-145‰, a high methane content, and can be associated with a typical seep fauna, such as *Bathymodiolus* sp. mussels and iron- and sulfur-precipitating microbial mats (MacDonald et al., 1990; Dupré et al., 2008a; Omoregie et al., 2008).

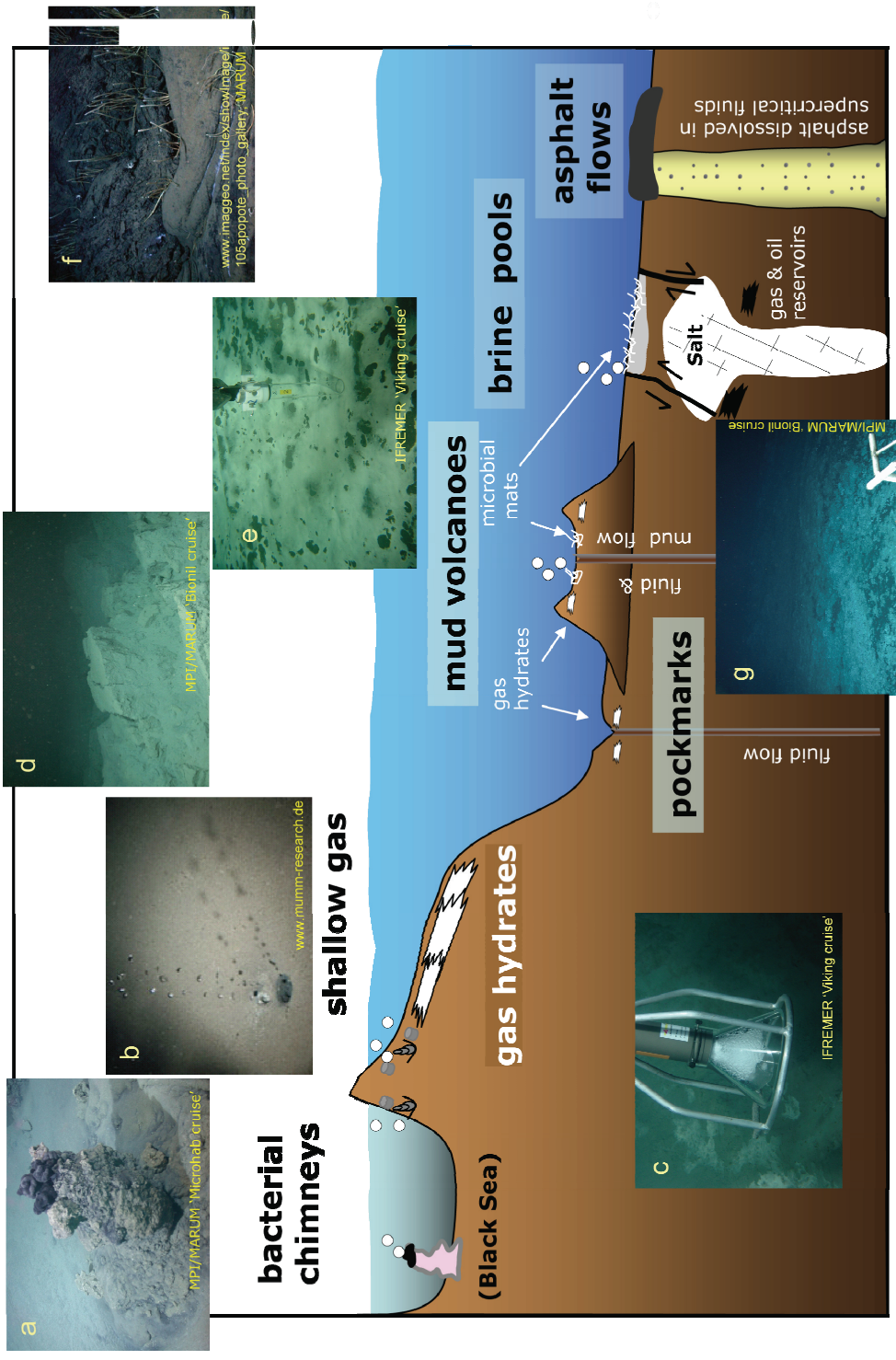


**Fig. 1:** **Various cold seep types at the marine seafloor, a) microbial chimney (about 1 m high) at the GHOSTDABS site, Black Sea, b) methane gas bubble release from the seafloor, c) methane hydrate formation during methane bubble sampling at an active seep site in the central area of the Håkon Mosby Mud Volcano off the coast of Norway, d) large sediment chunks in the central area of the Amon Mud Volcano in the Eastern Mediterranean, e) coring at the extensive *Beggiatoa* mat at the Håkon Mosby Mud Volcano, f) microbial mat associated with brine flow at the Chefren Mud Volcano in the Eastern Mediterranean, g) asphalt flow associated with tubeworms and microbial mats in the Gulf of Mexico.**

Besides methane, also higher hydrocarbons, like wet gasses ($C_2$-$C_5$ compounds) and more complex petroleum compounds ($C_{6+}$), are released from some seeps. For example at the Campeche Knolls in the southern Gulf of Mexico solidified asphalt deposits (Fig. 1f) are associated with active oil seepage and methane hydrates (MacDonald et al., 2004). Asphalt is thought to be dissolved in supercritical water (Hovland et al., 2005) which occurs above 405 °C and 300 atm. Supercritical fluids are highly hydrophobic, having similar solvent properties as strong organic solvents. The supercritical water-asphalt solution is brought to the sediment surface, where it cools, the solvent returns to normal water and the asphalt solidifies as a hard, porous slab. Asphalt seeps occur only at large depth (>2800m), where supercritical fluids can persist. In this study geostructures that are influences by brine flow and by the discharge of higher hydrocarbons were investigated in the Nile Deep Sea Fan (Grinth et al. in prep. (included as abstract), Felden et al. in prep. (included as abstract)).

*Shallow gas seeps*.- Methane formation by methanogenic bacteria is generally low in marine early diagenesis, due to competition for electron-donors with sulfate reducers (Reeburgh, 1983). Methane formation is more a characteristic for freshwater that has much lower sulfate levels than seawater. However, when in sediments with high organic load sulfate is depleted, methane can be formed close to the sediment surface from rather fresh organic matter and released into the water column. This occurs in sediments when organic matter deposition exceeds the stoichiometric sulfate penetration, e.g. in upwelling areas or estuaries. Also in coastal zones with high groundwater input with a relatively low sulfate content, methane can be formed. Seepage from shallow gas sites was detected e.g. at Cape Lookout Bay (North Carolina, USA) or Eckernförde Bay (Germany) (Martens and Val Klump, 1980; Anderson et al., 1998). During the course of this thesis, further investigations were done on the shallow seep site in Eckernförde Bay (Chapter 3).

### 1.2. Cold Seep Discharges: Nature, Origin, and Global Impact

Cold seeps constitute 3-phase-systems, where pore water, gas, and sediment rise from the subsurface and erupt. The mixture can originate from several kilometers depth and the upflow velocity and the origin of the three phases differ.

Sediment extrusion is typical for mud volcanoes, but also here sediments are ejected in different amounts, resulting in various mud volcano morphologies: the classic mud volcanoes are cone-shaped and several hundred meters high, like the Amon and the Isis Mud Volcano in the Nile Deep Sea Fan off the coast of Egypt (Dupré et al., 2008b). Flat, pancake shapes (e.g. the Håkon Mosby Mud Volcano off the coast of Norway), or mud pies with a steep outer rim (e.g. the Dvurechenskii mud volcano, Black Sea) are also found. Common to all mud volcanoes, the main discharge occurs through a central feeder channel that ends in a main crater or a central vent. In larger mud volcanoes often lateral pipes develop near the sediment surface, making the mud volcano morphology and the pathway

of the mud extrusion more complex. The extruded sediment is referred to as 'mud breccia' as a mud matrix supports a quantity of chaotically disturbed angular to rounded rock clasts that can range from millimeter to meter size. The clasts derive from the various lithological and stratigraphical horizons through which the gas-water-mud-mixture migrated (Dimitrov, 2002) and give a glance at deeply buried sedimentary units. The depth from which the mud derived and its geological origin can be inferred from vitrinite reflectance and the composition of the contained organic material (Schulz et al., 1997).

Sediments and fluids do not necessarily come from the same source. The matrix of the rising fluids is pore water squeezed from the sediment during burial, released during diagenetic processes or originating from submarine groundwater discharge, e.g. in near-costal zones. During its ascent, this pore water becomes enriched or depleted in various geochemical components and the composition depends on the geological source, the transport pathway and rate, and the chemically induced reactions during transport (Kukowski et al., 2002). Significant differences between seep fluids are found for conservative ions like chloride: fluids depleted in chloride indicate a deep freshwater source, whereas chloride-enriched fluids form from migration through evaporite deposits or from in situ methane hydrate formation. Also re-crystallization and precipitation of authigenic minerals in the sediment changes the fluid composition: for example carbonate re-crystallization at depth decreases the $Ca^{2+}$, but increase the $Sr^{2+}$ concentration (Martin et al., 1996). On the contrary, dissolution of buried barite ($BaSO_4$) deposits by sulfate depleted fluids, leads to fluid enrichment in $Ba^{2+}$ (Torres et al., 1996). Organic matter regeneration at depth is indicated by increased alkalinity, and high $NH_4^+$, $I^-$ and $Br^-$ content (Martin et al., 1996; Aloisi et al., 2004). Typically, silicate alteration processes, especially clay dehydration, are associated with fluid enrichment in geochemically important species such as $Ca^{2+}$, $Li^{2+}$, B, $Sr^{2+}$, and depletion in $K^+$ and $Mg^{2+}$, as found in the Dvurechenskii mud volcano (Aloisi et al., 2004). Similarly, in mud volcanoes in Trinidad (Dia et al., 1999) and the Eastern Mediterranean (Haese et al., 2006) fluid-rock interactions at elevated temperature were inferred from the correlation of $Na^+$, $Mg^{2+}$, and $K^+$, and the origin of the fluid with respect to the temperature regime and the source sediment could be deduced from the geochemical composition of the rising fluid.

In contrast to the highly variable solute composition, the variability in the fluid gas composition is much lower. Evidently, ancient fluids ascending through reduced sediments are anoxic; as the fluids are usually sulfate-free, also no sulfide is formed at depth. $H_2$, which is often found in hot smokers, is not present in cold seeps as it is converted to methane before it could reach the seafloor. Gases like $CO_2$ or noble gases are only occasionally found in cold seep fluids, mostly when seepage is connected to igneous volcanism (Kopf, 2002 and literature therein). The most important fluid constituent is always methane, which generally exceeds 90% of the dissolved gases (Dimitrov, 2002; Kopf, 2002).

Methane is formed in deeper zones of sediments by methanogenesis- the last step in the anaerobic degradation of biomass (Fig. 2①). As the competition for substrates is high, and the energy yield of methanogenesis is low compared to aerobic and other anaerobic metabolic processes, methanogenesis

only dominates when all common electron-acceptors in organic matter conversion ($O_2$, $NO_3^-$, metal-oxides, $SO_4^{2-}$) are depleted, or nearly so. Methanogenesis accounts for the re-mineralization of around 2-5% of the organic matter in coastal marine sediments (Canfield et al., 2005) and of up to 30% in environments with high organic load (Crill and Martens, 1986). At about 2 km sediment depth the geothermal temperature rise inhibits further microbial conversion and organic material that escaped microbial degradation is converted by thermocatalytic processes (Fig. 2②). At temperatures between 80-120 °C long-chain organic molecules are slowly broken down to heavy gaseous and liquid hydrocarbons (early thermogenic gas formation); these can be stored in petroleum reservoirs (Fig. 2③) or are converted to $C_1$ compounds (methane, Fig. 2④) at temperatures between 150-200 °C (late thermogenic gas formation) (Claypool and Kvenvolden, 1983). Large gas and oil reservoirs form if the hydrocarbons are trapped in structures like salt domes or beneath low-permeability sediments like clays. Isotopic fractionation can be used to distinguish microbially and thermogenically formed methane, as microbes preferentially use isotopically lighter substrates. Thus, microbially formed methane is lighter ($\delta^{13}C$ of -50 to -110‰ V-PDB) than geothermal methane ($\delta^{13}C$ of -20 to -50‰ V-PDB) (Whiticar, 1999). Altogether 75-320 Tg $CH_4$ $yr^{-1}$ is generated in marine sediments (Valentine, 2002), with methanogenesis as major source (Claypool and Kvenvolden, 1983).

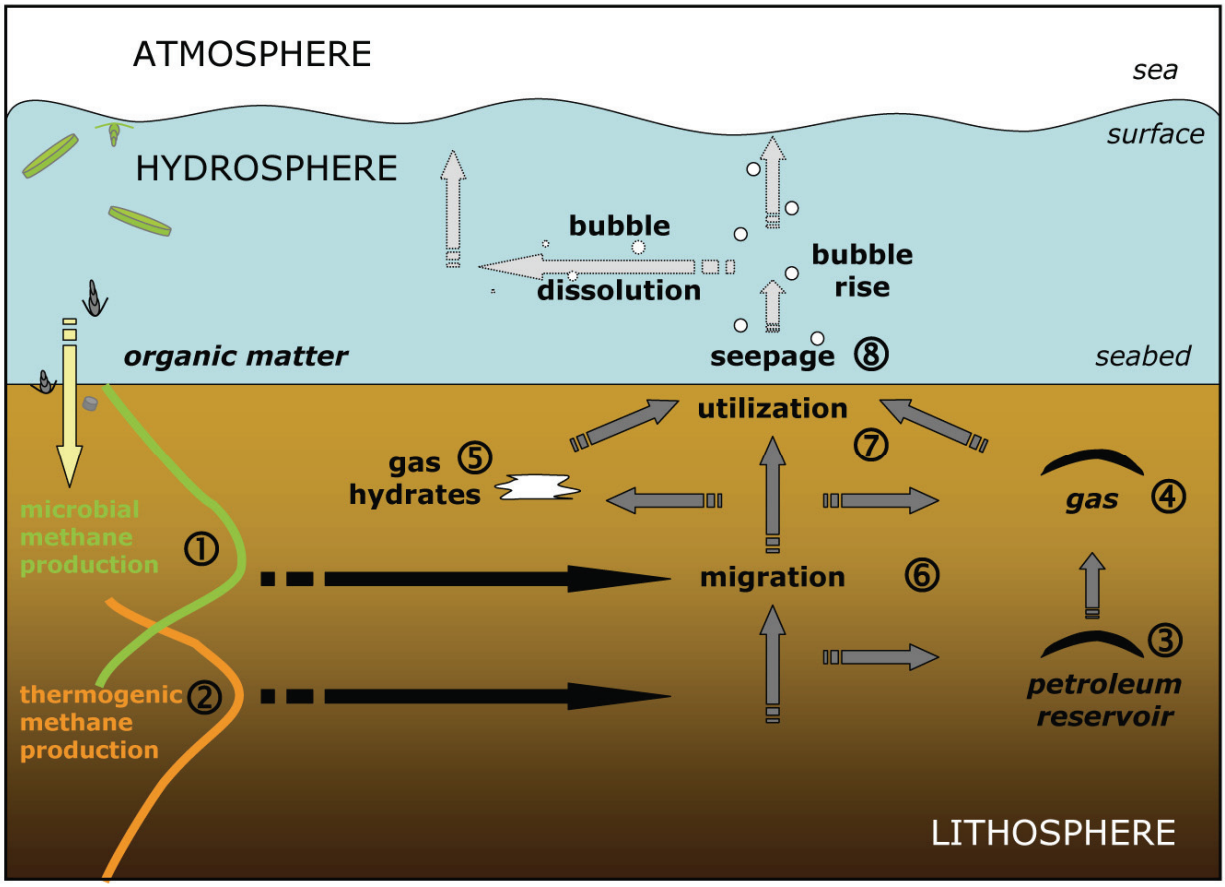


**Fig. 2: Principal sources, migration pathways, and fate of methane in marine sediments. Modified after Judd (2004). For detailed explanation see text.**

In the marine environment methane exists in different phases: gaseous, dissolved, and solid. The solid, ice-like form is called methane hydrate or 'clathrate', and methane is enclosed in a cage-like framework of water molecules (Fig. 2⑤) (Kvenvolden, 1993). Formation of methane hydrate needs methane oversaturation within the methane hydrate stability zone, a zone confined to marine settings with high hydrostatic pressure and low temperature. Methane hydrate formation and stability is influenced by salinity, and other gasses and hydrocarbons, a highly complex issue largely beyond the scope of this introduction and readers are referred to the review from Bohrmann and Torres (2006) and literature therein. Interestingly, due to equilibrium reactions with methane hydrates, the methane concentration in seawater has a different dependency on pressure and temperature than other gasses. In the methane hydrate stability zone, increasing pressure will not result in more dissolved methane, as it will precipitate to hydrates. Temperature increase in the methane hydrate stability zone leads to increased concentrations of dissolved methane, as the equilibrium of the hydrates shifts towards free methane. Above the dissociation temperature for methane hydrate (>15 °C at a water depth of >1000 m), increasing temperature leads to lower methane solubility, the common behavior of gasses. At further elevated temperature or lower pressure methane forms bubbles, if its solubility is exceeded. Methane moves dissolved in pore water to the seafloor, through cracks and channels in the sediment, or occasionally as bubbles (Fig. 2⑥). Also large oil and gas reservoirs release some hydrocarbons to the seabed as the sealing by the impermeable sediments and rocks leaks over geological time. Upward migrating methane is consumed in the near-surface sediment (see Section 1.4.1., Fig. 2⑦), but when the potential for utilization is exceeded, methane is released into the hydrosphere (Fig. 2⑧). Hydro-acoustic surveys showed that above cold seeps methane plumes can reach several hundred meters into the water column (Greinert et al., 2006; Sauter et al., 2006), and the detection of these plumes aids in the discovery of new seep sites. In some cases, e.g. if seeps are located in shallow waters, this methane reaches the atmosphere, and here it acts as greenhouse gas with a 21 times higher global warming potential than $CO_2$ (Lelieveld et al., 1998), and with a major impact on the climate. Latest estimates predict a methane contribution from geological sources to the atmosphere of 16-45 Tg $CH_4$ $yr^{-1}$ (Judd et al., 2002; Kvenvolden and Rogers, 2005), buried organic matter recycled through methane and released as methane-rich fluids thus plays a significant role in the global carbon cycle. The amount of methane gas hydrates retained in oceanic sediments is immense and global estimates are in the range of $10^5$ to $10^7$ Tg $CH_4$ (Reeburgh, 2007, and literature therein). Thus the yearly methane release from marine sediments is a very small fraction (<<0.1%) of a giant pool. Obviously, a small disturbance of this very large pool of methane hydrates may have severe consequences for the methane release. Such scenarios are discussed to be related with drastic and sudden global climate changes and mass extinctions in the geological past (Dickens et al., 1995; Dickens et al., 1997; Katz et al., 1999; Hesselbo et al., 2000; Thomas et al., 2002).

The accuracy of estimates for release and retention of methane depends on the availability of studies - and these are rare. One task of this thesis was to more accurately determine the consumption

and release of methane from cold seeps, which will help to finally make a precise global methane budget.

### 1.3. Life at Cold Seeps

Cold seep faunal assemblages were first described for the northern Gulf of Mexico (Kennicutt et al., 1985) and at a subduction zone in the northwestern Pacific (Suess et al., 1985). Since then cold seeps have been frequently reported as oases of life at an otherwise deserted seafloor (Sibuet and Olu, 1998). The primary producers at cold seeps are microbes metabolizing methane (methanotrophic) and sulfide (thiotrophic). The highest microbial yield is obtained by sulfide oxidation and by aerobic methane oxidation (0.33-0.66 mol C per mol electron-donor, Leak and Dalton, 1986; Hagen and Nelson, 1997); the efficiency in biomass yield from anaerobic methane oxidation is more than one order of magnitude lower (Nauhaus et al., 2007). However, when speaking of primary production at cold seeps, it should be realized that methane is mainly derived from the decay of organic matter produced from photosynthesis. Also the electron-acceptors for primary production - sulfate, oxygen and nitrate - derive from seawater oxidized by photosynthesis, thus the redox processes at cold seeps ultimately depend on sunlight.

Chemoautotrophic microbes form symbiotic associations with invertebrates. Bivalves and clams (e.g. *Mytilidae*, *Lucinidae* and *Vesicomyidae*) host symbionts in their gill tissue (Sibuet and Olu, 1998; Duperron et al., 2005), gut- and mouth-less siboglinid tubeworms rely on endosymbionts in their trophosome (Fig. 3) (Cordes et al., 2005; Lösekann et al., 2008), and methanotrophs are found in *Cladorhiza* sponges (Vacelet et al., 1995). However, methanotrophs and thiotrophs are also frequently found without a symbiotic partner. Diverse γ-proteobacteria were detected in seep sediments thriving on methane consumption with oxygen (Knittel et al., 2005; Lösekann et al., 2007; Omoregie et al., 2008). Representatives of free-living thiotrophs at seeps are sulfur-precipitating ε-proteobacteria like *Arcobacter* (Omoregie et al., 2008) or giant sulfur-oxidizing γ-proteobacteria like *Beggiatoa*, *Thiomargarita*, or *Thioploca* (Fig. 3). The giant sulfur-oxidizers are among the most prominent and widespread seep inhabitants. Extensive thiotrophic mats are found e.g. at Hydrate Ridge, the Håkon Mosby Mud Volcano, in the Gulf of Mexico (Sassen et al., 1993; Sahling et al., 2002; de Beer et al., 2006; Lösekann et al., 2007; Niemann et al., 2006) or at shallow methane seeps like Eckernförde Bay (Treude et al., 2005). Sulfide is consumed with oxygen or internally stored nitrate and sulfide oxidation proceeds via elemental sulfur to sulfate. This sulfur is an intermediate electron-donor storage, kept inside the filaments as internal globules, which give the bacteria the white appearance.

This primary production by free-living microorganisms, chemosynthetic macrofauna, and the precipitation of seep-related carbonates as substratum for sessile organisms form the basis for complex ecosystems at cold seeps. The presence of a chemosynthetic seep community is often used as indicator for near-surface methane and sulfide. At large features like mud volcanoes, giant pockmarks, and

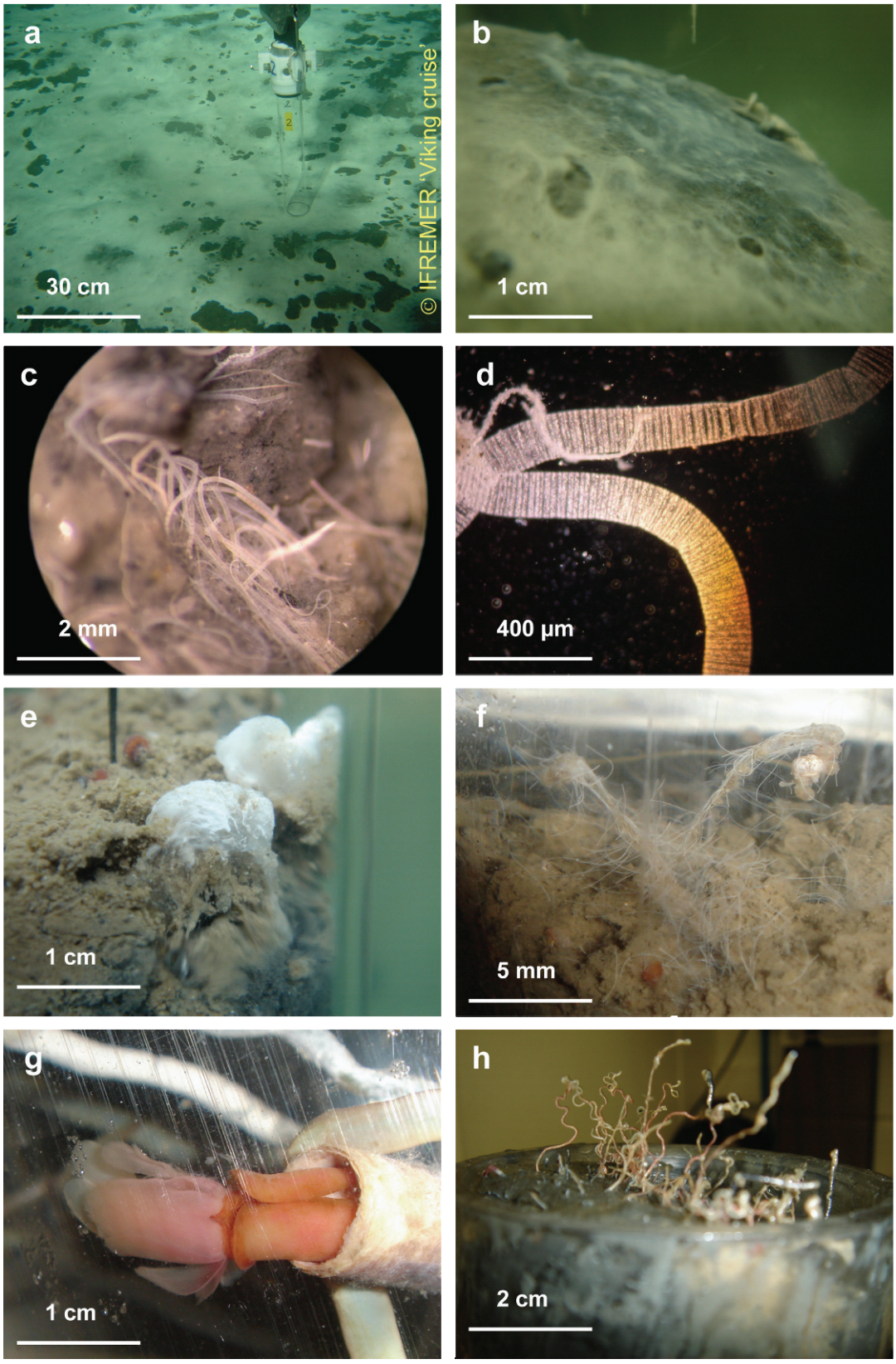


**Fig. 3: Thiotrophic bacteria and seep community. *Beggiatoa* mat from the Håkon Mosby Mud Volcano (a) as recorded with a deep-sea camera and (b) on top of sediment in a retrieved core. With light microscopy the interaction between, and the morphology of individual filaments can be assessed (c, d, provided from S. Grünke). Conspicuous sulfur globules related to thiotrophic bacteria are found at cold seeps ((e), Nyegga area). Macrofauna can be populated by thiotrophic bacteria ((f), Nyegga area) or host symbionts in their interior as do tubeworms retrieved from seeps (tubeworm retrieved from (g) the Nile Deep Sea Fan (h) the Norwegian Margin).**

massive near-surface methane hydrate deposits, different habitats with specific seep inhabitants are found (Sahling et al., 2002; Niemann et al., 2006; Sahling et al., 2008; Sommer et al., 2009b). It is hypothesized that this spatial distribution in habitats and the density of the faunal biomass is related to the fluid upflow velocity, and hence, the substrate supply at the local site (see Chapter 1.5., Sibuet and Olu, 1998; Treude et al., 2003; de Beer et al., 2006). In some cold seeps, like in the permanent anoxic waters of the Black Sea, indicator organisms are missing. Other strategies have to be found for the determination of zones with different levels of sulfate, methane and sulfide supply.

### 1.4. Biogeochemical Processes in Hydrocarbon-Rich Sediments

In cold seeps pore water, sediment, chemical constituents, and occasionally also heat are exchanged across the seabed-seawater interface. In near-surface seep sediments, the consumption of reduced compounds with oxidants contained in the pore water and sediment produces steep geochemical gradients, and stimulates the ecosystem 'cold seep'. The environmentally relevant redox cycle linked to methane oxidation (Section 1.4.1.) is the sulfur cycle (Section 1.4.2.), which itself is closely interconnected with the iron cycle (Section 1.4.3.).

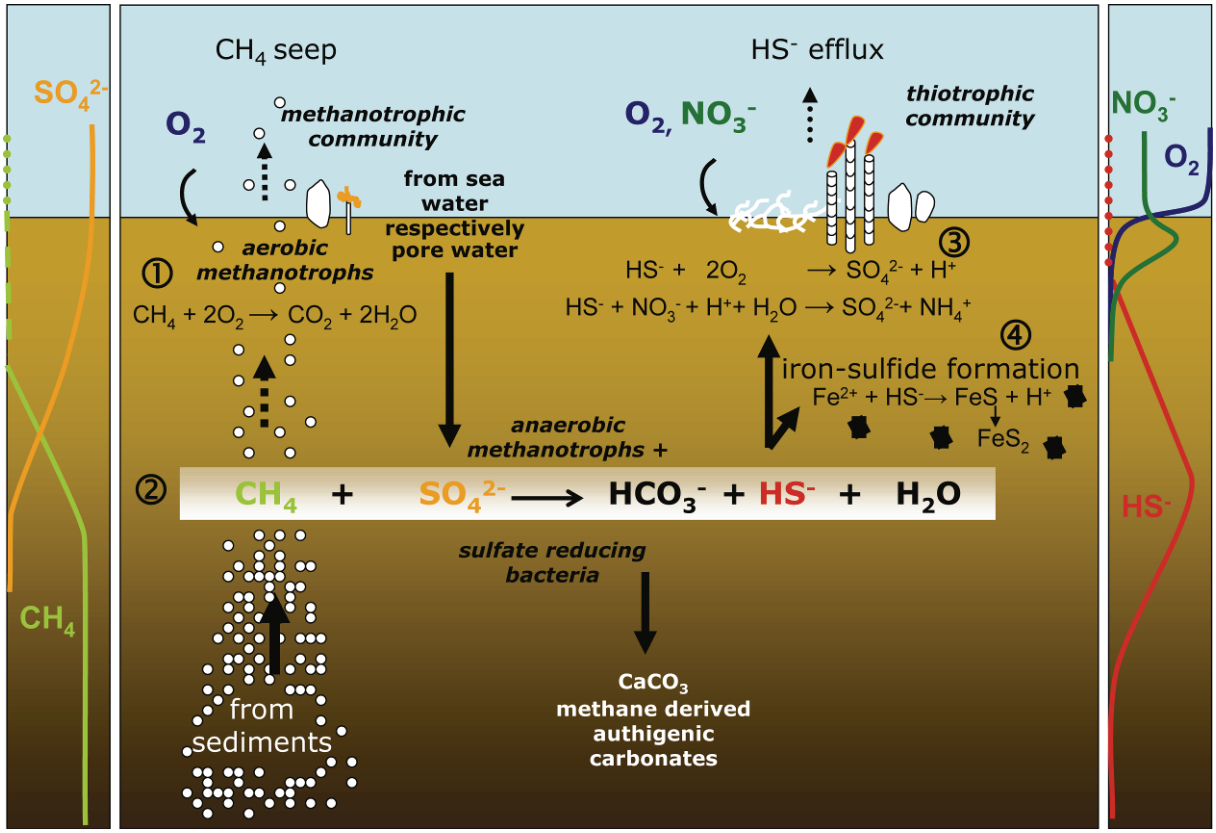


**Fig. 4: Main biogeochemical processes in hydrocarbon-rich near-surface sediments. Modified after Judd and Hovland (2007); left and right panels conceptually present profiles of the main reactants, for details see text.**

*1.4.1. Methane oxidation*

At the sediment-water interface of cold seeps methane consumption is mediated aerobically (Fig. 4①) and aerobic oxidation by epibenthic fauna can be a major sink for methane (Sommer et al., 2009a).

$$\textit{Aerobic methane oxidation}: \quad CH_4 + 2O_2 \rightarrow CO_2 + 2H_2O \qquad \text{(Eq. 1)}$$

However, within the seep sediment aerobic methane oxidation is strongly limited by the supply of oxygen (Suess et al., 1999; Wallmann et al., 1997), and only low methane turnover rates by aerobic microbes of 3-5 mmol $m^{-2}$ $d^{-1}$ have been reported (Niemann et al., 2006; Sommer et al., 2006). Sulfate, which is also known to oxidize methane (Martens and Berner, 1974; Barnes and Goldberg, 1976; Reeburgh, 1976), is 100 times more abundant than oxygen. Consequently, the main biological sink for methane in marine sediments is the anaerobic oxidation of methane (AOM) with sulfate (Fig. 4②):

$$\textit{Anaerobic methane oxidation}: \quad CH_4 + SO_4^{2-} \rightarrow HS^- + HCO_3^- + H_2O \qquad \text{(Eq. 2)}$$

Although essential details of the biochemical mechanism still need to be elucidated, the microbes mediating this reaction are well-known: methane oxidizing archaea (ANME-1, ANME-2 or ANME-3) and sulfate reducing bacteria (mainly *Desulfosarcina*, *Desulfococcus* or *Desulfobulbus*) are consistently detected in seep sediments where anaerobic methane oxidation and sulfate reduction proceeds (e.g. Boetius et al., 2000; Knittel et al., 2005; Lösekann et al., 2007). These microorganisms can be present as single cells, but mostly bacterial sulfate reducers and archaeal methanotrophs form aggregates with a biomass that exceeds that of the surrounding sediment by an order of magnitude. The very low energy yield of the reaction ($\Delta G^0$= -18 kJ per mol under standard conditions; Schink, 1997), which must be shared between the archaeon and the sulfate reducing bacterium, is apparently just enough for both populations. Methane oxidation coupled to sulfate reduction is a common process in diverse, anoxic environments where methane and sulfate are available. Sulfate and methane turnover rates at seeps typically are in the range of 30 mmol $m^{-2}$ $d^{-1}$ (Luff et al., 2004), but maximal rates of up to 100 mmol $m^{-2}$ $d^{-1}$ have been reported (Treude et al., 2003). Latest estimates predict that in marine sediments sulfate reduction can account for the consumption of up to 300 Tg $CH_4$ $yr^{-1}$ and thus of 80% of the methane flux from the sediment (Hinrichs and Boetius, 2002). However, such global numbers must be considered with caution. A much higher annual estimate is expected when the rarely surveyed seep areas will be taken into account. Thus, one task of this thesis was to extend the number and the accuracy of sulfate reduction and methane oxidation measurements in various cold seep sites and habitats.

*1.4.2. Biogeochemically relevant sulfur conversion pathways*

Sulfate reduction is one of the most relevant pathways in organic matter degradation (Eq. 3), and it is globally responsible for the mineralization of about 55% of the marine carbon (Canfield et al., 2005).

$$2CH_2O + SO_4^{2-} \rightarrow H_2S + 2HCO_3^- \qquad \text{(Eq. 3)}$$

Also in cold seeps sulfate reduction is a key process, as anaerobic methane oxidation with sulfate (Fig. 4②, Eq. 2) is the relevant filter preventing methane release from the sediment into the hydrosphere. One of the main products of either sulfate reduction pathway (organoclastic or methanotrophic) is sulfide. However, even in marine sediments with intense sulfide production, the sulfide flux from the sediment into the water column is small or absent: sulfide is either re-oxidized or precipitated (Fig. 4.③, ④), and an intense sulfur cycle with sulfur compounds with an oxidation level between –II ($H_2S$) and +VI ($SO_4^{2-}$) can establish (Fig. 5).

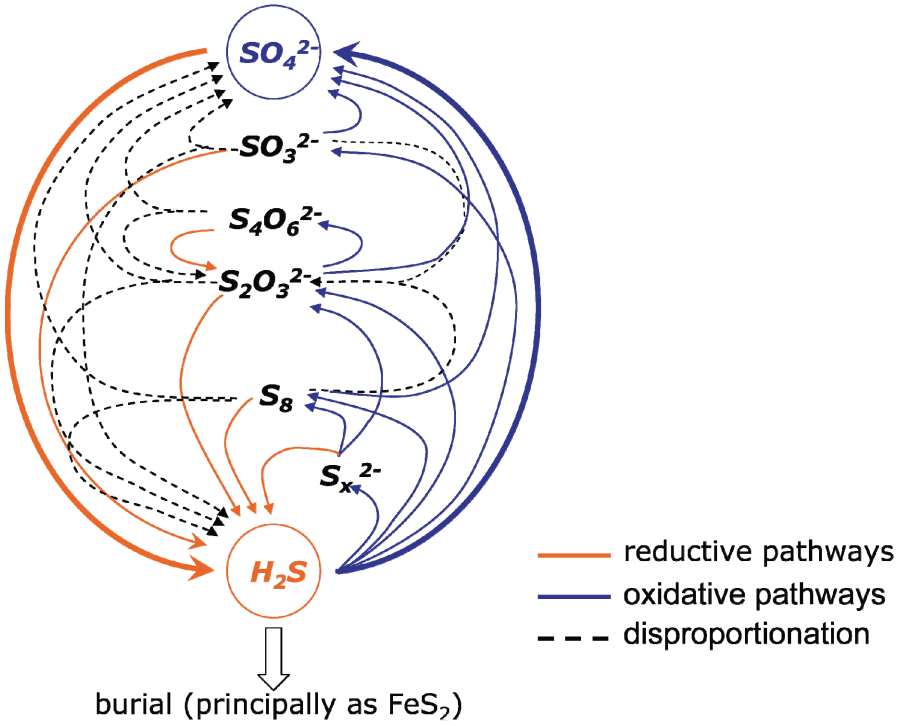


**Fig. 5: Schematic figure of the sedimentary sulfur cycle, with the important pathways for reductive processes, oxidative processes, disproportionation, and removal of sulfide from the cycle (precipitation as $FeS_2$) after Zopfi et al. (2004).**

As visible in Figure 5, the only product of sulfate reduction is sulfide, and sulfur compounds with a higher oxidation level such as elemental sulfur ($S_8$), thiosulfate ($S_2O_3^{2-}$), sulfite ($SO_3^{2-}$) and sulfate ($SO_4^{2-}$) derive from the oxidation of this sulfide (Zopfi et al., 2004). Sulfur intermediates or sulfate are formed chemically and/or by microbial processes when sulfide comes in direct contact with oxygen (Eq. 4), and microbial sulfide oxidation with nitrate (Eq. 5) is a well-known process for the giant

sulfur-oxidizing bacteria. The oxidation of sulfide with manganese(IV)- or iron(III)-oxides proceeds purely chemically (e.g. Eq. 6, 7, in detail in Section 1.4.3.), and is also often incomplete, leading to the formation of sulfur intermediates, such as elemental sulfur, sulfite or thiosulfate (Pyzik and Sommer, 1981; Burdige and Nealson, 1986; dos Santos Afonso and Stumm, 1992; Zopfi et al., 2004). Elemental sulfur can react with sulfide to form polysulfides ($S_x^{2-}$), known for their high reductive and nucleophilic reactivity and important e.g. in pyrite formation (Rickard, 1975; Luther, 1991) and sulfurization of sedimentary organic matter (Kohnen et al., 1989; Amrani and Aizenshtat, 2004).

Sulfur intermediates are then either reduced or oxidized chemically, or utilized by microbes. It should be noted at this point that redox processes are only performed by microorganisms when the chemical process is relatively slow and enough microbes are abundant. For example the reaction between oxygen and sulfide can proceed geochemically or microbially, and microbial turnover of sulfide in the presence of oxygen can be less than a second (e.g. in *Beggiatoa* mats, Jørgensen and Postgate, 1982). Purely chemical sulfide consumption with oxygen is in the range of several hours, depending on temperature, pH and ionic strength of the seawater and the presence of a probable catalyst, e.g. metals (Millero et al., 1987). However, microbes can exploit sulfur intermediates as energy source with oxygen, nitrate and metal-oxides as electron-acceptor or they reduce them to sulfide during the degradation of organic matter (Bak and Pfennig, 1987; Luther, 1991; Zopfi et al., 2004; Canfield et al., 2005). Some examples for microbial and/or geochemical reactions of sulfur compounds, that are common in marine surface sediments, can be found in Equation 4-7:

*Sulfur conversions with oxygen*

$$2HS^- + O_2 + 2H^+ \rightarrow 2S^0 + 2H_2O \quad \text{(Eq. 4a)}$$

$$2HS^- + 3O_2 \rightarrow 2H^+ + 2SO_3^{2-} \quad \text{(Eq. 4b)}$$

$$2HS^- + 2SO_3^{2-} + O_2 + 2H^+ \rightarrow 2S_2O_3^{2-} + 2H_2O \quad \text{(Eq. 4c)}$$

$$2SO_3^{2-} + O_2 \rightarrow 2SO_4^{2-} \quad \text{(Eq. 4d)}$$

$$HS^- + 2O_2 \rightarrow SO_4^{2-} + H^+ \quad \text{(Eq. 4e)}$$

*Sulfide oxidation with nitrate*

$$4HS^- + NO_3^- + 6H^+ \rightarrow 4S^0 + NH_4^+ + 3H_2O \quad \text{(Eq. 5a)}$$

$$HS^- + NO_3^- + H^+ + H_2O \rightarrow NH_4^+ + SO_4^{2-} \quad \text{(Eq. 5b)}$$

*Sulfide oxidation with manganese-oxide*

$$HS^- + MnO_2 + 3H^+ \rightarrow S^0 + 2H_2O + Mn^{2+} \quad \text{(Eq. 6)}$$

*Sulfide oxidation with iron-oxide*

$$HS^- + 2FeOOH + 5H^+ \rightarrow S^0 + 4H_2O + 2Fe^{2+} \quad \text{(Eq. 7)}$$

Under appropriate environmental conditions another shunt for the microbial usage of sulfur intermediates is the disproportionation of elemental sulfur, thiosulfate or sulfite (Bak and Pfennig, 1987). Disproportionation is the microbially induce, energy yielding conversion of an intermediate substrate into a more oxidized plus a more reduced compound without performing a redox-reaction. As the environmental constraints of the various sulfur transformation pathways are largely beyond the scope of this introduction the interested reader is referred to the review from Zopfi et al. (2004).

Important for investigations at cold seeps, the presence of sulfur intermediates in the sediment is a sign of sulfide oxidation. Elemental sulfur and, even better, the more unstable intermediates are the most direct indicators of active oxidation processes, but the abundance of sulfur intermediates is rarely studied in marine sediments and to our knowledge never in cold seeps. It is remarkably difficult to study sulfide oxidation rates in active sediments, due to the number of possible processes, the number of sulfur intermediates, the high turnover rates, and the very rapid exchange of isotope tracers among the sulfur species. However, due to new methods available for analyses of sulfur intermediates (see Chapter 5) it is now possible to assess the concentrations of individual sulfur species and thus define the limits of the oxidative potential of cold seep sediment, as done during this thesis for a mud volcano in the Black Sea (Chapter 5).

### *1.4.3. The Iron Cycle in Organic-Rich Sediments*

In sediments with high sulfate turnover, the sulfur cycle (1.4.2.) usually is strongly connected with the iron cycle: iron-oxides react with sulfide, and the generated iron-sulfides are the most important minerals associated with organoclastic and methanotrophic sulfate reduction. In ocean margins precipitation with iron is responsible for the removal of 5-20% of the sulfide from the sediments (Canfield and Teske, 1996; Jørgensen, 1990). For iron-sulfide formation dissolved sulfide is oxidized at the surface of solid state iron-oxides (Eq. 7), followed by the release of $Fe^{2+}$ that subsequently reacts with additional sulfide to form FeS (Pyzik and Sommer, 1981; Yao and Millero, 1996; Poulton et al., 2003). This initially formed amorphous iron-sulfide is rapidly transformed to metastable phases such as greigite ($Fe_3S_4$) or pyrrhotite ($Fe_{x-1}S$), which finally can be converted to the stable form pyrite ($FeS_2$). Several pyrite formation pathways have been proposed, whereas the most important are:

(i) the ‘hydrogen sulfide pathway’ (Wächtershäuser, 1988; Drobner et al., 1990; Rickard, 1997; Rickard and Luther, 1997)

$$FeS_{(aq)} + H_2S \rightarrow FeS_{2(s)} + H_2 \qquad \text{(Eq. 8)}$$

(ii) the ‘polysulfide pathway’ (Rickard, 1975; Luther, 1991)

$$FeS_{(s)} + S^0_{(s)} \rightarrow FeS_{2(s)} \qquad \text{(Eq. 9)}$$

(iii) the ‘iron-loss pathway’ (Wilkin and Barnes, 1996)

$$2FeS_{(s)} + \tfrac{1}{2}H_2O + \tfrac{3}{4}O_2 \rightarrow +FeS_{2(s)} + FeOOH_{(s)} \qquad \text{(Eq. 10)}$$

Iron minerals reactive towards sulfide are amorphous or crystalline oxides, or iron-containing silicates. In marine sediments iron may originate from allochthonous sources, brought into the ocean by aeolian, fluvial, and glacial transport from terrestrial environments, and discharge from hydrothermal vents, or iron-oxides are autochthonously formed in the sediment. The efficiency of the sulfide removal from the pore water depends on the mineral form, crystallinity, grain size, and the abundance of the particular iron mineral present. Half-life times of iron minerals in the presence of sulfide range from minutes, for highly reactive amorphous iron-oxides, to over thousands of years, for the essentially unreactive iron-containing silicates (Canfield et al., 1992; Poulton et al., 2004, Table 1).

**Table 1: Half-lives ($t_{½}$) of different iron-mineral species in a 1 mmol $L^{-1}$ sulfide solution, after [a)]Canfield et al. (1992), [b)]Poulton et al. (2004).**

| Mineral | $t_{½}$ |
|---|---|
| Freshly precipitated hydrous ferric oxide | 5 minutes [b)] |
| Ferrihydrite | 4 hours [a)] |
| Lepidocrocite | 11 hours [b)] / 4 days [a)] |
| Goethite | 17 days [a)] |
| Hematite | 30 days [a)] |
| Magnetite (uncoated) | 152 years [a)] |
| 'Reactive' silicates | 333 years [a)] |
| Sheet silicates | $10^5$ years [a)] |
| Ilmenite, garnets augite, amphibole | >1 x $10^5$ years [a)] |

As the most relevant educts (iron-oxides) and products (iron-sulfides) of sulfide removal with iron are solid minerals, the principal sedimentary iron-sulfide/iron-oxide cycle as shown in Figure 6 only can be maintained with solid phase transport. Bioirrigating organism or hydraulic forces bring iron-sulfides in the suboxic or oxic zone, where they get converted by oxidants with a higher redox potential, and sulfate and iron-oxides are formed. The freshly precipitated iron-oxides are in turn transported downwards into the sulfidic zone and constitute new electron-acceptors for sulfide precipitation.

Evidence on the carbon turnover activity of the environment in which pyrite was formed comes from isotopic studies. As sulfate reducers generally prefer the lighter $^{32}$S-sulfate and the fractionation between sulfide and pyrite is low during pyrite formation, a large depletion in the $\delta^{34}$S (‰ CDT) of pyrite is present in environments where sulfate reduction is not limited by the sulfate supply. Minor depletion in the $\delta^{34}$S of pyrite is found in sediments with intense sulfate reduction and sulfide production and fast sulfate depletion (Habicht and Canfield, 2001).

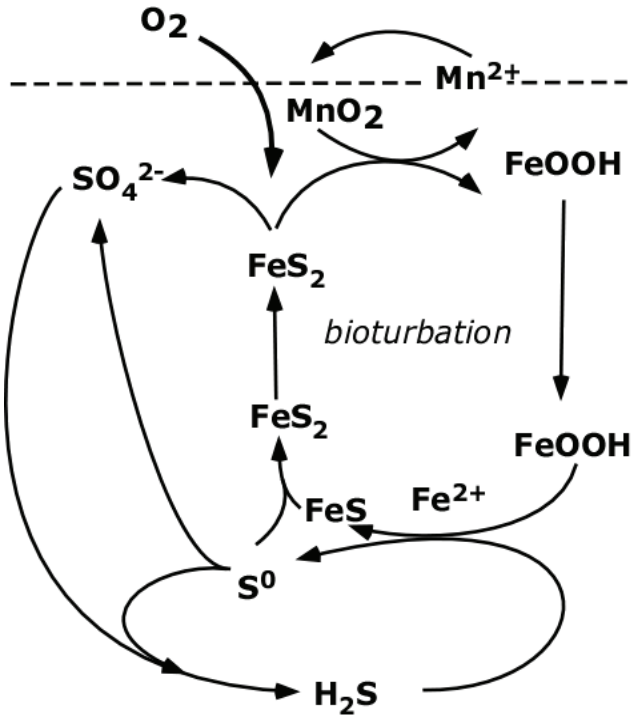


**Fig. 6: The principal sulfur and iron cycle in marine sediments. Sulfide produced from sulfate reduction reacts with iron-oxides to form iron-sulfide minerals, elemental sulfur or other sulfur intermediates. Oxygen and manganese-oxides are usually consumed during the re-oxidation of the iron-sulfide minerals. To keep this conveyer belt running the vertical transport of either iron-sulfide minerals into the oxic zone or iron-oxides into the anoxic zone, e.g. by bioturbation or by hydraulic forces, is needed (Jørgensen and Nelson, 2004).**

At present it is not known if the common iron-sulfur cycle as displayed in Figure 6 is valid for cold seep surface sediments. Iron minerals rising with the mud volcano sediments might be reactive towards sulfide and also in cold seeps metals could build an efficient barrier for sulfide. This is ecologically relevant as sulfide converted by geochemical processes is not available for thiotrophic primary production. On the other hand, at the high sulfide production rates from AOM, and at low sedimentation and bioirrigation rates limiting the common supply with iron-oxides, the sulfide concentration might exceed the reactive iron pool, sulfide can break through the suboxic zone, and can than be largely converted in microbial processes. One task of this thesis was to find out, which of the sulfide conversion processes dominates in cold seep sediments, and if the ancient mud volcano sediments contain iron-species reactive towards sulfide, which than would reduce primary production.

## 1.5. Cold Seep Mass Transfer Phenomena and their Implication on Substrate Turnover and Habitat Development

### *1.5.1. Mass transfer phenomena*

The high conversion rates at seeps need sufficient substrate supply, and substrates have to be transferred between the water column and the sediment, and between the oxic and the anoxic sediment layer. Two transport phenomena are relevant for this substrate supply in seep sediments: molecular diffusion and advection.

*Molecular diffusion.-* Molecular diffusion is a random migration of molecules, driven by a concentration gradient. No net water and sediment exchange takes place. The diffusional flux (J) of a solute through a plane is described by 'Fick's first law of diffusion':

$$J_{diff} = D \frac{dc}{dx} \qquad \text{(Eq. 11)}$$

where D = diffusion coefficient of a specific solute in water at a certain temperature and salinity and dc/dx = concentration change over a depth interval. For solute transport in sediments the porosity '$\phi$' needs to be considered as well and the specific diffusion coefficient $D_{sed}$ in the sediment has to be calculated (Iversen and Jørgensen, 1993).

$$J_{diff\_sed} = \phi D_{sed} \frac{dc}{dx} \qquad \text{(Eq. 12)}$$

Diffusive transport is highly efficient over short distances, but as the diffusion time is correlated with the square root of the length of the diffusion distance (according to the Stokes-Einstein relationship), diffusion is slow over longer distances. For example, diffusive transport of solutes in the length scale of microbes (µm) is extremely rapid with a diffusion time of less than a second. Relevant scales for diagenetic processes are often in the range of decimeter to meter, and diffusive transport will take months to years over these distances.

*Advective transport.-* Advection is a mass flow process with net sediment and water transport. Advection is always driven by a pressure gradient that can be induced by temperature differences, by bottom water currents interacting with uneven sediment surfaces or by sediment compaction (Schulz, 2006). Fauna can induce a similar spatial re-arrangement of sediment and pore water by physical reworking of the sediment (bioturbation) or indirectly e.g. by pumping activity (bioirrigation). The advective flux of a solute is calculated from the advection velocity 'v' and the concentration 'c' of the solute:

$$J_{adv} = v\, c \qquad \text{(Eq. 13)}$$

Advective solute transport rates can exceed those of diffusion by several orders of magnitude, but are also highly variable between different cold seep sites and habitats as are the fluid upflow velocities. Table 2 presents examples of fluid upflow velocities from different cold seep structures and habitats

with and without a particular chemosynthetic community. This table clearly shows how the advective flow varies over several orders of magnitude.

**Table 2: Fluid flow rates from cold seep sites determined with different approaches; MV: mud volcano.**

| Location | Upflow velocity (m $yr^{-1}$) | Cold seep chemosynthetic community | Method | |
|---|---|---|---|---|
| Håkon Mosby MV | 3-6<br>0.3-1<br>0.4 | *no fauna*<br>*bacterial mat*<br>*tube worms* | modeling | de Beer et al., 2006 |
| Eastern Mediterranean MV (Kazan MV, Amsterdam MV, Milano MV, Napoli MV) | 0.03-0.5 | *n.d.* | modeling | Haese et al., 2003; Haese et al., 2006; |
| Chefren MV | 0.6-15 | *bacterial mat* | modeling | Omoregie et al., 2008 |
| Dvurechenskii MV | 0.08-0.25 | *no fauna (Black Sea)* | modeling | Aloisi et al., 2004; Wallmann et al., 2006 |
| Costa Rica mud extrusions: | | | | |
| Mound 11<br>Mound 12 | 3<br>0.1 | *bacterial mat*<br>*bacterial mat* | modeling | Hensen et al., 2004; Linke et al., 2005 |
| Hydrate Ridge | $10^4$-$10^7$<br>0.1 -2.5<br>+/-0.05 | *bubble site*<br>*bacterial mat*<br>*clam field* | in situ measurement, modeling | Linke et al., 1994; Tryon et al., 1999; Torres et al., 2002; Tryon et al., 2002 |
| Peruvian Active Margin seeps | 400 | *clam field* | modeling | Olu et al., 1996 |
| Nankai Trough seeps off Japan | <10<br>100 | *bacterial mat*<br>*mussel bed* | modeling | Henry et al., 1992 |
| Bush Hill Seep (Gulf of Mexico) | 0.02-0.28<br>0.14 | *bacterial mat*<br>*no fauna* | modeling | Tryon and Brown, 2004 |
| Aleutian Subduction Zone | 3.4 | *clam field* | modeling | Wallmann et al., 1997 |

In cold seep fluids solutes can be transported by both mass transfer mechanisms - diffusion and advection - and the upward advection of fluids either intensifies or reduces the diffusive solute flux, depending on whether the diffusive transport is in upward or in downward direction:

$$J = J_{diff} + J_{adv} = D\frac{dc}{dx} + v\,c \qquad \text{(Eq. 14)}$$

Simply speaking for the ecologically and environmentally relevant seep processes, the fluids transport methane from large depth to the sediment layer containing oxidants such as sulfate and oxygen and the intensity of the fluid flow enables the occurrence of sulfate reduction, methane oxidation, and sulfide oxidation as schematically illustrated in Figure 7.

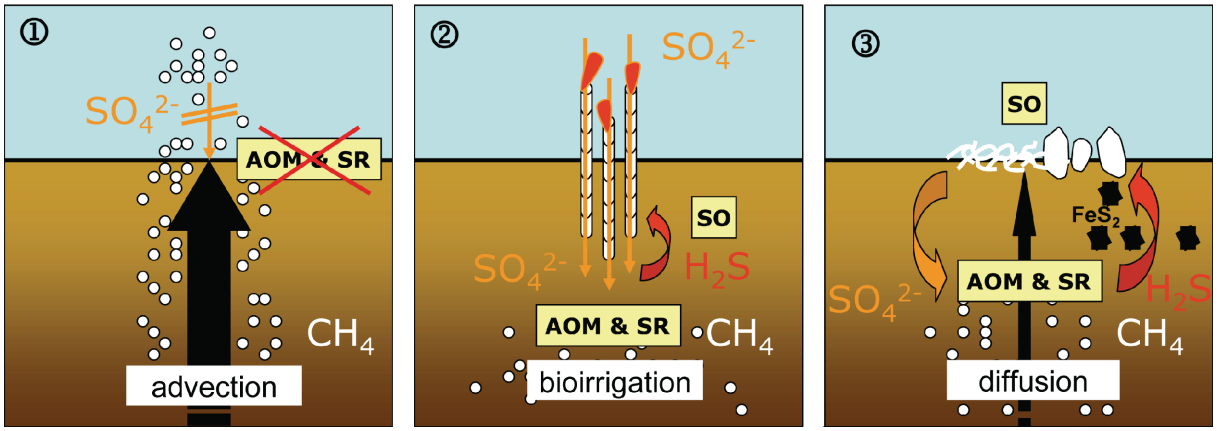


**Fig. 7: Examples for the impact of fluid flow intensity on the occurrence of methane release, methane oxidation, sulfate reduction, and sulfide consumption. AOM: anaerobic methane oxidation, SR: sulfate reduction, SO: sulfide oxidation.**

Intense advection transports large amounts of methane upwards, but minimizes the sediment supply with substrates from the water column. Seawater sulfate penetrates only millimeters to a few centimeters into the sediment, and anaerobic methane oxidation is limited by the sulfate availability. The aerobic filter for methane consumption is even less efficient and consequently large amounts of methane are released into the hydrosphere (Fig. 7①). This occurs in high upflow regions of mud volcanoes and pockmarks, like in the center of the Håkon Mosby Mud Volcano (de Beer et al., 2006; Niemann et al., 2006), and at other sites with a fluid upflow velocity >1 m $yr^{-1}$ (Luff et al., 2004).

Differently, enhanced supply with sulfate from the seawater can be induced by seep inhabitants like the bivalves *Acharax,* building U-shaped burrows, e.g. at Hydrate Ridge (Sahling et al., 2002). As well tubeworms transport sulfate to a depth of several decimeters by ventilation, as reported from the peripheral areas of the Håkon Mosby Mud Volcano (de Beer et al., 2006); at depth sulfide is produced from AOM, and nourishes the thiotrophic tube worm symbionts (Fig. 7②). In near-surface sediments, transport can even be dominated by the activity of the fauna with bioirrigation exceeding advection by 1-2 orders of magnitude (Wallmann et al., 1997; Haese et al., 2006).

If at sites with near-surface methane the fluid flow regime is diffusive or the advection is moderate (centimeter per year), like in the *Beggiatoa* habitat of the Håkon Mosby Mud Volcano (de Beer et al., 2006) and in the *Calyptogena* fields at Hydrate Ridge (Treude et al., 2003), sulfate penetrates naturally from the water column into the sediment and is largely converted by AOM. Large amounts of sulfide are formed, which can either precipitate as iron-sulfides or be utilized by thiotrophic bacteria and the thiotrophic symbionts in the invertebrates. Consequently, extensive thiotrophic surface mats or large chemosynthetic mussel beds are associated with medium to low fluid upflow, but high sulfide and methane turnover (Fig. 7③).

Thus to be able to explain the biogeochemical processes in cold seep sediments it is essential to know the intensity of the fluid flow. The actual upflow velocity can be obtained with different approaches (Table 2). Easiest, in situ instruments for fluid flow detection can be deployed at seeps (Linke et al., 1994; Tryon et al., 1999; Torres et al., 2002; Tryon and Brown, 2004). Furthermore, fluid upflow velocities can be obtained indirectly from different numerical and analytical modeling approaches. Cold seep fluids often transport heat, and as nonlinear vertical temperature profiles indicate fluid movement, the curvatures of profiles can be used to asses the fluid flow velocities, as done e.g. for the Håkon Mosby Mud Volcano (de Beer et al., 2006; Feseker et al., 2008). From the depth distribution of conservative ions like chloride, either depleted or enriched in the fluids compared to the seawater, the fluid seepage rate can be obtained by the best fit of the measured results with the model (Aloisi et al., 2004; Omoregie et al., 2008). The models become more complicated if the constituents do not behave conservatively and a reaction term has to be added as done for the determination of fluid upflow in mud volcanoes (Haese et al., 2003; Wallmann et al., 2006). However, the deployment of the in situ flow meter is difficult, costly, and time-consuming, the temperature approach is only applicable if the rising fluid has an enough elevated temperature, and all other efforts are based on the comparison of models with results that might have been subjected to biases from sediment retrieval (see below). To obtain more accurate results, the approach used in this study is a 1-dimensional-transport model, adapted from de Beer et al. (2006), that can be fitted to sulfide profiles measured in situ (see below). In cold seeps upflow is clearly indicated by the shape of the sulfide profile: as likely no oxidant for sulfide is available in the highly reduced sediment, a decrease in the sulfide concentration below the AOM zone is caused by the upflow of the sulfide-free fluid; if in contrast no upflow occurs, a constant concentration is reached and sulfide does not decrease below its production zones (Fig. 8). In steady state the diffusive flux downward ($J_{diff}$) equals the advective flux upward ($J_{adv}$):

$$J_{diff} = J_{adv} \qquad \text{(Eq. 15a)}$$

$$v\,c = D\frac{dc}{dx} \qquad \text{(Eq. 15b)}$$

$$C_x = C_0 e^{-\frac{vx}{D}} \qquad \text{(Eq. 15c)}$$

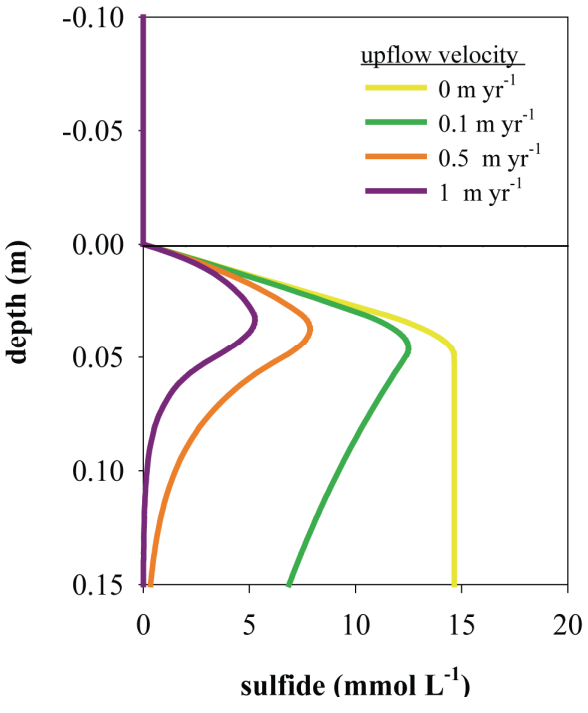


**Fig. 8: Example of the effect of different fluid flow velocities on the shape of a sulfide profile.**

where $C_x$ = the solute concentration at depth and $C_0$ = the concentration at the source, in this case the highest sulfide concentration in the AOM zone. The upflow velocity is obtained from solving Equation 15c for 'v'.

*1.5.2. In situ measurements*

Accurate sampling is critical for the correct interpretation of the results, and especially in cold seeps it is essential to understand the possible artifacts. The most important problem is the change of the sediments between sampling at the seafloor and analyses on the ship. During the transport the sediments increase in temperature and lyses of pressure-sensitive organisms occurs, and even exposure of less than an hour leads to long-term increases of aerobic respiration, typically with a factor of 2-3 (Reimers et al., 1986; Glud et al., 1994; Sauter et al., 2001). Sediments from seeps loose their main source of electron-donor, methane, which may lead to underestimations of AOM as shown in laboratory studies, where incubations at ambient concentration and pressure led to significantly higher turnover rates (Nauhaus et al., 2002). A much more serious artifact of extremely methane-rich sediments is gas formation during ascent. The cores are often literally boiling for hours, especially if hydrates are present. This leads to serious biases, like seawater mixing into the sediment, disturbing the distribution of sulfate, or of conservative solutes, like chloride, used for modeling upflow velocities. This methane also will flush out other gases, mainly $CO_2$ and $H_2S$. This can lead to drastic changes of the pore water composition, as the pH will go up leading to calcification and the sulfide removal can change the essential metal-sulfide reactions. As the upflow has stopped, retrieved sediment does not give meaningful information on exchange of pore water and water column solutes. Moreover, microbial mats, which normally are confined to the upper few millimeter of the sediment, will be mixed into the sediment, and only after a while recover to form new mats; the physiology of the large sulfur-oxidizers may have changed.

Due to these problems in situ measurements are needed. Devices useful for the determination of biogeochemical turnover processes are benthic chambers, in situ microprofiler, in-situ(-Rhizon)-pore water sampler, planar optods, and in situ sediment incubation tools.

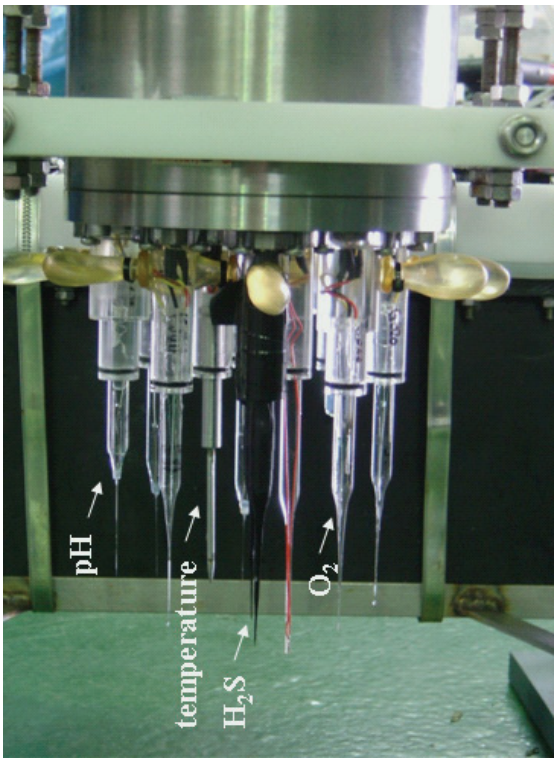


**Fig. 9: Microsensors mounted on a deep-sea profiling unit.**

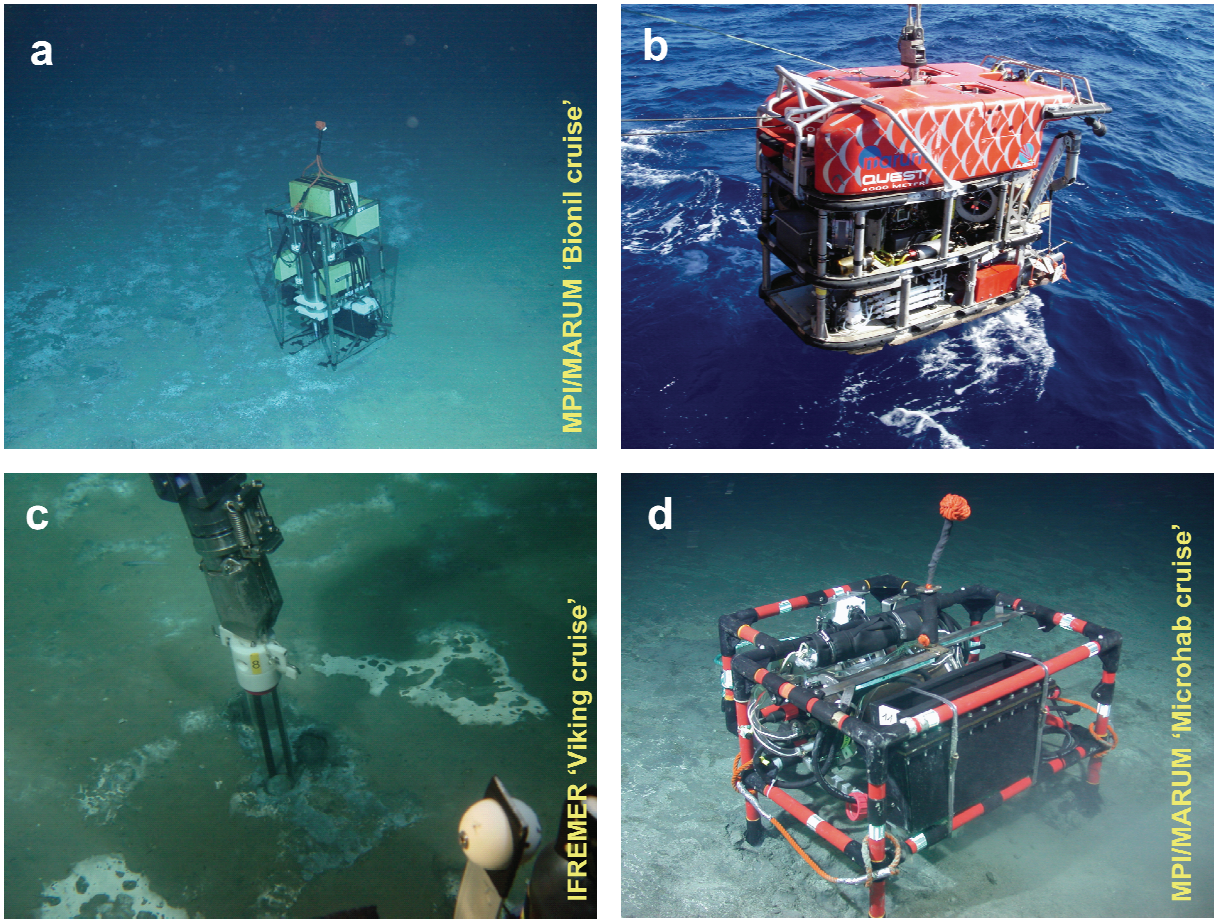


**Fig. 10: In situ tools and ROV sampling; a) microprofiler accurately positioned on the border of a microbial mat at the pockmark area in the central Nile Deep Sea Fan, b) deployment of the ROV Quest, c) ROV manipulator performing precise push coring of a small-scaled gray microbial mat at the Håkon Mosby Mud Volcano, d) benthic chamber at the seafloor close to the microbial reef structures southwest of the Crimean Peninsula (Black Sea).**

During this study a benthic chamber was used and high resolution geochemical gradients were measured in situ with microsensors. Microsensors are small, needle-shaped, and extremely sensitive measuring devices that can record geochemical gradients with high spatial and temporal resolution (Fig. 9). Gradients measured with oxygen and $H_2S$ microsensors provide highly relevant information about oxygen consumption rates, sulfide production, and sulfide consumption rates, e.g. aerobic and anaerobic sulfide oxidation can be distinguished. Depth changes in the redox potential can be measured directly with a redox sensor and peaks or dips in pH profiles can be ascribed to certain acidogenic or alkalogenic redox-reactions in the seep sediments. Temperature gradients, measured with macroelectrodes, can exhibit the degree of advection of warm seep fluids. To avoid the mentioned artifacts induced during sediment retrieval, during this work an in situ microprofiler (Fig. 10a) (Wenzhöfer et al., 2000) was deployed at various cold seep sites. This profiling unit consists of amplifiers and a computer kept in a titanium cylinder that is fixed in a frame. The energy supply for the device comes from a deep-sea battery. At the lower end of the cylinder up to 11 microsensors can be mounted. Depending on the programming, the sensors measure in the water column or move

stepwise into the sediment. Most importantly, this instrument can be deployed with a remotely operated vehicle (ROV, Fig. 10b) and can be precisely placed with the ROV manipulators and the help of cameras. With the ROV small scaled seep patches can be targeted for measuring and sampling (Fig. 10c) and the high spatial variability at cold seeps can be resolved.

To measure total exchange rates of solutes and gases across the sediment-water interface over a larger area (around 900 $cm^2$) a benthic chamber as introduced in Glud et al. (2009) has been used during this work (Fig. 10d). Inside the chamber different sensors can be mounted (e.g. oxygen, $H_2S$, temperature) that continuously record the increase or decrease of a constituent in the enclosed water column above the seep. In addition, water samples can be taken at pre-programmed time intervals. These samples can be used for the determination of e.g. sulfate, chloride, oxygen, or methane and from the linear regression or increase of the constituents, the exchange rates can be calculated.

### *1.5.3. Examples of in situ measurements on microbial mats related to fluid seepage*

Differences within cold seep sites support different structured microbial communities. Studies, where the microbial communities are related to the local conditions, possible dynamics, and substrate supplies, will lead to insight in the functioning of specific communities and strains that can not be cultivated, nor maintained under 'natural' conditions. Thus, from the high resolution geochemical gradients as measured with the microprofiler, we learn about microbial communities that are important for the functioning of the local ecosystem and may have unique adaptations that can only thrive in cold seeps. In that sense the combination of microbial analysis and direct measurements truly turns the cold seeps into natural laboratories. Finally, direct measurements allow us to assess how large the artifact of classical sampling is, since for very many measurements retrieval of sediment is needed.

To give examples for specific microbial seep communities thriving on different substrate supply, microprofiles measured at different spots with thiotrophic mats are shown in the following section. These measurements were conducted during cruises to the Norwegian shelf and to the Eastern Mediterranean (Nile Deep Sea Fan), are so far not published, but will be included in further publications (*see* abstracts in Section 3).

*Nyegga-the G12 mound*

The VIKING cruise (Ifremer, 2006) was a multidisciplinary study of focused fluid escape features off the coast of Norway. One sampling site, the Storegga area, is well-known for its giant Holocene slide, one of the largest ever mapped on continental margins. Gas hydrates occurrence and evidence for fluid escape make it a key area to study the relationships between fluids, gas hydrates, and slope stability. The Nyegga area is located on the northern flank of the Storegga Slide in 600-1000 m water depth, and is known for a large fluid escape features field, mainly pockmarks. The microprofiler was deployed here in a small pockmark-related structure (N 64° 39.83'; E 5° 17.39', 730 m water depth,

Fig. 11), identified from the black sediment covered by a white microbial mat. A second deployment was done 50 m away from this site on sediment that was obviously not affected by seepage activity, as no sulfide was detected in the upper 10 cm and oxygen penetrated deep, as normal for near-surface sediments of marine slops (Fig. 12a). With the high resolution recording of the microsensors oxygen depletion at only a few hundred micrometers depth was found for the Nyegga pockmark, exhibiting high oxygen conversion rates. A maximal concentration of 3 mmol $L^{-1}$ sulfide was reached in 4-5 cm depth (Fig. 12b). The constant concentration of sulfide below its production zone and the constant temperature of around 0.2 °C indicate that during the time of the deployment no warm seep fluids were rising. Microscopy revealed the presence of large thiotrophic bacteria, morphologically resembling *Beggiatoa*. Similar as in other sites investigated during this thesis (Chapter 2, 3), a gap has developed between the sulfide diffusing upwards from its production site in the sediment and the oxygen penetrating the sediment from the water column. Although the fluxes of sulfide and oxygen were in a ration of about 1:2 as needed for a complete sulfide conversion with oxygen (Eq. 4e), this gap excludes aerobic oxidation. This suboxic zone can either be formed from geochemical sulfide scavenging with e.g. iron, or by motile giant sulfur-oxidizers: many giant sulfur-oxidizers have an internal nitrate reservoir, which enables them to temporarily thrive on anaerobic conversion of sulfide with nitrate in the suboxic zone (Eq. 5a, b), and thus to outcompete obligate aerobic thiotrophs for sulfide. Also the near-surface pH peak, as recorded here (Fig. 12b), can be induced by both, geochemical and microbial sulfide turnover, and the different conditions required for either turnover pathway will be discussed in detail for other seeps in Chapter 2 and 3.

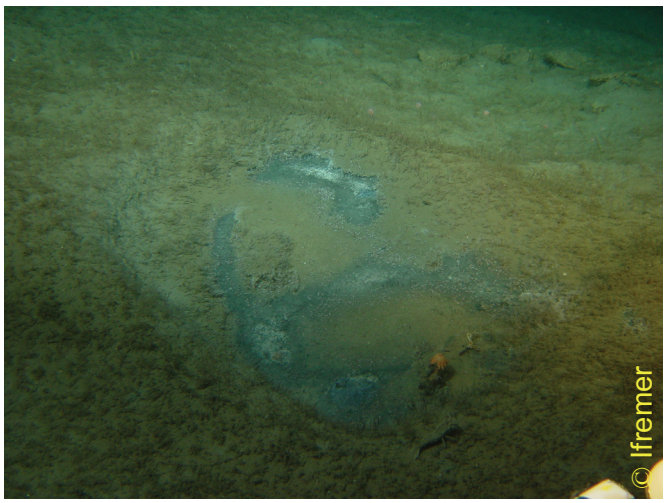


**Fig. 11: Fluid flow structure at the Nyegga site similar to the pockmark where the microprofiler was deployed. The diameter of the structure is about 1m.**

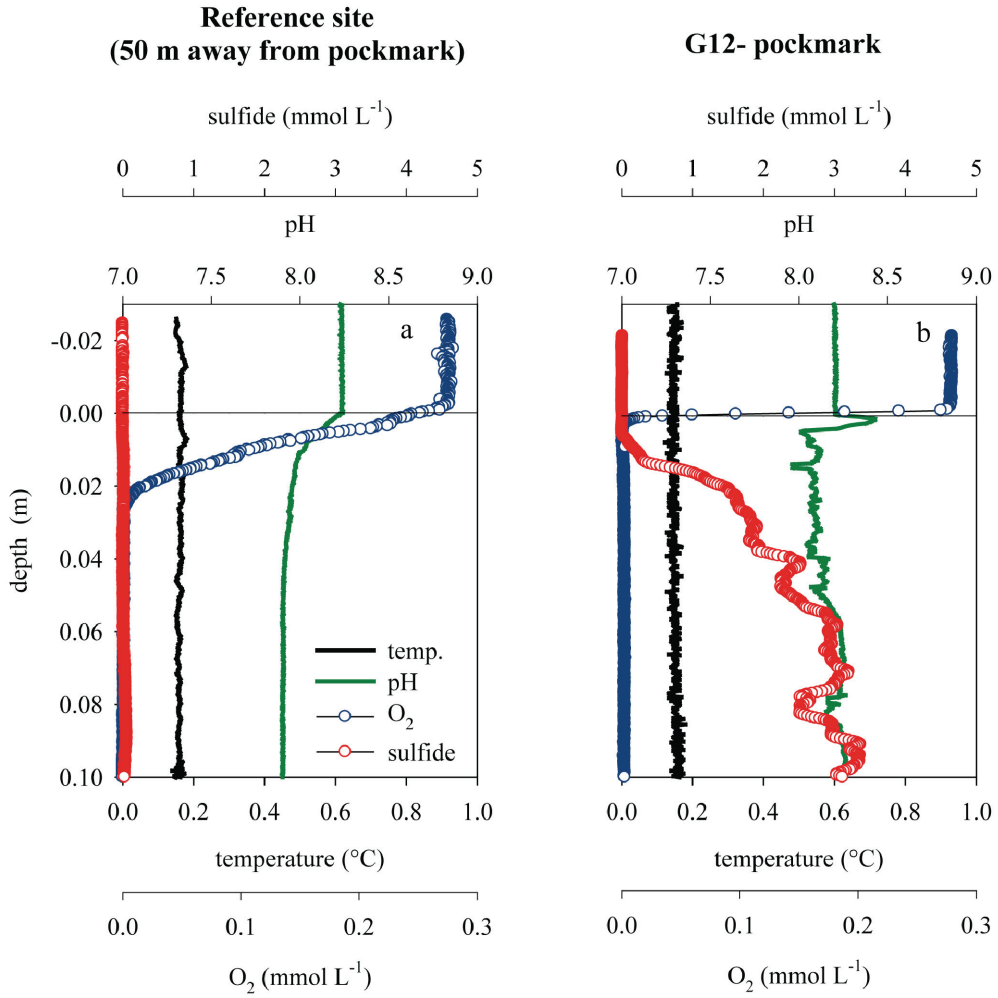


**Fig. 12: In situ microsensor measurements at the Nyegga pockmark area: a) reference site, b) pockmark sediment covered with a white microbial mat.**

*The Håkon Mosby Mud Volcano*

As it frequently was re-visited in the last decades, the Håkon Mosby Mud Volcano off the coast of Norway is one of the best surveyed mud volcanoes and represents a natural 'cold seep laboratory'. In situ microsensor measurements were carried out in different habitats, and also repeated in the same habitat in different years. The latest dataset (July 2009, kindly provided from D. de Beer) nicely shows the difference between the geochemical gradients in the 'hot spot' center and in the *Beggiatoa* inhabited area. In the 'hot spot' center the high fluid upflow velocity of 3-6 m $yr^{-1}$, as determined by de Beer et al. (2006), prevents sulfate from penetrating into the sediment; no sulfide is formed that could nourish *Beggiatoa* or other thiotrophic bacteria (Fig. 13a). The only methane consuming pathway is aerobic methan oxidation, however only a minor part (1-2%) of the advected methane is consumed in the center of the Håkon Mosby Mud Volcano and the reminder escapes into the water

column (Niemann et al., 2006). In contrast, in the *Beggiatoa* site the upflow velocity is reduced to <1 m $yr^{-1}$ (de Beer et al. 2006) and sulfate is available in the sediment up to a depth of several centimeter. The sulfide formed from AOM diffuses upwards and nourishes the dense *Beggiatoa* mat established on top of the sediment (Fig. 13b). Similar as in the Nyegga pockmark, a suboxic zone without oxygen or sulfide hints on either microbial sulfide conversion with nitrate or chemical sulfide oxidation with metal-oxides. A more detailed investiagtion of the biogeochmical processes and the limitations of primary prodcution in each habitat of the Håkon Mosby Mud Volcano can be found in Chapter 2.

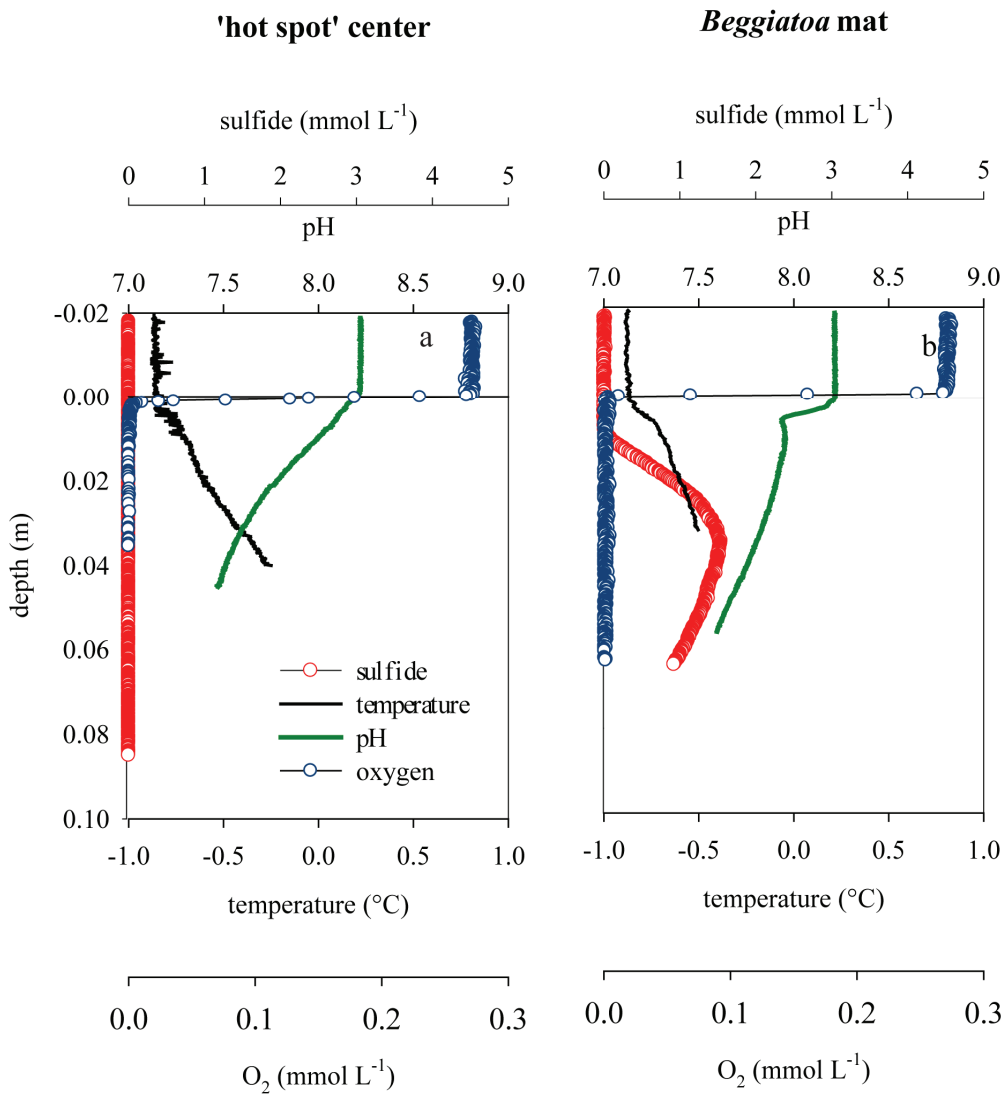


**Fig. 13: In situ measurements in a) the 'hot spot' center and b) the *Beggiatoa* habitat of the Håkon Mosby Mud Volcano.**

*Nile Deep Sea Fan - the pockmark area*

The Nile Deep Sea Fan comprises a variety of fluid seepage structures, such as mud volcanoes, pockmarks, authigenic carbonate deposits, and brine flows. In the Central Province of the Nile Deep Sea Fan, pockmark structures are found in a water depth of 1700 m, and were investigated during the M/70 Bionil cruise. At the Eastern border of this pockmark zone a kidney shaped area of about 60 x 100 m was discovered (N 32° 32.01'; E 30° 21.14'), where the sediment was densely covered by a bacterial mat (Fig. 14, 10a). A very convincing set of in situ microsensor profiles were measured on, at the border, and outside the mat, clearly relating the presence of the thiotrophic bacteria with sulfide formed by hydrocarbon turnover.

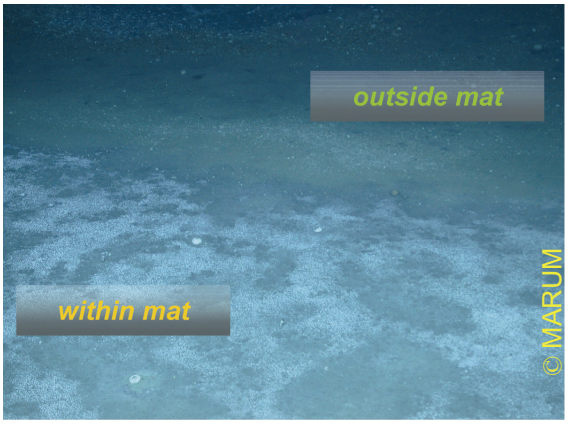


**Fig. 14: Dense, thiotrophic mat at the pockmark area of the Nile Deep Sea Fan. The sharp border of the mat is clearly visible on the picture made by the cameras of the ROV Quest (MARUM, Bremen).**

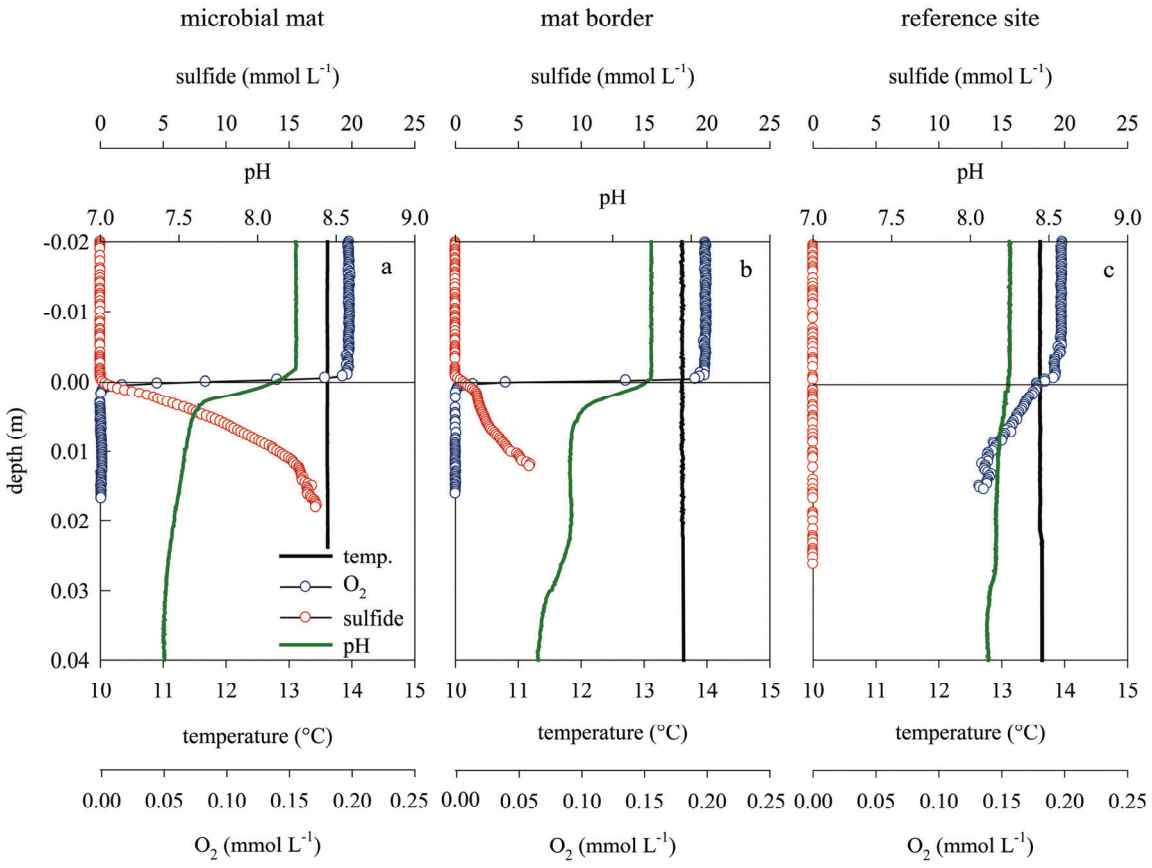


**Fig. 15: In situ microsensor measurements on a microbial mat in the pockmark area of the Central Province of the Nile Deep Sea Fan at a) the microbial mat, b) border of the mat, c) outside the mat.**

As visible in Figure 15a, oxygen did not penetrate more than 1 mm into the sediment inhabited by the sulfide oxidizing bacteria. Oxygen and sulfide profiles overlapped and showed steep gradients, resulting in high consumption rates. Concurrently a sharp pH decrease was recorded. The thiotrophic bacteria growing on the blackish, highly reduced sediment are relatives of the *Arcobacter* group (pers. comm. S. Grünke), and the presence of the bacterial mat can be linked to the sulfide produced from AOM. In contrast, oxygen penetrated deep into the sediment surrounding the microbial mat, while sulfide was not detected (Fig. 15c). Measurements at the border of the mat recorded intermediate sulfide concentrations. However, oxygen consumption was similarly high as in the mat and the turnover pathways might differ between the border of oxidized and reduced sediments (Fig. 15b) and the highly reduced sediments (Fig. 15a).

*Nile Deep Sea Fan - the Amon Mud Volcano*

The Amon Mud Volcano (water depth: 1120 m) is part of the Central Province fluid flow structures of the Nile Deep Sea Fan and exhibits a variety of chemosynthetic habitats, related to different fluid seepage phenomena. During the M/70 Bionil cruise patches with thiotrophic microbes were investigated at the very tip of the Amon (Fig. 16b, N 32° 22.13'; E 31° 42.66'), and the microprofiler was used to determine the sulfide turnover at those patches. Furthermore, at the southwestern flank of the Amon an extraordinary environment inhabited by thiotrophic bacteria was found: the sulfur river. Here, black, highly reduced sediment crops out from pelagic sediments and carbonate-crusts and is covered with a white microbial mat. This unique structure has a length of approximately 60 m and an average width of 2-3 m, in some areas reaching over 6 m.

*Microbial mats at the Amon tip.*- From all Amon Mud Volcano sites investigated with the microprofiler, only at the tip a temperature increase with depth was recorded (Fig. 16a), indicating that here the near-surface sediment is subjected to the upflow of warm fluids. Oxygen and sulfide overlapped and microbial sulfide consumption with oxygen will be the main pathway of primary production. In the sulfide profile a dip was recorded at 1 cm below the seafloor that is usually not detected in marine sediments. This could be formed either by a zone of sulfide oxidation in between two sulfide production zones or the dip displays a non steady state situation, e.g. a temporal change in fluid upflow. Similar dips in sulfide profiles were found at other sites and will be discussed in detail in Chapter 4.

*The sulfur river.*- A mat-forming population of the giant sulfur bacterium *Thiomargarita* was found on top of the highly reduced sediment of the sulfur river (Grinth et al. in prep.). These extremely large thiotrophic bacteria were up to now only characterized from the Namibian shelf (Schulz et al., 1999) and the Gulf of Mexico (Kalanetra et al., 2005), and are usually related to unstable conditions like seasonal upwelling and gas eruption events. This also holds true for the sulfur river.

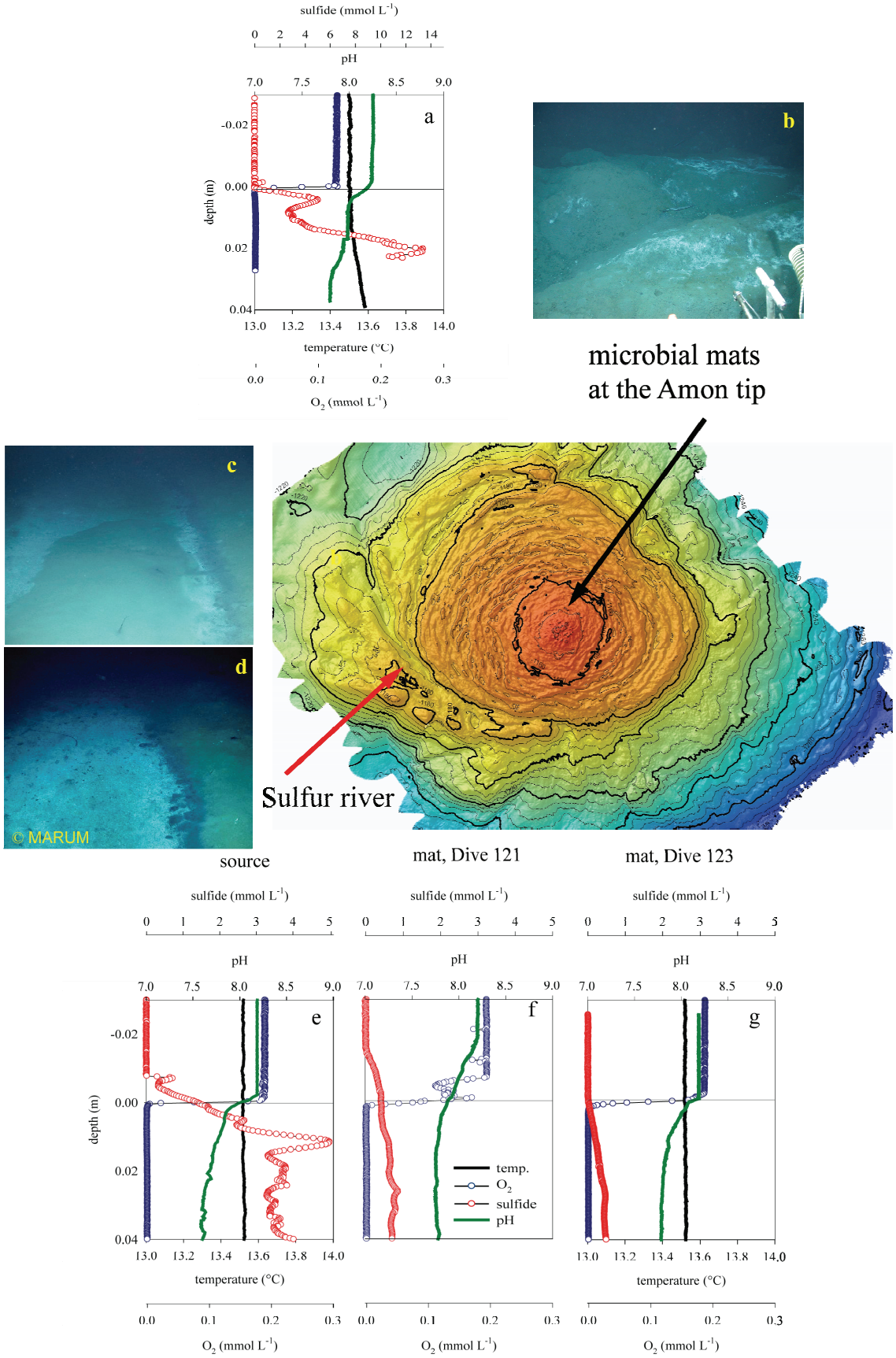


**Fig. 16: In situ microsensor measurements at the Amon Mud Volcano. The bathymetric map was generated during the M70/2 *Microhab* cruise (Dupré et al., 2008b).**

A probably temporal variation in lateral fluid flow was discovered here, as visible from the microsensor measurements. The microprofiler was deployed at close-by stations during two ROV dives (Dive 121, Dive 123). Unexpectedly, different profiles were recorded. During the first deployment (Fig. 16f) irregularities in oxygen concentration were measured in the water column, indicating plums of oxygen depleted water. Sulfide was present in a two cm thick zone above the sediment and a significant pH change was also recorded here. During the second deployment four days later (Fig. 16g) the profiles displayed a normal seep situation with oxygen penetrating the upper sediment, but without sulfide in the water column above the sediment. Also close to the source of the sulfur river sulfide was present in the water column above the sediment and here sulfide concentrations in the sediment were up to an order of magnitude higher (Fig. 16e).

The *Thiomargarita* present at the surface of this sulfur river are supposedly nourished by lateral outflow of sulfidic subsurface fluids (Grinth et al. in prep., included as abstract). The microsensor measurements show that this outflow is not constantly present. Accordingly, it is essential to address not only the spatial but also the temporal variation when doing research at cold seeps.

## 2. OBJECTIVES

As outlined in the previous section, cold seeps are rarely investigated, but highly valuable sites for research, forming unique natural laboratories to study biodiversity and the limitations of biogeochemical processes. The main objectives of this thesis were to investigate which parameters control the chemoautotrophic-driven primary production at cold seeps, and how transport processes control biogeochemical processes in the near-surface seep sediments. To be able to assess the heterogeneity between different cold seep structures and the habitats therein, rates of transformation, burial, transport, and exchange between the ocean water and the cold seeps were investigated at the Håkon Mosby Mud Volcano, the coastal seep site of Eckernförde Bay, the Dvurechenskii mud volcano in the permanent anoxia of the Black Sea, and a variety of seep related structures in the Nile Deep Sea Fan and at the Storegga Slide (Fig. 17).

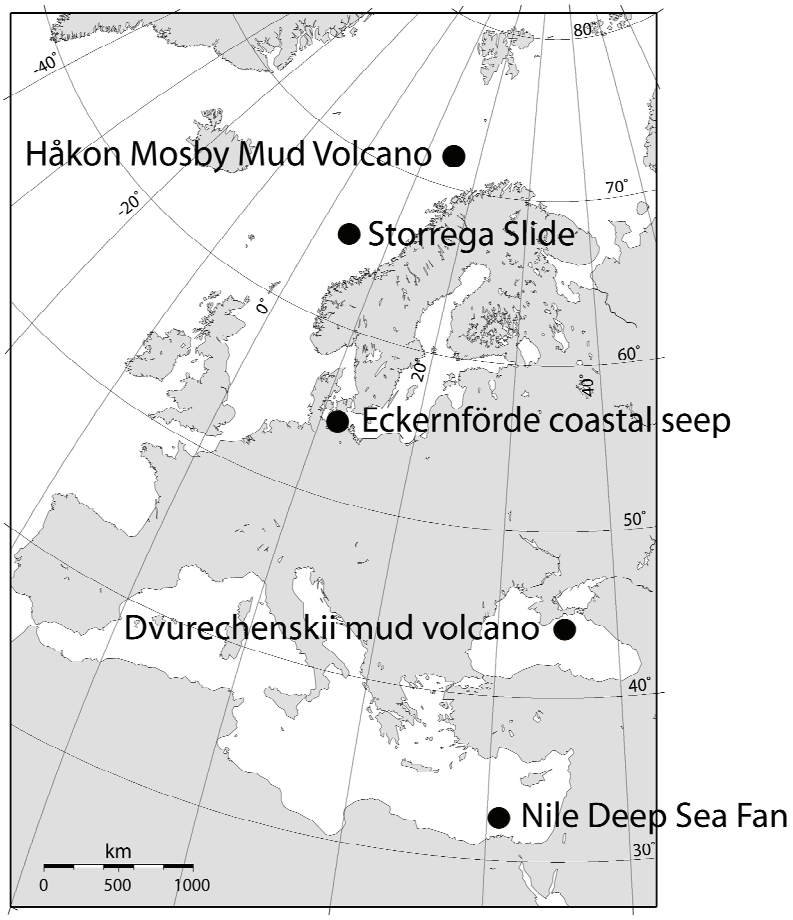


**Fig. 17: Map of study sites investigated during this thesis.**

In particular, the areal biogeochemical conversion rates of sulfate, methane, and sulfide, the potential for sulfide oxidation by various processes, and the impact of different fluid transport regimes on the geochemical gradients were studied with in situ, ex situ, and experimental approaches to answer the following questions:

I) How are sulfate reduction, methane oxidation, and sulfide production organized in cold seeps in oxic and in permanently anoxic environments?

II) How does the fluid flow regime influence the distribution of sulfide production and methane oxidation in the sediment, and the release of sulfide and methane from the sediment into the hydrosphere?

III) Which are the relevant pathways of sulfide oxidation in oxic and anoxic cold seep surface sediments?

IV) Can microbial sulfide oxidation compete with geochemical oxidation in cold seeps, or does geochemical sulfide oxidation limit the seep biomass production?

This work is part of the GEOTECHNOLOGIEN project MUMM$^{II}$ (Methane in the GeoBio-system - turnover, metabolism, and microorganisms), an interdisciplinary project covering the in situ quantification of microbial turnover and transport processes, as presented in this study, but also comprising controlled laboratory experiments of anaerobic methane oxidation and sulfate reduction, the specification of the involved organisms, and the research on the function of the organisms in seep systems.

## 3. OVREVIEW OF MANUSCRIPTS

*Chapter 2:*

**Geochemical processes and primary productivity in different thiotrophic mats of the Håkon Mosby Mud Volcano (Barents Sea)**

Anna Lichtschlag, Janine Felden, Volker Brüchert, Antje Boetius, Dirk de Beer

submitted to *Limnology and Oceanography*

This manuscript includes data from three research cruises to the Håkon Mosby Mud Volcano. Presented n situ measurements were conducted during the *Viking* cruise (2006) by A. Lichtschlag and D. de Beer. The deployment of the in situ microprofiler and the sediment sampling was performed with the help of the ROV Victor team (Ifremer) and the shipboard crew. Sampling and geochemical analyses of pore water and sediments as well as the nitrate uptake experiments, and the S-isotope analyzes were done by A. Lichtschlag. Sulfate reduction rates were determined by A. Boetius and J. Felden. *Beggiatoa* filament sampling on board was done by N. Weller with the help of H. Røy. The manuscript was written by A. Lichtschlag, with support and input from D. de Beer, A. Boetius, and V. Brüchert.

*Chapter 3:*

**Biological and chemical sulfide oxidation in a *Beggiatoa* inhabited marine sediment**

André Preisler, Dirk de Beer, Anna Lichtschlag, Gaute Lavik, Antje Boetius, Bo Barker Jørgensen

published in: *ISME Journal 1 341-353, 2007.*

The characterization of the ecophysiology of the *Beggiatoa* from Eckernförde Bay was done by A. Preisler, and the isotopic labeling experiments were performed by G. Lavik and A. Preisler. The characterization of the sediment by in situ measurements was done by D. de Beer, and the geochemical iron and manganese data were provided by A. Lichtschlag. This manuscript was written by D. de Beer with input from B. Jørgensen, A. Boetius, G. Lavik and A. Lichtschlag.

*Chapter 4:*

**Methane and sulfide fluxes in permanent anoxia: in situ studies at the Dvurechenskii mud volcano (Sorokin Trough, Black Sea)**

Anna Lichtschlag, Janine Felden, Frank Wenzhöfer, Florence Schubotz, Tobias Ertefai, Antje Boetius, Dirk de Beer

submitted to *Geochimica et Cosmochimica Acta*

This manuscript includes data from the *Microhab* cruise M72/2 (2007). In situ microsensor measurements were conducted by A. Lichtschlag and D. de Beer. The benthic chamber data was obtained by J. Felden and F. Wenzhöfer, and sulfate reduction and anaerobic methane oxidation rates were determined by J. Felden. The deployment of the in situ devices and the sediment sampling were done with the help of the Quest 4000 ROV team (MARUM, Bremen) and the shipboard crew. Pore water was sampled and analyzed by A. Lichtschlag, except the samples for carbon isotopes and methane, which were obtained and analyzed by F. Schubotz and T. Ertefai. The manuscript was written by A. Lichtschlag, with support and input from D. de Beer and A. Boetius.

*Chapter 5:*

**A deep reactive ferric iron source drives sulfide oxidation in the euxinic surface sediments of the Dvurechenskii mud volcano (Black Sea)**

Anna Lichtschlag, Alexey Kamyshny, Jr., Timothy G. Ferdelman, Dirk de Beer

in preparation for *Deep Sea Research Part I*

Sampling for the data of this manuscript was conducted during the M72/2 *Microhab* cruise (2007) and sediment samples were obtained with the help of the ROV Quest 4000 team and the shipboard crew. Pore water samples for analyzes of sulfate, dissolved iron, chloride as well as the samples for the solid phase iron, manganese and reduced sulfur species analyzes were obtained and measured by A. Lichtschlag. Samples for dissolved and particulate elemental sulfur, and pore water for sulfur intermediates and hydrogen sulfide determination were obtained and analyzed by A. Kamyshny. The calculations of the polysulfide were also performed by A. Kamyshny. The manuscript was written by A. Lichtschlag, with the help and input from D. de Beer , A. Kamyshny, and T. Ferdelman.

*Chapter 6:*

**The $H_2S$ microsensor & the dissociation constant $pK_1$: problems & solutions**

Miriam Weber, Anna Lichtschlag, Stefan Jansen, Dirk de Beer

The improvement of the calibration method for $H_2S$ microsensors and the experiments to test this method were conducted by A. Lichtschlag and M. Weber. The manuscript was written by M. Weber with support and input from A. Lichtschlag and D. de Beer.

## Related Work not Included in the Manuscripts

### Mud volcanism and associated biogeochemical processes in the Nile Deep Sea Fan - The Amon Mud Volcano

Janine Felden, Anna Lichtschlag, Frank Wenzhöfer, Dirk de Beer, Gert de Lange, Antje Boetius
in preparation for *Biogeosciences*

The highly active Amon mud volcano (AMV), located at 1250 m water depth between the Central and Eastern Province of the Nile Deep Sea Fan, was investigated during the BIONIL expedition with RV METEOR (M70/2) in autumn 2006. The AMV can be subdivided in four habitats: a central dome (I), the surrounding hummocky area with patches of bacterial mats (II), a wide slope covered by biogenic mounds (III), and a lateral mud flow at the foot of the AMV (IV). Here we investigated differences in the biogeochemistry of these four habitats and their relation to fluid flow regimes at AMV. Total and diffusive oxygen uptake was quantified in situ with a benthic chamber and a microsensor-profiler, respectively, deployed by an ROV. Microbial sulfate and methane consumption were measured by radiotracer incubations. Pore water chemistry was investigated to gain an understanding about the flow patterns and composition of subsurface fluids. Our results show that the concentric structure, morphology, and biogeochemistry of these habitats are mainly caused by spatial variations in gas and fluid flow on scales of meters to hundreds of meters. The central dome of the AMV was characterized by high temperature gradients and gas oversaturation, but low rates of microbial methane and sulfate consumption were detected despite the high availability of methane and sulfate. The biogeochemical hot spot of AMV were the patchy bacterial mats surrounding the central dome, with high rates of hydrocarbon oxidation, sulfide production, and oxygen consumption (20-55 mmol $m^{-2}$ $d^{-1}$). Another benthic hot spot habitat was found at the southeastern foot of the AMV where a lateral outflow of sulfidic, briny muds was partly covered by thiotrophic bacterial mats and siboglinid tubeworms. Here, the high oxygen uptake was fueled by sulfide transport rather than microbial production. Compared to other mud volcanoes, the AMV presents the unique case of a low efficiency of microbial methane consumption despite a high availability of methane and sulfate as electron-acceptor, causing a high methane emission to the hydrosphere.

**A novel, mat-forming *Thiomargarita* population associated with a sulfidic fluid flow from a deep-sea mud volcano**

Anne-Christin Girnth, Stefanie Grünke, Anna Lichtschlag, Janine Felden, Katrin Knittel, Frank Wenzhöfer, Dirk de Beer, Antje Boetius

in preparation for *Environmental Microbiology*

**Summary**

A mat-forming population of the giant sulfur bacterium *Thiomargarita* was discovered at the flank of the mud volcano Amon on the Nile Deep Sea Fan in the Eastern Mediterranean Sea. All cells were of a spherical and vacuolated phenotype and internally stored globules of elemental sulfur. With a diameter of 24-65 µm, *Thiomargarita* from the Eastern Mediterranean were substantially smaller than previously described species of this genus. A 16S rRNA gene fragment was amplified and could be associated to the *Thiomargarita*-resembling cells by fluorescence *in situ* hybridization techniques. This sequence is monophyletic with published *Thiomargarita* sequences but sequence similarities are only about 94%, indicating a distinct diversification. Fluctuating supply with oxygen and sulfide selects for the nitrate-storing *Thiomargarita* as previously observed in other marine habitats. In contrast to other populations, which rely on periodic resuspension from sulfidic sediment into the oxygenated water column, *Thiomargarita* at the Amon mud volcano remain stationary while environmental conditions change.

**Novel observations of *Thiobacterium*, a sulfur-storing *Gammaproteobacterium* producing gelatinous mats**

Stefanie Grünke, Anna Lichtschlag, Dirk de Beer, Marcel Kuypers, Tina Lösekann-Behrens, Alban Ramette, Antje Boetius

*sumbitted to the ISME Journal*

**Abstract**

This study examined the occurrence of *Thiobacterium* mats in three different sulfidic marine habitats: a submerged minke whale bone, deep-water seafloor and a submarine cave. The genus *Thiobacterium* includes rod-shaped microbes containing several spherical grains of elemental sulfur and forming conspicuous gelatinous mats. The gelatinous matrix contained massive amounts of *Thiobacterium* cells and was highly enriched in sulfur. Microsensor measurements and other biogeochemistry data suggest chemoautotrophic growth of *Thiobacterium*. Sulfide and oxygen microprofiles confirmed the dependence of *Thiobacterium* on hydrogen sulfide as energy source. Fluorescence *in situ* hybridization indicated that *Thiobacterium* spp. belong to the *Gammaproteobacteria*, a class that harbors many mat-forming sulfide-oxidizing bacteria. Further phylogenetic characterization of the gelatinous mats led to the discovery of an unexpected microbial diversity associated with *Thiobacterium* mats.

## REFERENCES

Aloisi, G., Drews, M., Wallmann, K., and Bohrmann, G., 2004. Fluid expulsion from the Dvurechenskii mud volcano (Black Sea) - Part I. Fluid sources and relevance to Li, B, Sr, I and dissolved inorganic nitrogen cycles. *Earth Planet. Sci. Lett.* **225**, 347-363.

Amrani, A. and Aizenshtat, Z., 2004. Reaction of polysulfide anions with a, b unsaturated isoprenoid aldehydes in aquatic media: simulation of oceanic conditions. *Org. Geochem.* **35**, 909-921.

Anderson, A. L., Abegg, F., Hawkins, J. A., Duncan, M. E., and Lyons, A. P., 1998. Bubble populations and acoustic interaction with the gassy floor of Eckernförde Bay. *Continent. Shelf Res.* **18**, 1807-1838.

Bak, F. and Pfennig, N., 1987. Chemolithotrophic growth of *Desulfovibrio sulfodismutans* sp. nov. by disproportionation of inorganic sulfur compounds. *Arch. Microbiol.* **147**, 184-189.

Barnes, R. O. and Goldberg, E. D., 1976. Methane production and consumption in anoxic marine sediments. *Geology* **4**, 297-300.

Bellaiche, G., Loncke, L., Gaullier, V., Mascle, J., Courp, T., Moreau, A., Radan, S., and Sardou, O., 2001. Le cône sous-marin du Nil et son réseau de chenaux profonds: nouveaux résultats (campagne Fanil). *CRAS* **333**, 399-404.

Boetius, A., Ravenschlag, K., Schubert, C. J., Rickert, D., Widdel, F., Gieseke, A., Amann, R., Jørgensen, B. B., Witte, U., and Pfannkuche, O., 2000. A marine microbial consortium apparently mediating anaerobic oxidation of methane. *Nature* **407**, 623-626.

Bohrmann, G. and Torres, M. E., 2006. Gas hydrates in marine sediments. In: Schulz, H. D. and Zabel, M. Eds.), *Marine Geochemistry*. Springer.

Burdige, D. J. and Nealson, K. H., 1986. Chemical and microbiological studies of sulfide-mediated manganese reduction. *Geomicrobiol. J.* **4**, 361-387.

Canfield, D., Kristensen, E., and Thamdrup, B., 2005. *Aquatic Geomicrobiology*. Elsevier, San Diego, California.

Canfield, D. E., Raiswell, R., and Bottrell, S., 1992. The reactivity of sedimentary iron minerals toward sulfide. *Am. J. Sci.* **292**, 659-683.

Canfield, D. E. and Teske, A., 1996. Late Proterozoic rise in atmospheric oxygen concentration inferred from phylogenetic and sulphur-isotope studies. *Nature* **382**, 127-132.

Claypool, G. E. and Kvenvolden, K. A., 1983. Methane and other hydrocarbon gases in marine sediment. *Annu. Rev. Earth Planet. Sci.* **11**, 299-327.

Cordes, E. E., Arthur, M. A., Shea, K., Arvidson, R. S., and Fisher, C. R., 2005. Modeling the mutualistic interactions between tubeworms and microbial consortia. *PLoS Biol.* **3**, 497-506.

Crill, P. M. and Martens, C. S., 1986. Methane production from bicarbonate and acetate in an anoxic marine sediment. *Geochim. Cosmochim. Acta* **50**, 2089-2097.

de Beer, D., Sauter, E., Niemann, H., Kaul, N., Foucher, J.-P., Witte, U., Schlüter, M., and Boetius, A., 2006. In situ fluxes and zonation of microbial activity in surface sediments of the Håkon Mosby Mud Volcano. *Limnol. Oceanogr.* **51**, 1315-1331.

Dia, A. N., Castrec-Rouelle, M., Boulegue, J., and Comeau, P., 1999. Trinidad mud volcanoes: Where do the expelled fluids come from? *Geochim. Cosmochim. Acta* **63**, 1023-1038.

Dickens, G. R., Castillo, M. M., and Walker, J. C. G., 1997. A blast of gas in the latest Paleocene; simulating first-order effects of massive dissociation of oceanic methane hydrate.

Dickens, G. R., O' Neil, J. R., Rea, D. K., and Owen, R. M., 1995. Dissociation of oceanic methane hydrate as a cause of the carbon isotope excursion at the end of the Paleocene. *Paleoceanography* **10**, 965-971.

Dimitrov, L. I., 2002. Mud volcanoes-the most important pathway for degassing deeply buried sediments. *Earth-Sci. Rev.* **59**, 49-76.

dos Santos Afonso, M. and Stumm, W., 1992. Reductive dissolution of iron(III) (hydr)oxides by hydrogen sulfide. *Langmuir* **8**, 1671-1675.

Drobner, E., Huber, H., Wächtershäuser, G., Rose, D., and Stetter, K. O., 1990. Pyrite formation linked with hydrogen evolution under anaerobic conditions. *Nature* **346**, 742-744.

Duperron, S., Nadalig, T., Caprais, J. C., Sibuet, M., Fiala-Medioni, A., Amann, R., and Dubilier, N., 2005. Dual symbiosis in a *Bathymodiolus* sp. mussel from a methane seep on the Gabon continental margin (southeast Atlantic): 16S rRNA phylogeny and distribution of the symbionts in gills. *Appl. Environ. Microbiol.* **71**, 1694-1700.

Dupré, S., Brosolo, L., Mascle, J., Pierre, C., Harmegnies, F., Mastalerz, V., Bayon, G., Ducassou, E., de Lange, G., Foucher, J.-P., Team6, t. V. R., and Party, t. M. L. S., 2008a. The Menes mud volcano caldera complex: an exceptional site of brine seepage in the deep waters off north-western Egypt*9th International Conference on gas in marine sediments*, Bremen, Germany.

Dupré, S., Buffet, G., Mascle, J., Foucher, J. P., Gauger, S., Boetius, A., Marfia, C., Team, A. A., Team, Q. R., and Party, B. S., 2008b. High-resolution mapping of large gas emitting mud volcanoes on the Egyptian continental margin (Nile Deep Sea Fan) by AUV surveys. *Mar. Geophys. Res.* **29**, 275-290.

Feseker, T., Foucher, J. P., and Harmegnies, F., 2008. Fluid flow or mud eruptions? Sediment temperature distributions on Håkon Mosby mud volcano, SW Barents Sea slope. *Mar. Geol.* **247**, 194-207.

Field, M. E. and Kvenvolden, K. A., 1985. Gas hydrates on the northern California continental margin. *Geology* **13**, 517-520.

Glud, R. N., Gundersen, J. K., Jørgensen, B. B., Revsbech, N. P., and Schulz, H. D., 1994. Diffusive and total oxygen uptake of deep-sea sediments in the Eastern South-Atlantic Ocean: *in situ* and laboratory measurements. *Deep-Sea Res. Pt. I* **41**, 1767-1788.

Glud, R. N., Stahl, H., Berg, P., Wenzhöfer, F., Oguri, K., and Kitazato, H., 2009. In situ microscale variation in distribution and consumption of $O_2$: A case study from a deep ocean margin sediment (Sagami Bay, Japan). *Limnol. Oceanogr.* **54**, 1-12.

Greinert, J., Artemov, Y., Egorov, V., De Batist, M., and McGinnis, D., 2006. 1300-m-high rising bubbles from mud volcanoes at 2080m in the Black Sea: Hydroacoustic characteristics and temporal variability. *Earth Planet. Sci. Lett.* **244**, 1-15.

Habicht, K. S. and Canfield, D. E., 2001. Isotope fractionation by sulfate-reducing natural populations and the isotopic composition of sulfide in marine sediments. *Geology* **29**, 555-558.

Haese, R. R., Hensen, C., and de Lange, G. J., 2006. Pore water geochemistry of eastern Mediterranean mud volcanoes: Implications for fluid transport and fluid origin. *Mar. Geol.* **225**, 191-208.

Haese, R. R., Meile, C., Van Cappellen, P., and de Lange, G. J., 2003. Carbon geochemistry of cold seeps: Methane fluxes and transformation in sediments from Kazan mud volcano, eastern Mediterranean Sea. *Earth Planet. Sci. Lett.* **212**, 361-375.

Hagen, K. D. and Nelson, D. C., 1997. Use of reduced sulfur compounds by *Beggiatoa* spp.: Enzymology and physiology of marine and freshwater strains in homogeneous and gradient cultures. *Appl. Environ. Microbiol.* **63**, 3957-3964.

Henry, P., Foucher, J. P., Lepichon, X., Sibuet, M., Kobayashi, K., Tarits, P., Chamotrooke, N., Furuta, T., and Schultheiss, P., 1992. Interpretation of temperature measurements from the Kaiko-Nankai cruise: Modeling of fluid flow in clam colonies. *Earth Planet. Sci. Lett.* **109**, 355-371.

Hensen, C., Wallmann, K., Schmidt, M., Ranero, C. R., and Suess, E., 2004. Fluid expulsion related to mud extrusion off Costa Rica - A window to the subducting slab. *Geology* **32**, 201-204.

Hesselbo, S. P., Grocke, D. R., Jenkyns, H. C., Bjerrum, C. J., Farrimond, P., Bell, H. S. M., and Green, O. R., 2000. Massive dissociation of gas hydrate during a Jurassic oceanic anoxic event. *Nature* **406**, 392-395.

Hinrichs, K. U. and Boetius, A., 2002. The anaerobic oxidation of methane: new insights in microbial ecology and biogeochemistry. In: Wefer, G., Billett, D., Hebbeln, D., Jørgensen, B. B., Schlüter, M., and van Weering, T. C. E. Eds.), *Ocean Margin Systems*. Springer-Verlag, Heidelberg.

Hovland, M. and Judd, A. G., 1988. *Seabed pockmarks and seepages*. Graham & Trotman, London.

Hovland, M., MacDonald, I. R., Rueslåtten, H., Johnsen, H. K., Naehr, T., and Bohrmann, G., 2005. Chapopote asphalt volcano may have been generated by supercritical water. *Eos Trans. AGU* **86**, 397-402.

Hovland, M. and Sommerville, J. H., 1985. Characteristics of two natural gas seepages in the North Sea. *Mar. Petrol. Geol.* **2**, 319-326.

Ivanov, M. K., Limonov, A. F., and vanWeering, T. C. E., 1996. Comparative characteristics of the Black Sea and Mediterranean Ridge mud volcanoes. *Mar. Geol.* **132**, 253-271.

Iversen, N. and Jørgensen, B. B., 1993. Diffusion coefficients of sulfate and methane in marine sediments: Influence of porosity. *Geochim. Cosmochim. Acta* **57**, 571-578.

Jørgensen, B. B., 1990. A thiosulfate shunt in the sulfur cycle of marine sediments. *Science* **249**, 152-154.

Jørgensen, B. B. and Nelson, D. C., 2004. Sulfide oxidation in marine sedimetns: Geochemistry meets microbiology. *Geological Society of America* **Special Paper 379**, 63 - 81.

Jørgensen, B. B. and Postgate, J. R., 1982. Ecology of the bacteria of the sulfur cycle with special reference to anoxic oxic interface environments. *Philos. T. Roy. Soc. B* **298**, 543-561.

Judd, A. and Hovland, M., 2007. *Seabed fluid flow: the impact on geology, biology and the marine environment*. Cambridge University Press, Cambridge.

Judd, A. G., 2004. Natural seabed gas seeps as sources of atmospheric methane. *Environ. Geol.* **46**, 988-996.

Judd, A. G., Hovland, M., Dimitrov, L. I., García Gil, S., and Jukes, V., 2002. The geological methane budget at Continental Margins and its influence on climate change. *Geofluids* **2**, 109-126.

Kalanetra, K. M., Joye, S. B., Sunseri, N. R., and Nelson, D. C., 2005. Novel vacuolate sulfur bacteria from the Gulf of Mexico reproduce by reductive division in three dimensions. *Environ. Microbiol.* **7**, 1451-1460.

Katz, M. E., Pak, D. K., Dickens, G. R., and Miller, K. G., 1999. The source and fate of massive carbon input during the latest Paleocene thermal maximum. *Science* **286**, 1531-1533.

Kennicutt, M. C., Brooks, J. M., Bidigare, R. R., Fay, R. R., Wade, T. L., and Mcdonald, T. J., 1985. Vent-type taxa in a hydrocarbon seep region on the Louisiana slope. *Nature* **317**, 351-353.

King, L. H. and MacLean, B., 1970. Pockmarks on the Scotian shelf. *Geol. Soc. Am. Bull.* **81**, 3141-3148.

Knittel, K., Lösekann, T., Boetius, A., Kort, R., and Amann, R., 2005. Diversity and distribution of methanotrophic archaea at cold seeps. *Appl. Environ. Microbiol.* **71**, 467-479.

Kobayashi, K., Ashi, J., Boulegue, J., Cambray, H., Chamot-Rooke, N., Fujimoto, H., Furuta, T., Iiyama, J. T., Koizumi, T., Mitsuzawa, K., Monma, H., Murayama, M., Naka, J., Nakanishi, M., Ogawa, Y., Otsuka, K., Okada, M., Oshida, A., Shima, N., Soh, W., Takeuchi, A., Watanabe, M., and Yamagata, T., 1992. Deep-tow survey in the KAIKO-Nankai cold seepage areas. *Earth Planet. Sci. Lett.* **109**, 347-354.

Kohnen, M. E. L., Damste, J. S. S., ten Haven, H. L., and de Leeuw, J. W., 1989. Early incorporation of polysulfides in sedimentary organic matter. *Nature* **341**, 640-641.

Kopf, A. J., 2002. Significance of mud volcanism. *Rev. Geophys.* **40**, 1-52.

Kukowski, N., Schlüter, M., Haese, R. R., Hensen, C., Hinkelmann, R., Sibuet, M., and Zabel, M., 2002. Subsurface fluid flow and material transport. In: Wefer, G., Billett, D., Hebbeln, D., Jørgensen, B. B., Schlüter, M., and van Weering, T. C. E. Eds.), *Ocean Margin Systems*. Springer-Verlag, Heidelberg.

Kvenvolden, K. A., 1993. Gas hydrates - geological perspective and global change. *Rev. Geophys.* **31**, 173-187.

Kvenvolden, K. A. and Rogers, B. W., 2005. Gaia's breath - global methane exhalations. *Mar. Petrol. Geol.* **22**, 579-590.

Leak, D. J. and Dalton, H., 1986. Growth yields of methanotrophs: 1. Effect of copper on the energetics of methane oxidation. *Appl. Microbiol. Biotechnol.* **23**, 470-476.

Lelieveld, J., Crutzen, P. l., and Dentener, F. J., 1998. Changing concentration, lifetime and climate forcing of atmospheric methane. *Tellus* **50**, 128-250.

Linke, P., Suess, E., Torres, M., Martens, V., Rugh, W. D., Ziebis, W., and Kulm, L. D., 1994. In situ measurement of fluid flow from cold seeps at active continental margins. *Deep Sea Research Part I: Oceanographic Research Papers* **41**, 721-739.

Linke, P., Wallmann, K., Suess, E., Hensen, C., and Rehder, G., 2005. In situ benthic fluxes from an intermittently active mud volcano at the Costa Rica convergent margin. *Earth Planet. Sci. Lett.* **235**, 79-95.

Lösekann, T., Knittel, K., Nadalig, T., Fuchs, B., Niemann, H., Boetius, A., and Amann, R., 2007. Diversity and abundance of aerobic and anaerobic methane oxidizers at the Haakon Mosby Mud Volcano, Barents Sea. *Appl. Environ. Microbiol.* **73**, 3348-3362.

Lösekann, T., Robador, A., Niemann, H., Knittel, K., Boetius, A., and Dubilier, N., 2008. Endosymbioses between bacteria and deep-sea siboglinid tubeworms from an Arctic Cold Seep (Haakon Mosby Mud Volcano, Barents Sea). *Environ. Microbiol.* **10**, 3237-3254.

Luff, R., Wallmann, K., and Aloisi, G., 2004. Numerical modeling of carbonate crust formation at cold vent sites: significance for fluid and methane budgets and chemosynthetic biological communities. *Earth Planet. Sci. Lett.* **221**, 337-353.

Luther, G. W., 1991. Pyrite synthesis via polysulfide compounds. *Geochim. Cosmochim. Acta* **55**, 2839-2849.

MacDonald, I. R., Bohrmann, G., Escobar, E., Abegg, F., Blanchon, P., Blinova, V., Bruckmann, W., Drews, M., Eisenhauer, A., Han, X., Heeschen, K., Meier, F., Mortera, C., Naehr, T., Orcutt, B., Bernard, B., Brooks, J., and de Farago, M., 2004. Asphalt volcanism and chemosynthetic life in the Campeche Knolls, Gulf of Mexico. *Science* **304**, 999-1002.

MacDonald, I. R., Reilly, J. F., II, Guinasso, N. L., Jr., Brooks, J. M., Carney, R. S., Bryant, W. A., and Bright, T. J., 1990. Chemosynthetic mussels at a brine-filled pockmark in the Northern Gulf of Mexico. *Science* **248**, 1096-1099.

Martens, C. S. and Berner, R. A., 1974. Methane production in the interstitial waters of sulfate-depleted marine sediments. *Science* **185**, 1167-1169.

Martens, C. S. and Val Klump, J., 1980. Biogeochemical cycling in an organic-rich coastal marine basin--I. Methane sediment-water exchange processes. *Geochim. Cosmochim. Acta* **44**, 471-490.

Martin, J. B., Kastner, M., Henry, P., Le Pichon, X., and Lallement, S., 1996. Chemical and isotopic evidence for sources of fluids in a mud volcano field seaward of the Barbados accretionary wedge. *J. Geophys. Res.* **101**.

Mascle, J., Benkhelil, J., Bellaiche, G., Zitter, T., Woodside, J., Loncke, L., and Party, P. I. S., 2000. Marine geologic evidence for a Levantine-Sinai plate, a new piece of the Mediterranean puzzle. *Geology* **28**, 779-782.

Milkov, A. V., 2000. Worldwide distribution of submarine mud volcanoes and associated gas hydrates. *Mar. Geol.* **167**, 29-42.

Millero, F. J., Hubinger, S., Fernandez, M., and Garnett, S., 1987. Oxidation of $H_2S$ in seawater as a function of temperature, pH, and ionic strength. *Environ. Sci. Technol.* **21**, 439-443.

Nauhaus, K., Albrecht, M., Elvert, M., Boetius, A., and Widdel, F., 2007. *In vitro* cell growth of marine archaeal-bacterial consortia during anaerobic oxidation of methane with sulfate. *Environ. Microbiol.* **9**, 187-196.

Nauhaus, K., Boetius, A., Kruger, M., and Widdel, F., 2002. In vitro demonstration of anaerobic oxidation of methane coupled to sulphate reduction in sediment from a marine gas hydrate area. *Environ. Microbiol.* **4**, 296-305.

Niemann, H., Lösekann, T., de Beer, D., Elvert, M., Nadalig, T., Knittel, K., Amann, R., Sauter, E. J., Schlüter, M., Klages, M., Foucher, J.-P., and Boetius, A., 2006. Novel microbial communities of the Haakon Mosby mud volcano and their role as a methane sink. *Nature* **443**, 854-858.

Olu, K., Duperret, A., Sibuet, M., Foucher, J. P., and Fiala-Medioni, A., 1996. Structure and distribution of cold seep communities along the Peruvian active margin: Relationship to geological and fluid patterns. *Mar. Ecol. Prog. Ser.* **132**, 109-125.

Omoregie, E. O., Mastalerz, V., de Lange, G., Straub, K. L., Kappler, A., Roy, H., Stadnitskaia, A., Foucher, J. P., and Boetius, A., 2008. Biogeochemistry and community composition of iron- and sulfur-precipitating microbial mats at the Chefren mud volcano (Nile Deep Sea Fan, Eastern Mediterranean). *Appl. Environ. Microbiol.* **74**, 3198-3215.

Ondreas, H., Olu, K., Fouquet, Y., Charlou, J. L., Gay, A., Dennielou, B., Donval, J. P., Fifis, A., Nadalig, T., Cochonat, P., Cauquil, E., Bourillet, J. F., Le Moigne, M., and Sibuet, M., 2005. ROV study of a giant pockmark on the Gabon continental margin. *Geo-Mar. Lett.* **25**, 281-292.

Poulton, S. W., Krom, M. D., and Raiswell, R., 2004. A revised scheme for the reactivity of iron (oxyhydr)oxide minerals towards dissolved sulfide. *Geochim. Cosmochim. Acta* **68**, 3703-3715.

Poulton, S. W., Krom, M. D., Van Rijn, J., Raiswell, R., and Bows, R., 2003. Detection and removal of dissolved hydrogen sulphide in flow-through systems via the sulphidation of hydrous iron (III) oxides. *Environ. Technol.* **24**, 217-229.

Pyzik, A. J. and Sommer, S. E., 1981. Sedimentary iron monosulfides - kinetics and mechanism of formation. *Geochim. Cosmochim. Acta* **45**, 687-698.

Reeburgh, W. S., 1976. Methane consumption in Cariaco trench waters and sediments. *Earth Planet. Sci. Lett.* **28**, 337-344.

Reeburgh, W. S., 1983. Rates of biogeochemical processes in anoxic sediments. *Annu. Rev. Earth Planet. Sci.* **11**, 269-298.

Reeburgh, W. S., 2007. Oceanic methane biogeochemistry. *Chem. Rev.*, 486-513.

Reimers, C. E., Fischer, K. M., Merewether, R., Smith, K. L., and Jahnke, R. A., 1986. Oxygen microprofiles measured in situ in deep ocean sediments. *Nature* **320**, 741-744.

Rickard, D., 1997. Kinetics of pyrite formation by the $H_2S$ oxidation of iron (II) monosulfide in aqueous solutions between 25 and 125 °C: The rate equation. *Geochim. Cosmochim. Acta* **61**, 115-134.

Rickard, D. and Luther, G. W., 1997. Kinetics of pyrite formation by the $H_2S$ oxidation of iron (II) monosulfide in aqueous solutions between 25 and 125 °C: The mechanism. *Geochim. Cosmochim. Acta* **61**, 135-147.

Rickard, D. T., 1975. Kinetics and mechanism of pyrite formation at low temperatures. *Am. J. Sci.* **275**, 636-652.

Sahling, H., Bohrmann, G., Spiess, V., Bialas, J., Breitzke, M., Ivanov, M., Kasten, S., Krastel, S., and Schneider, R., 2008. Pockmarks in the Northern Congo Fan area, SW Africa: Complex seafloor features shaped by fluid flow. *Mar. Geol.* **249**, 206-225.

Sahling, H., Rickert, D., Lee, R. W., Linke, P., and Suess, E., 2002. Macrofaunal community structure and sulfide flux at gas hydrate deposits from the Cascadia convergent margin, NE Pacific. *Mar. Ecol. Prog. Ser.* **231**, 121-138.

Sassen, R., Roberts, H. H., Aharon, P., Larkin, J., Chinn, E. W., and Carney, R., 1993. Chemosynthetic bacterial mats at cold hydrocarbon seeps, Gulf of Mexico continental slope. *Org. Geochem.* **20**, 77-89.

Sauter, E. J., Muyakshin, S. I., Charlou, J. L., Schlüter, M., Boetius, A., Jerosch, K., Damm, E., Foucher, J.-P., and Klages, M., 2006. Methane discharge from a deep-sea submarine mud volcano into the upper water column by gas hydrate-coated methane bubbles. *Earth Planet. Sci. Lett.* **243**, 354-365.

Sauter, E. J., Schlüter, M., and Suess, E., 2001. Organic carbon flux and remineralization in surface sediments from the northern North Atlantic derived from pore-water oxygen microprofiles. *Deep-Sea Res. Pt. I* **48**, 529-553.

Schink, B., 1997. Energetics of syntrophic cooperation in methanogenic degradation. *Microbiol. Mol. Biol. Rev.* **61**, 262-280.

Schulz, H. D., 2006. Quantification of early diagenesis: dissolved constituents in pore water and signals in the solid phase. In: Schulz, H. D. and Zabel, M. Eds.), *Marine Geochemistry*. Springer, Berlin, Heidelberg.

Schulz, H. M., Emeis, K. C., and Volkmann, N., 1997. Organic carbon provenance and maturity in the mud breccia from the Napoli mud volcano: Indicators of origin and burial depth. *Earth Planet. Sci. Lett.* **147**, 141-151.

Schulz, H. N., Brinkhoff, T., Ferdelman, T. G., Marine, M. H., Teske, A., and Jorgensen, B. B., 1999. Dense populations of a giant sulfur bacterium in Namibian shelf sediments. *Science* **284**, 493-495.

Sibuet, M. and Olu, K., 1998. Biogeography, biodiversity and fluid dependence of deep-sea cold-seep communities at active and passive margins. *Deep-Sea Res. Pt. II* **45**, 517-567.

Sommer, S., Linke, P., Pfannkuche, O., Niemann, H., Treude, T., and Haeckel, M., 2009a. Benthic respiration and energy transfer in cold seep habitats. *Geochim. Cosmochim. Acta* **73**, A1249-A1249.

Sommer, S., Linke, P., Pfannkuche, O., Schleicher, T., von Deimling, J. S., Reitz, A., Haeckel, M., Flogel, S., and Hensen, C., 2009b. Seabed methane emissions and the habitat of frenulate tubeworms on the Captain Arutyunov mud volcano (Gulf of Cadiz). *Mar. Ecol. Prog. Ser.* **382**, 69-86.

Sommer, S., Pfannkuche, O., Linke, P., Luff, R., Greinert, J., Drews, M., Gubsch, S., Pieper, M., Poser, M., and Viergutz, T., 2006. Efficiency of the benthic filter: Biological control of the emission of dissolved methane from sediments containing shallow gas hydrates at Hydrate Ridge. *Glob. Biogeochem. Cycles* **20**.

Suess, E., Bohrmann, G., von Huene, R., Linke, P., Wallmann, K., Lammers, S., Sahling, H., Winckler, G., Lutz, R. A., and Orange, D., 1998. Fluid venting in the eastern Aleutian subduction zone. *J. Geophys. Res.-Sol. Ea.* **103**, 2597-2614.

Suess, E., Carson, B., Ritger, S. D., Moore, J. C., Jones, M. L., Kulm, L. D., and Crochrane, G. R., 1985. Biological communities at vent sites along the subduction zone off Oregon. *Biol. Soc. Wash. Bull.* **6**, 475–484.

Suess, E., Torres, M. E., Bohrmann, G., Collier, R. W., Greinert, J., Linke, P., Rehder, G., Trehu, A., Wallmann, K., Winckler, G., and Zuleger, E., 1999. Gas hydrate destabilization: enhanced dewatering, benthic material turnover and large methane plumes at the Cascadia convergent margin. *Earth Planet. Sci. Lett.* **170**, 1-15.

Thomas, D. J., Zachos, J. C., Bralower, T. J., Thomas, E., and Bohaty, S., 2002. Warming the fuel for the fire: Evidence for the thermal dissociation of methane hydrate during the Paleocene-Eocene thermal maximum. *Geology* **30**, 1067-1070.

Torres, M. E., Bohrmann, G., and Suess, E., 1996. Authigenic barites and fluxes of barium associated with fluid seeps in the Peru subduction zone. *Earth Planet. Sci. Lett.* **144**, 469-481.

Torres, M. E., McManus, J., Hammond, D. E., de Angelis, M. A., Heeschen, K. U., Colbert, S. L., Tryon, M. D., Brown, K. M., and Suess, E., 2002. Fluid and chemical fluxes in and out of sediments hosting methane hydrate deposits on Hydrate Ridge, OR, I: Hydrological provinces. *Earth Planet. Sci. Lett.* **201**, 525-540.

Treude, T., Boetius, A., Knittel, K., Wallmann, K., and Jørgensen, B. B., 2003. Anaerobic oxidation of methane above gas hydrates at Hydrate Ridge, NE Pacific Ocean. *Mar. Ecol. Prog. Ser.* **264**, 1-14.

Treude, T., Krüger, M., Boetius, A., and Jørgensen, B. B., 2005. Environmental control on anaerobic oxidation of methane in the gassy sediments of Eckernförde Bay (German Baltic). *Limnol. Oceanogr.* **50**, 1771-1786.

Tryon, M. D. and Brown, K. M., 2004. Fluid and chemical cycling at Bush Hill: Implications for gas- and hydrate-rich environments. *Geochem. Geophys. Geosys.* **5**.

Tryon, M. D., Brown, K. M., and Torres, M. E., 2002. Fluid and chemical flux in and out of sediments hosting methane hydrate deposits on Hydrate Ridge, OR, II: Hydrological processes. *Earth Planet. Sci. Lett.* **201**, 541-557.

Tryon, M. D., Brown, K. M., Torres, M. E., Trehu, A. M., McManus, J., and Collier, R. W., 1999. Measurements of transience and downward fluid flow near episodic methane gas vents, Hydrate Ridge, Cascadia.

Vacelet, J., Bouryesnault, N., Fialamedioni, A., and Fisher, C. R., 1995. A methanotrophic carnivorous sponge. *Nature* **377**, 296-296.

Valentine, D. L., 2002. Biogeochemistry and microbial ecology of methane oxidation in anoxic environments: a review. *Antonie van Leeuwenhoek* **81**, 271-282.

Wächtershäuser, G., 1988. Pyrite formation, the first energy source for life - a hypothesis. *Syst. Appl. Microbiol.* **10**, 207-210.

Wallmann, K., Drews, M., Aloisi, G., and Bohrmann, G., 2006. Methane discharge into the Black Sea and the global ocean via fluid flow through submarine mud volcanoes. *Earth Planet. Sci. Lett.* **248**, 545-560.

Wallmann, K., Linke, P., Suess, E., Bohrmann, G., Sahling, H., Schlüter, M., Dählmann, A., Lammers, S., Greinert, J., and von Mirbach, N., 1997. Quantifying fluid flow, solute mixing, and

biogeochemical turnover at cold vents of the eastern Aleutian subduction zone. *Geochim. Cosmochim. Acta* **61**, 5209-5219.

Wenzhöfer, F., Holby, O., Glud, R. N., Nielsen, H. K., and Gundersen, J. K., 2000. In situ microsensor studies of a shallow water hydrothermal vent at Milos, Greece. *Mar. Chem.* **69**, 43-54.

Whiticar, M. J., 1999. Carbon and hydrogen isotope systematics of bacterial formation and oxidation of methane. *Chem. Geol.* **161**, 291-314.

Wilkin, R. T. and Barnes, H. L., 1996. Pyrite formation by reactions of iron monosulfides with dissolved inorganic and organic sulfur species. *Geochim. Cosmochim. Acta* **60**, 4167-4179.

Woodside, J. M. and Volgin, A. V., 1996. Brine pools associated with Mediterranean Ridge mud diapirs: an interpretation of echo-free patches in deep two sidescan sonar data. *Mar. Geol.* **132**, 55-61.

Yao, W. and Millero, F. J., 1996. Oxidation of hydrogen sulfide by hydrous Fe(III) oxides in seawater. *Mar. Chem.* **52**, 1-16.

Zopfi, J., Ferdelman, T.G., Fossing, H., 2004. Distribution and fate of sulfur intermediates – sulfite, tetrathionate, thiosulfate, and elemental sulfur – in marine sediments. In: Amend J., E. K., Lyons T. (Ed.), *Sulfur biogeochemistry: Past and present*. Geological Society of America Special Paper London.

Chapter 2

# Geochemical processes and chemosynthetic primary production in different thiotrophic mats of the Håkon Mosby Mud Volcano (Barents Sea)

Anna Lichtschlag[1], Janine Felden[1], Volker Brüchert[1+], Antje Boetius[1,2,3], Dirk de Beer[1]

[1]Max-Planck-Institute for Marine Microbiology, Celsiusstrasse 1, 28359 Bremen, Germany

[2]MARUM, University Bremen, Leobener Strasse, 28359 Bremen, Germany

[3]HGF MPG Research Group on Deep Sea Ecology and Technology, Alfred Wegener Institute for Polar and Marine Research, Am Handelshafen 12, 27570 Bremerhaven, Germany

[+]Present address: Department of Geology and Geochemistry, Stockholm University, Svante Arrhenius Väg 8c, 10691 Stockholm, Sweden

submitted to *Limnology and Oceanography*

*Acknowledgements.*

We thank the shipboard crews and scientific parties of the ARK XIX/3b cruise with the R/V Polarstern, of the ATL05/02-3 cruise with the R/V L'Atalante, of the Viking cruise with the R/V Pourquoi pas? and the ROV Victor 6000 team for the help with the work during the cruises. Special thanks to Nina Weller, Hans Røy and Susanne Hinck (Max-Planck-Institute for Marine Microbiology) for help on work with the bacterial samples and Michael Schlüter and Ludmilla Baumann (Alfred Wegener Institute for Polar and Marine Research) for providing the porosity data. We thank our colleague Stefanie Grünke for preparing the sampling map. We are grateful for the excellent microsensors from Gaby Eickert, Ines Schröder, Vera Hübner, Karin Hohmann, Ingrid Dohrmann and Cecilia Wiegand and thank Martina Alisch, Andrea Schipper and Martina Meyer for further technical support. Thanks to Frank Wenzhöfer and the Sea-Tech technicians of the Microbial Habitat group (Max-Planck-Institute for Marine Microbiology) for the construction and maintenance of the in situ devices. This study was supported by the GEOTECHNOLOGIEN project MUMM II (03G0608C) funded by the German Ministry of Education and Research (BMBF) and German Research Foundation (DFG), by the EU FP6 program HERMES (GOCE-CT-2005-511234-1) as well as by the Max-Planck and Helmholtz Societies.

**Abstract**

**In this study we have investigated if in a cold seep methane or sulfide is used for chemosynthetic primary production and if significant amounts of the sulfide produced by anaerobic oxidation of methane (AOM) are oxidized geochemically, hence are not available for chemosynthetic production. Geochemically controlled redox reactions and biological turnover were compared in different habitats of the Håkon Mosby Mud Volcano. The center of the mud volcano is characterized by the highest fluid flow, and most primary production by the microbial community depends on oxidation of methane. The small amount of sulfide produced is oxidized geochemically with oxygen or is precipitated with dissolved iron. In the medium flow peripheral *Beggiatoa* habitat sulfide is largely oxidized biologically. The oxygen and nitrate supply is high enough that *Beggiatoa* can oxidize the sulfide completely, and chemical sulfide oxidation or precipitation is not important. An internally stored nitrate reservoir with average concentrations of 110 mmol $L^{-1}$ enables the *Beggiatoa* to oxidize sulfide anaerobically. The pH profile indicates sequential sulfide oxidation with elemental sulfur as intermediate. The third habitat investigated were gray thiotrophic mats associated with perturbed sediments. These showed a high heterogeneity in sulfate turnover and high sulfide fluxes, which are balanced by the opposing oxygen and nitrate fluxes so that biological oxidation dominates over geochemical sulfide removal processes. The three habitats indicate substantial small-scale variability in carbon fixation pathways either through direct biological use of methane or through indirect carbon fixation of methane-derived carbon dioxide by chemolithotrophic sulfide oxidation.**

## 1. INTRODUCTION

Geochemical and microbiological processes at cold seeps, such as mud volcanoes, surface gas hydrate deposits, and methane-laden pockmarks differ significantly from processes in organic detritus-fueled deep-sea sediments. At cold seeps, methane is abundant near the sediment-water interface and methane-consuming microbial communities control its discharge to the water column (Boetius and Suess, 2004; Niemann et al., 2006; Wallmann et al., 2006). The key process in methane-rich seafloor sediment is the microbially mediated anaerobic oxidation of methane (AOM) coupled to sulfate reduction (Boetius et al., 2000). One product of this process is dissolved sulfide. However, not much is known about the fate of AOM-produced sulfide in cold seep sediments, but previous work indicated that it is almost completely oxidized within the seabed (Sahling et al., 2002; de Beer et al., 2006).

Both biological and geochemical processes can remove sulfide. In many cold seep ecosystems different thiotrophic communities gain energy from the chemolithoautotrophic oxidation of sulfide, such as the symbiotic siboglinid tubeworms (Cordes et al., 2005; Lösekann et al., 2008) and diverse bivalves including mytilids, lucinids, and vesicomyids (Sibuet and Olu, 1998; Duperron et al., 2005). Free-living thiotrophic bacteria form extensive mats, and representatives of these mat-forming organisms are giant sulfur-oxidizing γ-proteobacteria like *Beggiatoa*, *Thiomargarita* or *Thioploca*. Many members of these groups are able to store both nitrate and elemental sulfur intracellularly (McHatton et al., 1996; Teske and Nelson, 2006). *Thiomargarita* are sessile, spherical bacteria, whereas *Beggiatoa* and *Thioploca* are motile filamentous bacteria able to glide. They can move downward to a sediment zone where dissolved sulfide is abundant and use the stored nitrate as electron-acceptor, either oxidizing sulfide to sulfate (Eq. 1) or to elemental sulfur (Eq. 2):

$$HS^- + NO_3^- + H^+ + H_2O \rightarrow NH_4^+ + SO_4^{2-} \quad \text{(Eq. 1)}$$

$$4HS^- + NO_3^- + 6H^+ \rightarrow 4S^0 + NH_4^+ + 3H_2O \quad \text{(Eq. 2)}$$

In the upper zone of the sediment, where oxygen and nitrate are available but sulfide is depleted, they refill their vacuoles with nitrate and oxidize the internally stored sulfur aerobically:

$$2S^0 + 3O_2 + 2H_2O \rightarrow 2SO_4^{2-} + 4H^+ \quad \text{(Eq. 3)}$$

The most important abiotic process is the precipitation of sulfide with iron-oxides. Iron-oxides react with sulfide, forming mainly elemental sulfur and metastable, amorphous iron-sulfides. These metastable iron-sulfides can be converted to the stable species pyrite ($FeS_2$), e.g. by reaction with sulfide (Drobner et al., 1990) or by reaction with polysulfides (Luther, 1991). Iron-sulfides are either buried in the sediment or remain part of the sulfur and iron cycle by transport to the oxic zone, e.g. by

bioturbation, where they are re-oxidized. The oxidized iron is again available as an electron-acceptor for sulfide. In some marine settings, such as coastal zones, geochemical sulfide precipitation can totally dominate over microbial oxidation by *Beggiatoa* (Preisler et al., 2007). In the sediments of Limfjorden (Denmark) *Beggiatoa* is responsible for up to 50% of the sulfide oxidation (Mussmann et al., 2003). *Thioploca* off the coast of Chile mediate maximally one third of the total sulfide oxidation (Ferdelman et al., 1997). The causes for this variation in the partitioning of biotic and abiotic sulfide oxidation in marine sediments are not well constrained. At cold seeps in deep waters this has not been investigated.

The Håkon Mosby Mud Volcano is characterized by large gradients in fluid flow velocities and sulfide fluxes (de Beer et al., 2006), and, hence, represents an ideal natural laboratory to study the processes involved in sulfide consumption at cold seeps. The different fluid flow zones include: I) the central mud flows (fluid flow velocity >3-6 m $yr^{-1}$) dominated by aerobic methane oxidation, II) *Beggiatoa* mats (fluid flow velocity: 0.3-1 m $yr^{-1}$) and III) areas covered by gray mats (de Beer et al., 2006; Niemann et al., 2006; Lösekann et al., 2007). We have not studied the large outer rim of the Håkon Mosby Mud Volcano populated by thiotrophic siboglinid tubeworms (Lösekann et al., 2008) as we could not obtain in situ microsensor measurements from the dense subseafloor system of tubeworm roots. Part of the primary production at the Håkon Mosby Mud Volcano is based on the energy generation from microbial sulfide oxidation, and geochemical sulfide oxidation with iron-oxides or other electron-acceptors could potentially reduce the sulfide supply to bacteria, and, hence, the energy and carbon supply to this chemosynthetic ecosystem.

Thus our aims were 1) to determine if geochemical or biological processes dominate sulfide removal, 2) whether methane or sulfide is used for chemosynthetic biomass production, and 3) to estimate the areal primary production of the different microbial habitats. To answer these questions, the key pathways in sulfide oxidation were investigated, including the turnover of the geochemically and biologically relevant components ($SO_4^{2-}$, $O_2$, $NO_3^-$), the efflux of the emanating products (mainly $HS^-$, DIC), and the distribution of sulfide oxidizers.

## 2. MATERIAL AND METHODS

### 2.1. Sampling Site

The Håkon Mosby Mud Volcano is situated on the Norwegian-Barents-Svalbard continental margin (72°00.3’ N, 14°44.0’ E). It is located at a water depth of 1250 m, has a concentric shape with a diameter of 1 km and an elevation above the seafloor of 8-10 m (Vogt et al., 1997). The sediment layer thickness above the oceanic crust is more than 6 km and the deposits consist of Eocene-Pliocene preglacial hemipelagic sediments and Late Pliocene-Pleistocene glacial-marine sediments (Hjelstuen et al., 1999). The pore water rising in the Håkon Mosby Mud Volcano is highly enriched in methane,

and gas hydrate form around the central conduit for fluid flow (Milkov et al., 2004; Niemann et al., 2006).

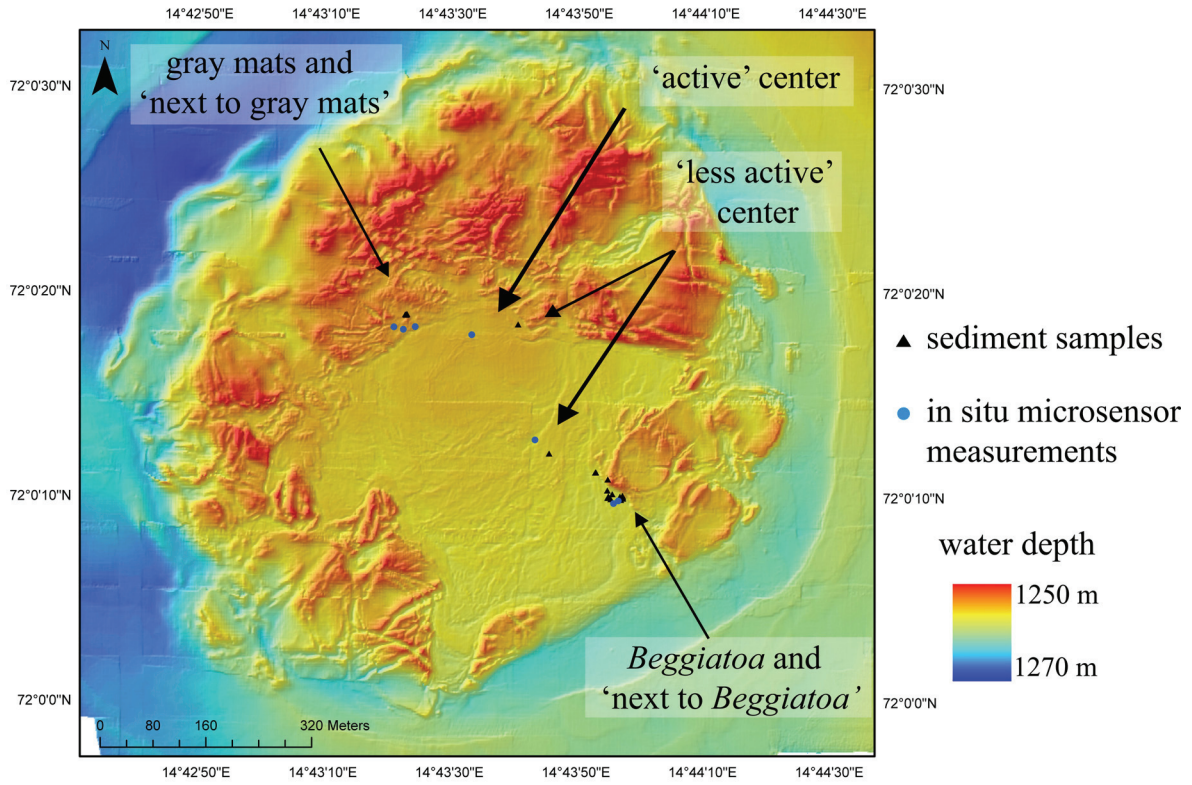


**Fig. 1: Map of the Håkon Mosby Mud Volcano showing the sampling and measurement positions in the different habitats. The topographic map was generated during the ARK XIX/3b by Ifremer, Brest (Foucher et al., 2009).**

## 2.2. Sampling

Sampling and measurements were performed in 2003 during the ARK XIX/3b cruise with the R/V Polarstern (PS64), in 2005 with the R/V L`Atalante (ATL05/02-3), and in 2006 during the HERMES cruise Viking (IFREMER) with the R/V Pourquoi pas?. On all expeditions the remotely operated vehicle (ROV) Victor 6000 (IFREMER) was used for sampling and positioning of instruments. Sampling and measurement details are summarized in Table 1 and sites are displayed in Fig. 1.

Push core samples with a sediment core length of 15-20 cm were obtained with the hydraulic ROV manipulator arm. Cores with 25-30 cm sediment length were retrieved with a multiple corer device (MUC), equipped with a POSIDONIA positioning system. As high gas load and decrease in pressure caused outgassing and sediment surface disturbances during retrieval, the sediment-filled liners were stored at in situ temperature (0 °C) for 1 day so that the mats appeared again and the geochemical gradients re-established. Subsequently the cores were transferred to a 4°C room for pore water extraction with Rhizons (type: CSS, Rhizosphere Research Products) connected to a peristaltic pump and glass syringes. The Rhizons with a filter pore diameter of 0.1 µm were horizontally inserted into the cores per 1 cm depth interval through predrilled holes that were sealed with diffusion-tight tape

before coring. The extracted pore water was immediately fixed in 5% ZnAc for sulfate, chloride and sulfide analyses or in 2 mol $L^{-1}$ HCl for analyses of dissolved iron. Samples for dissolved inorganic carbon (DIC) were fixed in $HgCl_2$ and stored at 4 °C without gas bubbles in glass vials with an additional butyl layer.

After pore water extraction, the remaining sediment was immediately cut in sections of 1 cm (depth interval 1-10 cm) or 2 cm (depth below 10 cm) slices and frozen at -20 °C in nitrogen flushed sampling bags. Before freezing, subsamples for porosity and elemental sulfur analyses were taken. For analysis of elemental sulfur, about 0.2 g sediment from each depth interval was put in 0.5 mL 5% ZnAc, 9.5 mL methanol were added and the mixture was vortex mixed. The samples were placed on a shaker for circa 12 h, decanted, and transferred to glass vials.

**Table 1: List of samples from all targeted habitats. Samples from measurements and experiments are labeled according to the PANGAEA database, in which the geochemical data are deposited (http://www.pangaea.de, doi:10.1594/PANGAEA.715022). Included are investigations during the Pourquoi pas? cruise 2006 (VKG), the L'Atalante cruise 2005 (ATL05/02-3), and the Polarstern cruise 2003 (PS64). Sediment was sampled either by a multiple corer (MTB-No.) or with push cores (PC-No./PUC-No.). In addition, in situ deployments of the microprofiler (MIC) are included.**

| Habitat | Measurements | PANGAEA database event label |
|---|---|---|
| 'Active' center | MIC | VKGD278/MIC-9 |
| 'Less active' center | MIC | VKGD277/MIC-4 |
| | Geochemistry | VKGD276/PC-7, VKGD276/PC-8 |
| | Sulfate reduction | PS64/377/PUC-1, PS64/377/PUC-2 |
| | Nitrate uptake | VKGD276/PC-8 |
| | S-isotopes | VKGD276/PC-8 |
| *Beggiatoa* | MIC | VKGD277/MIC-5 |
| | Geochemistry | VKGD276/PC-11, VKGD276/PC-12, VKGMTB6 |
| | Sulfate reduction | VKGD276/PC-2, VKGD276/PC-13, VKGMTB6 |
| | Nitrate uptake | ATL05/02-3/PUC-26, VKGD276/PC-1, VKGD276/PC-9, |
| | S-isotopes | VKGD276/PC-12 |
| | Microscopy/biology | ATL05/02-3/PUC-14, ATL05/02-3/PUC-15, ATL05/02-3/PUC-24, ATL05/02-3/PUC-23, VKGD276/PC-1, VKGD276/PC-3, VKGD276/PC-3 |
| 'Next to *Beggiatoa*' | MIC | VKGD277/MIC-6 |
| | Geochemistry | VKGD276/PC-5, VKGD276/PC-6 |
| Gray mat | MIC | VKGD278/MIC-7, VKGD278/MIC-8 |
| | Geochemistry | VKGD277/PC-7, VKGD277/PC-8 |
| | Sulfate reduction | VKGD277/PC-1, VKGD277/PC-3 |
| | Nitrate uptake | VKGD277/PC-7 |
| | S-Isotopes | VKGD277/PC-7 |
| | Microscopy | VKGD277/PC-8 |
| 'Next to gray mat' | MIC | VKGD278/MIC-10 |

### 2.3. Microscopy and Determination of Internally Stored Nitrate and Sulfur

To be able to evaluate the role of *Beggiatoa* in the environment, the morphology of the filaments and the internal storage capacity of substrates were assessed. The morphological diversity of the microorganisms from the gray and *Beggiatoa* mats was studied by transmitted light microscopy. Between 139 and 161 filaments were picked from four cores of the *Beggiatoa* habitat. The average biovolume and biomass of the filaments was calculated from their length and radius, assuming a cylindrical shape of the organisms. The filaments were transferred to vials with 250 µL of demineralized water and immediately frozen at -20 °C. This procedure breaks the cells and releases the vacuolar nitrate, which was measured after reduction to $N_2$ with a gas chromatograph-mass spectrometer (Hinck et al., 2007). Elemental sulfur was extracted from subsamples with methanol and analyzed as described below. In addition, sediment densely covered with *Beggiatoa* filaments was vertically sampled in high resolution, frozen and the nitrate content was measured as described below.

### 2.4. Geochemistry

*Solid phase geochemistry*. Different iron and sulfur solid phase species were identified and quantified. Elemental sulfur was determined on the methanol extracts of biological and sediment samples by high-performance liquid chromatography (Zopfi et al., 2004). The concentrations of AVS (acid volatile sulfides: FeS, some greigite: $Fe_3S_4$) and CRS (chromium reducible sulfur: $FeS_2$ and $S^0$, remaining greigite) were assessed with the modified two step acid distillation method (Fossing and Jørgensen 1989). In the following, the AVS and CRS will be referred to as their main components FeS and pyrite ($FeS_2$), respectively. Iron was extracted with the dithionite method (Canfield, 1989) and the ascorbic acid method (Ferdelman et al., 1991). The dithionite method extracts amorphous iron-oxides, crystalline iron-oxides, some iron-bearing silicates and some AVS (Canfield, 1989; Kostka and Luther, 1994). Triplicate samples of frozen sediment were extracted in 10 mL dithionite solution (0.5 g $L^{-1}$ sodium dithionite in 0.35 mol $L^{-1}$ acetate/0.2 mol $L^{-1}$ sodium citrate) on a shaker for 48 h at room temperature and the extracts were filtered afterwards. The extracts were left for at least 72 h to oxidize the remaining dithionite and were then analyzed with the Ferrozine method (see below) with 1% (w/v) hydroxylamine hydrochloride as reducing agent. To determine the amount of dithionite-soluble manganese, subsamples of the same extracts were measured with a Perkin Elmer 3110 flame atomic absorption spectrophotometer (AAS). The ascorbic acid method extracts the most reactive, amorphous iron-oxides, some AVS and some iron bound in clay minerals (Kostka and Luther, 1994). Triplicates of frozen sediment samples were extracted in 10 mL solution (10 g sodium citrate, 10 g sodium bicarbonate, 4 g ascorbic acid in 200 mL anoxic, demineralized water, adjusted to pH 8). Samples were shaken at 60 °C for 24 h, filtered, and iron concentrations were measured with the Ferrozine method.

*Pore water geochemistry*. Sulfate and chloride concentrations were measured by non-suppressed anion exchange chromatography (Waters IC-Pak anion exchange column, Waters 430 Conductivity detector). As eluent isophtalic acid (1 mmol $L^{-1}$, pH 4.6) containing 10% v/v methanol with a constant flow rate of 1 mL $min^{-1}$ was used. Total dissolved sulfide concentrations ($H_2S$ + $HS^-$ + $S^{2-}$) were determined with the diamine complexation method (Cline, 1969). For the determination of dissolved iron Ferrozine was used (1 g $L^{-1}$ Ferrozine in 50 mmol $L^{-1}$ HEPES buffer, adjusted to pH 7), and the concentration was measured spectrophotometrically (Stookey, 1970). DIC concentrations were assessed by flow injection (Hall and Aller, 1992) with 30 mmol $L^{-1}$ HCl and 10 mmol $L^{-1}$ NaOH as eluent and a conductivity detector (VWR scientific, model 1054).

### 2.5. Microsensor Measurements and Fluxes

High resolution in situ microsensor measurements were carried out with a deep-sea microprofiler as described previously (Wenzhöfer et al., 2000, see Fig. 2a). The ROV Victor was used to precisely position the microprofiler, to start the autonomous profiling routine, and for the instrument retrieval. The microsensors were stepwise driven from the water phase into the sediment to a depth of up to 8 cm. On the profiler electronic unit three pH, three oxygen, two sulfide microsensors (Revsbech and Ward, 1983; Jeroschewski et al., 1996; de Beer et al., 1997), and one temperature sensor (3 mm diameter, Pt100, UST Umweltsensorentechnik GmbH) were mounted and calibrated on board of the ship, as described previously (Wenzhöfer et al., 2000; de Beer et al., 2006).

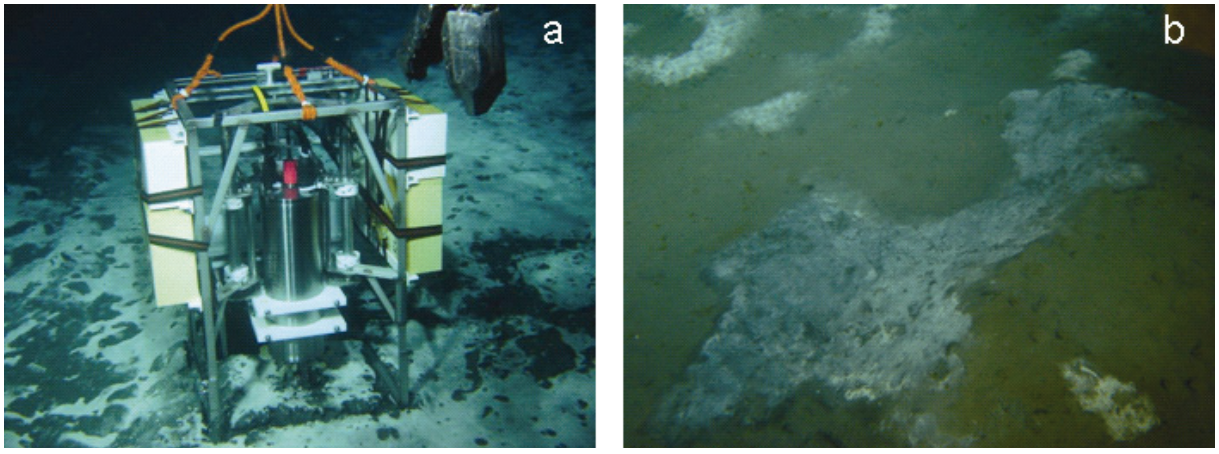


**Fig. 2: (a) Microprofiler unit standing on a dense mat of thiotrophic bacteria in the *Beggiatoa* habitat (source: Ifremer, Victor 6000); the height of the microprofiler is around 1 m; (b) gray mat patch prior to the deployment of the microprofiler; the extension of the patch (lower left to upper right end) is about 2 m (source: Ifremer, Victor 6000).**

In this study altogether seven deployments of the profiler were carried out at the center habitat, the *Beggiatoa* habitat, and at the gray mat site of the Håkon Mosby Mud Volcano (Fig. 1, Table 1). Measurements 'next to *Beggiatoa*' were conducted about 1 m next to a large *Beggiatoa* mat; 'next to

gray mat' was 20 cm away from a gray mat patch. As the surface was sometimes slightly undulating, the tilt of the profiler was estimated by image analyses and used to determine the position of the sediment surface.

Solute fluxes were calculated according to Fick's first law of diffusion, assuming steady state conditions. Oxygen fluxes were calculated from the oxygen gradients through the diffusive boundary layer according to Jørgensen and Revsbech (1985):

$$J = D\frac{dc}{dz} \qquad \text{(Eq. 4)}$$

where J = flux [mmol $m^{-2}$ $d^{-1}$], D = diffusion coefficient in water [$m^2$ $d^{-1}$] corrected for temperature and salinity (Li and Gregory 1974) and dc/dz = concentration gradient (dc [mmol $m^{-3}$]; dz [m]). Sulfide fluxes were calculated from gradients in the sediment according to following equation:

$$J = \phi D_{Sed}\frac{dc}{dz} \quad \text{(Eq. 5)}$$

where $\phi$ = porosity and $D_{Sed}$ = diffusion coefficient in the sediment [$m^2$ $d^{-1}$]. The diffusion coefficient $D_{sed}$ in the sediment was calculated according to Iversen and Jørgensen (1993):

$$D_{Sed} = \frac{D}{1+3(1-\phi)} \quad \text{(Eq. 6)}$$

The diffusion coefficient D at a salinity of 35‰ and a temperature of 0 °C was calculated to be $9.1 \times 10^{-5}$ $m^2$ $d^{-1}$ (Unisense Table, Seawater and Gases) for oxygen and of $6.9 \times 10^{-5}$ $m^2$ $d^{-1}$ for sulfide (Li and Gregory, 1974). Calculated diffusive in situ fluxes were corrected for advective upflow according to de Beer et al. (2006).

Fluxes of advected solutes were calculated as

$$J = v\,c \quad \text{(Eq. 7)}$$

where v is the fluid upflow velocity (m $d^{-1}$) and c is the concentration of the solute in the advected fluid. Fluid upflow velocities v of the different habitats can be found in de Beer et al. (2006) and in this manuscript.

### 2.6. Sulfate Reduction

Sulfate reduction was measured by the ex situ whole core injection method according to Jørgensen (1978), adapted as in Treude et al. (2003). On board 5-10 µL $^{35}SO_4^{2-}$ (dissolved in water, 50 kBq) radioactive tracer was injected into replicate subcores in depth intervals of 1 cm. Subcores were incubated in the dark at in situ temperature for 24 h. To stop the incubation, the sediment was sliced in 1 cm sections and fixed in 20 mL 20% ZnAc. Rates were determined with the single step cold distillation method (Kallmeyer et al., 2004).

### 2.7. Stable Sulfur Isotope Analyses of AVS and CRS

To determine potential sinks of reduced sulfide, subsamples of precipitated ZnS from the AVS and CRS distillations were filtered through 0.2 µm cellulose nitrate filters and converted to $Ag_2S$ in a 0.1 mol $L^{-1}$ $AgNO_3$ solution. The $Ag_2S$ precipitates were dried, weighed, and mixed with approximately 3.5 mg vanadium pentoxide in tin cups. The stable sulfur isotope composition of the samples was determined by isotope ratio mass spectrometry (irmMS) using a Eurovector elemental analyzer connected to a Finnigan Delta Plus gas isotope mass spectrometer via a Finnigan Conflo II split interface. Sulfur isotope compositions were determined for the center area, the *Beggiatoa* habitat, and the gray mat site. Isotopic ratios are displayed in the standard $\delta$-notation ($\delta^{34}S$) with respect to the Vienna Canyon Diablo Troilite (V-CDT). Accuracy and precision of the isotope mass spectrometer were tested after every tenth sample using IAEA Standard S2 ($\delta^{34}S$ 20.3‰ vs. V-CDT). Standard deviation based on all replicates was 0.4 ‰.

### 2.8. Nitrate Uptake

Defined amounts of nitrate were added to the overlying water of retrieved sediment cores. The water column was gently stirred with a jet stream. Water samples were taken after different time intervals, acidified and stored at 4 °C. Nitrate concentrations were measured with a chemiluminiscence $NO_x$ analyzer (Thermo Environmental Instruments) based on reduction of $NO_2^-$ and $NO_3^-$ and re-oxidation of the produced NO by ozone ($O_3$) (Braman and Hendrix, 1989). Random samples were checked for nitrite. No nitrite was detected and all $NO_x$ was assumed to be $NO_3^-$.

## 3. RESULTS

### 3.1. Characteristics of the Different Habitats

To study the effect of methane fluxes and upflow velocities on biological versus geochemical methane and sulfide conversions, we concentrated our study on three main habitats: the center site, the *Beggiatoa* habitat and the gray mat fields.

*Center.* Sediments in the center area were devoid of macrofauna and microbial mats. Based on visual observations we differentiated between an ‘active’ center in the northwest (Fig. 1) with a few sites of methane bubble release, disturbed sediments, and small cracks at the sediment surface. Southeast of this ‘active’ center, the seafloor showed a slightly undulating surface littered with small holes (diameter 2 cm). In this ‘less active’ center no gas bubble escape was observed.

*Beggiatoa habitat*. Sediments covered with *Beggiatoa* mats were sampled southeast of the center (Fig. 1) in an area with a dense mat of 1-2 mm thickness. The mats extended for hundreds of meters, with patches of several centimeters to decimeter large uncovered sediment (Fig. 2a). Some *Beggiatoa*

filaments reached a few millimeter into the sediment, but most filaments were present in the mat covering the sediment surface. *Beggiatoa* filaments had an average length of 1.3 mm and an average filament radius of 4.8 µm, resulting in a biovolume of $1.02 \times 10^{-10}$ L per filament. Filaments contained on average 120 mmol $L^{-1}$ elemental sulfur and 110 mmol $L^{-1}$ nitrate (Table 2).

**Table 2: General morphology and characteristics of *Beggiatoa* filaments picked from the surface mat of four different cores of the *Beggiatoa* habitat (ATL05/02-3/PUC-14, PUC-15, PUC-24, PUC-23); samples were taken in two different *Beggiatoa* patches close to each other.**

| | Length (mm) | Radius (mm) | Biovolume (L) | Biomass (µg) | Internal $S^0$ (mmol $L^{-1}$) | Internal nitrate (mmol $L^{-1}$) |
|---|---|---|---|---|---|---|
| $n_{cores}=4$ with $n_{filaments}=$ 139-161 | 1.33 (± 0.26) | $4.8 \times 10^{-3}$ ($\pm 0.5 \times 10^{-3}$) | $1.02 \times 10^{-10}$ ($\pm 0.3 \times 10^{-10}$) | 0.09 (± 0.05 ) | Min: 45 max: 289 Average: 120 (±113) | min: 73 Max: 149 Average: 110 (± 36) |

In sediments densely covered with *Beggiatoa*, a high total (internal plus pore water) nitrate content of on average 0.3 mmol $L^{-1}$ was measured in the uppermost 1.6 mm. This mainly originated from internally stored nitrate released after freezing and thawing and subsequent centrifugation. Below 1.6 mm the total nitrate content decreased rapidly (Fig. 3a). *Beggiatoa*-covered sediments, incubated at in situ temperature, lost all nitrate in the upper 2 cm of the sediment within 6 days (Fig. 3b).

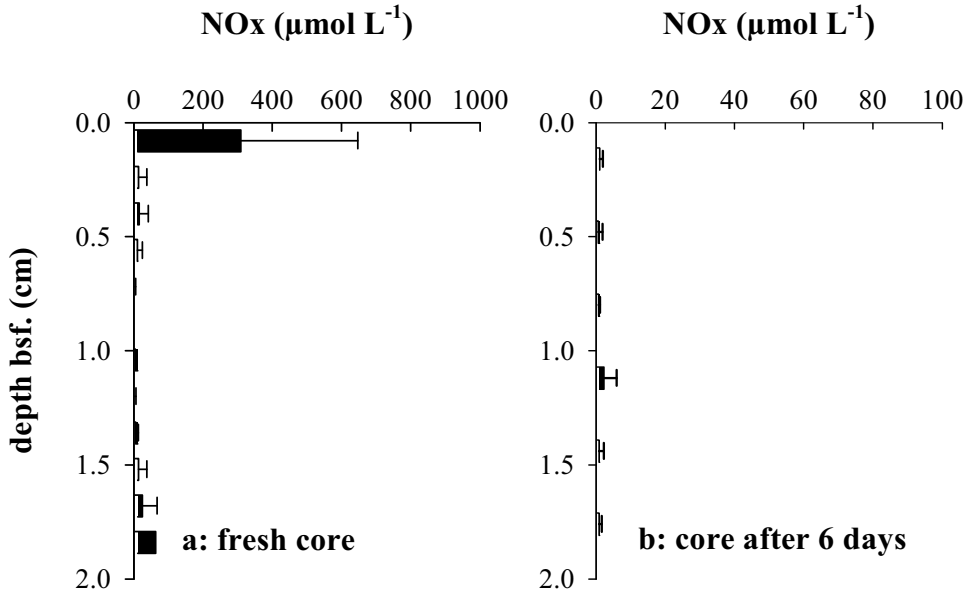


**Fig. 3: Distribution of the total nitrate content in (a) a fresh sediment core densely covered with *Beggiatoa* filaments and (b) a sediment core covered with *Beggiatoa* filament that stood for 6 days at in situ temperature; total nitrate content = pore water nitrate + nitrate released from disrupted *Beggiatoa* filaments . Note the different scales. Error bars display the standard error (*n*=3).**

*Gray mat area*. Patches of gray mats of 0.5-5 m diameter (Fig. 2b) occurred northwest of the center. Within a single patch the color changed from white to dark gray; often a gray mat was surrounded by a white mat. In this habitat about 50% of the sediment was covered by mats and the sediment surface was flat. At the seafloor some of the mats appeared quite thick and gelatinous, but in retrieved cores the average mat thickness was only approximately 1 mm. Microscopy showed a morphologically highly diverse community, as described previously (de Beer et al., 2006).

None of the sediment cores from the different habitats showed a visible color transition associated with redox gradients, the sediment color was typically dark grayish over the entire core length.

### 3.2. Geochemistry

*Solid phase geochemistry*. The results of all measured solid phase parameters are summarized in Figure 4. Concentrations of dithionite and ascorbic acid extractable iron, AVS and CRS were similar in all habitats over the entire core lengths. Only in the sediment under the gray mat, the pyrite (CRS) concentration was slightly lower in the top 4 cm, below which it increased to somewhat higher concentrations. In the center site and the gray mat habitat concentrations of FeS (AVS) slightly decreased with depth. The amount of dithionite-extractable manganese in the sediment was below 2 μmol $cm^{-3}$ in all habitats (data not shown). No subsurface peaks of manganese were detected in the surface sediments, indicating the absence of manganese-oxides. Clear differences between the habitats were observed in elemental sulfur concentrations and distributions. In the center site and in the 'next to Beggiatoa' sediments the elemental sulfur levels were less than 0.2 μmol $cm^{-3}$ throughout the core (Fig. 4c, k), whereas they were as high as 0.6 μmol $cm^{-3}$ in the near-surface sediments of the gray mat and the Beggiatoa site (Fig. 4g, n).

*Pore water geochemistry.* Results from pore water analyses are summarized in Figure 5. The sulfate gradients were steeper in the *Beggiatoa* site (Fig. 5f) than in the 'less active' center and the 'next to *Beggiatoa*' site (Fig. 5a, k). Sulfate concentrations decreased only slightly with depth in gray mat sediments (Fig. 5p). As chloride is not reactive, the steepness of its gradient can be used as a measure for upflow of mud and pore water with different chloride content (Aloisi et al. 2004; Wallmann et al. 2006). The chloride gradients differed only slightly between the 'active center', the *Beggiatoa*, and the 'next to *Beggiatoa*' sediments (Fig. 5c, h, m). In the top 15 cm of sediment below the gray mat chloride did not decrease (Fig. 5r). Sulfide concentrations were up to a magnitude lower in the extracted pore water than as measured in situ by microsensor measurements, due to stripping by degassing methane during retrieval. Below the sulfidic zones (Fig. 5b, g, i) dissolved iron was present (Fig. 5d, i, n). In zones with high sulfide content dissolved iron concentrations sometimes varied, likely due to sampling artifacts. DIC pore water profiles were scattered in the gray mats (Fig. 5t), probably due to disturbances by outgassing. In all other habitats DIC increased with depth (Fig. 5e, j, o).

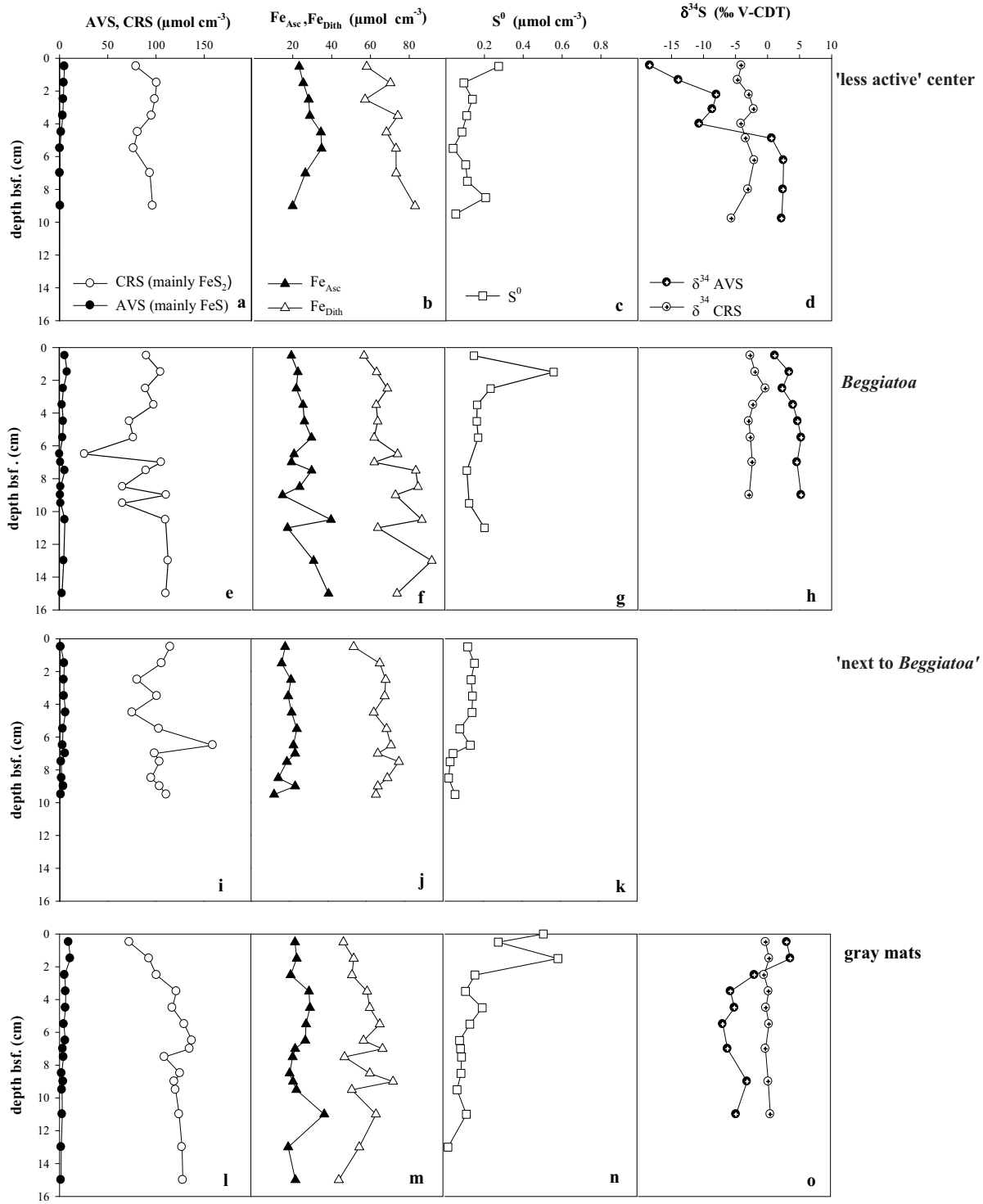


**Fig. 4: Iron and sulfur geochemistry and S-isotope distribution in the solid phase at different habitats ('less active' center: a-d, *Beggiatoa* site: e-h, 'next to *Beggiatoa*' site: i-k, gray mat area: l-o); CRS: chromium reducible sulfur ($FeS_2$, $S^0$, some greigite), AVS: acid reducible sulfur (FeS, some greigite), $Fe_{Asc}$: ascorbic acid-extractable iron, $Fe_{Dith}$: dithionite-extractable iron, $S^0$: elemental sulfur.**

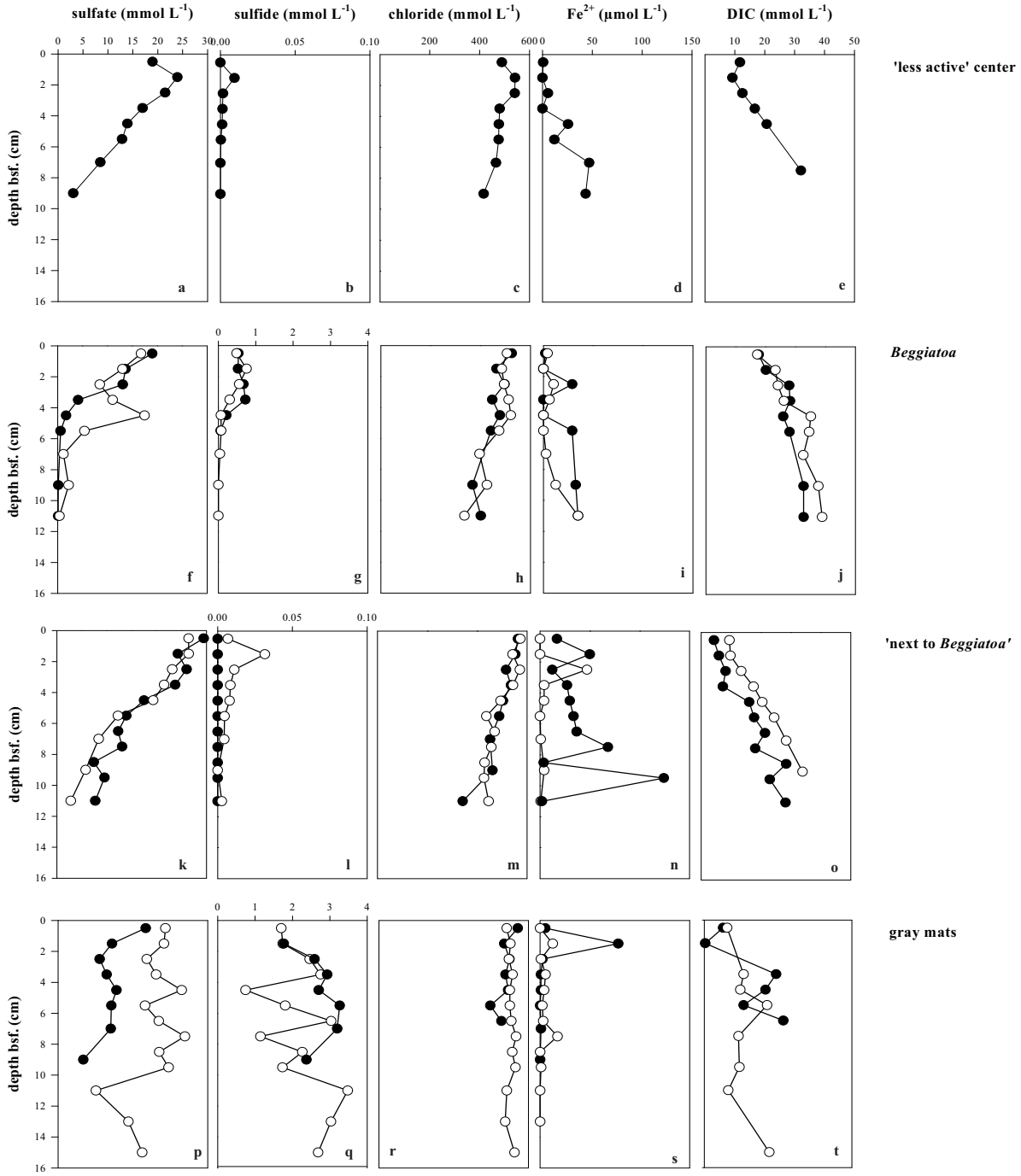


**Fig. 5: Vertical distribution of sulfate, sulfide, chloride, dissolved iron, and dissolved inorganic carbon (DIC) in the sediments of the 'less active' center site (a-e), the *Beggiatoa* fields (f-j), the 'next to *Beggiatoa*' site (k-o) and the gray mat site (p-t). Note the different scales for sulfide in the different habitats.**

### 3.3. Sulfur (S)-Isotope Composition

The stable isotope composition of the pyrite (CRS) was similar at the three sites and varied only between -5 to 0‰ vs. V-CDT with sediment depth (Fig. 4d, h, o). In contrast, the isotope composition of AVS varied strongly. In the top 2 cm of the gray mat sediments, AVS was enriched in $^{34}S$ (+5‰ vs. V-CDT) relative to CRS, but relatively depleted at depth (-5‰ vs. V-CDT). An inverse relationship was observed in the sediments from the 'less active' center, where AVS was more depleted relative to pyrite at the top, but became gradually more enriched with increasing sediment depth (Fig. 4d, h, o). Lastly, in the *Beggiatoa*-covered sediments, $\delta^{34}S_{FeS}$ was $^{34}S$-enriched relative to pyrite throughout the sediment core and varied little with depth.

### 3.4. In Situ Microsensor Measurements

The results from the in situ measurements are shown in Figures 6-8. In the 'active' center, where only pH and temperature measurements were successful, temperature increased sharply with depth (Table 3). The steep sediment temperature gradients indicate an upflow of warm fluids from the deeper subsurface. The pH decreased pronouncedly in the upper 5 cm (Fig. 6a).

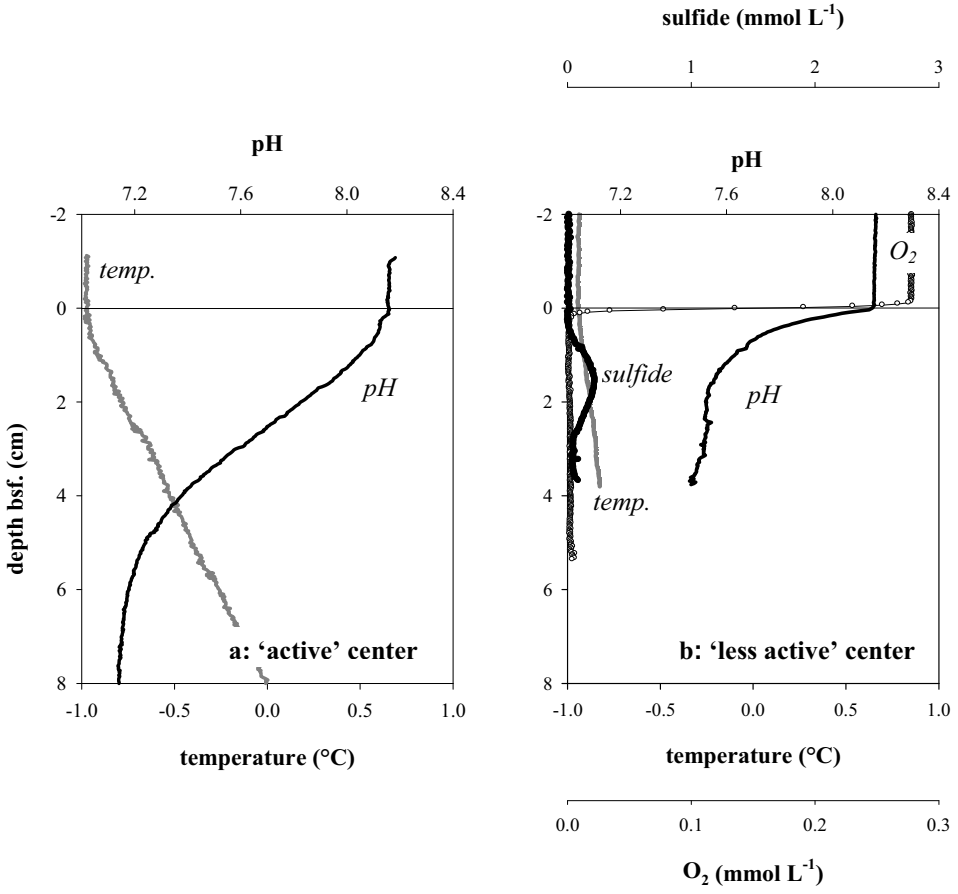


**Fig. 6: In situ measured microprofiles in sediments from (a) the 'active' center and (b) the 'less active' center.**

The pH profile in the 'less active' center showed a similar shape, but the decrease with depth was not as strong as in the 'active' center (Fig. 6b). Oxygen was present in the upper 1.3 mm of the sediment. Sulfide concentrations were low overall, peaked at 2 cm depth, and were below detection below 3 cm. Sulfide and oxygen profiles overlapped. The temperature gradient was less than 25% of the 'active' center temperature gradient (Table 3).

At the *Beggiatoa* site, oxygen penetration was only 0.5 mm (Table 4), and all oxygen was consumed within the mat. The sulfide profile showed highest concentrations at 2-4 cm (Fig. 7a), as reported previously (de Beer et al. 2006). All three replicate pH profiles showed a pH minimum near the mat surface and a pH maximum at 4 mm depth. The pH maximum coincided with the zone where the upward diffusing sulfide disappeared. This pH undulation was not observed before at this site.

In the 'next to *Beggiatoa*' site (Fig. 7b) oxygen penetrated 3.0 mm. This was the deepest oxygen penetration depth measured during our in situ deployments at the Håkon Mosby Mud Volcano, associated with the lowest temperature gradient. Sulfide and oxygen profiles overlapped. Sulfide concentrations were much lower than in the directly adjacent *Beggiatoa* covered sediments. The pH showed a gradual decrease from the overlying seawater.

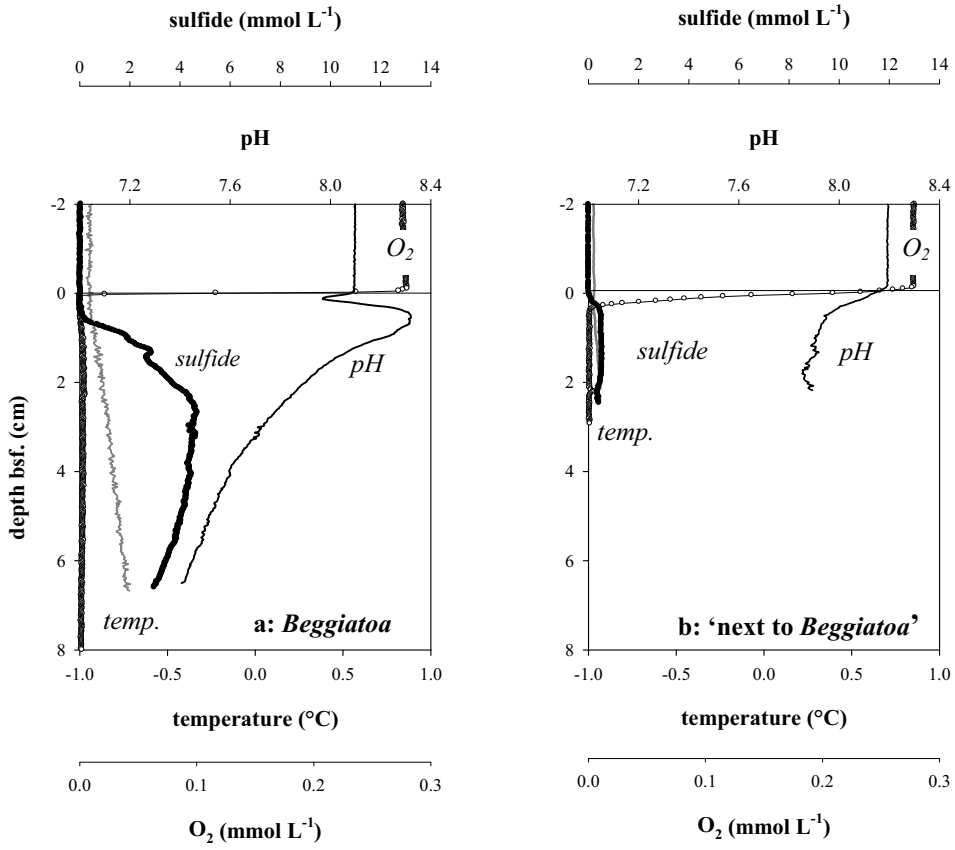


**Fig. 7: Oxygen, sulfide, pH, and temperature profiles measured in situ in (a) sediments densely covered with *Beggiatoa* filaments and (b) in sediments without a visible *Beggiatoa* mat: 'next to *Beggiatoa*'.**

Sulfide concentrations were always very high in gray mat sediments with the steepest gradients near the sediment surface (in Fig. 8a: average sulfide profile of two deployments). Oxygen penetration was comparable to the *Beggiatoa*-covered sediment, but sulfide and oxygen profiles overlapped. The pH profile showed a small peak just below the sediment surface; below this the pH decreased gradually.

In the 'next to gray mat' site (Fig. 8b) sulfide reached peak values that were 10 times lower than in the gray mat-covered area. The pH decreased only slightly from seawater values in the upper 6 cm. Oxygen penetrated only 0.3 mm into the sediment. Temperature gradients in both the gray mat and in the 'next to gray mat' sediments were higher than in the *Beggiatoa* habitat.

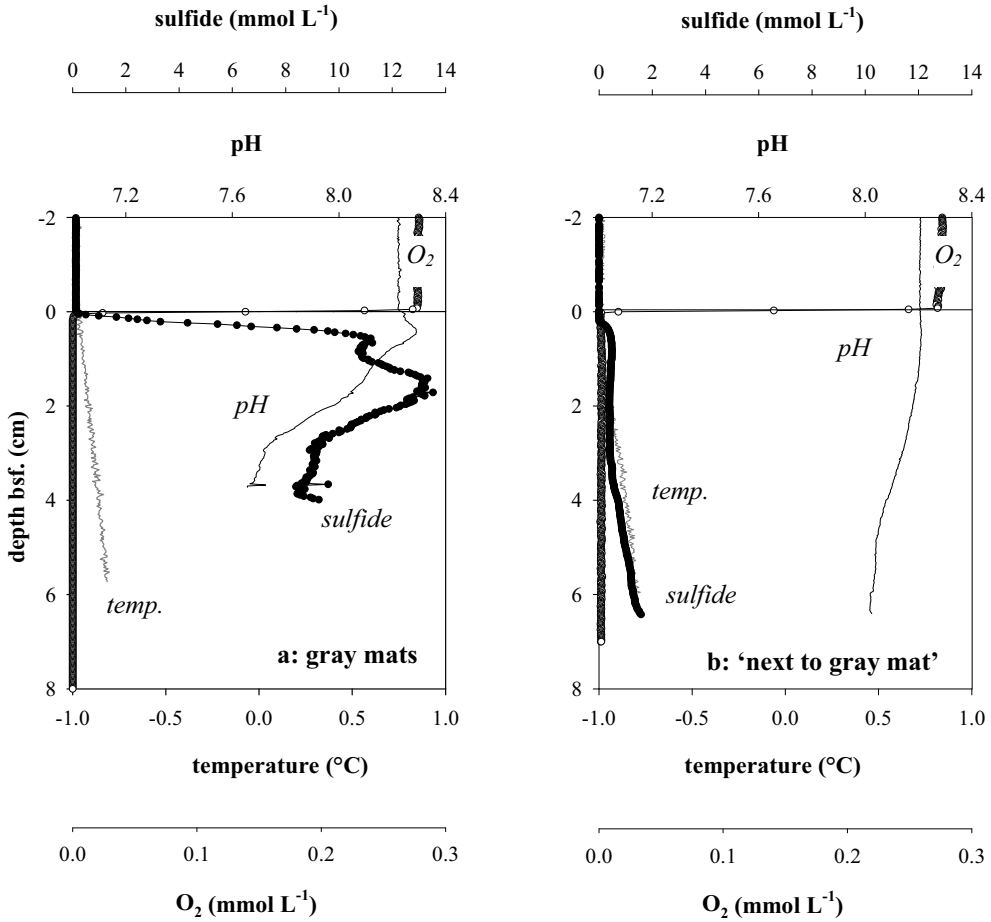


**Fig. 8: In situ microprofiles from sediments covered by (a) a gray mat and (b) 20 cm aside a gray mat: 'next to gray mat'. The sulfide profile in (a) the gray mat shows an average value gained during two microprofiler deployments.**

**Table 3: Temperature gradients measured in situ with the microprofiler.**

| habitat | Temperature gradient (°C $m^{-1}$) |
|---|---|
| 'Active' center | 13.9 |
| 'Less active' center | 3.2 |
| *Beggiatoa* | 2.8 |
| 'Next to *Beggiatoa*' | 1.6 |
| Gray mat | 2.8, 4.6 |
| 'Next to gray mat' | 3.2 |

### 3.5. Oxygen and Sulfide Fluxes

The fluxes calculated from in situ microsensor measurements (oxygen flux into the sediment and upward directed sulfide flux), corrected for upward advection, and the averaged oxygen penetration depths of all assessed habitats are shown in Table 4. Oxygen fluxes were highest in the gray mat habitat, slightly smaller in the 'next to gray mat' habitat and the *Beggiatoa* fields, and strongly reduced in the 'next to *Beggiatoa*' site and the center sediments. Sulfide fluxes followed a similar trend as those of oxygen, but the lowest were found 'next to gray mats'.

### 3.6. Sulfate Reduction Rates

Sulfate reduction was measured in the *Beggiatoa* habitat, the gray mat site, and the 'less active' center area. In *Beggiatoa*-covered sediments the highest sulfate reduction rate, 1200 nmol $cm^{-3}$ $d^{-1}$, occurred in the 1-3 cm depth interval and strongly decreased below 4 cm depth. In the gray mats sulfate reduction occurred irregularly in the top 15 cm with values ranging from 100-1400 nmol $cm^{-3}$ $d^{-1}$. At the center site sulfate reduction was low with maximally 20 nmol $cm^{-3}$ $d^{-1}$ and decreased strongly with depth. Integrated sulfate reduction rates for the upper 10 cm varied by a factor of 200 between habitats and ranged from an average of only 0.5 mmol $m^{-2}$ $d^{-1}$ in the 'less active' center to 59 mmol $m^{-2}$ $d^{-1}$ in the gray mat (Table 4). Despite the considerable small scale variability associated with the mat habitats, the average sulfate reduction rates measured explain very well the average sulfide fluxes measured in situ with the microsensors.

**Table 4: Summary of oxygen fluxes $J_{O2}$ (with standard deviations), oxygen penetration depths, upward directed sulfide fluxes $J_{sulfide\ upward}$, and sulfate reduction rates (SRR) from different habitats of the Håkon Mosby Mud Volcano. Calculations and measurements are based on the in situ deployments of the microprofiler and on the ex situ sulfate reduction rates integrated over the upper 10 cm. Displayed fluxes were calculated as diffusional fluxes and afterwards corrected for advection with a fluid upflow velocity as determined in de Beer et al., (2006). In the 'less active' center an upflow rate of *)1 m $yr^{-1}$ was assumed; only at an upflow rate of ≤1 m $yr^{-1}$ can sulfate penetrate to a depth of 2 cm and a sulfide peak can form (Fig. 6b). An upflow velocity of **)0.5 m $yr^{-1}$ was used for the *Beggiatoa* and 'next to *Beggiatoa*' site; no correction was applied to the gray mat and 'next to gray mat' site (upflow velocity: 0 m $yr^{-1}$, *see* Discussion). The negative notation of the fluxes stands for fluxes from the water column into the sediment, the positive notation stands for fluxes from the sediment in direction of the overlying water column. n.d.= not determined. Standard deviations and averages are derived from replicate measurements (*n*); for $J_{O2}$ and $O_2$ penetration depth *n*=6 for gray mat, *n*=3 for 'less active' center, *Beggiatoa* and 'next to gray mat' and *n*= 2 for 'next to *Beggiatoa*'. For SRR *n*= 5 for 'less active' center, *n*= 8 for *Beggiatoa* and *n*=2 for gray mat.**

| habitat | $J_{O2}$ (mmol $m^{-2}d^{-1}$) | $O_2$ penetration (mm) | $J_{sulfide\ upward}$ (mmol $m^{-2}d^{-1}$) | SRR (mmol $m^{-2}d^{-1}$) |
|---|---|---|---|---|
| 'Less active' center | -11.4 (± 3.7)*) | 1.3 | 0.7*) | 0.2-1.1<br>Average: 0.5 |
| *Beggiatoa* | -33.7 (± 8.8)**) | 0.5 | 11.6**) | 2.8-23.1<br>Average: 11.2 |
| 'Next to *Beggiatoa*' | -9.2 (± 0.9)**) | 3.0 | 7**) | n.d. |
| Gray mat | -45.2 (± 8.4) | 0.5 | 17/131 | 9.5-108<br>Average: 59 |
| 'Next to gray mat' | -35.2 (± 13) | 0.5 | 4.8 | n.d. |

### 3.7. Experimental Determination of Nitrate Uptake

Nitrate uptake was higher in *Beggiatoa* mats than in gray mats and the center sediments (Table 5). The initial uptake rate of starved *Beggiatoa* was up to eight times higher than after one hour of exposure. For the calculation of the nitrate flux the regression of the gradients (Fig. 9) after this initial hour was used. In the *Beggiatoa* sediments the nitrate uptake rate increased with higher nitrate concentrations in the water overlying the core. Increasing the seawater nitrate concentration 20-30 fold still resulted in constant decline after 66 h exposure (Fig. 9). As the nitrate decrease in the water is caused by both a) nitrate uptake by bacteria and b) molecular diffusion of nitrate from the water column into the sediment, the purely diffusional flux at given concentrations and time intervals was modeled (COMSOL multiphysics model) and subtracted from the value calculated from the regression of the gradient. This value then corresponds to the nitrate uptake by bacteria.

**Table 5: Summary of nitrate uptake experiments with the calculated nitrate fluxes. Uptake was calculated from linear nitrate regression after a time period >60 min; values for nitrate loss due to diffusive uptake into the sediment were achieved with the COMSOL multiphysics model and have been subtracted.**

| Habitat | Nitrate concentration before addition ($\mu mol\ L^{-1}$) | Amount of nitrate added ($\mu mol\ L^{-1}$) | $J_{NO3-}$ ($mmol\ m^{-2}d^{-1}$) |
|---|---|---|---|
| 'Less active' center | 9 | 29 (2 x environmental concentration) | -7 |
| *Beggiatoa* | 4 | 14 (environmental concentration) | -10.8 |
| | 1 | 29 (2 x environmental concentration) | -26 |
| | 6 | 52 (4 x environmental concentration) | -102 |
| | 6 | 270 (18 x environmental concentration) | -40 |
| | 184 | 310 (30 x environmental concentration) | -74 |
| | 3 | no nitrate addition | -1.5 |
| Gray mat | 9 | 28 (2 x environmental concentration) | -4.5 |
| Control (seawater without sediment) | 13 | 29 (2 x environmental concentration) | $-1.4x10^{-4}$ |

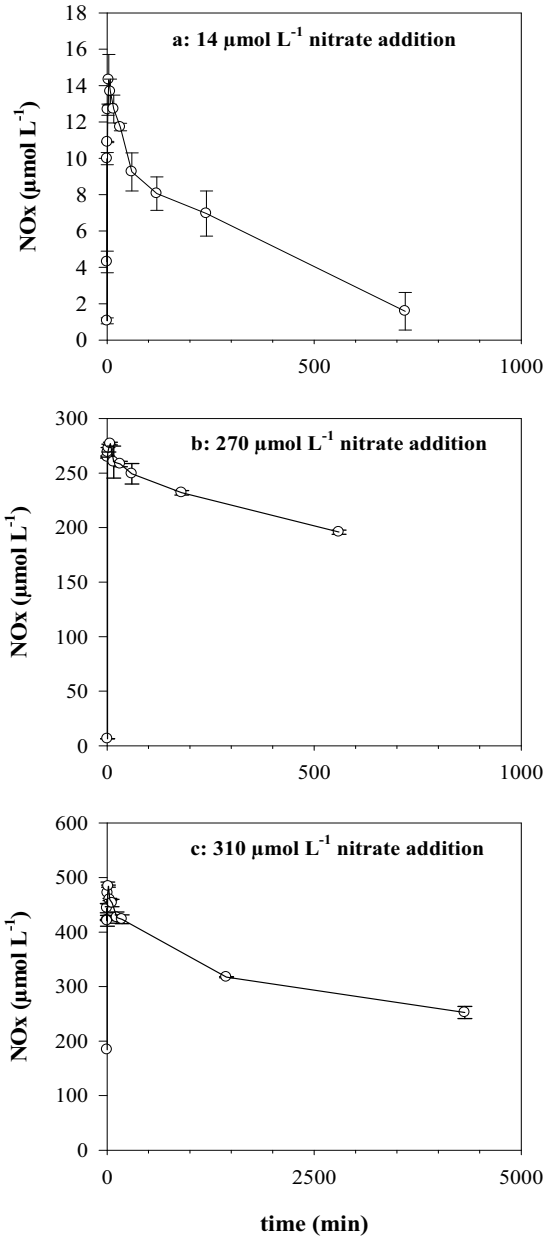


**Fig. 9: Uptake of nitrate by *Beggiatoa* was measured in bottom water overlying a densely *Beggiatoa* covered sediment. Different amounts of nitrate were added: (a) 14 µmol $L^{-1}$, (b) 270 µmol $L^{-1}$, (c) 310 µmol $L^{-1}$ (*see* also Table 5).**

## 4. DISCUSSION

At the Håkon Mosby Mud Volcano the presence and absence of thiotrophic mats can be explained by the sulfide fluxes from AOM. High fluxes of sulfide >10 mmol $m^{-2}$ $d^{-1}$ are exploited by thiotrophic mats. At a sulfide flux of 7 mmol $m^{-2}$ $d^{-1}$ and less, these mats do not form (Table 4). The patchiness of

the mats can vary on scales of centimeter to 100 m. This indicates a strong spatial heterogeneity in fluid upflow and methane supply to the seafloor, and hence spatially variable AOM activity. A third possible limitation of thiotrophic primary production could be the competition between geochemical and microbial sulfide oxidation. However, we found bacterial processes to be responsible for both the sulfide production as well as the removal, showing that a substantial fraction of the AOM-associated DIC production is efficiently channeled into chemosynthetic carbon fixation.

### 4.1. *Beggiatoa* Habitat

*Sulfide production.* Sulfate reduction rate measurements showed that in the *Beggiatoa* habitat most sulfide formed in the upper 3 cm. Also the sulfide microprofile indicated a hot spot of AOM at 2-4 cm bsf.. (Fig. 7a). The averaged depth integrated sulfate reduction rate was close to the sulfide flux obtained from the microprofiles (Table 4). Thus very little sulfide is consumed between the source of the sulfide and the zone of maximal thiotrophic consumption at 4 mm depth. Precipitation of iron-sulfides is minor and most of the sulfide is available for consumption by thiotrophic bacteria. To confirm that in the *Beggiatoa* habitat sulfide oxidation is mainly performed by thiotrophic bacteria, we addressed the questions I) whether *Beggiatoa* are actually capable of oxidizing the total sulfide supply and II) if indeed no geochemical sulfide oxidation is detected from the distribution of iron-sulfides and -oxides in the sediment.

*Biological sulfide oxidation.* As in situ microsensor measurements in the *Beggiatoa* habitat showed a pronounced gap between the depths of oxygen depletion and sulfide appearance, direct aerobic sulfide oxidation can be excluded. This characteristic gap was not observed in the other habitats and was likely caused by migrating *Beggiatoa* via anaerobic oxidation of sulfide with nitrate. At ambient nitrate concentrations the nitrate flux into the *Beggiatoa* mats was as high as the upward sulfide flux (Table 4, 5), thus the nitrate supply was sufficient to consume the total sulfide flux (Eq. 1, 2). *Beggiatoa* stored nitrate up to a concentration of 110 mmol $L^{-1}$ (Table 2), which is about 7,500-fold higher than the environmental background concentration of 0.015 mmol $L^{-1}$. From the storage capacity of individual filaments (Table 2) and the total nitrate content in the sediment we calculated that $2.7x10^4$ *Beggiatoa* filaments are present per $cm^3$ sediment in the zone with the high nitrate content (Fig. 3a, 0.3 mmol $L^{-1}$ nitrate / $1.12x10^{-8}$ mmol nitrate per 1 filament). The mat itself (thickness: 1.6 mm) hosts $4.2x10^7$ *Beggiatoa* filaments per $m^2$. *Beggiatoa* has a wet biomass of 3.8 g $m^{-2}$ ($4.2x10^7$ filaments $m^{-2}$ x $9x10^{-8}$ g wet weight per filament), corresponding to 0.8 g $m^{-2}$ dry weight assuming a water content of 80%. All nitrate disappeared from the sediment within 6 days (Fig. 3b), thus the vacuolar nitrate decrease was at least 18,000 mmol $m^{-3}d^{-1}$ (110 mmol $L^{-1}$ / 6 days), similar to a value reported previously (Preisler et al., 2007).

The unique shape of the pH profile can be caused by sequential sulfide oxidation. Anaerobic sulfide oxidation with nitrate is a proton-consuming process (Eq. 1, 2) leading to the observed local pH increase at around 4 mm sediment depth where the upward diffusing sulfide disappears (Fig. 7a). The pH minimum located at the lower boundary of the oxic zone can be a consequence of oxidation of $S^0$ to sulfate:

$$2S^0 + 3O_2 + 2H_2O \rightarrow 2SO_4^{2-} + 4H^+ \quad \text{(Eq. 8)}$$

Indeed a high $S^0$ content of 120 mmol $L^{-1}$ was found in the mat and thus $S^0$ will be the principal electron-donor for *Beggiatoa* in the sulfide-depleted sediment and mat layer. The oxygen flux (Table 4) is high enough to oxidize large amounts of $S^0$ (Eq. 8). When gliding between the oxic and the sulfidic zone internally stored energy sources (nitrate and $S^0$) will be used. Accordingly, the circa 0.4 µmol $cm^{-3}$ surplus sulfur in the surface sediments will be due to the intracellular sulfur pool of the filaments.

Spatially separated oxidation steps were used to explain pH microprofiles measured in laboratory incubated *Beggiatoa* mats (Sayama et al., 2005; Kamp et al., 2006). However, also a series of geochemical reactions can explain similar pH profiles. Preisler et al., (2007) reported an intense manganese and iron cycle in methane-containing sediments (Eckernförde Bay, Baltic Sea), where the chemical oxidation of sulfide with oxidized iron causes an increase in pH; produced $Fe^{2+}$ diffuses upwards and reduces manganese-oxides, and the concurrent iron-oxide precipitation causes a pH minimum.

*Potential role of iron for sulfide oxidation.* In the mud volcano fluids $Fe^{2+}$ is transported upwards with a flux of 0.05 mmol $m^{-2}$ $d^{-1}$. Dissolved iron will precipitate near the AOM zone as FeS and/or pyrite. However, this process does not balance the dissolved sulfide flux ($J_{sulfide}$ = 11.6 mmol $m^{-2}$ $d^{-1}$, Table 4), which is 230 times higher. The manganese concentration is too low to play a geochemical role in iron or sulfide oxidation. Bioturbating and bioirrigating organisms were absent in all sampled habitats, thus do not drive an iron oxidation and reduction cycle in the suboxic zone.

Potentially reactive dithionite and ascorbic acid-extractable iron remain the only detected species available for sulfide oxidation. Deposition or transport of rising mud from a deep reservoir most probably supplies each habitat with similar iron mineral species. In highly sulfidic environments, more iron-sulfide minerals than oxidized iron minerals are expected. Conversely, in habitats with little sulfide or suboxic habitats, more oxidized iron and a minor amount of iron-sulfides would be expected. However, different extraction methods showed similar concentrations of dithionite and of ascorbic acid-extractable iron in all habitats investigated here (Fig. 4), as could be the result from a relatively recent mud flow forming the inner flat crater of the Håkon Mosby Mud Volcano. Even the sediments from the ‘less-active’ center that had virtually no free sulfide showed the same extractable iron concentrations as the highly sulfidic gray mat sediments. Thus available iron-minerals are not or only

slowly reacting or the applied extractions overestimate the actual amount of reactive iron available for sulfide oxidation in the sediments of the Håkon Mosby Mud Volcano. As ascorbic acid and dithionite extract some iron-containing silicates (Kostka and Luther, 1994) and the extruded material has iron-containing minerals like chlorite (Lein et al., 1998), in this setting the methods might extract a larger amount of other iron minerals than previously thought. Most iron-containing silicates have a low reactivity with sulfide ranging from hundreds to thousands of years (Canfield et al., 1992).

Since the precipitation of pyrite produces sulfur isotope fractionations smaller than 1‰, the isotope composition of pyrite is a good approximation of the isotope composition of the source sulfide derived from sulfate reduction. In sediments with sulfate reduction rates of a similar magnitude as those reported here, pyrite that forms directly at the sediment surface is generally more depleted in $^{34}S$ than in the Håkon Mosby Mud Volcano sediments (Lyons, 1997; Schenau et al., 2002) due to biological isotope fractionation (Habicht and Canfield, 1996). Strong $^{34}S$-enrichment of sedimentary sulfides is usually indicative of precipitation from $^{34}S$-enriched dissolved sulfide (Brüchert et al., 2003; Dale et al., 2009). However, the homogeneity of the observed values with depth and between the three different sites supports a common allochthonous origin of the pyrite. We suggest that the pyrite in the mud volcano sediments derives largely from deeply-buried subseafloor deposits and is transported upwards with the mud-gas-fluid mixture. The slightly heavier $\delta^{34}S_{AVS}$ in the sediments under the *Beggiatoa* mat indicates the reservoir effect of an evolving dissolved sulfide pool due to ongoing bacterial sulfate reduction. The much stronger $^{34}S$-enrichment of near-surface AVS, e.g. compared to the sediments from the 'less active' center (Fig. 4d, h), indicates a smaller isotope effect from combined sulfate reduction and sulfide oxidation, in agreement with recent modeling studies on sediment inhabited by the phylogenetically related large sulfur bacteria *Thiomargarita* (Brüchert et al., 2003; Dale et al., 2009). AVS is generally considered as an intermediate in the formation of pyrite and as an active intermediate during sulfide oxidation (Berner, 1970; Schippers and Jørgensen, 2002). The overall low concentrations of AVS throughout the cored sediment indicate that AVS, like pyrite, is not an important sulfide sink. Although we cannot provide quantitative estimates of the turnover time of the AVS fraction, it is likely that the iron-sulfides make up only a small fraction of the total sulfide turnover in these sediments because the rate of supply of detrital reactive iron and the lack of bioturbating organisms limit the availability of reactive iron for iron-sulfide formation.

*Chemosynthetic biomass production*. We observed that most of the sulfide oxidation at the Håkon Mosby Mud Volcano is carried out by sulfide-oxidizing bacteria. Marine chemolithotrophic *Beggiatoa* gain a biomass of 8.4-15.9 g dry weight per mole sulfide oxidized (Nelson et al., 1986; Hagen and Nelson, 1997). Thus a sulfide flux of 11.6 mmol $m^{-2}\,d^{-1}$ (equal to 4.2 mol $m^{-2}\,yr^{-1}$) corresponds to 1.5-2.8 mol C production per $m^2$ in one year, assuming that 50% of the dry weight is carbon. On the whole densely *Beggiatoa* covered area of 38,244 $m^2$ (>50% dense bacterial coverage, Jerosch et al., 2007)

biomass production due to sulfide oxidation by *Beggiatoa* will then be $5.7x10^4$-$1.1x10^5$ mol C $yr^{-1}$. A complete turnover of thiotrophic biomass occurs within 4 days (0.8 g dry weight $m^{-2}$ respectively $1.2x10^3$ mol C in the total habitat / $1.1x10^5$ mol C $yr^{-1}$ biomass gain). This is realistic as the experimentally determined doubling time for *Beggiatoa* is approximately 1 day (Kamp et al., 2008), and high grazing pressure might control the standing stock efficiently (Van Gaever et al., 2006).

With the oxidation of one mole sulfide *Beggiatoa* fixes 0.35 mol $CO_2$ (Nelson et al., 1986). Thus 1.5 mol $CO_2$ is fixed per $m^2$ in one year (4.2 mol $m^{-2}$ $yr^{-1}$ x 0.35) respectively $5.6x10^4$ mol $CO_2$ is fixed in the total *Beggiatoa* habitat per year.

Compared to biomass production from sulfide oxidation, the biomass yield from AOM is low with a gain of 0.03 mol C fixed per mole methane oxidized (Nauhaus et al. 2007). Assuming methane consumption equals sulfide production (11.6 mmol $m^{-2}$ $d^{-1}$ or 4.2 mol $m^{-2}$ $yr^{-1}$), then 0.11 mol C $m^{-2}$ $yr^{-1}$ is produced by AOM. This is in total $4x10^3$ mol C $yr^{-1}$ for the *Beggiatoa* habitat. In the surface sediment of this habitat also aerobic methanotrophs are abundant (Lösekann et al., 2007). Biomass yield by aerobic methane oxidation is more difficult to calculate, as the amount of aerobically oxidized methane and the yield from methane oxidation at in situ conditions is not properly determined. Leak and Dalton (1986) came up with approximately 8 g biomass fixed per mole methane oxidized through the aerobic pathway. Assuming 10% of the oxygen consumption is due to aerobic methane oxidation as 10% of the microbes in the upper sediment layer of the *Beggiatoa* habitat are methanotrophs (Lösekann et al., 2007), 0.2 mol C $m^{-2}$ $yr^{-1}$ or $7.7x10^3$ mol C $yr^{-1}$ in the whole *Beggiatoa* area is fixed (note: stoichiometry $CH_4$:$O_2$ = 1:2). In summary, in this habitat the largest amount of biomass is produced by *Beggiatoa* via the oxidation of sulfide, whereas AOM and aerobic methane oxidation contribute maximally 20%.

### 4.2. Gray Mat Habitat

*Sulfide production*. Large differences in sulfide fluxes and sulfate reduction rates and variable but relatively high temperature gradients (Table 3, 4) indicate large heterogeneity of the gray mat habitat, which is most likely associated with dissociating gas hydrates. Sulfide concentrations were high and sulfide penetrated deep. This can be explained by absence of upward fluid flow and diffusion as dominant mass transport process. Assuming 1) steady state, 2) absence of advective flow, and 3) complete conversion of sulfate to sulfide as only S-converting process (e.g. no sulfide is oxidized), then at any depth below the oxic zone:

$$C_x\text{sulfide} = C_0\text{sulfide} - (C_x\text{sulfate} - C_0\text{sulfate})\,\frac{D_{\text{sulfate}}}{D_{\text{sulfide}}} \qquad \text{(Eq. 9)}$$

where $C_0$sulfide and $C_0$sulfate are sulfide and sulfate concentrations at the sediment-water interface, $C_x$sulfide and $C_x$sulfate are sulfide and sulfate concentrations at sediment depth x, and $D_{sulfide}$ and

$D_{sulfate}$ are molecular diffusion coefficients of the solutes in seawater ($D_{sulfate}$ = 4.3x10$^{-5}$ m$^2$ d$^{-1}$, Li and Gregory, 1974). With a seawater sulfate concentration of 28 mmol L$^{-1}$ and with sulfide in the water column and sulfate at large depth are zero, the maximal concentration of sulfide can be 17 mmol L$^{-1}$. Regarding the high heterogeneity in this habitat, this can be seen as close to what we measured. Thus the three assumptions for the above equation are valid: in gray mat sediments only little or no advective pore water flow occurs, the system is close to steady state and sulfide is not consumed in the anoxic zone. From the shape of the sulfide profile and the above equation it can be concluded that sulfate does not penetrate more than 2 cm. Diffusion as dominant mass transport process in an otherwise advective geosystem can occur, e.g. by spatial restricted blockage of fluid upflow by gas hydrates.

However, pore water profiles showed deeper sulfate penetration (Fig. 5p). This is in conflict with the high sulfate reduction and sulfide production rates and the estimated sulfate penetration depth. In diffusive systems maximum sulfate penetration depth ($Z_{sulfate}$) is controlled by sulfate reduction and can be approximated according to Jørgensen et al. (2004):

$$Z_{sulfate} = \frac{D_{sed}\text{sulfate}\ \phi\ C_0\text{sulfate}}{J_{sulfate}} \quad \text{(Eq. 10)}$$

with variables as defined previously and $J_{sulfate}$ is equal to the areal sulfate reduction rate. Maximum sulfate penetration depth at the averaged depth integrated sulfate reduction rate (59 mmol m$^{-2}$ d$^{-1}$) is approximately 1 cm, which is close to the penetration depth estimated before from the sulfide profile. The discrepancy to the measured pore water concentrations can be explained by mixing of water column sulfate with the gassy sediments during core recovery, which caused the sediments to bubble forcefully due to the pressure loss.

*Biological sulfide oxidation.* Whereas the sulfide flux measurements were variable, oxygen uptake rates were constant. As oxygen and sulfide profiles overlapped, part of the sulfide is oxidized aerobically and is fuelling the mixed thiotrophic mat. Oxidation of sulfide to sulfate with oxygen as terminal electron-acceptor occurs in a ratio of 2:1:

$$HS^- + 2O_2 \rightarrow SO_4^{2-} + H^+ \quad \text{(Eq. 11)}$$

Since the measured flux ratio was less than 1:1, the oxygen flux is too small to oxidize sulfide completely to sulfate. Elevated elemental sulfur concentrations in the upper part of the sediment indicate that sulfide is instead oxidized to elemental sulfur (Eq. 12), which can in turn be used either as electron-acceptor by sulfate-reducing bacteria or can be further oxidized to sulfate by sulfide-oxidizing bacteria.

$$2HS^- + O_2 + 2H^+ \rightarrow 2S^0 + 2H_2O \quad (Eq.12)$$

Active nitrate uptake by the gray mat was indicated by the nitrate uptake experiments (Table 5). Since no sulfide leaked from the sediment, the sum of oxygen and nitrate fluxes should approximate the opposing sulfide flux if precipitation or chemical oxidation with iron is insignificant. Assuming an oxidation of sulfide to elemental sulfur, the nitrate flux into the gray mat habitat therefore will be maximally $^1/_4$ of the sulfide flux (Eq. 2). The morphological diversity and patchy white (sulfur storing filaments) and gray (non sulfur storing filaments) mats hint to a patchwork of sulfide-oxidizing processes in this habitat. The density of motile bacteria that convert nitrate in the anoxic zone is too low to produce a gap between the oxic and the sulfidic zone.

*Potential role of iron in sulfide oxidation.* Sulfide oxidation takes place in the upper centimeter of the sediment (Fig. 8a). Only a very active iron oxidation cycle could supply the system with sufficient iron-oxides to consume the high sulfide fluxes. No elevated concentrations of dithionite or ascorbic acid-extractable iron were found in the top centimeter of the sediment. Oxygen penetration depth (0.5 mm) was smaller than the mat thickness (1 mm) and thus all oxygen was consumed within the mat leaving no oxygen for the chemical oxidation of sedimentary iron-sulfides.

If reactive iron minerals had reacted with sulfide, elemental sulfur would have formed over the full depth and not only in the upper centimeter were the thiotrophic community is present. $S^0$ concentrations in the deeper sediment layers were in the same range as in the center site. Although pyrite concentrations were slightly elevated in the gray mat habitat, the isotopic composition does not show an AOM-derived signal for pyrite sulfur. As in the *Beggiatoa* habitat, the $\delta^{34}S$ values imply that pyrite originated from a deep source, and was not recently formed.

For the role of iron-oxides in sulfide oxidation in the gray mats the same arguments as for the *Beggiatoa* habitat hold: geochemical oxidation of sulfide does not limit bacterial primary production. The most important characteristic of this habitat seems to be its heterogeneity concerning sulfate reduction and thus sulfide flux and diffusion as dominant mass transport processes. However, the gray mat habitat covers only a very small fraction of the Håkon Mosby Mud Volcano and may represent pioneer communities in transient AOM hotspots above dissociating gas hydrate.

### 4.3. 'Less Active' Center Site

*Sulfide production.* The decreased temperature gradient suggests substantially less fluid upflow in the outer rim NE and S of the 'active' center, here referred to as 'less active' center, and marked by small elevations in the seafloor bathymetry (Fig. 1; Table 3). Low sulfate reduction rates were

measured at the northern site and sulfide was detected in pore water and in situ microsensor measurements in the southern 'less active' site. Obviously, decreased fluid upflow in contrast to the 'active center' allows some sulfate to penetrate the sediment and enables AOM-driven sulfate reduction to some extent (de Beer et al., 2006).

*Geochemical and biological turnover and chemosynthetic biomass production.* In the 'less active' center site $Fe^{2+}$ is migrating upwards with the mud volcano fluids with a flux of 0.1 mmol $m^{-2}$ $d^{-1}$ and is vanishing at the interface concurrent with sulfide. As the sulfide flux in this area is substantially lower than in all other habitats (Table 4), chemical immobilization with dissolved iron is significant and removes around 10% of the sulfide (Fig. 10). Precipitation of dissolved iron with isotopically light sulfide derived from AOM is visible in the sulfur isotope distribution (Fig. 4d). The isotope composition of AVS indicates the active involvement of this iron-sulfide pool in the sulfur cycling near the sediment surface. The strong $^{34}S$-depletion of AVS in the sediments from the 'less active' center reflects the strong fractionation effect of sulfate-reducing bacteria under conditions where sulfate is not limiting (Canfield, 2001). Iron-sulfides extracted in the AVS fraction are known to exchange sulfide rapidly with ambient pore water (Fossing and Jørgensen, 1989). The continuous enrichment in AVS with depth in these sediments therefore indicates the exchange of iron-bound sulfide with coexisting hydrogen sulfide that becomes more $^{34}S$-enriched with depth. Below 5 cm depth FeS showed an isotopic composition as in other habitats and this displays background values from the deep sediment source. No thiotrophic mat was visible on top of the center sediments. Sulfide and oxygen profiles did overlap (Fig. 6b) and 20% of the oxygen flux will be used for oxidation of the remaining sulfide flux. This process might be purely chemical as Lösekann et al. (2007) reported that the oxic part of the center sediment is clearly dominated by methylotrophic γ-proteobacteria (affiliated with *Methylobacter*, *Methylophaga*). Indeed major oxygen uptake will be by aerobic methanotrophs. Assuming the same growth yields for aerobic methane oxidation as stated above, maximally 0.6 mol C $m^{-2}$ $yr^{-1}$ will be produced. In the mud volcano center without the active parts (115,000 $m^2$ (Jerosch et al., 2007) – 10,000 $m^2$ active area as estimated from visual observations) maximally $6.1 \times 10^4$ mol C $yr^{-1}$ will be produced by aerobic methane oxidation. Biomass production due to AOM (calculated from sulfide fluxes) will be as small as $6.7 \times 10^2$ mol C $yr^{-1}$.

In the 'active' center only aerobic methane oxidation occurs. Here in total 1.9 mol $m^{-2}$ $yr^{-1}$ methane are consumed (Niemann et al., 2006). This produces a biomass of 0.6 mol C $m^{-2}$ $yr^{-1}$ or $6 \times 10^3$ mol C $yr^{-1}$. In total approximately $6.8 \times 10^4$ mol C $yr^{-1}$ will be formed in the center habitat of the Håkon Mosby Mud Volcano, mainly by aerobic oxidation of methane. These are rough estimates as the subdivision in 'active' and 'less active' center is only by sediment surface structure and the in situ energy yield for aerobic methane oxidation has so far not been determined properly.

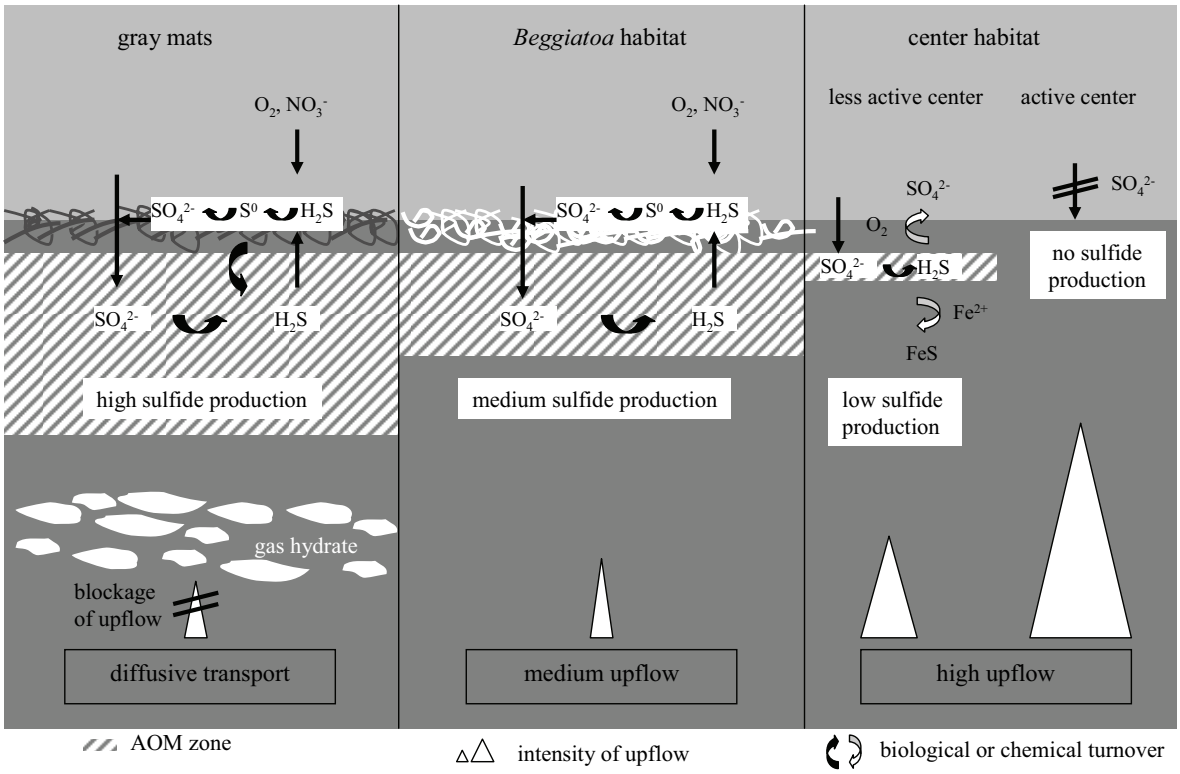


**Fig. 10: Schema of the most important geochemical and microbiological processes in the three investigated areas of the Håkon Mosby Mud Volcano.**

## 5. CONCLUSIONS

At the Håkon Mosby Mud Volcano habitats associated with methane-fueled sulfide production >10 mmol $m^{-2}$ $d^{-1}$ were populated by *Beggiatoa* or thiotrophic bacteria forming gray mats. Geochemical sulfide oxidation with iron-oxides or manganese-oxides, which could reduce the primary production by the thiotrophic bacteria, is of minor importance. Fluxes of oxygen and nitrate are sufficient for a complete consumption of sulfide by the thiotrophs, which assimilate a substantial amount of the AOM-derived $CO_2$ for growth. Sulfide availability depends on the upflow regime, which varies on spatial scales of cm to hundreds of meters. Advective upflow shapes the *Beggiatoa* habitat; in the gray mat area mass transport is mainly by diffusion, resulting in high sulfide concentrations close to the sediment surface. Although methane oxidation coupled to sulfate reduction is mandatory for the sulfide supply, primary productivity in the *Beggiatoa* and gray mat habitat of the Håkon Mosby Mud Volcano is in general dominated by thiotrophic bacteria, and methanotrophs contribute <20%. Because sulfate is limiting sulfide production in both hotspot habitats, AOM leaves a relatively $^{34}S$-enriched isotope signature in the iron monosulfide pool. Pyrite, however, does not represent a significant sink for sulfide formed at the sediment surface. In the zones of the center area with reduced fluid flow, some sulfate can penetrate into the sediment, which results in some sulfide production by AOM-coupled sulfate reduction. The rates, however, appear too low to support thiotrophic mats and chemical oxidation of the upward directed sulfide flux with oxygen and dissolved iron predominates. Thus, in the center of the Håkon Mosby Mud Volcano geochemical sulfide oxidation processes predominate and biomass production is largely limited to direct energy conservation from aerobic and anaerobic methane oxidation.

## REFERENCES

Aloisi, G., M. Drews, K. Wallmann, and G. Bohrmann, 2004. Fluid expulsion from the Dvurechenskii mud volcano (Black Sea) - Part I. Fluid sources and relevance to Li, B, Sr, I and dissolved inorganic nitrogen cycles. *Earth Planet. Sci. Lett.* **225:** 347-363.

Berner, R. A., 1970. Sedimentary pyrite formation. *Am. J. Sci*. **268:** 1-23.

Boetius, A., K. Ravenschlag, C. J. Schubert, D. Rickert, F. Widdel, A. Gieseke, R. Amann, B. B. Jørgensen, U. Witte, and O. Pfannkuche, 2000. A marine microbial consortium apparently mediating anaerobic oxidation of methane. *Nature* **407:** 623-626.

Boetius, A., and E. Suess, 2004. Hydrate Ridge: a natural laboratory for the study of microbial life fueled by methane from near-surface gas hydrates. *Chem. Geol.* **205:** 291-310.

Braman, R. S., and S. A. Hendrix, 1989. Nanogram nitrite and nitrate determination in environmental and biological materials by vanadium(III) reduction with chemiluminescence detection. *Anal. Chem.* **61:** 2715-2718.

Brüchert, V., B. B. Jørgensen, K. Neumann, D. Riechmann, M. Schlösser, and H. Schulz, 2003. Regulation of bacterial sulfate reduction and hydrogen sulfide fluxes in the central Namibian coastal upwelling zone. *Geochim. Cosmochim. Acta* **67:** 4505-4518.

Canfield, D. E., 1989. Reactive iron in marine sediments. *Geochim. Cosmochim. Acta* **53:** 619-632.

Canfield, D. E., 2001. Isotope fractionation by natural populations of sulfate-reducing bacteria. *Geochim. Cosmochim. Acta* **65:** 1117-1124.

Canfield, D. E., R. Raiswell, and S. Bottrell, 1992. The reactivity of sedimentary iron minerals toward sulfide. *Am. J. Sci.* **292:** 659-683.

Cline, J. D., 1969. Spectrophotometric determination of hydrogen sulfide in natural waters. *Limnol. Oceanogr.* **14:** 454-458.

Cordes, E. E., M. A. Arthur, K. Shea, R. S. Arvidson, and C. R. Fisher, 2005. Modeling the mutualistic interactions between tubeworms and microbial consortia. *PLoS Biol*. **3:** 497-506.

Dale, A. W., V. Brüchert, M. Alperin, and P. Regnier, 2009. An integrated sulfur isotope model for Namibian shelf sediments. *Geochim. Cosmochim. Acta* **73:** 1924-1944.

de Beer, D., A. Glud, E. Epping, and M. Kühl, 1997. A fast responding $CO_2$ microelectrode for profiling sediments, microbial mats and biofilms. *Limnol. Oceanogr.* **42:** 1590-1600.

de Beer, D., E. Sauter, H. Niemann, N. Kaul, J.-P. Foucher, U. Witte, M. Schlüter, and A. Boetius, 2006. In situ fluxes and zonation of microbial activity in surface sediments of the Håkon Mosby Mud Volcano. *Limnol. Oceanogr.* **51:** 1315-1331.

Drobner, E., H. Huber, G. Wächtershäuser, D. Rose, and K. O. Stetter, 1990. Pyrite formation linked with hydrogen evolution under anaerobic conditions. *Nature* **346:** 742-744.

Duperron, S., T. Nadalig, J. C. Caprais, M. Sibuet, A. Fiala-Medioni, R. Amann, and N. Dubilier, 2005. Dual symbiosis in a *Bathymodiolus* sp. mussel from a methane seep on the Gabon

continental margin (southeast Atlantic): 16S rRNA phylogeny and distribution of the symbionts in gills. *Appl. Environ. Microbiol.* **71:** 1694-1700.

Ferdelman, T. G., T. M. Church, and G. W. Luther, 1991. Sulfur enrichment of humic substances in a Delaware salt marsh sediment core. *Geochim. Cosmochim. Acta* **55:** 979-988.

Ferdelman, T. G., C. Lee, S. Pantoja, J. Harder, B. M. Bebout, and H. Fossing, 1997. Sulfate reduction and methanogenesis in a *Thioploca*-dominated sediment off the coast of Chile. *Geochim. Cosmochim. Acta* **61:** 3065-3079.

Fossing, H., and B. B. Jørgensen, 1989. Measurement of bacterial sulfate reduction in sediments: evaluation of a single-step chromium reduction method. *Biogeochemistry* **8:** 205-222.

Foucher, J. P., G. K. Westbrook, A. Boetius, S. Ceramicola, S. Dupre, J. Mascle, J. Mienert, O. Pfannkuche, C. Pierre, and D. Praeg, 2009. Structure and drivers of cold seep ecosystems. *Oceanography* **22:** 92-109.

Habicht, K., and D. E. Canfield, 1996. Sulphur isotope fractionation in modern microbial mats and the evolution of the sulphur cycle. *Nature* **382:** 342-343.

Hagen, K. D., and D. C. Nelson, 1997. Use of reduced sulfur compounds by *Beggiatoa* spp.: Enzymology and physiology of marine and freshwater strains in homogeneous and gradient cultures. *Appl. Environ. Microbiol.* **63:** 3957-3964.

Hall, P. O., and R. C. Aller, 1992. Rapid, small-volume, flow injection analysis for $\Sigma CO_2$ and $NH_4^+$ in marine and freshwaters. *Limnol. Oceanogr.* **37:** 1113-1119.

Hinck, S., T. R. Neu, G. Lavik, M. Mussmann, D. de Beer, and H. M. Jonkers, 2007. Physiological adaptation of a nitrate-storing *Beggiatoa* sp. to diel cycling in a phototrophic hypersaline mat. *Appl. Environ. Microbiol.* **73:** 7013-7022.

Hjelstuen, B. O., O. Eldholm, J. I. Faleide, and P. R. Vogt, 1999. Regional setting of Håkon Mosby Mud Volcano, SW Barents Sea margin. *Geo-Mar. Lett.* **19:** 22-28.

Iversen, N., and B. B. Jørgensen, 1993. Diffusion coefficients of sulfate and methane in marine sediments: Influence of porosity. *Geochim. Cosmochim. Acta* **57:** 571-578.

Jerosch, K., M. Schlüter, J.-P. Foucher, A.-G. Allais, M. Klages, and C. Edy, 2007. Spatial distribution of mud flows, chemoautotrophic communities, and biogeochemical habitats at Håkon Mosby Mud Volcano. *Mar. Geol.* **243:** 1-17.

Jeroschewski, P., C. Steuckart, and M. Kühl, 1996. An amperometric microsensor for the determination of $H_2S$ in aquatic environments. *Anal. Chem.* **68:** 4351-4357.

Jørgensen, B. B., 1978. A comparison of methods for the quantification of bacterial sulfate reduction in coastal marine sediments: 1. Measurements with radiotracer techniques. *Geomicrobiol. J.* **1:** 11-27.

Jørgensen, B. B., M. E. Böttcher, H. Lüschen, L. N. Neretin, and I. I. Volkov, 2004. Anaerobic methane oxidation and a deep $H_2S$ sink generate isotopically heavy sulfides in Black Sea sediments. *Geochim. Cosmochim. Acta* **68:** 2095-2118.

Jørgensen, B. B., and N. P. Revsbech, 1985. Diffusive boundary layers and the oxygen uptake of sediments and detritus. *Limnol. Oceanogr.* **30:** 111-122.

Kallmeyer, J., T. G. Ferdelman, A. Weber, H. Fossing, and B. B. Jørgensen, 2004. A cold chromium distillation procedure for radiolabeled sulfide applied to sulfate reduction measurements. *Limnol. Oceanogr.: Methods* **2:** 171-180.

Kamp, A., H. Røy, and H. N. Schulz-Vogt, 2008. Video-supported analysis of *Beggiatoa* filament growth, breakage, and movement. *Microb. Ecol.* **56:** 484-491.

Kamp, A., P. Stief, and H. N. Schulz-Vogt, 2006. Anaerobic sulfide oxidation with nitrate by a freshwater *Beggiatoa* enrichment culture. *Appl. Environ. Microbiol.* **72:** 4755-4760.

Kostka, J. E., and G. W. Luther, 1994. Partitioning and speciation of solid phase iron in saltmarsh sediments. *Geochim. Cosmochim. Acta* **58:** 1701-1710.

Leak, D. J., and H. Dalton, 1986. Growth yields of methanotrophs: 1. Effect of copper on the energetics of methane oxidation. *Appl. Microbiol. Biotechnol.* **23:** 470-476.

Lein, A. Y., P. Vogt, K. Crane, A. V. Egorov, N. V. Pimenov, A. S. Savichev, G. D. Ginsburg, G. I. Ivanov, G. A. Cherkashev, and M. V. Ivanov, 1998. Geochemical features of gas-bearing ($CH_4$) deposits of a submarine mud volcano in the Norwegian sea. *Geokhimiya***:** 230-249.

Li, Y.-H., and S. Gregory, 1974. Diffusion of ions in sea water and in deep-sea sediments. *Geochim. Cosmochim. Acta* **38:** 703-714.

Lösekann, T., K. Knittel, T. Nadalig, B. Fuchs, H. Niemann, A. Boetius, and R. Amann, 2007. Diversity and abundance of aerobic and anaerobic methane oxidizers at the Haakon Mosby Mud Volcano, Barents Sea. *Appl. Environ. Microbiol.* **73:** 3348-3362.

Lösekann, T., A. Robador, H. Niemann, K. Knittel, A. Boetius, and N. Dubilier, 2008. Endosymbioses between bacteria and deep-sea siboglinid tubeworms from an Arctic Cold Seep (Haakon Mosby Mud Volcano, Barents Sea). *Environ. Microbiol.* **10:** 3237-3254.

Luther, G. W., 1991. Pyrite synthesis via polysulfide compounds. *Geochim. Cosmochim. Acta* **55:** 2839-2849.

Lyons, T. W., 1997. Sulfur isotopic trends and pathways of iron sulfide formation in upper Holocene sediments of the anoxic Black Sea. *Geochim. Cosmochim. Acta* **61:** 3367-3382.

McHatton, S. C., J. P. Barry, H. W. Jannasch, and D. C. Nelson, 1996. High nitrate concentrations in vacuolate, autotrophic marine *Beggiatoa* spp. *Appl. Environ. Microbiol.* **62:** 954-958.

Milkov, A. V., P. R. Vogt, K. Crane, A. Y. Lein, R. Sassen, and G. A. Cherkashev, 2004. Geological, geochemical, and microbial processes at the hydrate-bearing Håkon Mosby mud volcano: a review. *Chem. Geol.* **205:** 347-366.

Mussmann, M., H. N. Schulz, B. Strotmann, T. Kjaer, L. P. Nielsen, R. A. Rossello-Mora, R. I. Amann, and B. B. Jørgensen, 2003. Phylogeny and distribution of nitrate-storing *Beggiatoa* spp. in coastal marine sediments. *Environ. Microbiol.* **5:** 523-533.

Nauhaus, K., M. Albrecht, M. Elvert, A. Boetius, and F. Widdel, 2007. *In vitro* cell growth of marine archaeal-bacterial consortia during anaerobic oxidation of methane with sulfate. *Environ. Microbiol.* **9:** 187-196.

Nelson, D. C., B. B. Jørgensen, and N. P. Revsbech, 1986. Growth pattern and yield of a chemoautotrophic *Beggiatoa* sp. in oxygen-sulfide microgradients. *Appl. Environ. Microbiol.* **52:** 225-233.

Niemann, H., T. Lösekann, D. de Beer, M. Elvert, T. Nadalig, K. Knittel, R. Amann, E. J. Sauter, M. Schlüter, M. Klages, J.-P. Foucher, and A. Boetius, 2006. Novel microbial communities of the Haakon Mosby mud volcano and their role as a methane sink. *Nature* **443:** 854-858.

Preisler, A., D. de Beer, A. Lichtschlag, G. Lavik, A. Boetius, and B. B. Jørgensen, 2007. Biological and chemical sulfide oxidation in a *Beggiatoa* inhabited marine sediment. *ISME J.* **1:** 341-353.

Revsbech, N. P., and D. M. Ward, 1983. Oxygen microelectrode that is insensitive to medium chemical composition - use in an acid microbial mat dominated by *Cyanidium caldarium*. *Appl. Environ. Microbiol.* **45:** 755-759.

Sahling, H., D. Rickert, R. W. Lee, P. Linke, and E. Suess., 2002. Macrofaunal community structure and sulfide flux at gas hydrate deposits from the Cascadia convergent margin, NE Pacific. *Mar. Ecol. Prog. Ser.* **231:** 121-138.

Sayama, M., N. Risgaard-Petersen, L. P. Nielsen, H. Fossing, and P. B. Christensen, 2005. Impact of bacterial $NO_3^-$ transport on sediment biogeochemistry. *Appl. Environ. Microbiol.* **71:** 7575-7577.

Schenau, S. J., H. F. Passier, G. J. Reichart, and G. J. de Lange, 2002. Sedimentary pyrite formation in the Arabian Sea. *Mar. Geol.* **185:** 393-402.

Schippers, A., and B. B. Jørgensen, 2002. Biogeochemistry of pyrite and iron sulfide oxidation in marine sediments. *Geochim. Cosmochim. Acta* **66:** 85-92.

Sibuet, M., and K. Olu, 1998. Biogeography, biodiversity and fluid dependence of deep-sea cold-seep communities at active and passive margins. *Deep-Sea Res. Pt. II* **45:** 517-567.

Stookey, L. L. 1970, Ferrozine - a new spectrophotometric reagent for iron. *Anal. Chem.* **42:** 779-781.

Teske, A., Nelson, D.C. 2006, The genera *Beggiatoa* and *Thioploca*, p. 784-810. *In* M. Dworkin, Falkow, S., Rosenberg, E., Schleifer, K-H, and Stackebrandt, E. [ed.], *Prokaryotes*. Springer.

Treude, T., A. Boetius, K. Knittel, K. Wallmann, and B. B. Jørgensen, 2003. Anaerobic oxidation of methane above gas hydrates at Hydrate Ridge, NE Pacific Ocean. *Mar. Ecol. Prog. Ser.* **264:** 1-14.

Van Gaever, S., L. Moodley, D. de Beer, and A. Vanreusel, 2006. Meiobenthos at the Arctic Håkon Mosby Mud Volcano, with a parental-caring nematode thriving in sulphide-rich sediments. *Mar. Ecol. Prog. Ser.* **321:** 143-155.

Vogt, P. R., G. Cherkashev, G. Ginsburg, G. Ivanov, A. Milkov, K. Crane, A. Lein, E. Sundvor, N. Pimenov, and A. Egorov, 1997. Haakon Mosby mud volcano provides unusual example of venting. *EOS* **78:** 549-549.

Wallmann, K., M. Drews, G. Aloisi, and G. Bohrmann, 2006. Methane discharge into the Black Sea and the global ocean via fluid flow through submarine mud volcanoes. *Earth Planet. Sci. Lett.* **248:** 545-560.

Wenzhöfer, F., O. Holby, R. N. Glud, H. K. Nielsen, and J. K. Gundersen, 2000. In situ microsensor studies of a shallow water hydrothermal vent at Milos, Greece. *Mar. Chem.* **69:** 43-54.

Zopfi, J., Ferdelman, T.G., Fossing, H., 2004. Distribution and fate of sulfur intermediates – sulfite, tetrathionate, thiosulfate, and elemental sulfur – in marine sediments., p. 97-116. *In* E. K. Amend J., Lyons T. [eds.], Sulfur biogeochemistry: Past and present. *Geological Society of America Special Paper.*

Chapter 3

# Biological and chemical sulfide oxidation in a *Beggiatoa* inhabited marine sediment

André Preisler, Dirk de Beer, Anna Lichtschlag, Gaute Lavik, Antje Boetius and Bo Barker Jørgensen

Max-Planck-Institute for Marine Microbiology, Celsiusstrasse 1, 28359 Bremen, Germany

published in the *ISME Journal 1(2007)**1**:341-353*

*Acknowledgements.*

We thank our colleagues Tim Ferdelman, Tina Treude and Susanne Hinck for valuable comments, and our technicians Gaby Eickert, Ines Schröder, Karin Hohmann for supply of excellent microsensors and assistance during the measurements. Else Wieringa is acknowledged for the nitrate measurements. We thank Wolfgang Queisser (IfM-GEOMAR) for his generous hospitality and for using his workshop as laboratory. We thank the crew of the Littorina (IfM-GEOMAR) for the sampling and help with deployments. The study is supported by the Bundesministerium für Bildung und Forschung and the Deutsche Forschungsgemeinschaft in the frame of the GEOTECHNOLOGIEN project MUMM (FKZ G0554A, 03G0608A) and the Max-Planck-Institute for Marine Microbiology.

**Abstract**

**The ecological niche of nitrate-storing *Beggiatoa*, and their contribution to the removal of sulfide were investigated in coastal sediment. With microsensors a clear suboxic zone of 2-10cm thick was identified, where neither oxygen nor free sulfide was detectable. In this zone most of the *Beggiatoa* were found, where they oxidize sulfide with internally stored nitrate. The sulfide input into the suboxic zone was dominated by an upward sulfide flux from deeper sediment, whereas the local production in the suboxic zone was much smaller. Despite their abundance, the calculated sulfide oxidizing capacity of the *Beggiatoa* could account for only a small fraction of the total sulfide removal in the sediment. Consequently, most of the sulfide flux into the suboxic layer must have been removed by chemical processes, mainly by precipitation with $Fe^{2+}$ and oxidation by Fe(III), which was coupled with a pH increase. The free $Fe^{2+}$ diffusing upwards was oxidized by Mn(IV), resulting in a strong pH decrease. The nitrate storage capacity allows *Beggiatoa* to migrate randomly up and down in anoxic sediments with an accumulated gliding distance of 4 m before running out of nitrate. We propose that the steep sulfide gradient and corresponding high sulfide flux, a typical characteristic of *Beggiatoa* habitats, is not needed for their metabolic performance, but rather used as a chemotactic cue by the highly motile filaments to avoid getting lost at depth in the sediment. Indeed sulfide is a repellant for *Beggiatoa*.**

## 1. INTRODUCTION

*Beggiatoa* are multicellular, filamentous, colorless sulfur bacteria of the γ-proteobacteria clade, inhabiting freshwater, marine and hypersaline sediments and forming distinct white mats. The large marine sulfide oxidizers *Beggiatoa* and *Thioploca*, with filament diameters >10 μm, and *Thiomargarita*, can all store nitrate in vacuoles (Fossing et al., 1995; Schulz et al., 1999) up to a concentration of 370 mM (McHatton et al., 1996; Ahmad et al., 1999). In sediments containing *Beggiatoa*, total nitrate concentrations can be orders of magnitude higher than in the overlying seawater due to intracellular storage (Sayama, 2001; de Beer et al., 2006). This intracellular nitrate is used to oxidize sulfide in deeper anoxic zones of sediments. The oxidation most probably proceeds via dissimilatory nitrate reduction to ammonium (DNRA) (Vargas and Strohl, 1985; McHatton et al., 1996; Schulz and Jørgensen, 2001; Sayama et al., 2005). Sulfide is oxidized first to elemental sulfur (Nelson et al., 1986) and stored in globules that give the mats a white appearance. In a second step, the sulfur is further oxidized to sulfate (Otte et al., 1999).

*Beggiatoa* inhabits strongly reduced, organic-rich or hydrocarbon-rich, porous sediments, with sufficient interstitial space for motility (Jørgensen, 1977). Commonly, the oxic and sulfidic zones are separated by a zone where neither is present in measurable concentration (≤1 μM), further called the suboxic zone (Froelich et al., 1979; Berner, 1981). *Beggiatoa* is thought to be a cause of the separation, because of its abundance and its capacity to anaerobically oxidize sulfide with nitrate (Sayama et al., 2005). Indeed, up to 20 g *Beggiatoa* biomass per $m^2$ was found in Limfjorden (Jørgensen, 1977). A more classical explanation for the suboxic zone is chemical sulfide oxidation with Fe(III) as electron-acceptor. Fe(III) is rapidly formed by oxidation of $Fe^{2+}$ with oxygen. As Fe(III) is insoluble, it needs to be transported into the suboxic zone by sediment reworking, for example by bioturbation or by hydrodynamics. Both the transport rate and the specific reactivity of Fe(III)-bearing minerals can limit the chemical oxidation of sulfide in sediments (Canfield, 1989).

Thus, sulfide oxidation by *Beggiatoa*, or other sulfur bacteria, may compete with chemical oxidation. In Limfjorden sediments, *Beggiatoa* can oxidize 50% or more of the produced free sulfide (Jørgensen, 1977; Mussmann et al., 2003). Experimental studies showed that *Thioploca* communities off the coast of Chile have the potential to oxidize 25-91% of the free sulfide produced by sulfate reduction (Otte et al., 1999). Field studies suggest that *Thioploca* can oxidize a maximum of 16-34% of sulfide production (Ferdelman et al., 1997). The actual importance of nitrate-storing bacteria for the benthic sulfur cycle can thus vary strongly, whereas the contribution by chemical oxidation remains uncertain.

We studied the physiology and chemotactic responses of *Beggiatoa* to explain its role in the N and S conversions in their preferred habitat. We characterized sediments that are densely colonized by

*Beggiatoa* using microsensors, we studied the metal chemistry in the *Beggiatoa* zone, and estimated the sulfide oxidation rates by *Beggiatoa* and by chemical processes.

## 2. METHODS

### 2.1. Sampling

Sediments were sampled in cores with a diameter of 10 cm, using a small multiple corer (Barnett et al., 1984), on four fieldtrips in 2002 and 2003 in Eckernförde Bay, Germany (54°31.30N, 10°02.18E, 54°31.15N, 10°01.28E) at a water depth of 25-28 m. A detailed description of the sampling site is published (Treude et al., 2005). The sediments were transported to a laboratory near the sampling site (IfM-Geomar, Kiel, Germany), where the analyses were immediately started. The vertical distributions of the light (oxidized) and dark (reduced) zones were similar in parallel cores used for porosity, chemical analysis, biomass determinations and microsensor analyses. Cores that were not immediately used were stored at 15 ºC.

### 2.2. Microsensor Measurements

*Retrieved sediments*. Microprofiles in retrieved sediment cores were measured within 3 days after sampling. The measurements were performed at 15 ºC. The overlying water was stirred gently by an air jet over the water surface. Profiles of nitrate plus nitrite were measured with a biomicrosensor (Larsen et al., 1997), having a tip diameter of 100 µm and a 90% response time ($t_{90}$) of 2 min. Microsensors for $O_2$, $H_2S$ and pH were made and used as described previously (Revsbech, 1989; Jeroschewski et al., 1996; de Beer, 2000). The tip diameters were ca. 10 µm, the $t_{90}$ <3 s. The microsensors were mounted on a motor-driven micromanipulator. Motor control and data acquisition were done using a computer. The position of the sediment surface was determined with a dissection scope. The total dissolved sulfide profiles were calculated from the measured $H_2S$ and pH microprofiles (Jeroschewski et al., 1996). The value for p$K_1$ (for the equilibrium between $H_2S$ and $HS^-$) used was corrected for temperature and salinity (22%) (Millero et al., 1988).

*In situ*. The shafts of $O_2$, $H_2S$ and pH microsensors (three each) were elongated with 40 cm glass tubes, to a total length of 57 cm. The sensors were calibrated after mounting on a deep-sea profiler (Wenzhöfer et al., 2000). The sensors were mounted on the bottom of the titanium housing within a horizontal distance of maximally 11 cm. The titanium housing, containing amplifiers and a computer for data acquisition and motor control, could be moved vertically by a spindle in a threading on the frame, with a smallest step size of 25 µm. The motor on top of the housing was connected directly to the spindle. The relative vertical positions of the sensor tips were carefully measured, so that the resulting profiles could be aligned. The profiler was preprogrammed to measure a vertical profile, with

steps of 250 µm, over a depth of 50 cm. Each step included a waiting time of 4 s before a reading was made, consisting of the average of four samplings in a time interval of 4 s. The profiling started 2 h after deployment. The profiler was mounted on a frame and deployed with a winch.

For profile analysis, the surface was taken as reference point (depth = 0), defined by the steepest slope of the oxygen profile. From the in situ and ex situ measured steady state sulfide profiles, we calculated the local diffusive fluxes, using Ficks law of diffusion ($J = D_s dC/dx$, with $D_s$ the effective diffusion coefficient and dC/dx the local gradients). $D_s$ was calculated from the molecular diffusion coefficient ($D_w$), corrected for salinity and temperature (Li and Gregory, 1974) and the porosity ($\varphi$) (Ullman and Aller, 1982) using $D_s = \varphi^2 D_w$, resulting in $8.3 \times 10^{-10}$ $m^2/s$ for sulfide at 15 °C. Porosity was determined from the weight loss upon drying at 60 °C for 72 h. The density was determined by weighing known volumes of sediment. The local sulfide conversion rates were obtained from reaction-transport calculations (Gieseke and de Beer, 2004). As no sulfide left the sediment, the sum of the local sulfate reduction rates, as published by Treude et al. (2005) and the influx of free sulfide from deeper sediments was equal to the total free sulfide consumption in the suboxic zone.

### 2.3. Biomass Determination

*Beggiatoa* biomass was determined within 1 day after sampling. A core was sliced in 0.5-1 cm intervals, and subsamples from each interval (300-500 mg) were suspended in filtered seawater (10 mL). From 300-400 mg of this suspension, the *Beggiatoa* filaments were enumerated by microscopy. The biomass was calculated from the filament volume (cylindrical shape) assuming a density of 1 g $cm^{-3}$.

### 2.4. Cell-specific Nitrate Reduction and Sulfide Oxidation Rates

Samples (0.8 mL) from the upper 3 cm of sediment were transferred into glass vials, 0.2 mL seawater was added, and the vials sealed by a rubber stopper. One vial was left open to serve as oxygenated reference. After 12, 20 and 42 days, two vials were used for intracellular nitrate, biomass and motility measurements. Cell motility, as a measure for viability, was determined from a parallel vial by microscopy. The nitrate reduction rate by *Beggiatoa* was determined from the decrease of the intracellular nitrate. Sulfide oxidation rates were calculated from the nitrate reduction rates assuming a stoichiometry $H_2S/NO_3^-$ of 1 or 4, for the oxidation to sulfate or sulfur, respectively.

### 2.5. Total Sedimentary Nitrate and Elemental Sulfur Measurements

Sediment cores were sliced in 0.5-1 cm intervals, fixed in ZnAc (20 mL, 20% solution), frozen and thawed. Pore water was extracted by centrifugation at 3000 g for 10 min. This procedure was found to reproducibly release and extract vacuolar nitrate. Nitrite plus nitrate were measured in the supernatant

with a $NO_x$ Analyser (Thermo Environmental Instruments, Franklin, MA, USA) based on $NO_3^-$ and $NO_2^-$ reduction to NO by $V(III)Cl_3$ (in 1M HCl) (Braman and Hendrix, 1989).

Sulfur was extracted from the pellet of the centrifuged samples with methanol (100%). Elemental sulfur, S(0), was determined by high performance liquid chromatography (Zopfi et al., 2004).

**2.6. Intracellular Nitrate and Intracellular Sulfur Determination**

Intracellular nitrate was measured in *Beggiatoa* filaments immediately after sectioning of the core. Filaments from the different sediment depths were transferred into artificial seawater (22%) using a glass needle. Their length and width were determined by microscopy and the biovolume was calculated assuming a cylindrical shape. The whole procedure took about 1-2 h per sediment layer. Several filaments (7-11) of the same diameter (24 or 30 µm) were transferred into 250 µL of demineralized water and frozen at -20 °C, causing cell rupture. After thawing, the samples were centrifuged (3000 g) and nitrate was measured in the supernatant as described above. On the basis of biovolume and the dilution factor, the average intracellular nitrate concentrations were determined. The remaining pellet was dried in air and the intracellular elemental sulfur grains of *Beggiatoa* were dissolved in methanol (100%) over 2-3 days. The elemental sulfur was measured as described above.

**2.7. Nitrate Reduction Rates Measured with Stable Isotope**

From a sediment core of 10 cm diameter, the upper 2 cm that contained the *Beggiatoa* was removed. Three subcores of 2.5 cm diameter were taken from the remaining sediment. The sediment from the upper layer (0-2 cm) was split, two parts were frozen and thawed, to kill all *Beggiatoa*, and one part was left untreated. The three subcores were then topped up with 2 cm of the differently treated sediment, leaving 5 cm overlying water. Nitrification was inhibited in the untreated sediment that contained *Beggiatoa*, and in one treated core by addition of thiourea to a final concentration of 86 µM. The third core with frozen and thawed sediment, but otherwise untreated, was considered as the control. The overlying water was gently stirred and the cores were incubated in the dark. Directly after preparation of the cores, microsensor measurements of $O_2$, $H_2S$ and pH were performed, and repeated at weekly intervals. After 3 weeks 25 µM $^{15}NO_3^-$ was added to the overlying water, obtaining a total $NO_3^-$ concentration of ca. 40 µM. The cores were left open for 24 h to allow the *Beggiatoa*, if present, to accumulate the $^{15}NO_3^-$. Then the cores were sealed to prevent escape of $^{15}N$-labelled $N_2$ and left for another 24 h. Subsequently, the cores were sectioned in 0.5 cm intervals (0-3 cm depth) or 1 cm intervals (3-5 cm depth) into gastight Exetainers (6 mL, Labco Ltd, High Wycombe, UK) prefilled with 1 mL $HgCl_2$ solution (0.6%) and filled completely with demineralized water and sealed. A 1 mL headspace (helium) was introduced to the Exetainers to extract the labeled $N_2$ gas ($^{29}N_2$ and $^{30}N_2$) from the water phase and, after vigorous shaking of the Exetainers, injected into a gas chromatography-mass spectrometry (GC-MS; VG, Optima, ISOTECH, Middlewich, UK). The 1 mL of sample slurry

extracted by the introduction of the headspace was used to determine the $NO_x$ concentration by the $NO_x$ analyzer, described above. To determine the fraction of the labeled intracellular $NO_3^-$ (% $^{15}NO_3^-$ of total $NO_3^-$) at each depth, we transferred 2 ml of the slurry to another Exetainer, subsequently filled up with demineralized water. After the introduction of a 1 mL helium headspace, all $NO_x$ were reduced to NO by adding 0.5 mL of $TiCl_3$ (Cox and Earp, 1982). This was injected into the GC-MS-injection port, reduced to $N_2$ by the reduction oven (copper at 650 °C) and analyzed by MS. To the remaining slurry (3.5 ml), 0.5 mL of HBr was added to oxidize $^{15}NH_4^+$ to $N_2$ before analysis by GC-MS (Warembourg, 1993), before determination of $^{15}N_2$ by GC-MS. The efficiencies were measured with $^{15}NO_x$ and $^{15}NH_4^+$ standards. To obtain the total DNRA for each depth, the amount of produced $^{15}NH_4^+$ was divided by the $^{15}N$-labeled fraction of $NO_3^-$. The areal nitrate consumption rates were calculated from the decrease of nitrate in the overlying water. The local DNRA was determined from the evolution of $^{15}NH_4^+$, and local denitrification from the evolution of $^{15}N_2$ in each depth interval. The areal rates of DNRA and denitrification were then obtained by integration over depth. The biomass-specific DNRA rates for *Beggiatoa* were calculated as the ratio of the volumetric DNRA (corrected for the DNRA in the cores without *Beggiatoa*) and the volume fraction of *Beggiatoa* in the sediment.

**2.8. Iron and Manganese Analyses**

To obtain the concentrations of dissolved $Fe^{2+}$ and solid-phase iron and manganese, one core was sliced in 1 cm depth intervals within 2 days after sampling. Pore water was extracted using a pore water press, pressurized by nitrogen. During extraction the surface of the core was constantly flushed with nitrogen. Pore water aliquots were immediately acidified and used for the spectrophotometric determination of dissolved $Fe^{2+}$ with the Ferrozine method (Stookey, 1970). The remaining sediment was immediately frozen for later solid-phase analyses. For the determination of various solid iron phases, different iron extraction methods were applied, whereas here only the results of ascorbic acid extractions (Canfield, 1989; Ferdelman et al., 1991) are shown, a method designed to extract reactive iron minerals. For each extraction, 0.4 g frozen sediment was used and the extracts were analyzed with the Ferrozine method (see above).

Solid-phase Mn(IV) concentrations were quantified by extracting 0.2 g of the sediment with the dithionite method (Canfield, 1989). The extracts were analyzed with flame atomic absorption spectrometry. All iron and manganese measurements were carried out in triplicates. The diffusive $Fe^{2+}$ flux was calculated from its profile using an effective diffusion coefficient of $0.52 \times 10^{-10}$ mol $m^{-2}$ $s^{-1}$, assuming $OH^-$ as counter ion (Li and Gregory, 1974), corrected for temperature, salinity and porosity as described above.

## 3. RESULTS

The sediments of Eckernförde Bay consisted of fine mud, with a mean porosity of 0.88 and density of 1.3 g $cm^{-3}$. The top 3-6 cm were dark gray, whereas the deeper sediments were black. The sediments were covered by thin white mats of a *Beggiatoa* community consisting of different size classes with diameters varying from 14 to 40 µm. Although the white film covering the sediments was eye-catching, it represents only a small fraction of the benthic population, by far most of the filaments were inside the sediment (Fig. 1 and 2). Most filaments had a diameter of 24 or 30 µm and were phylogenetically closely related to strains found in Limfjorden (*Beggiatoa* sp., Limfjord, Denmark) and Dangast (*Beggiatoa* sp., Dangast, Germany) (Mussmann et al., 2003; M. Mussmann, personal communication).

### 3.1. Biogeochemistry

In retrieved cores oxygen penetrated 0.1-0.2 cm into the sediment, and nitrate penetrated a few millimeters deeper than oxygen, as measured with microsensors (Fig. 1). Sulfide was detected (>1 µM) only below a depth of 2-6 cm (Fig. 2). All measurements showed a separation between the oxic and sulfidic zone, but the width of this suboxic zone varied. In all investigated sediment cores, *Beggiatoa* was predominantly present above the sulfidic zone (Fig. 2). The distribution was either bell-shaped or a gradual decrease of cell densities with depth was observed. Although occasionally living filaments were found in the sulfidic zone, free sulfide, in concentrations above 1 µM, was clearly not an attractant for *Beggiatoa*. The upward sulfide flux from the sulfidic zone into the suboxic zone varied from core to core, and averaged 4.3 mmol $m^{-2}$ $day^{-1}$ (±2 mmol $m^{-2}$ $day^{-1}$).

Nitrate was measured in sediments that were Zn-treated, frozen, and thawed to open vacuoles and cell membranes of the nitrate-storing organisms. These nitrate profiles strongly differed from the nitrate profiles measured with microsensors. With microsensors only extracellular nitrate is detected. The total nitrate concentrations in *Beggiatoa*-inhabited sediments were much higher than in the overlying water, thus nitrate was actively accumulated inside the cells. The distribution of this intracellular nitrate correlated well with that of *Beggiatoa* biomass (Fig. 1). Occasionally, near the sediment surface, nitrate was much higher than estimated from *Beggiatoa* abundance (Fig. 3a), which indicates that other nitrate-accumulating organisms were present, probably diatoms (Lomstein et al., 1990). In that case, a good agreement between nitrate content and *Beggiatoa* biomass could only be achieved by a procedure where *Beggiatoa* filaments were first removed from sediments, counted and their volume determined. Then they were pooled per sediment depth, and their nitrate was extracted and quantified (Fig. 3a). In conclusion, the nitrate found inside the sediments below 0.3 cm depth originated entirely from *Beggiatoa* vacuoles.

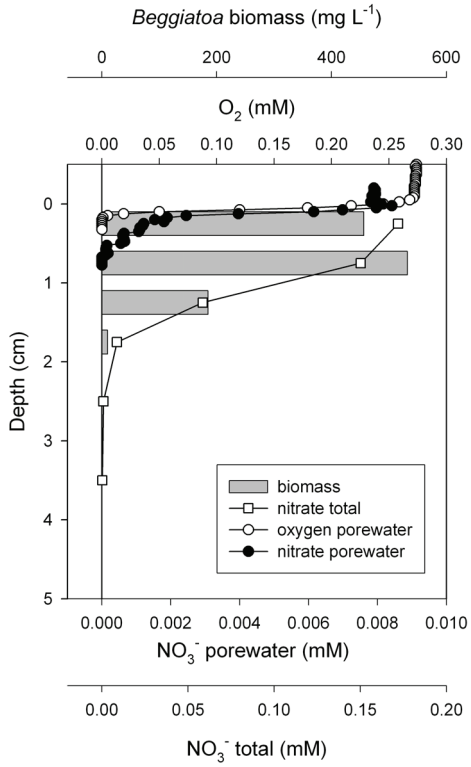


**Fig. 1: Profiles in Eckernförde Bay sediment measured on a retrieved core. Shown are distributions of oxygen and nitrate in pore water, measured with microsensors, total nitrate extracted from frozen and thawed sediment, and *Beggiatoa* biomass.**

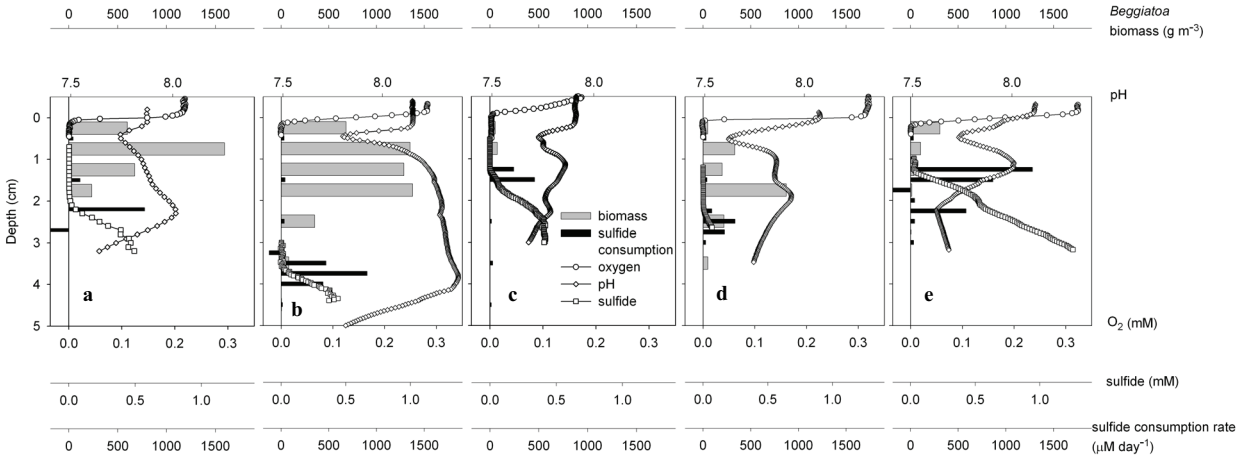


**Fig. 2: Distribution of *Beggiatoa* biomass, microsensor profiles of oxygen, sulfide, and pH, and the rates of sulfide consumption calculated from the local sulfate reduction rates and the sulfide microprofiles. The measurements were made on retrieved cores in a) March 2002, b) March 2002, c) June 2002, d) June 2002, and e) January 2003.**

In contrast to nitrate, only a small fraction of the sulfur in sediments is associated with *Beggiatoa*. Even in the zone with the highest *Beggiatoa* density, less than 10% of the sulfur is intracellular, and the distribution pattern of sulfur is clearly different from that of *Beggiatoa*. Significant sulfur pools are present below the suboxic zone (Fig. 3b).

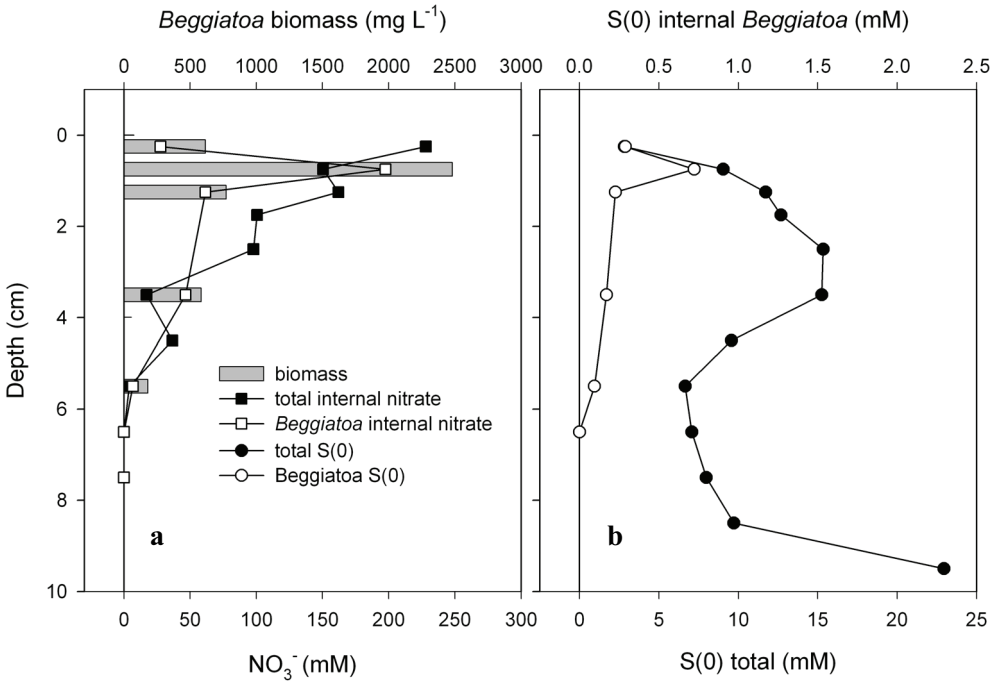


**Fig. 3: a) Distribution of *Beggiatoa* biomass, total intracellular nitrate determined from frozen and thawed cores, and intracellular nitrate from *Beggiatoa*, total S(0) and intracellular S(0) from *Beggiatoa*. b) Distribution from total sedimentary S(0) and intracellular *Beggiatoa* S(0). Observe the different scales.**

From experiments with stable isotope tracers ($^{15}NO_3^-$), a cell-specific DNRA rate of similar magnitude was found. The $^{15}NH_4^+$ formation coincided well with the *Beggiatoa* distribution (Fig. 4a), with a local maximum at 2 cm depth. As nitrate from the overlying water does not diffuse to that depth, *Beggiatoa* must be responsible for the ammonium production and have transported the nitrate intracellularly into the sediment. This was confirmed by control experiments without *Beggiatoa*, where significant $^{15}NH_4^+$ production (DNRA) was only found near the oxic zone in the upper sediment (Fig. 4b). When subtracting the $NH_4^+$ production of the control core from the *Beggiatoa* core, *Beggiatoa* seems not to contribute to DNRA in the upper 1 cm. The upper 1 cm of the sediments with *Beggiatoa* produced twice as much $N_2$ as in the controls without *Beggiatoa*. Below 1 cm depth, the depth distribution of the labeled $N_2$ gas was the same with or without *Beggiatoa* present. The $^{15}NO_3^-$ tracer had labeled the vacuolar nitrate pool over the full suboxic zone as can be seen from the $^{15}NO_3^-$ fraction (Fig. 4a). From the specific labeling intensity and the $^{15}NH_4^+$ production rate, the total $NH_4^+$

production rate was calculated. The areal DNRA rate was 43 mmol $m^{-2}$ $day^{-1}$ in a sediment with 3 g *Beggiatoa* $m^{-2}$. Assuming 1 mL of *Beggiatoa* per g biomass, this DNRA rate is equivalent to 14 mM $day^{-1}$ of vacuolar nitrate concentration decrease. The same results were obtained in two replicate stable isotope experiments.

The pH profiles in retrieved cores showed a local minimum at a depth of ca. 0.5-1 cm, and a clear local maximum near the top of the sulfidic zone, that is the zone where upwardly diffusing sulfide disappeared (Fig. 2a–e).

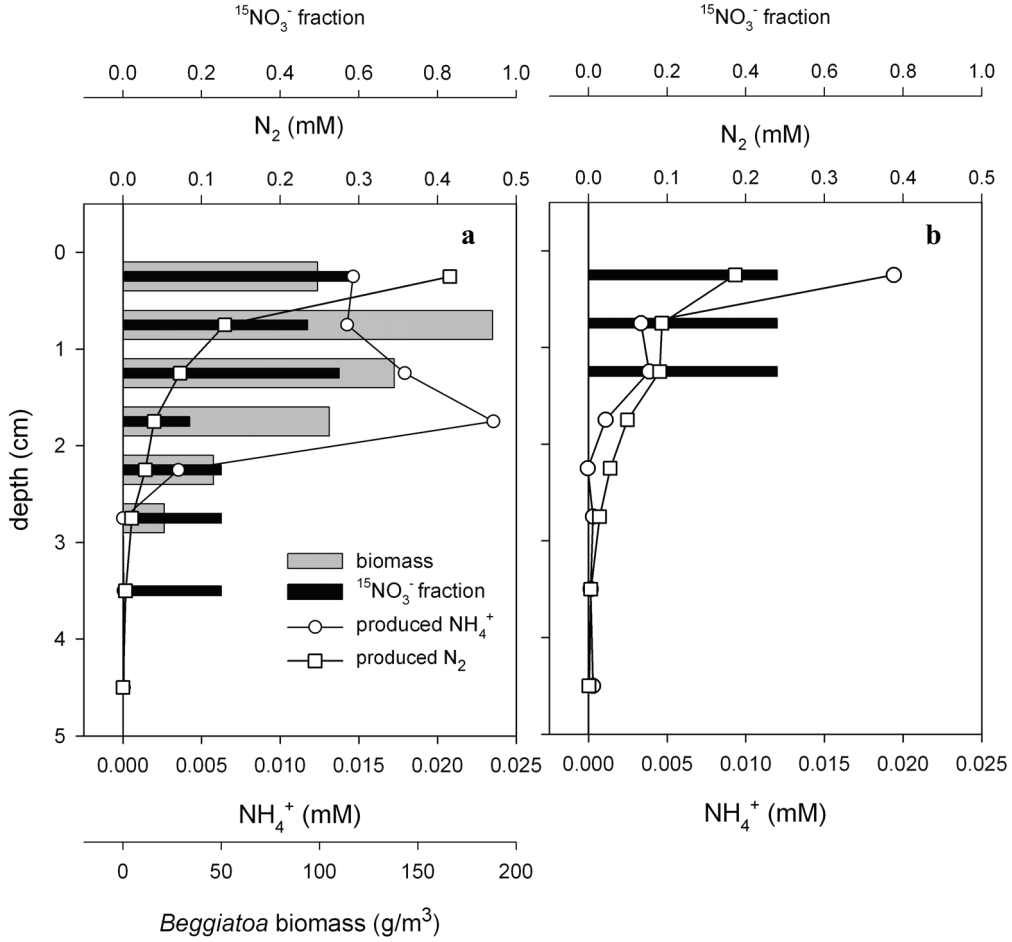


**Fig. 4: Results from the $^{15}N$ tracer experiment. a) The distribution of *Beggiatoa* biomass, the $^{15}N$-nitrate fraction of total nitrate, total produced $NH_4^+$ as calculated from the label fraction and produced $^{15}NH_4^+$, and produced $N_2$, calculated from the label fraction and the produced $^{15}N_2$. b) The produced $NH_4^+$ and $N_2$ in a control core without *Beggiatoa*. From the difference in $NH_4^+$ production between the two cores and the biomass distribution, the DNRA rates per *Beggiatoa* volume in sediments were calculated. DNRA, dissimilatory nitrate reduction to ammonium.**

The concentration of internal nitrate was ca. 100-300 mM and the cellular sulfur content was ca. 300-400 mM (both expressed per volume of *Beggiatoa*). Thus the amount of intracellular e-donor and e-acceptor are rather well balanced, with a slight surplus towards the e-donor, for the oxidation of

sulfur to sulfate ($4S(0) + 3NO_3^- + 7H_2O \rightarrow 4SO_4^{2-} + 3NH_4^+ + 2H^+$). As in the suboxic zone sulfide is supplied to the filaments continuously, most probably nitrate limits the time that filaments can reside in the sediments.

The internal stores of sulfur and nitrate allow *Beggiatoa* to live independently from external resources for up to 2 weeks, as concluded from an experiment where filaments containing 270 mM nitrate were incubated in oxygen and nitrate-free sediment. These filaments lost 70% of their intracellular nitrate in 2 weeks, and were depleted after 3 weeks, during which they remained motile. After 5 weeks the filaments were still intact, but had lost motility. The calculated mean rate of vacuolar nitrate decrease was 13 mM $day^{-1}$.

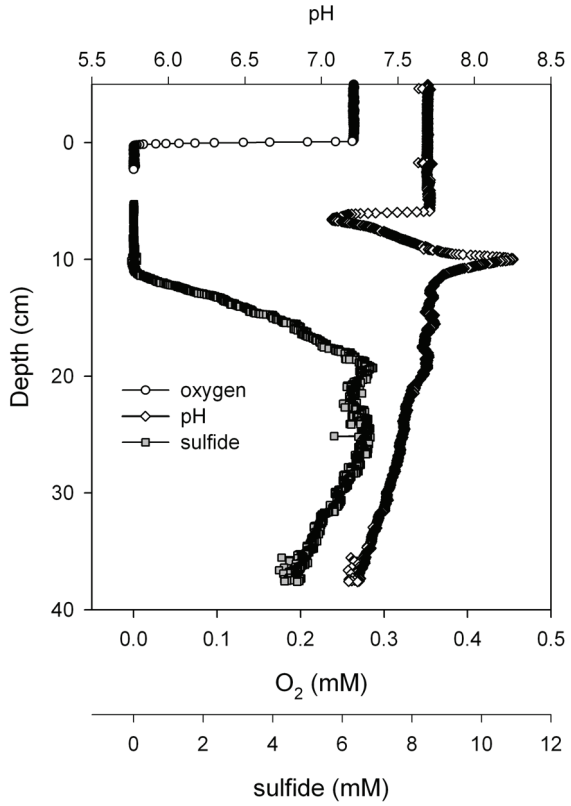


**Fig. 5: Microprofiles of oxygen, sulfide and pH measured in situ with microsensors mounted on an autonomous profiler. The sediment surface was determined as the depth with the steepest oxygen concentration gradient.**

The in situ profiles showed an oxygen penetration depth of 0.1-0.2 cm, and a sulfidic zone below ca. 10 cm depth (Fig. 5). The sulfide levels peaked between 20 and 30 cm depth, reaching ca. 7 mM,

and below 30 cm the concentration decreased. The pH profiles showed a minimum value at ca. 6 cm depth, and a maximum value at the top of the sulfidic zone. The separation between the oxic and sulfidic zone was much larger than observed in retrieved cores. During the in situ measurements, strong winds (40-50 km $h^{-1}$) possibly caused turbulences at the seafloor and disturbance of the top sediments. Also, ship movement might have caused rough positioning on the seafloor causing replacement of sediment, and covering of the sediments below the profiler. Nevertheless, the pH profiles peaked at the top of the sulfidic zone and showed a local minimum in the suboxic zone, similar to the retrieved cores.

Solid-phase iron and manganese species had increased concentrations in the upper sediment (Fig. 6). Dissolved pore water $Fe^{2+}$ was elevated in the top 2 cm, with a local maximum of ca. 130 µM at 1 cm depth. It was lower (<50 µM) in the oxic zone, obviously due to oxidation with oxygen, and close to 0 below 2 cm depth, probably due to precipitation with free sulfide. The ascorbate-extractable Fe(III) had increased concentrations up to 30 mM in the top 4 cm. In principle, the method extracts also some of the FeS pool; however, the independent extraction of FeS only showed insignificant amounts. Manganese extracted with dithionite peaked in the upper centimeter with 3 mM, about three times the background level found below.

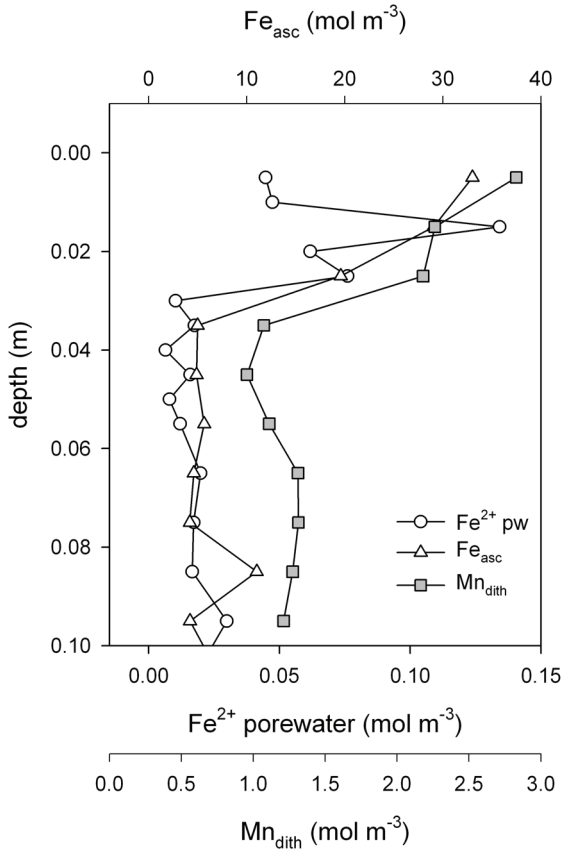


**Fig. 6: Distributions of dithionite extracted manganese ($Mn_{dith}$), $Fe^{2+}$ dissolved in the porewater, and ascorbic acid extractable sedimentary iron ($Fe_{asc}$), which is regarded as the most reactive Fe(III) fraction.**

### 3.2. Effects of Nitrate, Oxygen and Sulfide

To investigate the distinct pH profiles, we tested the hypothesis that the local pH minimum in the suboxic zone was caused by aerobic oxidation of sulfur to sulfate, a process well known to reduce the pH value. The oxygen in the overlying water was experimentally reduced to <40 µM $O_2$ by flushing with argon, for a period of 6 h. The penetration depth of oxygen became close to 0. The only effect on pH was a slight increase in the overlying water due to $CO_2$ outgassing, but the local pH minimum remained unchanged (Fig. 7a), thus it was concluded that the local pH minimum was not related to an oxygen-dependent process. Also the addition of 200 µM nitrate (10-fold the in situ concentration) to the overlying water did not change the pH profile in the sediment (Fig. 7b), suggesting that also nitrate respiration did not cause the pH minimum.

To investigate the possibility that the local pH maximum at the top of the sulfidic zone was caused by interaction of free sulfide with oxidized compounds in the sediment, 0.3 mM sulfide was added to the overlying water. This resulted in an immediate increase in the pH in the upper zone of the sediment, to which sulfide could penetrate (Fig. 8). The pH reached a maximum value of 9.5. The sediment surface turned instantly black, indicating FeS formation. Overnight the sulfide disappeared and the pH profile recovered to the original shape.

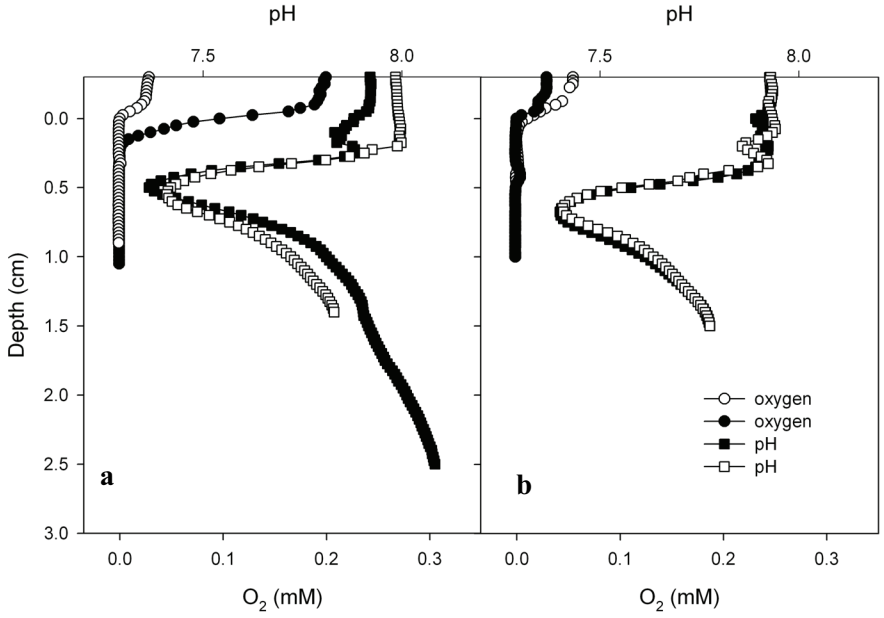


**Fig. 7: The effect of (a) oxygen decrease and (b) addition of 200 µM nitrate on the subsurface pH profile, measured with microsensors. Closed symbols indicate profiles before treatment, open symbols represent the situation 6-8 hours after the change. Oxygen or nitrate have no effect on the pH profiles.**

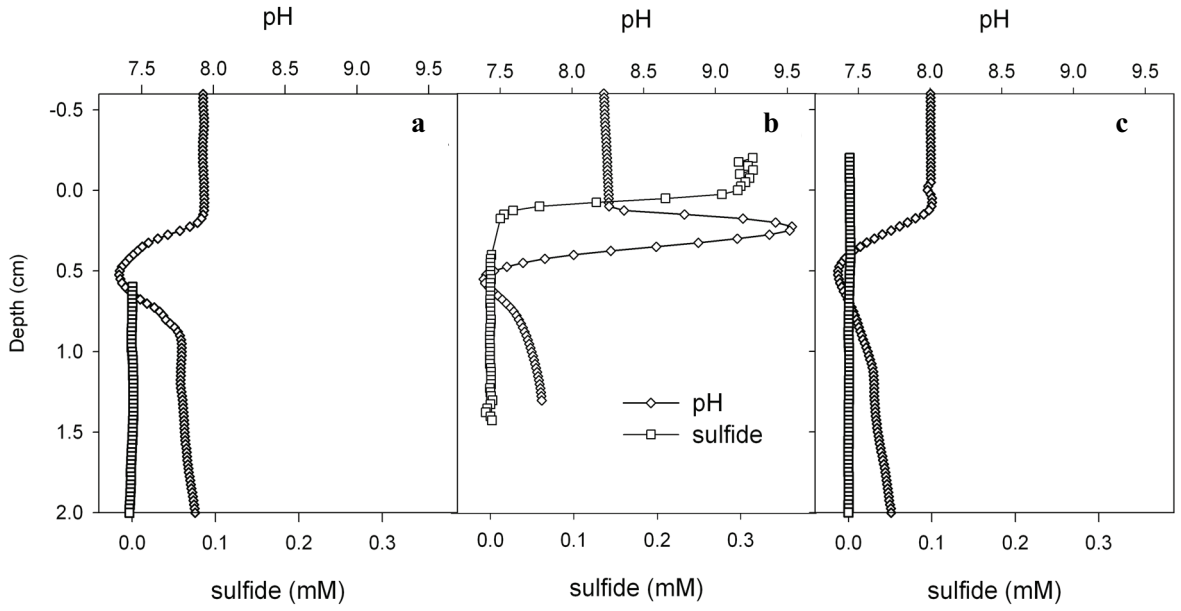


**Fig. 8: Effect of sulfide addition to the overlying water on the pH profile. The experiment was done under reduced oxygen, by flushing with argon. a) Before addition, b) 10 minutes after addition, c) 8 hours after addition.**

## 4. DISCUSSION

The in situ and ex situ microsensor measurements all showed a clear separation between the sulfidic and the oxic zone, and a local pH maximum at the top of the sulfidic zone. The in situ profile has a larger suboxic zone between the oxic and sulfidic zone than those measured on retrieved cores. This indicates that before or during the in situ deployment of the microsensor profiler sediment was deposited in the area of profiling, either by wind driven bottom water currents or by the deployment of the equipment. This changed the oxygen distribution, but the local pH in the upper 3 cm remained that of seawater. Also irregular topography can lead to an overestimation of the suboxic zone. The local pH maximum at the top of the sulfidic zone and the local minimum below the oxic zone were observed both in situ and in the retrieved cores. Thus the characteristic local pH maximum and minimum in the profiles were not an artifact of the retrieval.

Our observations show that *Beggiatoa* is predominantly distributed in the suboxic and oxic zone, and avoids the sulfidic zone. Sulfide enters the suboxic *Beggiatoa* zone by local sulfate reduction and by diffusion upwards from the sulfidic zone. Our in situ microprofiles showed a sulfide maximum between 25 and 35 cm depth. At this depth the sulfate to methane transition zone is found, and the highest rates of anaerobic oxidation to methane (Treude et al., 2005). From the sulfide oxidation rates calculated for *Beggiatoa*, the published local sulfate reduction rates that were measured at the same stations (Treude et al., 2005), and the calculated sulfide influx, we obtained a budget for the suboxic

zone and estimated the importance of *Beggiatoa* for sulfide oxidation (Table 1). The biomass-specific DNRA was found to be ca. 13-14 mM $day^{-1}$ close to values previously found for *Thioploca* (Otte et al., 1999). Thus the biomass-specific sulfide oxidation rate of *Beggiatoa* is ca. 13 mM $day^{-1}$, when sulfide is oxidized to sulfate:

$$HS^- + NO_3^- + H^+ + H_2O \rightarrow SO_4^{2-} + NH_4^+ \qquad \text{(Eq. 1)}$$

or ca. 52 mM $day^{-1}$ for the first step in sulfide oxidation to elemental sulfur:

$$6H^+ + 4HS^- + NO_3^- \rightarrow 4S(0) + NH_4^+ + 3H_2O \text{ (Eq. 2)}$$

Combining the estimated biomass-specific conversion rate (13 mM $day^{-1}$) and the measured biomass quantities (Fig. 2), the areal rates of sulfide oxidation to sulfate by *Beggiatoa* were estimated to vary between 0.0086 and 0.38 mmol $m^{-2}$ $day^{-1}$, averaging 0.16 ±0.15 mmol $m^{-2}$ $day^{-1}$. The actual sulfide oxidation rate during balanced growth, when all sulfides are oxidized to sulfates, will be slightly higher, as a part of the reducing power is used for cell growth. Therefore, per mol of nitrate ca. 1.2 mol of sulfide can be oxidized to sulfate, if the growth yield with nitrate is the same as with oxygen (Nelson et al., 1986).

**Table 1: S-budget of the suboxic zone inhabited by *Beggiatoa* (upper 2 cm).**

| Sulfide input (mmol $m^{-2}$ $day^{-1}$) | | Sulfide consumption (mmol $m^{-2}$ $day^{-1}$) | |
|---|---|---|---|
| Diffusion from sulfidic zone | Local sulfate reduction | *Beggiatoa* | Inferred chemical oxidation |
| 4.3 (±2) (86%) | 0.7 (14%) | 0.16 (±0.15) (3%) | 4.84 (97%) |

The budget calculation (Table 1) shows that only a small fraction of the sulfide input into the suboxic zone is oxidized by *Beggiatoa*, as the influx and local production far exceeds the estimated nitrate reduction rate. Even if we assume that sulfide oxidation locally stops at the level of sulfur

(Sayama et al., 2005), allowing four sulfides to be oxidized with one nitrate, *Beggiatoa* activity is insignificant for the total sulfide oxidation. The sulfide input into the suboxic zone was mostly the influx from deeper sediments, and was consumed at the interface of the sulfidic zone and the suboxic zone, causing the local maximum in sulfide consumption (Fig. 2). This distribution of sulfide consumption rates did not correlate with the distribution of *Beggiatoa* (Fig. 2). Whereas *Beggiatoa* consumed ca. 20% of the sulfide produced by sulfate reduction in the suboxic zone, almost all of the influx from deeper sediments must be consumed by chemical oxidation. The most likely electron-acceptor for such anaerobic sulfide oxidation is Fe(III).

$$2FeOOH + HS^- + 3H^+ \rightarrow 2Fe^{2+} + S(0) + 4H_2O \quad \text{(Eq. 3)}$$

A part of the soluble reduced iron and sulfide will form iron sulfides

$$Fe^{2+} + HS^- \rightarrow FeS + H^+ \quad \text{(Eq. 3a)}$$

Whereas the first reaction involves dissipation of protons and thus a pH increase, the second step leads to a small pH decrease. In a gradient system, the second step is not 100% efficient, and a part of the $Fe^{2+}$ escapes into the suboxic zone, where its concentration is indeed elevated (Fig. 6). This mechanism is corroborated by the local pH maximum consistently found at the interface between the suboxic zone and the sulfidic zone (Fig. 2). The product of sulfide oxidation by Fe(III) is elemental sulfur, which is indeed abundantly found in the sediments (Fig. 3b).

The local pH minimum near the surface was very stable (Fig. 7 and 8), which also points to a chemical process. The local pH minimum was not influenced by oxygen or nitrate (Fig. 7), making a biological oxidation process unlikely:

$$2S(0) + 3O_2 + 2H_2O \rightarrow 2SO_4^{2-} + 4H^+ \quad \text{(Eq. 4)}$$

or

$$4S(0) + 3NO_3^- + 7H_2O \rightarrow 4SO_4^{2-} + 3NH_4^+ + 2H^+ \quad \text{(Eq. 5)}$$

Also aerobic iron oxidation cannot explain the pH profile, as the pH minimum was always below the oxic zone, and not affected by oxygen levels in the water phase. In the absence of oxygen, $Fe^{2+}$ may rapidly be oxidized by manganese oxides (Postma, 1985), which leads to a pH decrease:

$$2Fe^{2+} + MnO_2 + 4H_2O \rightarrow 2Fe(OH)_3 + Mn^{2+} + 2H^+ \text{ (Eq. 6)}$$

The analyses of sedimentary iron and manganese support these hypotheses (Fig. 6). Elevated amounts of oxidized iron were found in the upper 3 cm, and were thus available for sulfide oxidation. The iron minerals in the upper sediment were very reactive, as shown by the experimental sulfide addition to the overlying water (Fig. 8). Sulfide penetration into the upper sediment was limited, and an immediate very strong pH increase was observed. Below 3 cm depth low levels of Fe(III) were found, which were probably less reactive. Also a clear elevation of manganese was found in the upper 3 cm, including the oxic zone. The manganese extracted with dithionite is thought to be the reactive pool, and the elevated levels in the upper sediments is dominated by Mn(IV) (Kostka and Luther, 1994).

The steep $Fe^{2+}$ peak indicates strong Fe(III)- driven mineralization in the suboxic zone. The $Fe^{2+}$ is produced just below or in the Mn(IV)-rich layer, and we propose that it is the $Fe^{2+}$ oxidation by $MnO_2$ which leads to the observed pH minimum below the oxic zone. The reaction of Equation 6 is not instant, but proceeds on a timescale of hours (Postma, 1985), thus indeed free $Fe^{2+}$ can be present at detectable levels in Mn(IV)-containing sediments. If the effective diffusion coefficient for $Fe^{2+}$ is 0.52 $x10^{-9}$ $m^2$ $s^{-1}$, 3 mM of $MnO_2$ in the upper 1 cm is sufficient to absorb the $Fe^{2+}$ diffusing upwards from its peak for several weeks. This solid-phase electron-acceptor for iron oxidation might also explain why the local pH minimum was observed in the in situ profiles at 6 cm depth (Fig. 5): the $MnO_2$-containing layer had been covered with reduced mud, but was not yet depleted.

Other $MnO_2$ reduction processes lead to pH increase, for example when coupled to the oxidation of FeS or $FeS_2$ or to organic compounds:

$$2FeS_2 + 15MnO_2 + 22H^+ \rightarrow 2FeOOH + 4SO_4^{2-} + 15Mn^{2+} + 10H_2O \text{ (Eq. 7)}$$

$$2FeS + 3MnO_2 + 6H^+ \rightarrow 2FeOOH + 2S(0) + 3Mn^{2+} + 2H_2O \text{ (Eq. 8)}$$

$$CH_2O + 2MnO_2 + H_2O \rightarrow CO_2 + 2Mn^{2+} + 4OH^- \text{ (Eq. 9)}$$

These processes are thought to be partly microbially catalyzed (Schippers and Jørgensen, 2001). Because no pH increase was observed in the upper sediment, however, they were apparently not dominant.

Thus, the pH profiles can be explained from manganese and iron cycling, and the metal cycling drives the oxidative sulfur cycling. Frequent resuspension and bioturbation is needed for intense iron and manganese cycling in muddy sediments (Canfield et al., 2005). The upper layer of the sediment is, possibly due to storms or methane ebullition (Roden and Wetzel, 1996), regularly resuspended in the aerated bottom water leading to oxidation of $Mn^{2+}$ and $Fe^{2+}$. Irregular resuspension of upper sediment layers was considered to explain the presence of potentially active aerobic methanotrophs in the upper 5 cm (Treude et al., 2005).

Bioventilation and bioturbation may be less important for the oxidation of reduced iron and manganese, as signs of bioturbation were found in the upper centimeter only (Treude et al., 2005). The oxidized layer can be 10 cm thick as observed in situ, but is more often 2-4 cm thick. This layer, in the sediments we investigated, is the habitat for *Beggiatoa*. As summarized in Fig. 9, sulfide diffusing from below into this layer is rapidly oxidized by Fe(III), forming a steep sulfide gradient and a local maximum in pH. $Fe^{2+}$ diffuses upwards and reaches the $MnO_2$-rich zone, where it is oxidized, leading to a local minimum in pH.

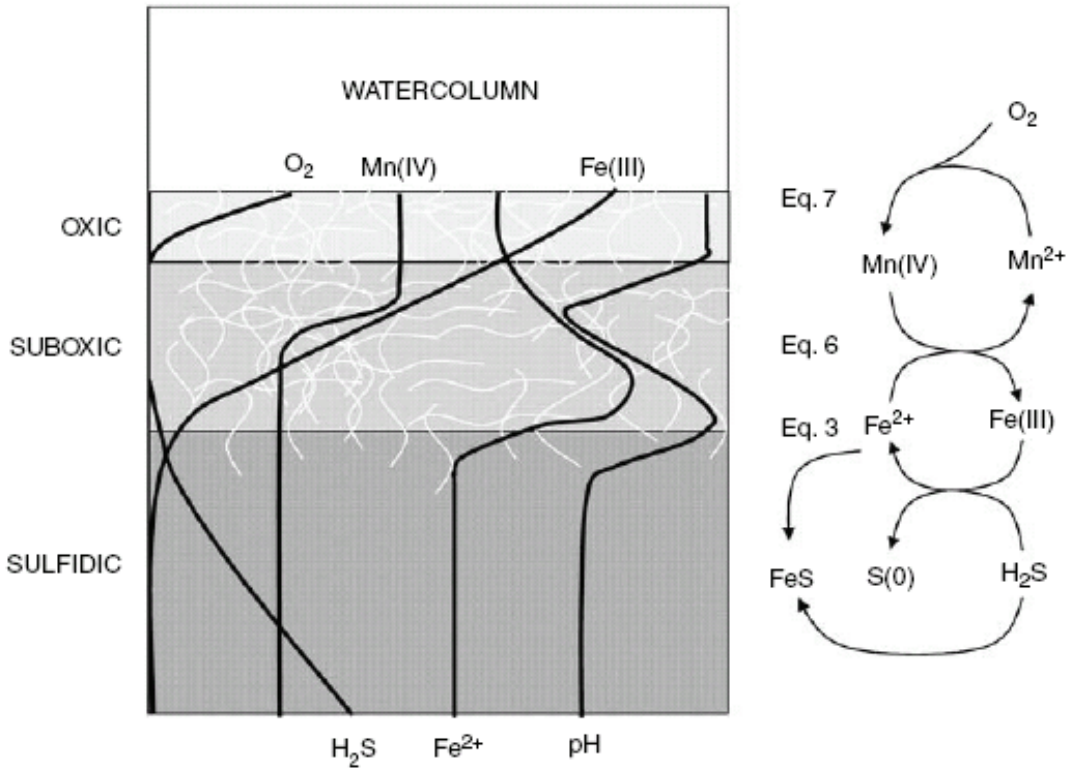


**Fig. 9: Overview of the main geochemical reactions in the oxic (dashed), suboxic (light gray) and sulfidic (dark gray) zones, and the pore water profiles. The profiles are not quantitative. The distribution of *Beggiatoa* is indicated by the white filaments.**

Whereas we conclude that most sulfide is oxidized through chemical processes, a recent study (Sayama et al., 2005) came to the opposite conclusion that the observed pH microprofiles and sulfide oxidation must be explained by the metabolic activities of *Beggiatoa.* Their study was done in *Beggiatoa* mats transplanted experimentally on sulfidic sediments. The authors explained the local pH maximum at the upper sulfidic zone by the oxidation of sulfide by nitrate to S(0) (Eq. 1), and the local pH minimum by the aerobic oxidation of S(0) to sulfate (Eq. 4). The sulfide fluxes we calculated from their published profiles are four- to fivefold lower than their measured DNRA rates (which were very high and entirely attributed to *Beggiatoa*), implying that DNRA could easily oxidize all sulfide diffusing upwards to sulfate (Eq. 1). The differences could be explained by a *Beggiatoa* density that was much higher than in our study; however, cell densities were not reported.

Why is *Beggiatoa* so abundant in the studied sediment? A prerequisite for *Beggiatoa* is a highly porous sediment (Jørgensen, 1977), like indeed the sediments in this study. The sulfate reduction rate in the zone where *Beggiatoa* occurs was comparable to rates found in temperate intertidal sediments, in subtidal sediments, and in many other sediments (Canfield et al., 2005), where, however, no conspicuous *Beggiatoa* mats were found. Thus the abundance of *Beggiatoa* in the sediments studied here cannot be explained by a high volumetric sulfate reduction rate, as in other sediments without *Beggiatoa* similar rates were found. The pH in the sediments we investigated was between 7 and 8, a typical marine sediment value (Boehme et al., 1998). In summary, in the suboxic zone where *Beggiatoa* resides we could not detect unique characteristics that could explain the presence of *Beggiatoa.* One distinguishing characteristic of habitats where *Beggiatoa* is found appears to be the presence of detectable free sulfide. Typical habitats include cold seeps (Barry et al., 1996; Kalanetra et al., 2003), upwelling areas with high organic input (Brüchert et al., 2003), whale carcasses, sulfidic springs (Martinez et al., 1997; Mattison et al., 1998), hydrothermal vents (Nelson et al., 1989) and hypersaline mats (Garcia-Pichel et al., 1994; Jonkers et al., 2003), all of which have steep sulfide gradients. High temperatures seem to exclude *Beggiatoa* as they are not reported from sulfidic hot springs. In principle, a suboxic zone is not essential, because also when sulfidic and oxic zones overlap *Beggiatoa* can persist and develop a mat on the surface (Jørgensen and Revsbech, 1983). In our studies, the sulfide diffusing upwards was scavenged by Fe(III), thus this source reached only the very small fraction of the *Beggiatoa* population that is present at the sulfidic interface. Therefore, sulfide diffusing from below the suboxic zone could not insignificantly feed the *Beggiatoa* population in the suboxic zone. The amount of sulfide produced locally was sufficient for their metabolic needs, and they had a sufficiently high affinity for $H_2S$ to compete with the chemical oxidation processes. Although most of the *Beggiatoa* reside in the suboxic zone, where sulfide concentrations were low (≤1 µM), sulfide may not be very toxic for *Beggiatoa*. Occasionally, filaments were found deep in the sulfidic zone, and despite high sulfide concentrations, they were motile. However, generally the sulfidic zone is avoided.

We propose that *Beggiatoa* needs a steep sulfide gradient for orientation. Owing to their internal stores of sulfur and nitrate they can travel independent from external supplies for a period of days to weeks. With a gliding velocity of 2 μm $s^{-1}$ (Nelson et al., 1989), their linear path length is 70 cm in 4 days if the vacuolar nitrate concentration is 50 mM, and even 5 m in 3 weeks when they start the journey with the highest measured nitrate concentration of 370 mM. When moving in random direction in sediments without a signal to return to the surface, the cells would sooner or later reach depths in the sediments from which they cannot return to the oxidized zone before their stored nitrate is depleted. A steep sulfide gradient could provide a signal to return. Indeed, we observed a phobic response to sulfide in the *Beggiatoa* mats from the Håkon Mosby mud volcano, a cold seep in the Barents Sea. When 2 cm thick agar plugs containing 3 mM sulfide (pH 7.8) were inserted into *Beggiatoa* mats, filaments cleared a ring of several millimeters wide around the plug within hours. No repulsion was observed with sulfide-free controls (data not shown). A vacuolated nitrate storing hypersaline *Beggiatoa* strain was repelled by sulfide, as shown in sulfide gradient tubes (S. Hinck, personal communication). Several authors have alluded to a phobic response by *Beggiatoa* to sulfide (for example, Garcia-Pichel et al., 1994; Canfield et al., 2005), but it is not yet properly documented. More detailed investigations are needed towards the negative tactile response towards sulfide, for example it is not known how steep the gradient should be to function as repellant, and at which concentrations sulfide may become toxic for *Beggiatoa*. Random motion in a narrow zone between the surface and the steep sulfide gradient would allow *Beggiatoa* to reach the surface with a sufficient frequency to reload the vacuole with nitrate. Consequently, the negative tactile response towards sulfide allows them to persist and thrive in anoxic sediments. The special ecological niche for large nitrate storing *Beggiatoa* is thus not explained by substrate supply, thermodynamics or kinetic options, but by behavior.

## REFERENCES

Ahmad A., Barry J. P., Nelson D. C., 1999. Phylogenetic affinity of a wide, vacuolate, nitrate-accumulatlng *Beggiatoa* sp. from Monterey Canyon, California, with *Thioploca* spp. *Appl. Environ. Microbiol.* **65**: 270–277.

Barnett P. R. O., Watson J., Connelly D., 1984. A multiple corer for taking virtually undisturbed samples from shelf, bathyal and abyssal sediments. *Oceanolica Acta* **7**: 399–408.

Barry J. P., Greene H. G., Orange D. L., Baxter C. H., Robison B. H., Kochevar R. E. *et al.*, 1996. Biologic and geologic characteristics of cold seeps in Monterey Bay, California. *Deep-Sea Res. Pt. I.* **43**: 1739–1762.

Berner R. A., 1981. A new geochemical classification of sedimentary environments. *J. Sed. Petrol.* **51**: 359–365.

Boehme S. E., Sabine C. L., Reimers C. E., 1998. $CO_2$ fluxes from a coastal transect: a time-series approach. *Mar. Chem.* **63**: 49–67.

Braman R. S, Hendrix S. A., 1989. Nanogram nitrite and nitrate determination in environmental and biological materials by Vanadium(III) reduction with chemiluminescence detection. *Anal. Chem.* ***61***: 2715–2718.

Brüchert V., Jørgensen B. B., Neumann K., Riechmann D., Schlösser M., Schulz H. N., 2003. Regulation of bacterial sulfate reduction and hydrogen sulfide fluxes in the central Namibian coastal upwelling zone. *Geochim. Cosmochim. Acta* **67**: 4505–4518

Canfield D., Thamdrup B., Kristensen E., 2005. *Aquatic Geomicrobiology*. Elsevier, San Diego, California

Canfield D. E., 1989. Reactive iron in marine sediments. *Geochim. Cosmochim. Acta* **53**: 619–632.

Cox R. D., Earp R. F., 1982. Determination of trace level organics in ambient air by high-resolution gas chromatography with simultaneous photoionization and flame ionization detection. *Anal. Chem.* **54**: 2265–2270.

de Beer D., 2000. Potentiometric microsensors for in situ measurements in aquatic environments. In: Buffle J, Horvai G (eds). *In situ monitoring of aquatic systems: chemical analysis and speciation.* Wiley & Sons: Chichester, UK. pp 161–194.

de Beer D., Sauter E., Niemann H., Kaul N., Foucher J. P., Witte U. *et al.,* 2006. In situ fluxes and zonation of microbial activity in surface sediments of the Håkon Mosby Mud Volcano. *Limnol. Oceanog.r* **51**: 1315–1331.

Ferdelman T. G., Church T. M., Luther G. W. I., 1991. Sulfur enrichment of humic substances in a Delaware salt marsh sediment core. *Geochim. Cosmochim, Acta* **55**: 979–988.

Ferdelman T. G., Lee C., Pantoja S., Harder J., Bebout B., Fossing H., 1997. Sulfate reduction and methanogenesis in a *Thioploca*-dominated sediment off the coast of Chile. *Geochim. Cosmochim. Acta* **61**: 3065–3079.

Fossing H., Gallardo V.A., Jørgensen B. B., Hüttel M., Nielsen L. P., Schulz H. *et al.*, 1995. Concentration and transport of nitrate by the mat-forming sulphur bacterium *Thioploca*. *Nature* **374**: 713–715.

Froelich P. N., Klinkhammer G. P., Bender M. L., Luedtke N. A., Heath G. R., Cullen D. *et al*., 1979. Early oxidation of organic matter in pelagic sediments of the eastern equatorial Atlantic: suboxic diagenesis. *Geochim. Cosmochim. Acta* **43**: 1075–1090.

Garcia-Pichel F., Mechling M., Castenholz R. W., 1994. Diel migrations of microorganisms within a benthic, hypersaline mat community. *Appl. Environ. Microbiol.* **60**: 1500–1511.

Gieseke A., de Beer D., 2004. Use of microelectrodes to measure in situ microbial activities in biofilms, sediments, and microbial mats. In: Akkermans A. D. L., van Elsas D. (eds). *Molecular Microbial Ecology Manual*. Kluwer: Dordrecht, the Netherlands, pp 1581–1612.

Jeroschewski P., Steukart C., Kühl M., 1996. An amperometric microsensor for the determination of $H_2S$ in aquatic environments. *Anal. Chem.* **68**: 4351–4357.

Jonkers H. M., Ludwig R., De Wit R., Pringault O., Muyzer G., Niemann H. *et al.*, 2003. Structural and functional analysis of a microbial mat ecosystem from a unique permanent hypersaline inland lake: 'La Salada de Chiprana' (NE Spain). *FEMS Microbiol. Ecol.* **44**: 175–189.

Jørgensen B. B., 1977. Distribution of colorless sulfur bacteria (*Beggiatoa* spp.) in a coastal marine sediment. *Mar. Biol.* **41**: 19–28.

Jørgensen B. B., Revsbech N. P., 1983. Colorless sulfur bacteria, *Beggiatoa* spp. and *Thiovulum* spp. in $O_2$ and $H_2S$ microgradients. *Appl. Environm. Microbiol.* **45**: 1261–1270.

Kalanetra K. M., Nelson D. C., Joye S. B., 2003. Evolutionary relationships of novel, vacuolate, sulfur-oxidizing bacteria from hydrothermal vents and cold seeps. *Abstracts of the General Meeting of the American Society for Microbiology* **103-N**: 362.

Kostka J. E., Luther G. W., 1994. Partitioning and speciation of solid-phase iron in salt-marsh sediments. *Geochim. Cosmochim. Acta* **58**: 1701–1710.

Larsen L. H., Kjaer T., Revsbech N. P., 1997. A microscale $NO_3^-$ biosensor for environmental applications. *Anal. Chem.* **69**: 3527–3531.

Li Y.-H., Gregory S., 1974. Diffusion of ions in sea water and deep-sea sediments. *Geochim. Cosmochim. Acta* **38**: 703–714.

Lomstein E., Jensen M. H., Sorensen J., 1990. Intracellular $NH_4^+$ and $NO_3^-$ pools associated with deposited phytoplankton in a marine sediment (Aarhus Bight, Denmark). *Mar. Ecol. Prog. Ser.* **61**: 97–105.

Martinez A., Pibernat I., Figueras J., Garcia-Gil J., 1997. Structure and composition of freshwater microbial mats from a sulfur spring (''Font Pudosa'', NE Spain). *Microbiologia* **13**: 45–56.

Mattison R. G., Abbiati M., Dando P. R., Fitzsimons M. F., Pratt S. M., Southward A. J. *et al*., 1998. Chemoautotrophic microbial mats in submarine caves with hydrothermal sulphidic springs at Cape Palinuro, Italy. *Microb. Ecol.* **35**: 58–71.

McHatton S., Barry J. P., Jannasch H. W., Nelson D. C., 1996. High nitrate concentrations in vacuolate autotrophic marine *Beggiatoa* spp. *Appl. Environ. Microbiol.* **62**: 954–958.

Millero F. J., Plese T., Fernandez M., 1988. The dissociation of hydrogen sulfide in seawater. *Limnol. Oceanogr.* **33**: 269–274.

Mussmann M., Schulz H. N., Strotmann B., Kjaer T., Nielsen L. P., Rossello-Mora R. A. *et al.,* 2003. Phylogeny and distribution of nitrate-storing *Beggiatoa* spp. in coastal marine sediments. *Environ. Microbiol.* **5**: 523–533.

Nelson D. C., Jørgensen B. B., Revsbech N. P., 1986. Growth pattern and yield of a chemoautotrophic *Beggiatoa* sp. in oxygen-sulfide microgradients. *Appl. Environ. Microbiol.* **52**: 225–233.

Nelson D. C., Wirsen C. O., Jannasch H. W., 1989. Characterization of large, autotrophic *Beggiatoa* spp. abundant at hydrothermal vents of the Guaymas Basin. *Appl. Environ. Microbiol.* **55**: 2909–2917.

Otte S., Kuenen J. G., Nielsen L. P., Paerl H. W., Zopfi J., Schulz H. N. *et al.,* 1999. Nitrogen, carbon, and sulfur metabolism in natural *Thioploca* samples. *Appl. Environ. Microbiol*. **65**: 3148–3157.

Postma D., 1985. Concentrations of Mn and separation of Fe in sediments. 1. Kinetics and stoichiometry of the reaction between birnessite and dissolved Fe(II) at 10 °C. *Geochim. Cosmochim. Acta* **49**: 1023–1033.

Revsbech N. P., 1989. An oxygen microelectrode with a guard cathode. *Limnol. Oceanogr.* **55**: 1907–1910.

Roden E. E., Wetzel R. G., 1996. Organic carbon oxidation and suppression of methane production by microbial Fe(III) oxide reduction in vegetated and unvegetated wetland sediments. *Limnol. Oceanogr*. **41**: 1733–1748.

Sayama M., 2001. Presence of nitrate-accumulating sulfur bacteria and their influence on nitrogen cycling in a shallow coastal marine sediment. *Appl. Environ. Microbiol.* **67**: 3481–3487.

Sayama M., Risgaard-Petersen N., Nielsen L. P., Fossing H., Christensen P. B., 2005. Impact of bacterial $NO_3^-$ transport on sediment biogeochemistry. *Appl. Environ. Microbiol.* **71**: 7575–7577.

Schippers A., Jørgensen B. B., 2001. Oxidation of pyrite and iron sulfide by manganese dioxide in marine sediments. *Geochim. Cosmochim. Acta* **65**: 915–922.

Schulz H. N., Brinkhoff T., Ferdelman T. G., Hernandez Marine M., Teske A., Jørgensen B. B., 1999. Dense populations of a giant sulfur bacterium in Namibian shelf sediments. *Science* **284**: 493–495.

Schulz H. N., Jørgensen B. B., 2001. Big bacteria. *Ann. Rev. Microbiol.* **55**: 105–137.

Stookey L. L., 1970. Ferrozine - a new spectrophotometric reagent for iron. *Anal. Chem.* **42**: 779–785.

Treude T., Krüger M., Boetius A., Jørgensen B. B., 2005. Environmental control on anaerobic oxidation of methane in the gassy sediments of Eckernförde Bay (German Baltic). *Limnol. Oceanogr.* **50**: 1771–1786.

Ullman W. J., Aller R. C., 1982. Diffusion coefficients in nearshore marine sediments. *Limnol. Oceanogr.* **27**: 552–556.

Vargas A., Strohl W. R., 1985. Utilization of nitrate by *Beggiatoa alba*. *Arch. Microb.* **142**: 279–284.

Warembourg F., 1993. Nitrogen fixation in soil and plant systems. In: Paul E, Melillo J, Knowles R, Blackburn H (eds). *Nitrogen Isotope Techniques*. Elsevier: Amsterdam, the Netherlands, pp 127–156.

Wenzhöfer F., Holby O., Glud R. N., Nielsen H. K., 2000. In situ microsensor studies of a shallow hydrothermal vent at Milos, Greece. *Mar. Chem.* **69**: 43–54.

Zopfi J., Ferdelman T. G., Fossing H., 2004. Distribution and fate of sulfur intermediates - sulfite tetrathionate, thiosulfate, and elemental sulfur - in marine sediments. In: Amend J, Edwards K, Lyons T (eds). *The Biogeochemistry of Sulfur.* GSA Special Paper. Geol. Soc. America: London, UK, pp 97–116.

Chapter 4

# Methane and sulfide fluxes in permanent anoxia: in situ studies at the Dvurechenskii mud volcano (Sorokin Trough, Black Sea)

Anna Lichtschlag[1], Janine Felden[1], Frank Wenzhöfer[1, 2], Florence Schubotz[3], Tobias Ertefai[3+], Antje Boetius[1, 2], Dirk de Beer[1]

[1]Max-Planck-Institute for Marine Microbiology, Celsiusstrasse 1, 28359 Bremen, Germany

[2]HGF MPG Research Group on Deep Sea Ecology and Technology, Alfred Wegener Institute for Polar and Marine Research, Am Handelshafen 12, 27570 Bremerhaven, Germany

[3]MARUM, University Bremen, Leobener Strasse, 28359 Bremen, Germany

[+]current address: Department of Applied Chemistry, Curtin University of Technology, Kent St, Perth, WA 6845, Australia

submitted to *Geochimica et Cosmochimica Acta*

*Acknowledgments.*

We thank the members of the shipboard crew of the RV Meteor, the Quest 4000 team (MARUM, Bremen) and the scientific party for the excellent support during the M72/2 Microhab cruise. Special thanks are to Gaby Eickert, Ines Schröder, Vera Hübner, Karin Hohmann, Ingrid Dohrmann and Cecilia Wiegand for the excellent microsensors, and to Martina Alisch and Gabi Schüßler for further technical support. We thank our colleague Stefanie Grünke for preparing the sampling map. We are grateful for the support from the Sea-Tech technicians of the Microbial Habitat group (Max-Planck-Institute for Marine Microbiology) for the construction and maintenance of the in situ devices. This study was supported by the GEOTECHNOLOGIEN project MUMM II (03G0608C) funded by the German Ministry of Education and Research (BMBF) and German Research Foundation (DFG), by the EU FP6 program HERMES (GOCE-CT-2005-511234-1) as well as by the Max Planck Society and MARUM (funded though DFG).

**Abstract**

**Benthic fluxes of methane and sulfide, and the factors controlling transport, consumption and production of both compounds within the sediment were investigated at a cold seep in permanently anoxic waters (Dvurechenskii mud volcano (DMV), 2060 m water depth, Black Sea). The pie-shaped mud volcano showed temperature anomalies as well as solute and gas fluxes indicating high fluid flow at a small elevation north of the geographical center. This is probably the missing source of the previously reported methane flares above the DMV. The anaerobic oxidation of methane (AOM) coupled to sulfate reduction (SR) was excluded from this zone due to fluid-flow induced sulfate limitation. Consequently the emission of dissolved methane into the water column was high, with an estimated rate of 0.44 mol $m^{-2}$ $d^{-1}$. Fluid flow and total methane flux were decreased in the outer center of the mud volcano, correlating with an increase in sulfate penetration into the sediment, and with higher SR and AOM rates. Additional signs of seepage were seen at the edges of the mud volcano. Outside the summit area between 50-70% of the methane flux (0.07-0.1 mol $m^{-2}$ $d^{-1}$) was consumed within the upper 10 cm of the sediment. The total amount of dissolved methane released from the DMV into the water column was still significant with a discharge of $1.4x10^{7}$ mol $yr^{-1}$. The DMV maintains also high areal rates of methane-fueled sulfide production of on average 0.05 mol $m^{-2}$ $d^{-1}$. However, we concluded that sulfide and methane emission into the hydrosphere from deep-water mud volcanoes does not significantly contribute to the sulfide and methane inventory of the Black Sea.**

## 1. INTRODUCTION

Below the chemocline in the permanently anoxic waters of the Black Sea, oxygen, nitrate and most of the reactive iron- and manganese-oxides are depleted. Sulfate is the principal electron-acceptor in organic matter mineralization in the water column and the upper seabed (Eq. 1). This leads to an accumulation of sulfide in the anoxic water column to concentrations of up to 370 µmol $L^{-1}$ (Neretin et al., 2001).

$$2CH_2O + SO_4^{2-} \rightarrow HS^- + 2HCO_3^- + H^+ \qquad \text{(Eq. 1)}$$

At the Dvurechenskii mud volcano (Bohrmann et al., 2003) and at other methane seeps on the slope off Crimea (Kruglyakova et al., 2002; Michaelis et al., 2002) the anaerobic oxidation of methane (AOM) coupled to sulfate reduction (SR) is another metabolic pathway with significant sulfide production. This process is performed by methane oxidizing archaea and associated sulfate reducing bacteria (Hinrichs et al., 1999; Boetius et al., 2000), which gain energy by the following reaction:

$$CH_4 + SO_4^{2-} \rightarrow HS^- + HCO_3^- + H_2O \qquad \text{(Eq. 2)}$$

At many active seeps, methane oxidation is limited by the availability of sulfate and oxygen, which must diffuse against an upward pore water flow (de Beer et al., 2006; Niemann et al., 2006). Hence, fluid flow velocities control the amount of methane and sulfide that is consumed or released into the water column, and their fluxes often differ locally depending on the geological structure of the cold seep system.

Here we investigated how spatial variations in fluid flow and the absence of oxygen as an electron-acceptor influence fluxes of methane and sulfide from an active mud volcano to the Black Sea hydrosphere. Our target site, the Dvurechenskii mud volcano (DMV), is a large cold seep structure located in the central part of the Sorokin Trough at a water depth of 2060 m. It has a wide flat center with an elliptic shape of 1200 by 800 m diameter, and a steep outer edge with an elevation 80 m above the seafloor. Mud is diapirically rising from a deep source originating in the Maikopian formation (Oligocene-Lower Miocene) (Woodside et al., 1997). Fluids ascend from up to 3 km depth and are formed by thermogenic organic matter and silicate alteration processes, resulting in enrichment in $Ba^{2+}$, $I^-$, $Cl^-$, $Sr^{2+}$, $Li^+$, and ammonium compared to the Black Sea bottom water. The fluids are depleted in sulfide and sulfate and have a higher salinity than seawater. Particulate organic matter content is 2-6 wt.% at the sediment surface, but decreases to about 1 wt%. below 5 cm sediment depth (Aloisi et al., 2004; Wallmann et al., 2006). Temperature anomalies in the water column and in the sediments of the DMV indicated areas with increased fluid and/or mud upflow (Bohrmann et al., 2003). The

distribution of pore water components in retrieved cores could be fitted to a transport model assuming upward flow velocities from 0.08 to 0.25 m $yr^{-1}$, with highest upflow in the central part of the mud volcano, decreasing towards the edge (Aloisi et al., 2004; Wallmann et al., 2006). Rates of anaerobic methane oxidation coupled to sulfate reduction were also highest in the central part, and the model predicted a consumption of up to 80% of the average methane flux (Wallmann et al., 2006). Gas flares extended up to 1300 m into the water column above the DMV (Greinert et al., 2006), but their source was not located. The expelled gas was mainly composed of methane with low amounts of ethane and propane. Previous investigations from other seep structures have shown that modeling of pore water gradients from retrieved cores tends to underestimate fluid flow rates, and that the relationship between fluid flow and methane consumption is not linear (de Beer et al., 2006; Niemann et al., 2006). In this study we revisited the DMV to investigate the spatial variation of fluid flow, methane and sulfide fluxes as well as associated biogeochemical processes using in situ methods. We aimed to find the hot spot of the DMV with regard to methane emission. We further tested the hypotheses that 1) fluid flow, methane efflux and consumption decrease radially from the source to the outer edge, 2) that methane consumption and sulfide production are controlled by fluid flow and 3) that mud volcanoes are a significant source for methane and sulfide to the Black Sea hydrosphere.

## 2. MATERIALS AND METHODS

### 2.1. Sampling

The DMV was visited during the RV Meteor M72/2 cruise in February/March 2007. High quality videographic observation at this site was accomplished using the cameras of the remotely operated vehicle (ROV) Quest 4000 (MARUM, Bremen), and recording of high resolution topographic maps was carried out with the sonar of the research vessel (Fig. 1). In a small area (N 44° 17.03'; E 34° 58.88') north of the geographical center of the mud volcano the multibeam maps showed an elevation of the seafloor of around 2-3 m above the surrounding area. Here temperature loggers mounted on the ROV frame recorded a temperature anomaly of +0.014 °C in the bottom water (Feseker et al., in press). Elevated water temperature is a reliable indicator for discharge of warm fluids, hence we planned sampling transects from the DMV summit as an area of increased fluid seepage to the outer edge of the mud volcano. Sediments were sampled from the summit (St. 1), the geographical center (St. 2), the edge (St. 3, St. 8), and sites north and south of the DMV (St. 9, St. 10), with short sediment cores (push cores: 10-20 cm sediment length) operated by the ROV manipulator, with a TV-guided multiple corer (TV-MUC, 20-40 cm sediment core length) equipped with a POSIDONIA positioning system or with a gravity corer (up to 4 m sediment length). Sampling locations are displayed in Fig. 1 and samples were labeled according to the international geoscience database PANGAEA (Table 1).

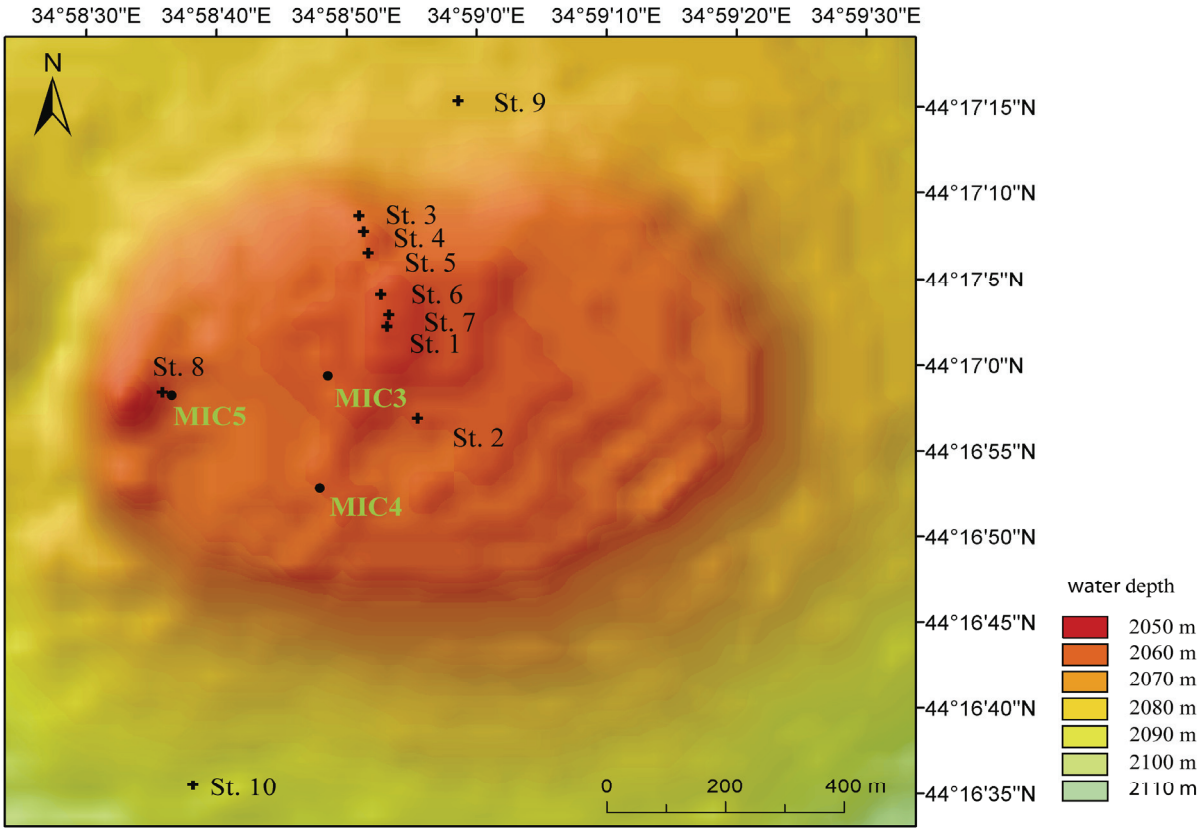


**Fig. 1: Bathymetric map of the DMV generated during the M 72/2 cruise with sampling stations (St. 1 - St. 10, displayed as ✚). Additionally, sampling positions MIC 3-5 from Wallmann et al. (2006) and Aloisi et al. (2004) are displayed as ●.**

### 2.2. In Situ Microsensor Measurements and Flux Calculations

High resolution geochemical gradients were measured in situ with a deep sea microprofiler (Fig. 2a), a similar unit as mounted on free-falling lander (Gundersen and Jørgensen, 1990; Wenzhöfer et al., 2000). However, instead of recording one set of profiles, the program could be restarted by a button (activated by the ROV arm), allowing multiple recordings per deployment (Treude et al., 2009). For measurements the profiler was precisely positioned at the seafloor and profiling was started with the ROV manipulator. The microprofiler was equipped with three $H_2S$ sensors, two pH sensors, one $N_2O$ sensor and one 3 mm thick temperature sensor (PT 100, Umweltsensorentechnik GmbH, Germany) (Jeroschewski et al., 1996; de Beer et al. 1997, Andersen et al., 2001). The sensors were calibrated at in situ temperature as described previously (Wenzhöfer et al., 2000; de Beer et al., 2006). The results from the $H_2S$ sensors were converted to total sulfide concentrations with a $pK_1$ for sulfide in seawater after Goldhaber and Kaplan (1975) and will further be referred to as sulfide (= $H_2S+HS^-+S^{2-}$).

Eight microprofile measurements were done along a transect from the geographical center (St. 2, in the 'outer center') as the most southward measuring point towards the northern edge (St. 3) (Fig. 1).

Here the profiler was deployed as close as possible (10 cm) to a crack in the sediment that was filled with white matter (further referred to as 'white patches'). The transect crossed the summit twice (St. 1a, b). Between the summit and the station at the northern edge, four other stations (St. 4-7, 'outer center') were sampled along the transect.

Diffusive sediment-water exchange fluxes of sulfide were calculated from the gradients in the diffusive boundary layer (DBL) using Ficks first law of diffusion:

$$J_{diff} = D \frac{dc}{dz} \qquad \text{(Eq. 3)},$$

where $J_{diff}$ = diffusive flux [mmol $m^{-2}$ $d^{-1}$], D = diffusion coefficient in water [$m^2$ $d^{-1}$] corrected for temperature and salinity (Li and Gregory, 1974), and dc/dz = concentration gradient [mmol $m^{-3}$ $m^{-1}$]. A diffusion coefficient D for $HS^-$ of $1.05 \times 10^{-4}$ $m^2$ $d^{-1}$ was used. Fluxes in the sediment were calculated from the gradients:

$$J_{diff} = \phi D_{sed} \frac{dc}{dz} \qquad \text{(Eq. 4)},$$

where $\phi$ = porosity and $D_{sed}$ = diffusion coefficient in the sediment [$m^2$ $d^{-1}$]. The diffusion coefficient $D_{sed}$ in the sediment was calculated according to Iversen and Jørgensen (1993):

$$D_{sed} = \frac{D}{1 + 3(1 - \phi)} \qquad \text{(Eq. 5)}$$

**2.3. Benthic Chamber Measurements**

A benthic chamber module constructed for the deployment by an ROV as described in Glud et al. (2009) was positioned at St. 1 on the DMV summit (Fig. 2b). Subsamples of the water enclosed in the chamber were taken with syringes after certain time intervals. The total deployment time of the benthic chamber was 8 hours. After retrieval of the chamber module, subsamples of each water sample were immediately fixed in ZnAc (2%) for chloride analyses (1 mL sample in 0.5 mL ZnAc), stored in sealed glass vials for methane concentration measurements, or frozen for nutrient analyses. Nutrients were measured with a Skalar Continuous-Flow Analyzer according to the method of Grasshoff et al. (1983). Concentrations of chloride were measured with non-suppressed ion-chromatography (Waters 510 HPLC Pump; Waters IC-Pak 50 x 4.6 mm anion exchange column; Waters 430 Conductivity

detector). Methane was measured in the headspace of the glass vial after heating to 60 °C for 30 minutes with a gas chromatograph (5890A, Hewlett Packard) coupled to a flame ionization detector (HP 5890 GC-FID). A GFT-Poropak-Q column (6 ft., 80/100) was installed for the chromatographic separation using the following temperature program: initial oven temperature: 40 °C, hold for 1 minute, heating rate of 20 °C $min^{-1}$ to 200 °C (1 minute). The precision of the gas chromatography measurements was ±5%.

**2.4. Bottom Water and Sediment Pore Water Analyses**

Seawater was sampled at defined spots 10 cm above the seafloor with the ROV fluid sampling system KIPS (Schmidt et al., 2007). The samples were enclosed in PFA (perfluoralkoxy) flasks, where they stayed during the dive. The pH was measured immediately after retrieval of the water samples. Subsamples for nutrient concentrations analyses were treated and measured as described above.

For analyses of sediment solutes either push cores or TV-MUC cores were taken north and south of the DMV (St. 9, St. 10) and close to the microprofiler stations at the summit (St. 1), the geographical center (St. 2) and the northern and the western edge with the conspicuous white patches on the seafloor (St. 3, St. 8). For methane analyses sediments were sampled with a gravity corer at the same stations. Pore water was extracted from the sediment with Rhizons (type: CSS, Rhizosphere Research Products, filter capacity of 0.1 µm). To allow Rhizon insertion, holes were drilled in the core liners at depth intervals of 1 cm and sealed with diffusion-tight PVC tape before sampling. The Rhizons were horizontally inserted into the sediment through the tape covering the predrilled holes and pore water was extracted gently with a syringe. Pore water subsamples for dissolved inorganic carbon (DIC) were quickly transferred into glass vials and poisoned with $HgCl_2$ for concentration measurements or sterile filtered for the determination of the DIC isotopic composition. Further subsamples (1 mL) were transferred into plastic vials with 0.5 mL ZnAc (2%) for sulfate, chloride and total sulfide determination. Sulfate and chloride were measured with non-suppressed ion-chromatography as described above. The photometric methylene blue method (Cline, 1969) was used to measure the sulfide concentration (= $H_2S+HS^-+S^{2-}$). DIC concentrations were measured with a conductivity detector (VWR scientific, model 1054) with 30 mmol $L^{-1}$ HCl and 10 mmol $L^{-1}$ NaOH as eluent according to the method of Hall and Aller (1992).

For methane concentration measurements 3 mL wet sediment samples were taken in cut off syringes, extruded into 20 mL vials and closed gas tight. 100 µL subsamples were taken from the gas phase with gas tight syringes and measured as described above. For onshore isotopic analysis, headspace gas (5 mL) was transferred into vials filled with saturated NaCl-solution using gas tight syringes and volume-volume exchange with hypodermic needles, and stored up-side-down.

The DIC isotopic composition was measured with a GasBench automated sampler, interfaced to a Finnigan MAT 251 mass spectrometer. Prior to analysis, a pore water aliquot (~0.5 to 1 mL) was

flushed with helium and subsequently acidified with phosphoric acid to allow $CO_2$ extraction. Analyses were calibrated with a known standard of defined isotopic value, primary standardization occurred by tank $CO_2$. Standard deviation was estimated to be less than 0.1‰. The stable carbon isotopic compositions of methane was analyzed by gas chromatography-isotope ratio mass spectrometry using a Thermo Finnigan Trace GC ultra coupled to a Thermo Finnigan Deltaplus XP mass spectrometer via a Thermo Finnigan GC Combustion III interface. The GC was equipped with a Supelco Carboxen 1006 Plot fused-silica capillary column (30 m x 0.32 mm in diameter). The initial oven temperature was set to 40 °C, held for 4 minute, raised by 20 to 50 °C $min^{-1}$ to 240 °C, held for 1 minute. Standard deviations were usually less than 1‰. Isotope ratios are given in δ-notation relative to the Vienna Peedee Belemnite Standard (V-PDB).

### 2.5. Sulfate Reduction (SR) and Anaerobic Methane Oxidation (AOM)

Rate measurements of anaerobic methane oxidation and sulfate reduction were done on retrieved cores with the whole core injection method. Samples were digested and analyzed as described before (Jørgensen, 1978; Treude et al., 2003; Kallmeyer et al., 2004). Briefly, push core sediments were vertically sub-sampled with small subcore liners (diameter = 2.5 cm). For each sampling station and method 3-4 replicate subcores were used. For sulfate reduction rate measurements 10 µL $^{35}SO_4^{2-}$ (75 kBq activity in water) and for anaerobic methane oxidation rate measurements 20 µL $^{14}CH_4$ (1.4 kBq activity in water) were injected. Measurements were carried out on sediment samples from the summit (St. 1), the geographical center (St. 2), the western edge in an area with white patches on top of the sediment (St. 8), as well as north (St. 9) and south (St. 10) of the DMV.

### 2.6. Acridine Orange Direct Counts (AODC)

Sediments were sliced in 1 cm intervals, fixed in formalin/seawater and the total number of microbial cells present in 1 $cm^3$ sediment was determined with acridine orange direct counts (AODC) via epifluoresence microscopy (Meyer-Reil, 1983; Boetius and Lochte, 1996). Cell counts include only single cell and no aggregates.

**Table 1: Sampling and analysis details from the different areas of the Dvurechenskii mud volcano (DMV). Samples and in situ instruments are labeled as in the PANGAEA database (http://www.pangaea.de). SR: sulfate reduction, AOM: anaerobic methane oxidation, AODC: acridine orange direct counts, DIC isotopes: $\delta^{13}C$ of dissolved inorganic carbon.**

| *Station* | *Mud volcano area* | *Coordinates* | *Measurement and PANGAEA event label* |
|---|---|---|---|
| St. 1a, St. 1b | Summit | 44° 17.03' N, 34° 58.88' E | Microsensor measurements (M72/2_309_MICP-1, MICP-8), benthic chamber deployment (M72/2_319_CHAM-1), SR, AOM (M72/2_309_PUC-68, -36,), Geochemical analyses (M72/2_309_PUC-51, -21, M72/2_319_PUC-2, M72/2_310), AODC (M72/2_309_PUC-36), |
| St. 2 | Outer center: geographical center of the DMV | 44° 16.95' N, 34° 58.94' E | Microsensor measurements (M72/2_309_MICP-2), SR, AOM (M72/2_270), Geochemical analyses (M72/2_269, M72/2_300), AODC (M72/2_270), |
| St. 3 | Northern edge | 44° 17.14' N, 34° 58.84' E | Microsensor measurements (M72/2_309_MICP-3), Geochemical analyses (M72/2_319_PUC-43) |
| St. 4 | Outer center | 44° 17.12' N, 34° 58.85' E | Microsensor measurements (M72/2_309_MICP-4) |
| St. 5 | Outer center | 44° 17.10' N, 34° 58.86' E | Microsensor measurements (M72/2_309_MICP-5) |
| St. 6 | Outer center | 44° 17.06' N, 34° 58.87' E | Microsensor measurements (M72/2_309_MICP-6) |
| St. 7 | Outer center | 44° 17.04' N, 34° 58.88' E | Microsensor measurements (M72/2_309_MICP-7) |
| St. 8 | Western edge | 44° 16.97' N, 34° 58.59' E | SR, AOM (M72/2_282_PUC-26, -67), Geochemical analyses (M72/2_282_PUC-27) |
| St. 9 | North of DMV | 44° 17.26' N, 34° 58.98' E | SR, AOM (M72/2_280), Geochemical analyses (M72/2_279, M72/2_314), AODC (M72/2_280) |
| St. 10 | South of DMV | 44° 16.58' N, 34° 58.64' E | SR, AOM (M72/2_291), Geochemical analyses (M72/2_291, M82/2_306) AODC (M72/2_291) |

## 3. RESULTS

### 3.1. Site and Sediment Description

The videotransects showed spatial differences in the surface morphology across the DMV (Fig. 2). At the geographical center (St. 2) the sediment surface was uneven with small hills (maximal heights of 20 cm). As visible by video observation and on retrieved sediments, a beige-brown fluffy layer of sedimented detritus of a thickness of about 1 cm was visible on top of the sediment. At the summit (St. 1) the sediment surface was even more hummocky, and ripple-like structures with a wavelength of approximately 50 cm were present. Here, no fluff layer was observed on top of the seafloor. At all stations of the outer center (St. 4 - St. 7) the seafloor was flat and the fluffy layer was covering the seafloor completely. At the northern edge (St. 3) and the western edge (St. 8) the thickness of the fluffy layer increased to 2 cm. Here, the sediment surface was again very hummocky and many cracks in the seafloor were observed. Sediments retrieved from the site north of the DMV (St. 9) were covered with up to 7 cm of the fluff. Here, no ROV dives were carried out but samples were recovered with a TV-guided multiple corer.

The material forming the fluffy layer comprises deposits of marine snow often found on top of Black Sea sediments. It was stratified with interspersed brown-green layers separating about 1 mm thick whitish zones representing the sedimentation of the coccolithophorid blooms. Below the fluffy layer sediment cores recovered from the DMV were homogeneous over the whole core length, with a dark, olive-green sediment color, a fine grained sediment texture and the presence of gas bubbles from methane oversaturation after retrieval. In the inner center of the DMV (between St. 1, 2, 6 and 7) gas bubbles were released from the sediment upon touching the seafloor with our instruments and samplers (Fig. 2e), indicating that methane was oversaturated in situ, at a depth of 2060 m. This is related to the high in situ methane concentrations of 118 mmol $L^{-1}$ in the warm summit and close-by sediments (Feseker et al., in press). A lower methane concentration of 85 mmol $L^{-1}$ was estimated for the DMV for the presence of methane hydrates in equilibrium with pore water in the outer center area with lower in situ temperatures (Wallmann et al., 2006). At the northern, western and southern edge of the DMV video observation showed white patches on the seafloor (Fig. 2f). Microscopy of recovered samples from these white patches showed needle shaped minerals (possibly barite). The white material did not contain sulfide-oxidizing bacteria, which are usually forming conspicuous whitish mats at cold seeps that reside in oxic and suboxic bottom waters.

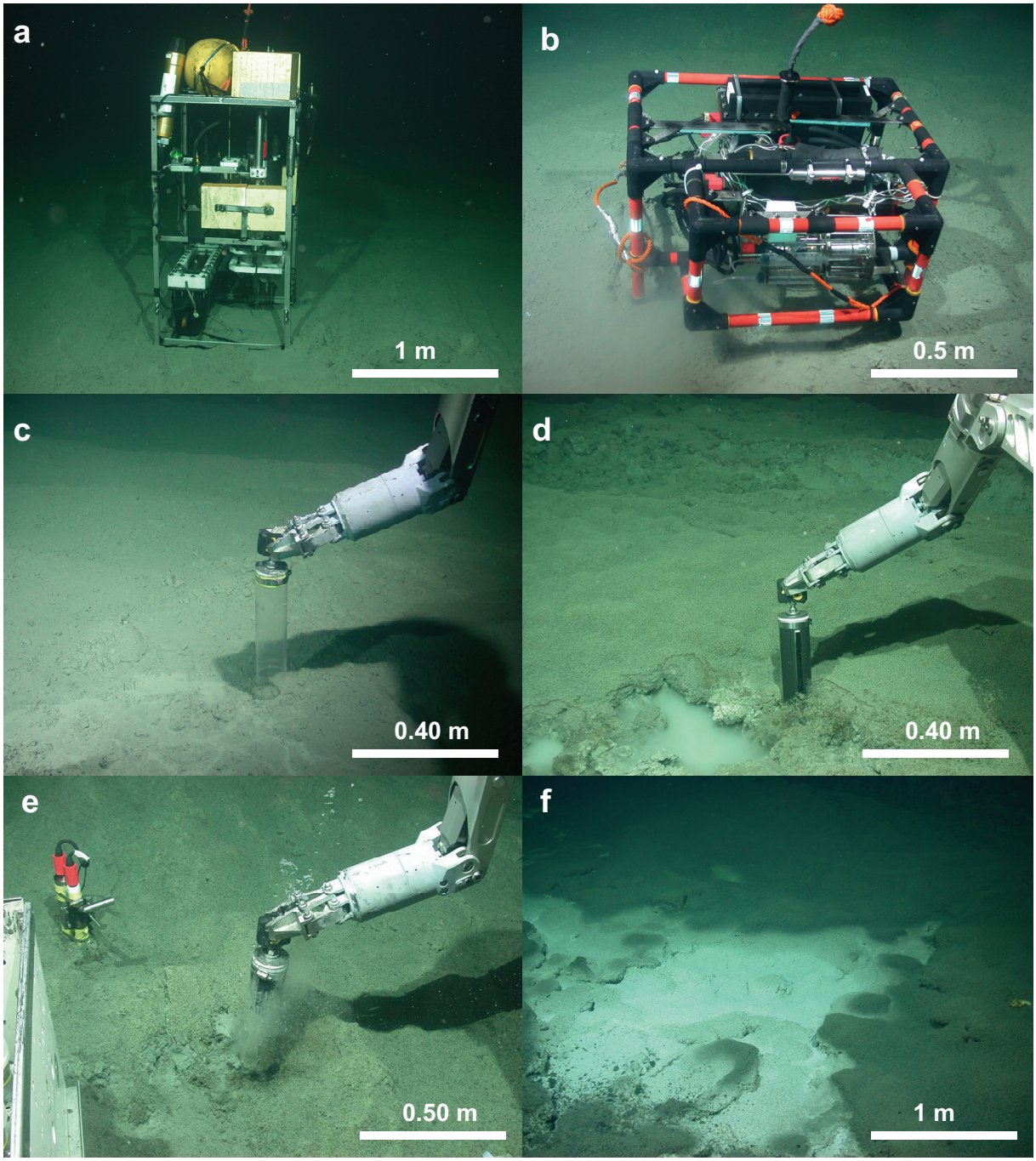


**Fig. 2: a) Microprofiler measurements, b) benthic chamber module deployment, and c) sediment sampling at the summit lacking the fluffy layer on top of the sediment; d) sediment sampling at the outer center with a thick fluffy layer on top of the sediment; e) gas bubble escape during coring at the geographical center; f) white patch at the western edge (diameter of about 2 m). Source: ROV Quest 4000 (MARUM, Bremen).**

## 3.2. In Situ Microsensor Measurements and Flux Calculations

### *3.2.1. Temperature*

With our microprofiler the highest sediment temperature gradients of up to 10.2 °C $m^{-1}$ were found at the summit of the DMV (St. 1; Fig. 3b, c). Here the temperature in the water column was also slightly elevated (+0.1 °C, 5 cm above the sediment). At St. 7 the temperature gradient was already reduced to 15% of the value at the summit (Fig. 3d) and declined further towards the northern edge. The temperature gradient at the geographical center (St. 2) was 1.2 °C $m^{-1}$, in between those of St. 6 and St. 5. At the outer edge (Fig. 3h) the gradient was only 2% of that of the summit. Sediment temperature gradients are summarized in Table 2.

### ***3.2.2. Sulfide***

Sulfide concentrations were the lowest in sediments of the summit of the DMV (St. 1, Fig. 3). The stations at the edge (St. 3) and outer center (St. 2, 4-7) showed elevated concentrations of sulfide in the sediment indicating local production. Neither the sulfide depth distributions, nor the concentration maxima of sulfide showed a gradual succession with distance from the summit, in contrast to the temperature gradients. Interestingly, at most sites two sulfide peaks were found in the sediment: one at the sediment-water interface and a second one at 3 - 15 cm bsf (below surface). In several profiles the sulfide steadily decreased with sediment depth below the second concentration maximum. The peaks indicate zones of net production separated by a sulfide sink. From the sum of the diffusive fluxes below and above these zones, an average volumetric consumption rate of 1,300 mmol $m^{-3}$ $d^{-1}$ was calculated from profiles with dips. The time needed for leveling of the two concentration maxima into a straight line by diffusion, was modeled using a 1-dimensional COMSOL multiphysics modeling suite.

Sulfide fluxes are summarized in Table 2 and are displayed as (I) fluxes calculated from the DBL (diffusive boundary layer)and thus representing the sulfide that is released from the sediment into the water column and (II) upward directed sulfide fluxes of the second, deeper located sulfide peak. The DBL sulfide fluxes (I) showed an increase along the transect from the summit to the northern edge. The sulfide fluxes calculated from the gradients in the subsurface sediment (II) were substantially lower with lowest fluxes at the summit, intermediate fluxes in the outer center area and highest fluxes at the edge.

Below the lower sulfide peak downward diffusion equals upward advection, in steady state. Fluid upflow velocities can then be calculated from the shape of the sulfide profiles below the peak (de Beer et al., 2006)

$$c_x = c_0 e^{-\frac{vx}{D_{sed}\phi}} \qquad \text{(Eq. 6)},$$

where $c_x$ is the solute concentration at sediment depth x, $c_0$ the concentration at the source (in this case the maximal concentration of the lower sulfide peak), v is the upflow velocity (m $yr^{-1}$) and all other variables are as described before. Modeling of the fluid upflow velocities from sulfide profiles was possible at St. 1 a, b, St. 2, and St. 3. The upflow velocities obtained by this modeling approach are displayed in Table 2. To estimate the effect of fluid flow on the sulfide fluxes, which in Table 2 are displayed as diffusive fluxes ($J_{diff}$), the total flux ($J_{tot}$) was calculated as described previously (de Beer et al., 2006):

$$J_{tot} = J_{diff} + J_{adv} = D\frac{dc}{dx} + vc \qquad \text{(Eq. 7)},$$

where $J_{adv}$ is the advective flux and c is the local concentration of the solute. The interfacial fluxes appeared to be hardly influenced by the upflow velocities obtained with Equation 6. Less than 5% of the total sulfide flux across the DBL was due to the advectional term. Depending on the upflow velocity used in Equation 7, the efflux from the second peak was 40-90% higher at the summit, and 25% higher at the geographical center. As this is in the range of the standard deviations of the measurements, in the further discussion the diffusive fluxes are considered accurate.

*3.2.3. pH*

At one deployment at the DMV summit (St. 1a) both pH sensors recorded a very distinct profile with a dip right below the sediment surface followed by a peak at 3.5 cm bsf, and a gradual decline below this depth (Fig. 3b). The replicate measurement at the summit (St. 1b, about 15 m away from the first one), showed a gradual decline of pH (Fig. 3c). At the outer center area north of the summit the pH was more or less constant with depth (Fig. 3d-g). The pH profiles at the edge (Fig. 3h) showed a steady decrease with depth with a similar profile as in St. 1b. At the geographical center (St. 2, outer center) there was a clear and strong peak in pH at a depth of 2 cm (Fig. 3a).

*3.2.4. $N_2O$*

The signal of the $N_2O$ sensor (data not displayed) showed a strong increase with depth at the summit and at the edge, but not in the stations in between. As no $N_2O$ can be present in the sediments of the DMV, the sensor must have responded to another gaseous species. In laboratory experiments, the sensor showed a response to sulfide, methanethiol but not to dimethyl sulfide. At the summit, where the $N_2O$ sensor showed a response, sulfide was absent, so sulfide cannot have caused the strong signal of the $N_2O$ sensor. Although it is unknown what substance the sensor has measured, the locations suggest release of a very labile, possibly oxidizing, compound in seepage areas of the DMV.

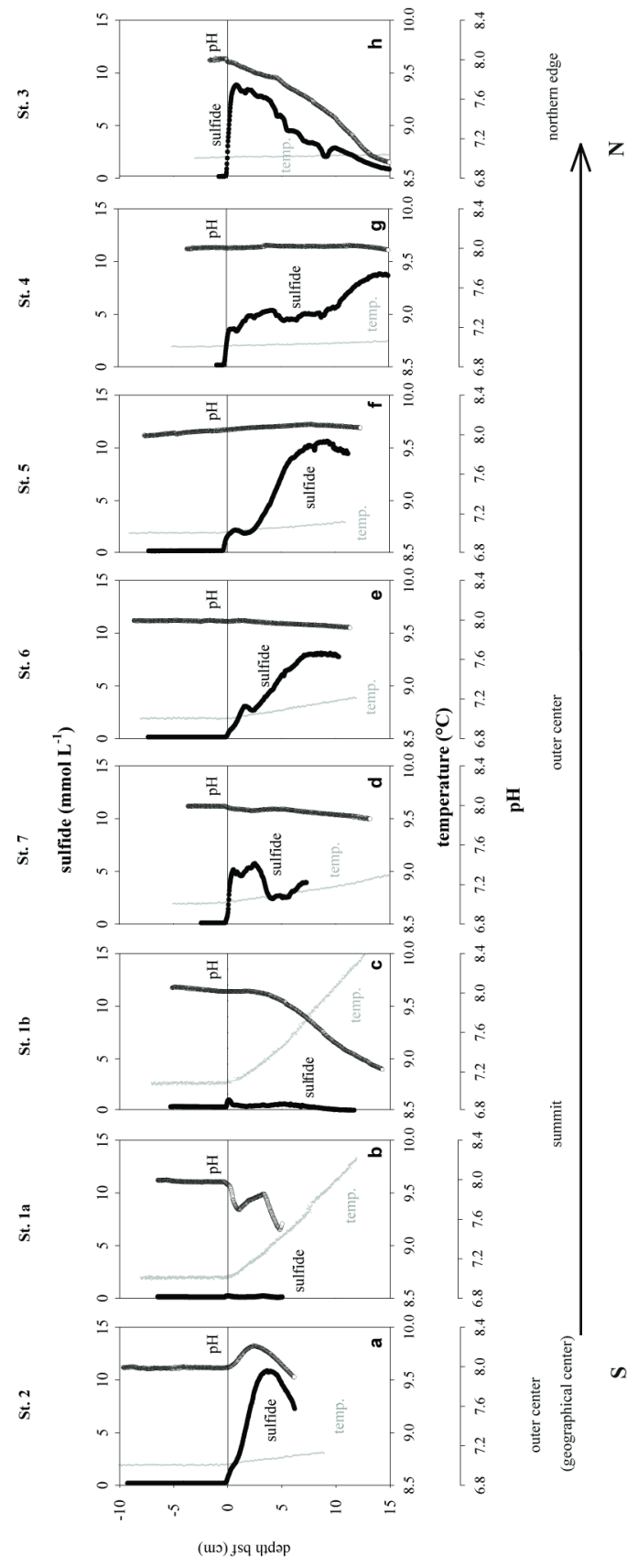


**Fig. 3: a-h) High resolution in situ microsensor profiles of sulfide ($H_2S$+$HS^-$+$S^{2-}$), pH. and temperature. Graphs are arranged in geographical order from the most southward station (outer center, geographical center, St. 2), crossing the summit (St. 1a, 1b), the outer center (St. 7-4), and ending at the northern edge (St. 3). Sulfide profiles from St. 1 to St. 6 are averages of results from three different sensors. At St. 7 only two sensors worked. Except for St. 1 only one of the two pH sensors was functional.**

### 3.3. Benthic Chamber Measurements

The summit of the DMV emits large amounts of methane, ammonium and chloride, as indicated by their concentration increase with time in the benthic chamber (Fig. 4; Table 3). Using the effluxes and pore water concentrations of these solutes, an upflow velocity of the mud volcano fluid of 1-3 m $yr^{-1}$ was estimated, assuming no consumption of the solutes in the sediment (Table 3).

**Table 3: Results from the 8 hour deployment of the benthic chamber at the summit of the DMV (St. 1). The upflow was calculated from the flux of solutes into the chamber and the solute fluid concentrations. *Methane concentration at the summit at equilibrium at ambient salinity, temperature and pressure as in Feseker et al. (in press); it was assumed that no methane was consumed in the summit sediments (*see* discussion); **ammonium concentration of the fluid as in Aloisi et al. (2004).**

| | Methane | Ammonium | Chloride |
|---|---|---|---|
| Total emission (mmol $m^{-2}$ $d^{-1}$) | 440 | 40 | 6.6 x$10^3$ |
| Concentration in mud volcano fluid (mmol $L^{-1}$) | 118* | 20** | 810 |
| Upflow (m $yr^{-1}$) | 1.2 | 0.7 | 2.8 |

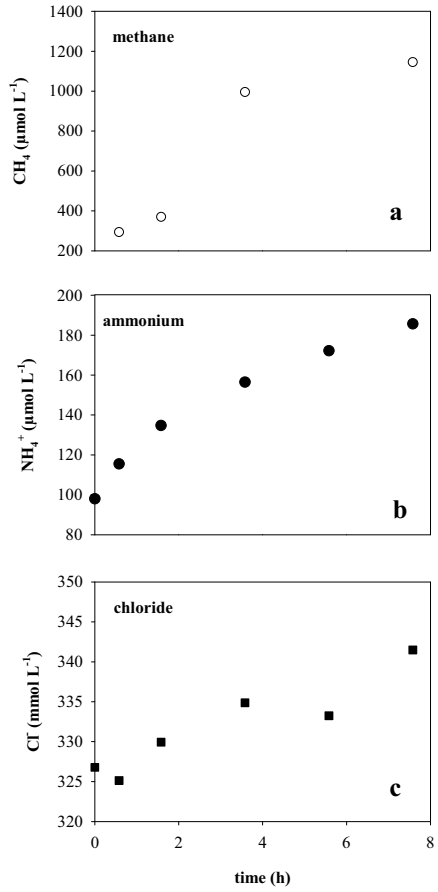


**Fig. 4: Results from analyses of a) methane, b) ammonium, and c) chloride in water collected inside the benthic chamber during the 8 hour deployment at the summit. Fluxes are calculated from the linear increase of the compounds inside the chamber.**

### 3.4. Geochemistry of Bottom Water and Pore Water

The pH of the Black Sea water at 10 cm above the seafloor of the DMV was 8.0. No nitrate or nitrite was found. Ammonium was equally high in the water above the summit and the geographical center. At the edge ammonium values were reduced to half of the amount of the other sites.

Solute distributions in recovered sediment cores differed substantially between the sampling stations. In the core from the summit (St. 1) a strong outgassing was observed after retrieval. In this core sulfate was detected to a depth of up to 10 cm after retrieval (Fig. 5a). In the less gaseous geographical center (St. 2) sulfate was found only to a depth of 5 cm (Fig. 5g). From the rather variable data it is clear that the pore water in the mud volcano is depleted in sulfate, and is elevated in chloride and DIC (Fig. 5). Outside the volcano (St. 9) concentrations of sulfate, chloride, sulfide, DIC, and the isotopic composition of the DIC were almost constant, and close to seawater values. The sulfide concentrations (Fig. 5c, i, o, s) were always lower than as measured in situ with the microprofiler, probably an effect of degassing during retrieval of the sediment cores. Methane concentrations after retrieval exceeded atmospheric saturation levels in all cores from the DMV (data not shown). The $\delta^{13}C$ signature of methane retrieved from the summit of the DMV was around -60‰ V-PDB. The DIC carbon isotope signature was similar over the whole sediment core (+8‰ V-PDB, Fig. 5d), and the same as found in several meters depth (data from gravity core 310, not shown), thus conversion of methane to DIC is slow at the summit compared to the transport of DIC from the subsurface. At the geographical center the DIC concentration increased to maximally 17 mmol $L^{-1}$ in 10 cm depth. Here the lowest DIC $\delta^{13}C$ value (-30‰ V-PDB) was found 2 cm below the sediment surface, and the signature became less depleted with depth (Fig. 5j), thus part of the DIC originated from AOM. Also at the edge stations the DIC was increased (Fig. 5 p, t). At the reference site (St. 9) outside the DMV the $\delta^{13}C$ signature was constant over the upper 10 sediment depth (Fig. 5z), and methane concentrations were <0.1 mmol $L^{-1}$ in the top 100 cm (data not shown).

### 3.5. Rates of Sulfate Reduction (SR) and Anaerobic Oxidation of Methane (AOM)

Depth-integrated rates (0-10 cm) of SR and AOM are summarized in Table 2. At the summit (St. 1, Fig. 5e) SR and AOM were very low in the upper 10 cm, but above detection limit. In the geographical center of the DMV (St. 2, Fig. 5k) SR reached 20 mmol $m^{-2}$ $d^{-1}$. The highest SR was detected directly at the seafloor-water interface, where it exceeded AOM significantly. Below the first cm, AOM and SR were similar. AOM rates were similar also at the western edge (St. 8), but SR exceeded AOM considerably (Fig. 5u). All sites except the summit showed considerably higher SR and AOM rates than the sites outside the DMV (Table 2, St. 9, St. 10, Fig. 5 aa; St. 10, not included in Fig. 5). Outside the mud volcano, integrated SR rates were only 0.2-1% of those in the outer center, but slightly higher than those of the summit.

| | St. 1 a/b Summit | St. 2 Outer center (geographical center) | St. 3 Northern edge | St. 4 Outer center | St. 5 Outer center | St. 6 Outer center | St. 7 Outer center | St. 8 Western edge | St. 9 North of DMV | St. 10 South of DMV |
|---|---|---|---|---|---|---|---|---|---|---|
| *Temperature gradient (°C $m^{-1}$)* | 9.7/10.2 | 1.2 | 0.2 | 0.3 | 0.8 | 1.7 | 1.7 | n.d. | n.d. | n.d. |
| *Fluid upflow from sulfide profile (m $yr^{-1}$)* | n.d. | 0.3 | 0.3 | n.d. | n.d. | n.d. | n.d. | n.d. | n.d. | n.d. |
| *(I) Diffusive sulfide flux across DBL (mmol $m^{-2}$ $d^{-1}$) ±SD* | 10 ±8 | 27 ±17 | 105 ±128 (sulfide flux I+II) | 74 ±45 | 45 ±29 | 15 ±16 | 37 ±1 | n.d. | n.d. | n.d. |
| *(II) Upward directed diffusive sulfide flux of second sulfide peak (mmol $m^{-2}$ $d^{-1}$) ±SD* | 0.7 ±0.5/ 0.3 | 18 ±4 | see (I) sulfide flux across the DBL | 5 ±2 | 10 ±1 | 7 ±2 | 3 ±1 | n.d. | n.d. | n.d. |
| *Depth integrated sulfate reduction rates (ex situ) (mmol $m^{-2}$ $d^{-1}$) ±SD* | 0.05 ±0 | 19.8 ±5.7 | n.d. | n.d. | n.d. | n.d. | n.d. | 108 ±38 | 0.2 ±0 | 0.2 ±0.1 |
| *Depth integrated methane oxidation rates (ex situ) (mmol $m^{-2}$ $d^{-1}$) ±SD* | 0.07 ±0.1 | 9.1 ±6 | n.d. | n.d. | n.d | n.d. | n.d. | 11.2 ±9.6 | <0.01 | 0.2 ±0.1 |

**Table 2: Results from in situ microsensor measurements and ex situ AOM and SR rate measurements. For the sulfide fluxes averages are given with standard deviation (SD) wherever possible (St. 1-6: *n*=3; St.7: *n*=2); for rate measurements *n*=3; rates are integrated over 0-10 cm sediment depth. n.d. = not determined.**

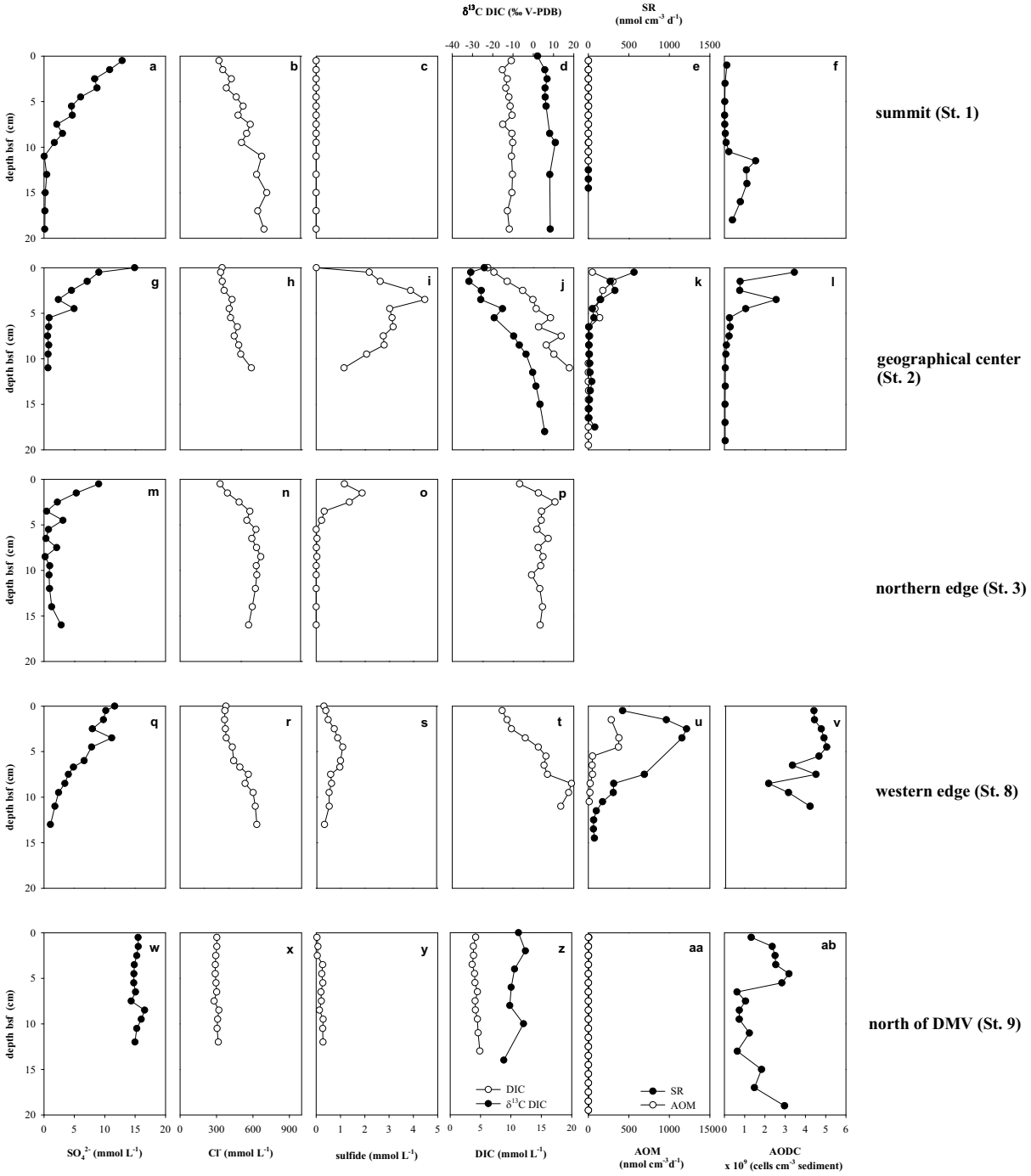


**Fig. 5: Pore water characteristics, anaerobic methane oxidation (AOM) and sulfate reduction (SR) rates, and acridine orange direct counts of cells in the sediments (AODC) of the DMV sampling stations.**

### 3.6. AODC Counts

Cell counts from the summit showed an unusual depletion in cells in the first 10 cm of the sediment with values of on average $10^7$ cells per $cm^3$ sediment (Fig. 5f). This is one to two orders of magnitude lower than in the same sediment depth at the sites north and south of the DMV (Fig. 5 ab). Below the depth of 10 cm the amount of cells in sediments from the summit increased to $10^9$ cells per $cm^3$ sediment. At the geographical center the number decreased with depth from $10^9$ cells per $cm^3$ sediment at the sediment surface to $10^7$ cells per $cm^3$ sediment in 18 cm depth (Fig. 5l). Numbers of cells were constantly high over the upper 10 cm at the western edge (St. 8). These cell counts always comprise only single cells and not aggregated microbial cells.

## 4. DISCUSSION

### 4.1. Patterns of Fluid Flow and Methane Flux

The Dvurechenskii mud volcano has the shape of a flat mud pie with a steep outer edge, and consists of a warm inner mud and fluid flow channel with a decreasing temperature gradient to the outside (Feseker et al., in press). Previous ex situ biogeochemical measurements at the DMV indicated a radial zonation of the DMV with highest fluid upflow and most intense anaerobic oxidation of methane in the central part, gradually decreasing towards the outer zone (Wallmann et al., 2006). During our investigations we studied the geochemical structure of the DMV with in situ tools to circumvent artifacts during recovery such as disturbances by degassing of cores. The in situ analyses and higher sampling resolution of our study revealed a more complex distribution and relationship of fluid flow and microbial methane and sulfur turnover than previously observed. This may reflect temporal and spatial changes in volcanic activity or a more precise picture of consistent local patterns. Combining detailed bathymetry and temperature probing, we found a hotspot of fluid flow and mud transport, associated with a small elevation (summit) north of the geographical center of the DMV, characterized by a high methane emission and low microbial methane consumption. This is most likely the source of the flare previously reported (Greinert et al., 2006), as we observed intensive gas ebullition after local disturbances of the seafloor during sampling. This hot spot area was not found before and thus was not investigated geochemically. Here, a fluid upflow velocity of 0.6-0.9 m $yr^{-1}$ was calculated from in situ microsensor measurements. From benthic chamber measurements the fluid flow was found to be 0.7-2.8 m $yr^{-1}$, so of the same order of magnitude. At the geographical center (St. 2) and outer edge (St. 3) we calculated from the lower peak of the in situ sulfide profile a fluid flow of 0.3 m $yr^{-1}$, similar to velocities previously observed in this area (Aloisi et al., 2004; Wallmann et al., 2006). In the summit area very low SR and AOM rates were found while outside the summit area, we measured considerable SR and AOM rates. However, the AOM and SR rates did not follow the

radially decreasing temperature gradients (Fig. 6). Although the fluid upflow velocity was similar as in the outer center, the temperature gradient was substantially lower at the edge than in all other zones of the DMV (Table 2). This may indicate different sources for warm and cold mud volcano fluids. Differences in sources could also explain the white patches on top of the sediment of the outer edge, which consist of mineral precipitations (presumably barite) and not of bacterial mats as previously thought (Bohrmann et al., 2003). Alternatively, the water seeping out at the edge has lost more heat than the water seeping out of the center, because of longer pathways or because it was cooled by methane hydrates (Feseker et al., in press).

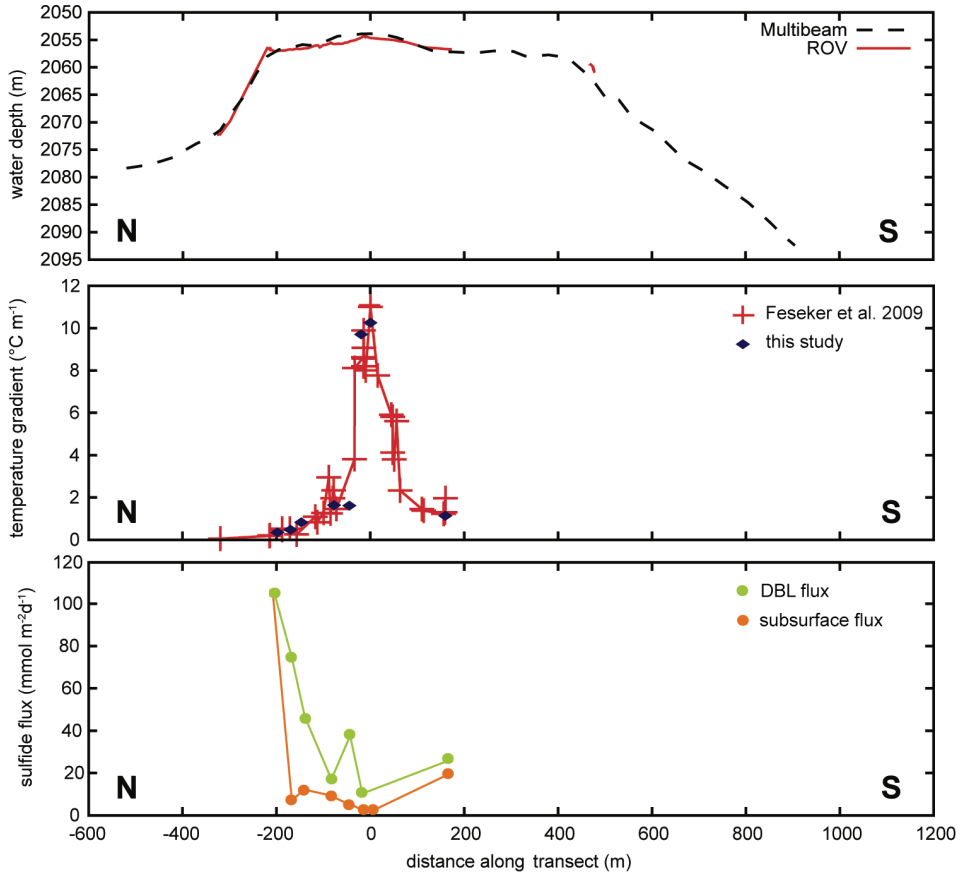


**Fig. 6: Temperature gradients and sulfide fluxes along a transect across the DMV compared to measurements from Feseker et al. (in press). a) bathymetry of the DMV, b) temperature gradients from Feseker et al. (in press) and from this study, c) DBL (diffusive boundary layer) and subsurface sulfide fluxes from this study.**

### 4.2. Factors Controlling Methane Consumption and Sulfide Production

Most mud volcanoes release methane in dissolved and gaseous phases. At the DMV we did not find active gas vents, but observed the release of gaseous methane upon disturbances of the seafloor such as the touch down of the ROV or coring (Fig. 2e). Measuring emission of dissolved methane in situ with the benthic chamber at the summit of the DMV resulted in estimates of a methane seepage rate of 440 mmol $m^{-2}$ $d^{-1}$. This is in the upper range of methane emission rates reported from other cold seeps, e.g. 15 mmol $m^{-2}$ $d^{-1}$ off the coast of Costa Rica (Mau et al., 2006), or maximally 100 mmol $m^{-2}$ $d^{-1}$ at Hydrate Ridge (Torres et al., 2002). Consumption of methane was virtually absent in the upper 15 cm of the summit sediment (Fig. 5e). The constant $\delta^{13}C$ DIC values with depth and low DIC pore water concentrations (Fig. 5d) confirm that no methane oxidation occurred in the sediment. In the more peripheral areas of the DMV, sulfate reduction and AOM reached around 10-100 mmol $m^{-2}$ $d^{-1}$, similar to the range previously reported from the DMV (Wallmann et al. 2006), or from other mud volcanoes like the Håkon Mosby Mud Volcano (Niemann et al., 2006) and the Kazan Mud Volcano (Haese et al., 2003). The discrepancy between sulfate reduction and methane oxidation rates (Table 2, Fig. 5) can be caused by the high patchiness of the sedimentary processes as observed from the in situ sulfide profiles.

Two factors may be responsible for the low AOM rates despite high methane concentrations at the summit. A striking difference with other methane seeps is the low number of cells in the upper 10 cm of the summit sediment, of on average $10^7$ cells per $cm^3$ (Fig. 5f). As a comparison, the sediments of the active Håkon Mosby Mud Volcano area and sediments of Hydrate Ridge contain up to $10^9$-$10^{10}$ cells per $cm^3$ (Knittel et al., 2003; Lösekann et al., 2007). At the reference site north of the DMV 50 times more cells were present than in the upper 10 cm of the summit sediment (Fig. 5 ab). Such a cell number anomaly could have been caused by the extrusion of a 'microbe-depleted' subsurface mud package that flew over the former seafloor, diluting out the slowly growing anaerobic methane oxidizers. Fresh mud flow at certain areas of the DMV was proposed earlier (Bohrmann et al., 2003; Aloisi et al., 2004; Wallmann et al., 2006) and also explains the absence of the fluffy layer on top of the seafloor at the summit. Consequently, sulfate reduction was even lower than at the reference station outside the DMV, where the contribution of organoclastic sulfate reduction was around 0.2 mmol $m^{-2}$ $d^{-1}$.

An additional factor explaining the low AOM rates at high methane flux sites could be sulfate limitation by high upward flow of sulfate-depleted fluids, preventing diffusion of seawater sulfate into the seafloor (de Beer et al., 2006; Niemann et al., 2006). At the high fluid upflow velocity as calculated for the summit (Table 2, 3) in situ sulfate penetration would be restricted to the upper few centimeter of the sediment, hence limiting AOM. High rates of AOM and a clear geochemical signature of DIC production from AOM was observed in the sediments of the DMV around the summit, which are subjected to lower upflow velocities of around 0.3 m $yr^{-1}$. Accordingly, DIC

concentrations increased considerably with depth and, associated with the peak in methane oxidation, DIC carbon showed the lowest $\delta^{13}C$ values at 2 cm bsf ($\delta^{13}C$ DIC: -30‰ V-PDB). This value comprises the isotopic signature of the DIC of the advected mud volcano fluids (+8‰ V-PDB), the DIC diffusing into the sediment from the overlying seawater (Black Sea seawater $\delta^{13}C$ DIC: +0.8‰ V-PDB, (Fry et al., 1991)), and the $^{13}C$ depleted DIC produced in the sediment from methane oxidation ($\delta^{13}C$-methane: -60‰ V-PDB).

As the diffusion coefficient of sulfate is around 1.7 times lower than that of sulfide, the maximal sulfide concentration at steady state conditions, under diffusional transport and complete sulfate conversion without re-oxidation, can reach 10 mmol $L^{-1}$ in Black Sea sediments (maximal sulfate concentration is 17 mmol $L^{-1}$). This value was approximated in some profiles of the DMV outer center, and the fluid upflow or the sulfide concentration might be an overestimation here. Interestingly, the sediment depths of the sulfide peaks were different in all center sites and this implies irregularities in the fluid flow across the mud volcano surface and disturbances by mud flow.

The concentration minima in the sulfide profiles are highly unusual and difficult to explain. Minima between peaks in the sulfide profiles indicate a sink for sulfide, by oxidation or precipitation. Oxygen and nitrate are absent below the chemocline of the Black Sea. However, atypical for Black Sea sediments, about 20-80 µmol $cm^{-3}$ amorphous and crystalline Fe(III)oxides or iron silicates and up to 150 µmol $L^{-1}$ dissolved iron were detected in the summit (data not shown) and might be responsible for the sulfide concentration minimum. Outside the summit no dissolved iron was found, concentrations of Fe(III)oxides were much lower and sulfide fluxes significantly higher. However, also here sulfide concentration minima were observed (St. 4-7). There is no dissolved iron and not enough Fe(III) to sustain the volumetric sulfide consumption of on average 1,300 mmol $m^{-3}$ $d^{-1}$ for a prolonged period. With a concentration of reactive iron of maximally 20,000 mmol $m^{-3}$ as found for the geographical center (data not shown), consumption can be maintained for about two weeks. Thus, we may have sampled a fresh mud flow not yet in steady state, or other processes must be responsible for consuming sulfide. A recent deposition and decomposition of fresh organic matter during a winter or spring bloom of *Emiliania huxleyi* as common in the Black Sea (Sorokin, 1983; Hay et al., 1990) could cause a non-steady state situation with two sulfide peaks. However, the sulfate reduction rates outside the mud volcano were not elevated compared to other observations in the abyssal part of the Black Sea (Jørgensen et al., 2001; Weber et al., 2001). Mud volcanoes are dynamic environments and transient state can be caused e.g. by changes in upward fluid flow velocity, hydrate dissociation, and mud flow events. However, over short distances of several centimeter, leveling of the two concentration maxima into a straight line by diffusion is in the order of days and the dip must be a transient phenomenon.

### 4.3. Mud Volcanoes as Source for Methane and Sulfide to the Black Sea

We identified an elevated zone with a radius of approximately 50 m (7800 $m^2$), which showed evidence of high fluid flow velocities and methane seepage. As no methane was consumed in the upper seafloor, the methane emission at the summit equaled a methane flux of $1.3x10^6$ mol $yr^{-1}$ (0.44 mol $m^{-2}$ $d^{-1}$ x 7800 $m^2$ x 365, Table 3). Methane emission in the surrounding center was not measured in situ, but can be calculated from the upflow velocity and the ambient concentration of dissolved methane. At the in situ methane concentration as estimated for methane hydrates in equilibrium with methane (0.085 mol $L^{-1}$, Wallmann et al., 2006), we determined an average methane transport of 0.07 mol $m^{-2}$ $d^{-1}$ or $1.9x10^7$ mol $yr^{-1}$ for the entire DMV center area and edge ($7.5x10^5$ $m^2$). However, as gas bubbles were released from the sediment, the in situ concentration will be higher and at the methane concentration as calculated for the ambient conditions (0.118 mol $L^{-1}$, Feseker et al., in press), the methane flux could be up to 0.1 mol $m^{-2}$ $d^{-1}$ or $2.7x10^7$ mol $yr^{-1}$ in the DMV center area. In the sediments of the DMV, methane utilization as inferred from the averaged sulfide flux (0.05 mol $m^{-2}$ $d^{-1}$, average of fluxes except from the summit) was $1.4x10^7$ mol $CH_4$ $yr^{-1}$, i.e. between 50-70% of the total methane flux was consumed. Accordingly, from the summit plus the outer center up to $1.4x10^7$ mol $CH_4$ $yr^{-1}$ was discharged in form of dissolved methane, which is about an order of magnitude higher than previous estimates of $1.9x10^6$ mol $CH_4$ $yr^{-1}$ (Wallmann et al., 2006). The Black Sea is the world's largest surface water reservoir of dissolved methane, with concentrations of around 11 µmol $L^{-1}$, and a methane inventory of $6x10^{12}$ mol with 5-20 yr turnover time (Reeburgh et al., 1991). Less than 15% of the methane comes from methanogenesis in the sediment, and seeps and gashydrates are thought to provide the remainder (Kessler et al., 2006). Even with our higher estimate for methane discharge at least 15,000 mud volcanoes with similar emission rates as the DMV would be needed to account for the Black Sea water column methane flux of 2.3 - $3.5x10^{11}$ mol $yr^{-1}$ as estimated from Kessler et al. (2006). To date the presence of more than 65 submarine mud volcanoes is known for the total Black Sea (Kruglyakova et al., 2002). Thus mud volcanoes are not relevant for the methane budgets of the Black Sea. Instead, gas seeps with strong and focused methane gas venting such as frequently found on shelves and slopes of the Black Sea (Polikarpov et al., 1992; Luth et al., 1999; Dimitrov, 2002; Michaelis et al., 2002) play the dominant role in the methane inventory of the Black Sea.

Also the amount of sulfide produced in the DMV is low compared to the total sulfide inventory of $1.4x10^{14}$ mol of the Black Sea (Neretin et al., 2001). It was previously estimated that the largest contribution to the sulfide inventory ($8.8x10^{11}$ - $1.5x10^{12}$ mol $yr^{-1}$) comes from the water column and only $9.4x10^{10}$ - $1.5x10^{11}$ mol $yr^{-1}$ sulfide is derived from the sediment (Neretin et al., 2001). The $1.4x10^7$ mol $yr^{-1}$ sulfide released from the DMV contributes maximally 0.01% to the total sediment derived sulfide content. Thus, although sulfate reduction and sulfide production are significant processes in the sediments of the DMV, the sulfide flux from mud volcanoes does not significantly add to the sulfide inventory of the Black Sea.

## 5. CONCLUSIONS

Our results show that the Dvurechenskii mud volcano represents an active methane seep and a highly dynamic geobio-system. Fluid and mud flow have a significant impact on the efflux of methane and sulfide, as well as on the anaerobic oxidation of methane. Medium to low fluid upflow allows high sulfate and methane consumption and reduces the methane emission to the water column by circa 50-70%. High fluid upflow >1 m $yr^{-1}$, and the extrusion of subsurface muds depleted in microbial assemblages prevents methane oxidation and leads to very high methane emission rates of >400 mmol $m^{-2}$ $d^{-1}$ at the summit of the DMV. This rather small elevation north of the geographical center of the DMV shows the highest temperature gradients, but almost no microbial sulfide production is detected. Hence, while temperature gradients, fluid flow, methane emission and consumption affect each other, they are not directly correlated in space. Our results suggest that deep-water mud volcanoes have only a small contribution on the methane and sulfide inventory of the Black Sea, and that most methane is derived from the abundant gas vents in shallower areas of the Black Sea margin.

## REFERENCES

Aloisi G., Drews M., Wallmann K., and Bohrmann G., 2004. Fluid expulsion from the Dvurechenskii mud volcano (Black Sea) - Part I. Fluid sources and relevance to Li, B, Sr, I and dissolved inorganic nitrogen cycles. *Earth Planet. Sci. Lett.* **225**, 347-363.

Andersen K., Kjær T., and Revsbech N. P., 2001. An oxygen insensitive microsensor for nitrous oxide. *Sensors Actuators B Chem.* **81**, 42-48.

Boetius A. and Lochte K., 1996. Effect of organic enrichments on hydrolytic potentials and growth of bacteria in deep-sea sediments. *Mar. Ecol. Prog. Ser.* **140**, 239-250.

Boetius A., Ravenschlag K., Schubert C. J., Rickert D., Widdel F., Gieseke A., Amann R., Jørgensen B. B., Witte U., and Pfannkuche O., 2000. A marine microbial consortium apparently mediating anaerobic oxidation of methane. *Nature* **407**, 623-626.

Bohrmann G., Ivanov M., Foucher J. P., Spiess V., Bialas J., Greinert J., Weinrebe W., Abegg F., Aloisi G., Artemov Y., Blinova V., Drews M., Heidersdorf F., Krabbenhoft A., Klaucke I., Krastel S., Leder T., Polikarpov I., Saburova M., Schmale O., Seifert R., Volkonskaya A., and Zillmer M., 2003. Mud volcanoes and gas hydrates in the Black Sea: new data from Dvurechenskii and Odessa mud volcanoes. *Geo-Mar. Lett.* **23**, 239-249.

Cline J. D., 1969. Spectrophotometric determination of hydrogen sulfide in natural waters. *Limnol. Oceanogr.* **14**, 454-458.

de Beer D., A. Schramm, C. M. Santegoeds, and M. Kühl, 1997. A nitrite microsensor for profiling environmental biofilms. *Appl. Environ. Microbiol*. **63:** 973-977.

de Beer D., Sauter E., Niemann H., Kaul N., Foucher J.-P., Witte U., Schlüter M., and Boetius A., 2006. In situ fluxes and zonation of microbial activity in surface sediments of the Håkon Mosby Mud Volcano. *Limnol. Oceanogr.* **51**, 1315-1331.

Dimitrov L., 2002. Contribution to atmospheric methane by natural seepages on the Bulgarian continental shelf. *Continent. Shelf Res.* **22**, 2429-2442.

Feseker T., Pape T., Wallmann K., Klapp S. A., Schmidt-Schierhorn F., and Bohrmann G. The thermal structure of the Dvurechenskii mud volcano and its implications for gas hydrate stability and eruption dynamics. *Mar. Petrol. Geol.* **In Press, Corrected Proof**.

Fry B., Jannasch H. W., Molyneaux S. J., Wirsen C. O., Muramoto J. A., and King S., 1991. Stable isotope studies of the carbon, nitrogen and sulfur cycles in the Black Sea and the Cariaco Trench. *Deep-Sea Res. Pt. A* **38**, S1003-S1019.

Glud R. N., Stahl H., Berg P., Wenzhöfer F., Oguri K., and Kitazato H., 2009. In situ microscale variation in distribution and consumption of $O_2$: A case study from a deep ocean margin sediment (Sagami Bay, Japan). *Limnol. Oceanogr.* **54**, 1-12.

Goldhaber M. B. and Kaplan I. R., 1975. Apparent dissociation constants of hydrogen sulfide in chloride solutions. *Mar. Chem.* **3**, 83-104.

Grasshoff K., Ehrhardt M., and Kremling K., 1983. *Methods of seawater analysis*. Verlag Chemie, Weinheim.

Greinert J., Artemov Y., Egorov V., De Batist M., and McGinnis D., 2006. 1300-m-high rising bubbles from mud volcanoes at 2080m in the Black Sea: Hydroacoustic characteristics and temporal variability. *Earth Planet. Sci. Lett.* **244**, 1-15.

Gundersen J. K. and Jørgensen B. B., 1990. Microstructure of diffusive boundary layers and the oxygen uptake of the sea floor. *Nature* **345**, 604-607.

Haese R. R., Meile C., Van Cappellen P., and de Lange G. J., 2003. Carbon geochemistry of cold seeps: Methane fluxes and transformation in sediments from Kazan mud volcano, eastern Mediterranean Sea. *Earth Planet. Sci. Lett.* **212**, 361-375.

Hall P. O. and Aller R. C., 1992. Rapid, small-volume, flow injection analysis for $\Sigma CO_2$ and $NH_4^+$ in marine and freshwaters. *Limnol. Oceanogr.* **37**, 1113-1119.

Hay B. J., Honjo S., Kempe S., Ittekkot V. A., Degens E. T., Konuk T., and Izdar E., 1990. Interannual variability in particle flux in the southwestern Black Sea. *Deep-Sea Res. Pt. A* **37**, 911-928.

Hinrichs K. U., Hayes J. M., Sylva S. P., Brewer P. G., and DeLong E. F., 1999. Methane-consuming archaebacteria in marine sediments. *Nature* **398**, 802-805.

Iversen N. and Jørgensen B. B., 1993. Diffusion coefficients of sulfate and methane in marine sediments: Influence of porosity. *Geochim. Cosmochim. Acta* **57**, 571-578.

Jeroschewski P., Steuckart C., and Kühl M., 1996. An amperometric microsensor for the determination of $H_2S$ in aquatic environments. *Anal. Chem.* **68**, 4351-4357.

Jørgensen B. B., 1978. A comparison of methods for the quantification of bacterial sulfate reduction in coastal marine sediments: 1. Measurements with radiotracer techniques. *Geomicrobiol. J.* **1**, 11-27.

Jørgensen B. B., Weber A., and Zopfi J., 2001. Sulfate reduction and anaerobic methane oxidation in Black Sea sediments. *Deep-Sea Res. Pt. I* **48**, 2097-2120.

Kallmeyer J., Ferdelman T. G., Weber A., Fossing H., and Jørgensen B. B., 2004. A cold chromium distillation procedure for radiolabeled sulfide applied to sulfate reduction measurements. *Limnol. Oceanogr.: Methods* **2**, 171-180.

Kessler J. D., Reeburgh W. S., Southon J., Seifert R., Michaelis W., and Tyler S. C., 2006. Basin-wide estimates of the input of methane from seeps and clathrates to the Black Sea. *Earth Planet. Sci. Lett.* **243**, 366-375.

Knittel K., Boetius A., Lemke A., Eilers H., Lochte K., Pfannkuche O., Linke P., and Amann R., 2003. Activity, distribution, and diversity of sulfate reducers and other bacteria in sediments above gas hydrate (Cascadia margin, Oregon). *Geomicrobiol. J.* **20**, 269-294.

Kruglyakova R., Gubanov Y., Kruglyakov V., and Prokoptsev G., 2002. Assessment of technogenic and natural hydrocarbon supply into the Black Sea and seabed sediments. *Continent. Shelf Res.* **22**, 2395-2407.

Li Y.-H. and Gregory S., 1974. Diffusion of ions in sea water and in deep-sea sediments. *Geochim. Cosmochim. Acta* **38**, 703-714.

Lösekann T., Knittel K., Nadalig T., Fuchs B., Niemann H., Boetius A., and Amann R., 2007. Diversity and abundance of aerobic and anaerobic methane oxidizers at the Haakon Mosby Mud Volcano, Barents Sea. *Appl. Environ. Microbiol.* **73**, 3348-3362.

Luth C., Luth U., Gebruk A. V., and Thiel H., 1999. Methane gas seeps along the oxic/anoxic gradient in the Black Sea: manifestations, biogenic sediment compounds and preliminary results on benthic ecology. *Mar. Ecol.* **20**, 221-249.

Mau S., Sahling H., Rehder G., Suess E., Linke P., and Soeding E., 2006. Estimates of methane output from mud extrusions at the erosive convergent margin off Costa Rica. *Mar. Geol.* **225**, 129-144.

Meyer-Reil L.-A., 1983. Benthic response to sedimentation events during autumn to spring at a shallow water station in the Western Kiel Bight: 2. Analysis of benthic bacterial populations. *Mar. Biol.* **77**, 247-256.

Michaelis W., Seifert R., Nauhaus K., Treude T., Thiel V., Blumenberg M., Knittel K., Gieseke A., Peterknecht K., Pape T., Boetius A., Amann R., Jørgensen B. B., Widdel F., Peckmann J. R., Pimenov N. V., and Gulin M. B., 2002. Microbial reefs in the Black Sea fueled by anaerobic oxidation of methane. *Science* **297**, 1013-1015.

Neretin L. N., Volkov I. I., Böttcher M. E., and Grinenko V. A., 2001. A sulfur budget for the Black Sea anoxic zone. *Deep-Sea Res. Pt. I* **48**, 2569-2593.

Niemann H., Lösekann T., de Beer D., Elvert M., Nadalig T., Knittel K., Amann R., Sauter E. J., Schlüter M., Klages M., Foucher J.-P., and Boetius A., 2006. Novel microbial communities of the Haakon Mosby mud volcano and their role as a methane sink. *Nature* **443**, 854-858.

Polikarpov G. G., Egorov V. N., Gulin S. B., Gulin M. B., and Stokozov N. A., 1992. Gas seeps from the bottom of the Black Sea - a new object of molismology. In: Polikarpov, G. G. (Ed.), *Molismology of the Black Sea*, Nauka, Kiev.

Reeburgh W. S., Ward B. B., Whalen S. C., Sandbeck K. A., Kilpatrick K. A., and Kerkhof L. J., 1991. Black Sea methane geochemistry. *Deep-Sea Res. Pt. A* **38**, S1189-S1210.

Revsbech N. P. and Ward D. M., 1983. Oxygen microelectrode that is insensitive to medium chemical composition - use in an acid microbial mat dominated by *Cyanidium caldarium*. *Appl. Environ. Microbiol.* **45**, 755-759.

Schmidt K., Koschinsky A., Garbe-Schönberg D., de Carvalho L. M., and Seifert R., 2007. Geochemistry of hydrothermal fluids from the ultramafic-hosted Logatchev hydrothermal field, 15 degrees N on the Mid-Atlantic Ridge: Temporal and spatial investigation. *Chem. Geol.* **242**, 1-21.

Sorokin Y. I., 1983. The Black Sea. In: Ketchum, B. H. (Ed.), *Ecosystems of the World. Estuaries and Enclosed Seas.* Elsevier, Amsterdam.

Torres M. E., McManus J., Hammond D. E., de Angelis M. A., Heeschen K. U., Colbert S. L., Tryon M. D., Brown K. M., and Suess E., 2002. Fluid and chemical fluxes in and out of sediments hosting methane hydrate deposits on Hydrate Ridge, OR, I: Hydrological provinces. *Earth Planet. Sci. Lett.* **201**, 525-540.

Treude T., Boetius A., Knittel K., Wallmann K., and Jørgensen B. B., 2003. Anaerobic oxidation of methane above gas hydrates at Hydrate Ridge, NE Pacific Ocean. *Mar. Ecol. Prog. Ser.* **264**, 1-14.

Treude T., Smith C. R., Wenzhöfer F., Carney E., Bernardino A. F., Hannides A. K., Krüger M., and Boetius A., 2009. Biogeochemistry of a deep-sea whale fall: sulfate reduction, sulfide efflux and methanogenesis. *Mar. Ecol. Prog. Ser.* **382:** 1-21.

Wallmann K., Drews M., Aloisi G., and Bohrmann G., 2006. Methane discharge into the Black Sea and the global ocean via fluid flow through submarine mud volcanoes. *Earth Planet. Sci. Lett.* **248**, 545-560.

Weber A., Riess W., Wenzhöfer F., and Jørgensen B. B., 2001. Sulfate reduction in Black Sea sediments: in situ and laboratory radiotracer measurements from the shelf to 2000m depth. *Deep-Sea Res. Pt. I* **48**, 2073-2096.

Wenzhöfer F., Holby O., Glud R. N., Nielsen H. K., and Gundersen J. K., 2000. In situ microsensor studies of a shallow water hydrothermal vent at Milos, Greece. *Mar. Chem.* **69**, 43-54.

Woodside J., Ivanov M. K., and Limonov A. F., 1997. *Neotectonics and fluid flow through seafloor sediments in the Eastern Mediterranean and Black Sea, Preliminary results of the geological and geophysical investigations during the ANAXIPROBE/TTR-6 cruise of the R/V Gelendzhik (July-August 1996)*. UNESCO, Paris.

Chapter 5

# A deep reactive ferric iron source drives sulfide oxidation in the euxinic surface sediments of the Dvurechenskii mud volcano (Black Sea)

Anna Lichtschlag, Alexey Kamyshny, Jr.*, Timothy G. Ferdelman and Dirk de Beer

Max-Planck-Institute for Marine Microbiology, Celsiusstrasse 1, 28359 Bremen, Germany

*current address: Department of Geology and ESSIC, University of Maryland, College Park, Maryland 20742, USA

in preparation for *Dee Sea Research Part I*

*Acknowledgements.*

We thank captain, crew and shipboard scientists of the R/V Meteor cruise M72/2 and the ROV Quest team (MARUM, Bremen) for their excellent support for work at sea. We are grateful for technical assistance from Martina Alisch and Duygu Sevgi Sevilgen. We also would like to thank Stefanie Grünke for the preparation of the sampling map.

This project was made possible by the GEOTECHNOLOGIEN project MUMM II (03G0608C) funded by the German Ministry of Education and Research (BMBF) and German Research Foundation (DFG), by the EU FP6 program HERMES (GOCE-CT-2005-511234-1) as well as by the Helmholtz Societies. A K thanks the Max-Planck-Society and the MPG Minerva Program for support.

**Abstract**

**The depth distribution of sulfur species (S(II), S(0), $S_n^{2-}$, $S_2O_3^{2-}$, $SO_3^{2-}$, $SO_4^{2-}$) were studied in the Dvurechenskii mud volcano, a cold seep situated in the permanent anoxia of the eastern Black Sea Basin (Sorokin Trough, 2060 m water depth). Unusually high sulfite concentrations of up to 11 µmol $L^{-1}$, thiosulfate concentrations of up to 22 µmol $L^{-1}$, pore water zero-valent sulfur concentrations of up to 150 µmol $L^{-1}$ and up to 5 polysulfide species were measured in the upper sediment. The only available electron-acceptors for the oxidation of hydrogen sulfide to sulfur intermediates are iron-minerals, detected in the sediments and expelled from the Dvurechenskii mud volcano with the mud. Up to 60 µmol $g^{-1}$ of reactive iron-minerals and up to 170 µmol $L^{-1}$ dissolved iron were present in the central summit with the highest fluid upflow and obviously fresh mud outflow. The iron-mineral content decreased towards the edge of the mud volcano, however sulfur intermediate concentrations and speciation concurrently increased, with the most intense sulfur speciation found also at the edge of the mud volcano. Calculations of the equilibrium between the polysulfides and the zero-valent elemental sulfur showed that in the whole mud volcano the sulfur system is not in equilibrium. The deviation from equilibrium increases with depth and decreases from the geographical center towards the edge.**

## 1. INTRODUCTION

The main pathway for hydrogen sulfide formation in the marine environment is bacterial sulfate reduction coupled to mineralization of organic matter buried in the seafloor. However, hydrogen sulfide is also produced during the anaerobic oxidation of methane (AOM) with sulfate (Eq. 1) (Barnes and Goldberg, 1976; Martens and Berner, 1974). This is the most important pathway for the removal of methane derived from organic-rich sediments where methane is produced on site (Jørgensen et al., 2004; Treude et al., 2005) and from cold seep structures such as microbial reefs, pockmarks and mud volcanoes, where methane is largely supplied from a deep reservoir (e.g. Haese et al., 2003; Joye et al., 2004; Mau et al., 2006; Michaelis et al., 2002; Niemann et al., 2005; Sauter et al., 2006). In such systems methanotrophic archaea and sulfate reducing bacteria are responsible for the anaerobic turnover of the ascending methane with sulfate from the seawater (Boetius et al., 2000) and hydrogen sulfide is produced in equimolar amounts as methane is consumed.

$$CH_4 + SO_4^{2-} \rightarrow HS^- + HCO_3^- + H_2O \qquad \text{(Eq. 1)}$$

Hydrogen sulfide formed through either pathway flows in a complex microbiological and geochemical redox cycle, with sulfate as the most oxidized end product and pyrite as the dominant buried reduced product (Zopfi et al., 2004). In most methane-rich cold seeps the turnover of hydrogen sulfide with oxygen or nitrate supports a rich chemolithotrophic community. Macrobenthos with thiotrophic symbionts, and giant sulfur bacteria forming extensive mats on the sediment surface, oxidize hydrogen sulfide either completely to sulfate or transform it to elemental sulfur (de Beer et al., 2006; Niemann et al., 2006; Olu-Le Roy et al., 2004; Olu et al., 1997). In normal marine sediments without the abundant chemoautotrophic fauna the hydrogen sulfide is also either completely re-oxidized to sulfate or sulfur intermediates form, whereas different shunts with various sulfur intermediate production and consumption processes are known (Zopfi et al., 2004, and reference therein).

In the oxidation of hydrogen sulfide elemental sulfur is a common intermediate produced by various electron-acceptors. Elemental sulfur content in sediments is usually higher than of other intermediate oxidation state sulfur compounds because it is less bio-available than other sulfide oxidation products (Zopfi et al., 2004). Sulfur itself reacts with hydrogen sulfide, producing polysulfides ($S_n^{2-}$) and their protonated forms with n = 2-8 (Maronny, 1959; Boulegue and Michard, 1978; Kamyshny et al., 2004; Kamyshny et al., 2007). Thiosulfate is produced in marine sediments by oxidation of hydrogen sulfide with oxygen (both chemically and microbiologically), oxidized iron and manganese (chemically), nitrate (microbiologically), and also during the chemical oxidation of FeS and $FeS_2$. Sulfite in marine sediments is produced by similar processes of hydrogen sulfide oxidation with oxygen (both chemically and microbiologically), or with iron- and manganese-oxides (chemically) (Zopfi et al., 2004, and reference therein).

In the Black Sea the electron-acceptors for microbiological and geochemical hydrogen sulfide oxidation are depleted below the pycnocline and sulfide oxidation processes are limited by the small flux of settling metal-oxides. At cold seeps in the anoxic waters of the Black Sea thiotrophic mats or macrobenthos adapted to extreme conditions have not been found. However, cold seeps are unique environments where many geochemical processes deviate from normal and where the sulfur cycle has not been completely deciphered. Although the presence of intermediate sulfur species as elemental sulfur, thiosulfate and tetrathionate in anoxic marine sediments is well documented (Troelsen and Jørgensen, 1982; Podgorsek and Imhoff, 1999; Zopfi et al., 2004), the distribution of these compounds, and their sources and sinks, have never been studied in cold seep systems, where sulfur turnover plays a key role. The aim of this work was to determine whether also sulfur intermediates are formed in a reduced environment combined to advective flow. With a variety of analytical techniques (Fahey and Newton, 1987; Zopfi et al., 2001; Zopfi et al., 2004; Kamyshny et al., 2006; Kamyshny, 2009; Kamyshny et al., 2009), we can assess the speciation and concentrations of a range of hydrogen sulfide oxidation products, such as polysulfides ($S_n^{2-}$), colloidal and solid elemental sulfur (S(0)), thiosulfate ($S_2O_3^{2-}$), sulfite ($SO_3^{2-}$), and polythionates ($S_nO_6^{2-}$). Methods for analysis of individual polysulfides (Kamyshny et al., 2004; Kamyshny et al., 2006) are now available and allow to calculate how far the polysulfides are from equilibrium with zero-valent sulfur in the sediment (Kamyshny et al., 2008). Deviation from equilibrium might be a proof of ongoing conversion processes. We tested the hypothesis that oxidation processes can be driven by oxidants originating from a cold seep, the Dvurechenskii mud volcano, situated in the permanent anoxic waters in the Black Sea (Sorokin Trough).

## 2. MATERIAL AND METHODS

### 2.1. Sampling Site

The Sorokin Trough in the northeastern part of the Black Sea is a 150 km long and 50 km wide depression zone that has developed as a foredeep of the Crimean Mountains (Tugolesov et al., 1985). In the Sorokin Trough diapiric mud volcanoes have formed due to a SE-NW directed tectonical compression regime (Krastel et al., 2003). The Dvurechenskii mud volcano (DMV) is located in the central part of the Sorokin Trough (N 44° 17'; E 34° 59') at a water depth of 2060 m and thus in permanently anoxic waters (Fig. 1). The hydrogen sulfide concentration is around 370 µmol $L^{-1}$ at this depth (Neretin et al., 2001) and the ambient bottom water temperature is 9 °C (Bohrmann et al., 2003). The DMV is elevated 80 m above the seafloor, and has an extension of about 1200 by 800 m. Morphologically, it resembles a flat mud pie with a steep outer edge.

Submarine mud volcanoes are tectonic windows where pore waters, gases and mud from a deep located source are released into the marine environment. At the DMV the source of origin of the expelled mud is the 4-5 km thick Maikopian formation (Oligocene-Lower Miocene), which is overlain by a 2-3 km thick layer of Pliocene to Quaternary sediments (Tugolesov et al., 1985). The ascending fluids contain large amounts of methane and are characterized by an enrichment in $Cl^-$, $Li^+$, $Ba^{2+}$, $Sr^{2+}$, $I^-$, and dissolved inorganic nitrogen and a depletion in sulfate and hydrogen sulfide (Aloisi et al., 2004). The intensity of fluid flow and the occurrence of mud extrusions change laterally. North of the 'geographical center' an approximately 8000 $m^2$ large 'summit' with fresh mud flow and high upflow of methane-rich fluids was detected by visual observation, by multibeam survey, and by temperature anomalies in the water column. In the peripheral area surrounding this summit, no recent mud flow was detected, and fluid upflow is substantially lower. At the edge of the DMV seepage occurs locally and is indicated by white patches covering the sediment (Feseker et al. in press.; Bohrmann et al., 2003; Aloisi et al., 2004; Wallmann et al., 2006, Lichtschlag et al., subm.).

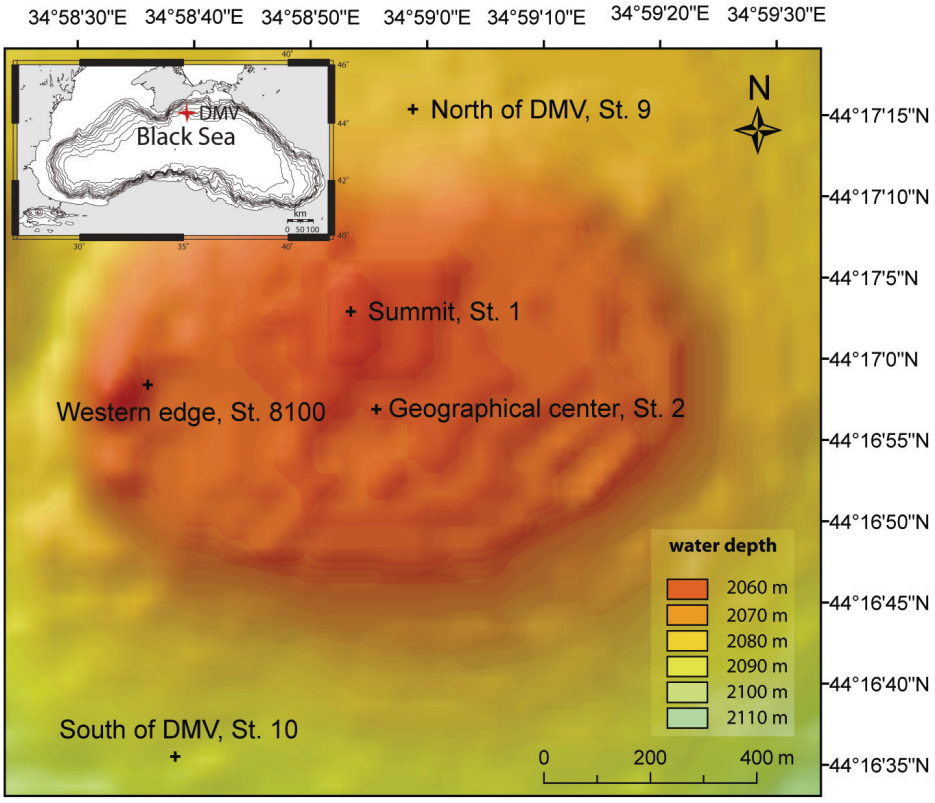


**Fig. 1: Bathymetric map with sampling locations at the Dvurechenskii mud volcano (DMV), generated with the ship multibeam of the R/V Meteor during the M72/2 cruise.**

## 2.2. Sampling Technique

Sampling was conducted on board of the German research vessel Meteor (cruise M72/2). Push cores operated by the ROV Quest 4000 from the MARUM (Bremen) were used to obtain precisely targeted sediment cores of 20 cm length. A video-guided multiple corer (MUC) was used to obtain

sediment cores with a maximal length of 30 cm. Sediment cores were sampled at the 'summit' (St. 1), at the 'geographical center' of the mud volcano (St. 2), at the 'western edge' with white patches on top of the sediment (St. 8), and north and south of the DMV (St. 9, St. 10) (Table 1, Fig. 1).

All cores were immediately after retrieval stored and processed at in situ temperature (9 °C). Samples for sulfide and sulfide oxidation intermediates content measurements were placed in a glove-box flushed with nitrogen (≤0.3% $O_2$ in the gas phase), and all samples were treated under anoxic conditions until they were fixed.

The pore water was extracted with Rhizon samplers (type: CSS, Rhizosphere Research Products, NL-Wageningen) with a filter pore diameter of 100 nm. The Rhizons were horizontally inserted in cores through predrilled holes that had been sealed with gas tight tape before sampling. After insertion, the Rhizons were connected to syringes with which a small under-pressure was applied. Prior to sulfur intermediates extraction, the Rhizons were stored for at least one hour in anoxic water in the glove-box. The syringes for pore water extraction were flushed several times with the glove-box atmosphere before they were attached to the Rhizons. The first milliliter of the extracted pore water was discharged to avoid any possible contamination from oxygen absorbed on the Rhizons and/or syringe plunger and the dilution of seawater sample with anoxic Milli-Q in which the Rhizons were stored.

The introduction of substantial biases in sulfur species concentrations due to the pore water extraction with Rhizons was excluded by testing the Rhizons in the laboratory under conditions similar to the conditions during sampling. For this test a liquid phase with a known sulfur species concentration was sucked through the Rhizon samplers and samples were stored in plastic syringes for different time intervals. After 2 hours (average duration of sampling) the decrease in the initial sulfide concentration was less than 4.5%, the decrease in the initial thiosulfate concentration less than 10%, and the increase in S(0) was less than 0.13% of the initial sulfide concentration at a pH of 8.3. At a pH of 7.2 the decrease in sulfide concentration was less than 10%, the decrease in thiosulfate concentration was less than 8%, and the increase in S(0) was less than 0.14% of the initial sulfide concentration. The tests show that the decrease in the sulfide recovery can be attributed to degassing rather than to oxidation, especially taking into account the higher sulfide loss at the lower pH value. This is consistent with theoretical estimations of sulfide oxidation rates in the presence of oxygen. Under fully oxygenated conditions, the production rate of e.g. sulfite by oxidation of hydrogen sulfide (realistic concentration: 1000 µmol $L^{-1}$) with $O_2$ (314 µmol $L^{-1}$ dissolved at 22‰ and 9 °C) would be 0.1 µmol $L^{-1}$ $min^{-1}$ ($dSO_3^{2-}/dt = k\ [H_2S]\ [O_2] = 3 \times 10^{-7}$ µmol $L^{-1}$ $min^{-1}$ [1000 µmol $L^{-1}$] [314 µmol $L^{-1}$], Zhang and Millero, 1993). Two hours of contact with fully oxygenated water is needed per 10 µmol $L^{-1}$ sulfite produced and this scenario can be excluded from our sample handling.

**Table 1: Sampling stations at the Dvurechenskii mud volcano. All data presented as graphs will be available in the international database PANGAEA (http://www.pangaea.de). In 'Core 1' hydrogen sulfide, polysulfides, polythionates, thiosulfate, sulfite, and colloidal solid sulfur were sampled in the pore waters; 'Core 2' was used for analysis of total sulfur in wet sediment, and 'Core 3' was used for analyses of sulfate, dissolved iron, and chloride in pore waters and solid phase iron, manganese, and reduced sulfur in wet sediment. From 'Core 3' of each sampling site after pore water extraction the sediment was sliced in 1 or 2 cm intervals, transferred to plastic bags, immediately flushed with nitrogen, and frozen at -20 °C.**

| *Station and mud volcano area* | | *PANGAEA event label* | *Coordinates* |
|---|---|---|---|
| St. 1 Summit | *Core 1* | M72/2_309_PUC-43 | N 44° 17.03'; E 34° 58.88' |
| | *Core 2* | M72/2_309_PUC-16 | |
| | *Core 3* | M72/2_309_PUC-51 | |
| St. 2 Geographical center | *Core 1* | M72/2_269 | N 44° 16.95'; E 34° 58.94' |
| | *Core 2* | not sampled | |
| | *Core 3* | M72/2_269 | |
| St. 8 Western edge | *Core 1* | M72/2_282_PUC-32 | N 44° 16.97'; E 34° 58.59' |
| | *Core 2* | M72/2_282_PUC-51 | |
| | *Core 3* | M72/2_282_PC-27 | |
| St. 9 North of DMV | *Core 1* | not sampled | N 44° 17.26'; E 34° 58.98' |
| | *Core 2* | M72/2_279 | |
| | *Core 3* | M72/2_279 | |
| St. 10 South of DMV | *Core 1* | M72/2_291 | N 44° 16.58'; E 34° 58.64' |
| | *Core 2* | M72/2_291 | |
| | *Core 3* | not sampled | |

## 2.3. Analytical Techniques

### *2.3.1. Pore water*

The protocol for the quantification of zero-valent sulfur compounds in the pore water samples (1-5 mL) consisted of three methods (Kamyshny et al., 2009).

i) The polysulfide speciation was detected by rapid single-phase derivatization, based on the conversion of inorganic polysulfides to more stable dimethylpolysulfanes (Kamyshny et al., 2004; Kamyshny et al., 2006). After the derivatization of a sample with 300 µl methyl trifluoromethanesulfonate in 40 mL methanol and 5 mL phosphate-buffer (50 mmol $L^{-1}$, pH 7.8), it was stored dark at -20 ºC for less than 1 month. In the home laboratory sodium sulfate solution (80 mL, 375 mmol $L^{-1}$) and internal standard (dibenzo(a,h)anthracene in 1,4-dioxane) were added to the sample, and it was extracted by 2 x 1 mL n-dodecane. Samples were analyzed by HPLC with a Dionex GP50 Gradient Pump equipped with a Dionex UVD340S Diode Array Detector using the Discovery

C18 reverse phase column (250 mm x 4.6 mm x 5 µm) and pure methanol at a flow rate of 1 mL $min^{-1}$ as a mobile phase with detection at 220 nm and 230 nm. Calibration was made by secondary standards of polysulfides mixture derivatized according to conditions described in Kamyshny et al. (2006).

ii) The sum of polysulfidic, polythionate, colloidal, and dissolved elemental sulfur was quantified, based on the conversion to thiocyanate by the reaction with hydrogen cyanide (cyanolysis). The procedure for cyanolysis extraction was adapted from Kamyshny (2009), and was adjusted to smaller sample volumes by using proportionally smaller volumes of reactants. Extracted samples were frozen and stored at -20 ºC until analysis. Thiocyanate concentration was detected according to the method of Rong et al. (2005), using a Dionex GP50 Gradient Pump equipped with a Dionex UVD340S Diode Array Detector and a Nomura Chemical, Japan, Develosil RPAQUEOUS C30 reverse phase column (150 mm x 4.6 mm x 5 µm). Retention time for $SCN^-$ was 5.2 minutes.

iii) Samples for total zero-valent sulfur were preserved by mixing with zinc chloride solution (5%), frozen, and stored at -20 ºC until analysis. After thawing, an internal standard (4,4´-dibrombiphenyl in methanol) was added to the samples, and it was extracted with 2 x 1 mL chloroform. The extract was diluted twice with methanol to improve the peak shape and analyzed as the samples from the single-phase derivatization (i).

For polythionates analyses pore water was sampled in the glove-box, sealed under nitrogen, frozen immediately, and stored at -20 ºC. Samples were analyzed without pre-treatment by the same chromatographic technique as samples for thiocyanate. Retention times for $S_4O_6^{2-}$, $S_5O_6^{2-}$, and $S_6O_6^{2-}$ were 2.3, 3.2 and 9.9 minutes respectively.

Thiosulfate and sulfite were analyzed with the monobromobimane derivatization method. Derivatization and analysis were performed as described by Zopfi et al. (2004).

Samples for analysis of the total S(II) content (sum of sulfide, bisulfide, all polysulfide species, and acid soluble metal sulfides (MetS) nanoparticles, which pass through the Rhizon samplers, Eq. 2) were preserved by adding ½ volume of zinc chloride solution (5%). Samples were frozen and stored at -20 ºC. Analysis was performed according to the method of Cline (1969).

$$\sum \mathrm{S(II)} = \sum_{1}^{8} \mathrm{S_n^{2-}} + \sum_{1}^{8} \mathrm{HS_n^-} + \sum_{1}^{8} \mathrm{H_2S_n} + \sum \mathrm{MetS} \qquad \text{(Eq. 2)}$$

For analyses of dissolved iron 1 mL pore water was fixed in 200 µL 2 mol $L^{-1}$ HCl (pH after addition <1). Dissolved iron was measured spectrophotometrically with Ferrozine (1 g $L^{-1}$ in 50 mmol $L^{-1}$ HEPES buffer, pH 7) at 562 nm (Stookey, 1970).

For analyses of the sulfate and chloride concentrations 1 mL pore water was fixed in 0.5 mL zinc acetate solution (2%). Sulfate and chloride were determined after filtration and dilution with non-suppressed anion exchange chromatography with a Waters IC-Pak anion exchange column equipped

with a Waters 430 Conductivity detector. As eluent 1 mmol $L^{-1}$ isophtalic acid with 10% v/v methanol (pH 4.6) was used at a flow rate of 1 mL $min^{-1}$.

*2.3.2. Solid phase*

Sediment samples for analysis of total zero-valent sulfur content were preserved in zinc acetate solution (5%). After preservation samples were frozen and stored at -20 ºC until analysis. Sulfur was extracted from the preserved sediment with methanol and analyzed by HPLC. The detailed procedure for analysis can be found elsewhere (Zopfi et al., 2004).

Concentrations of acid volatile sulfides (AVS: FeS, some $Fe_3S_4$) and chromium reducible sulfur (CRS: $FeS_2$, S(0), remaining $Fe_3S_4$ ) were measured with the modified two step acid distillation method (Fossing and Jørgensen, 1989); 3-4 g of frozen sediment was used. Concentrations of iron were measured on dithionite ($Fe_D$), HCl ($Fe_{HCl}$), and ascorbic acid ($Fe_{Asc}$) extracts. For each leaching method 0.2-0.3 g frozen sediment was put in 10 mL extractant. With the dithionite method (Canfield, 1989) amorphous Fe(III)oxide, crystalline Fe(III)oxide, some AVS, and a minor amount of silicate bound iron is extracted (Canfield, 1989; Kostka and Luther, 1994). Sediment samples were shaken in the dithionite-acetate-sodium citrate solution for 48 h at room temperature and the extracts were left for 72 h to oxidize the remaining dithionite. With the ascorbic acid method reactive, amorphous Fe(III)oxides as well as some AVS is extracted (Kostka and Luther, 1994) in an anoxic sodium citrate/sodium bicarbonate/ascorbic acid mixture adjusted to pH 8 (Ferdelman et al., 1991). Samples were shaken at 60 °C for 24 h. With the HCl method (1h extraction in 0.5 mol $L^{-1}$ HCl at room temperature) amorphous Fe(III)oxides, some silicate bound iron, and all AVS is extracted (Kostka and Luther, 1994). All extractions were performed in duplicates and the iron concentrations were determined spectrophotometrically (Stookey, 1970) with Ferrozine as described above.

The amount of dithionite and HCl dissolvable manganese ($Mn_D$, $Mn_{HCl}$), was measured on subsamples of the extracts with a Perkin Elmer 3110 flame atomic absorption spectrophotometer (AAS) equipped with a Mn hollow cathode lamp adjusted to a wavelength of 422.7 nm.

## 3. RESULTS

### 3.1. North of the DMV (St. 9)

Pore water and solid phase analyses from St. 9 north of the DMV showed a sediment geochemistry as expected from near-surface sediments of the deep Black Sea basin with rather constant S(II) and chloride concentrations, no dissolved iron, and sulfate concentrations only slightly decreasing over the upper 15 cm of the sediment (Fig. 2 a-d). With the solid phase extractions elevated amounts of iron were only leached with HCl. The other iron and manganese extractions exhibited overall low concentrations. Concentrations of AVS, CRS, and of total zero-valent sulfur in the wet sediment slightly increased within the upper 15-20 cm bsf (below surface) (Fig. 2f, g). No core for sulfur intermediate measurements was sampled here.

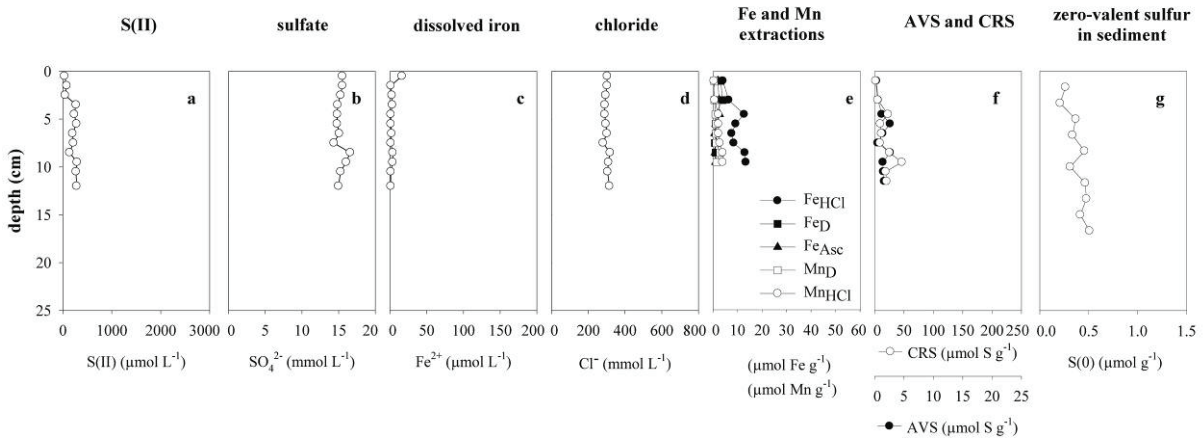


**Fig. 2: Distribution of (a-d) solutes, (e) extractable iron and manganese, (f) AVS (acid volatile sulfide) and CRS (chromium reducible sulfur), and (g) zero-valent sulfur in sediments from the reference site north of the DMV (St. 9).**

### 3.2. Summit (St. 1)

Upon retrieval, the sediments in the cores from the DMV were usually bubbling, and due to this outgassing mixing of seawater and pore water occurred. This mixing will have affected especially the most gaseous sediments as at the summit, and should be kept in mind while comparing distributions of different sites. Sediments in DMV areas with substantial fluid upflow are subjected to sulfate-free and chloride-rich mud volcano fluids (Aloisi et al., 2004), accordingly in summit sediments sulfate was depleted at 11 cm depth (Fig. 3a) and the chloride concentration doubled in the upper 20 cm (Fig. 3c).

A striking observation only made at the summit station was the presence of dissolved iron immediately below the seawater-seafloor interface, and with concentrations rapidly increasing with depth to up to 170 µmol $L^{-1}$ (Fig. 3b). Additionally, the highest solid phase iron concentrations of all sampling sites were measured here and up to 60 µmol Fe $g^{-1}$ was extracted with HCl. $Fe_{Asc}$ and $Fe_D$ extractions were also higher than in all other stations and leached 20-30 µmol Fe $g^{-1}$ (Fig. 3d). Reduced solid sulfur species were constant over the whole core length with low AVS (<2 µmol S $g^{-1}$) and high CRS (170 µmol S $g^{-1}$) concentrations (Fig. 3e).

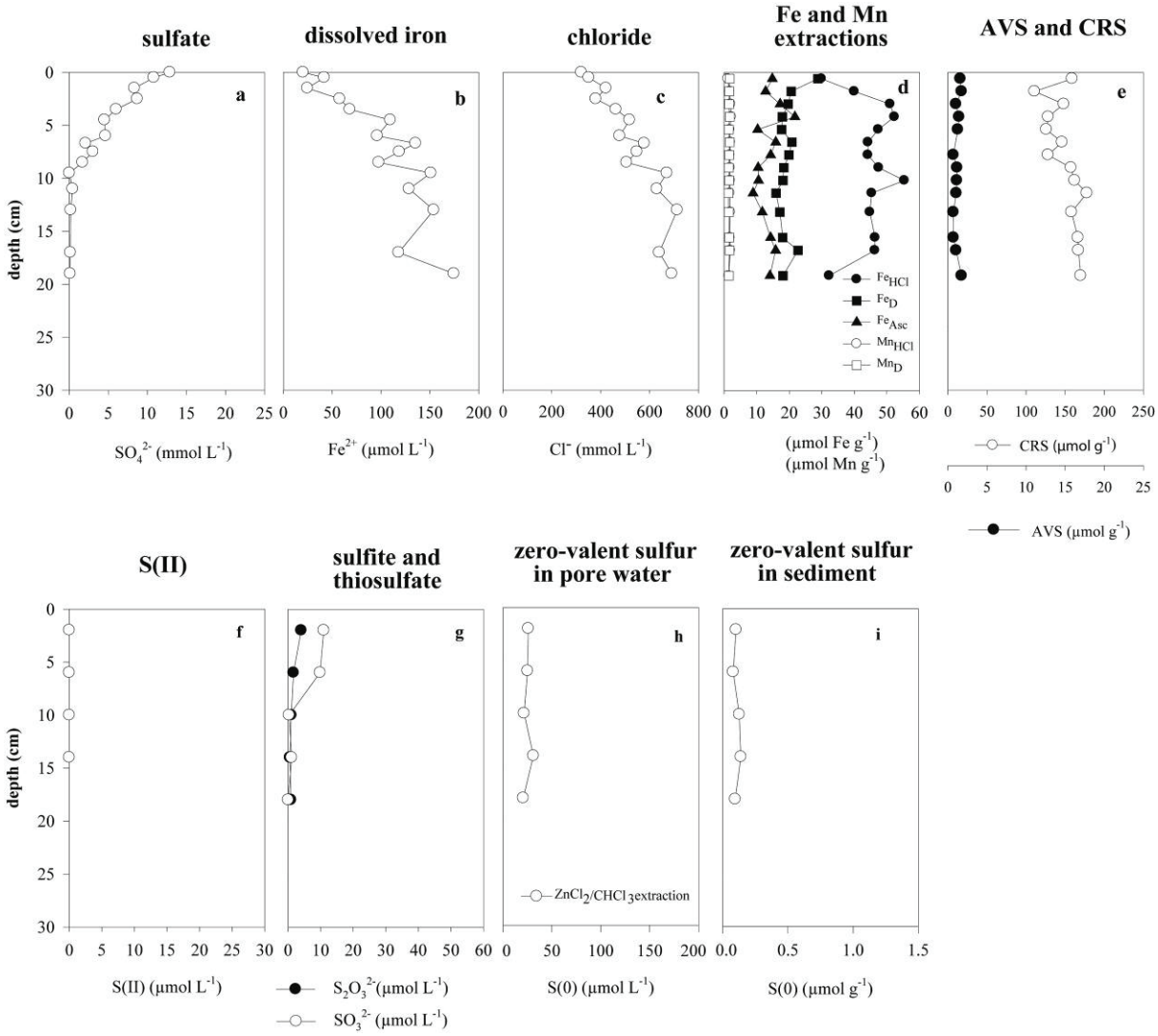


**Fig. 3: Distribution of (a-c) solutes, (d) extractable iron and manganese, (e) AVS and CRS, (f-h) S(II), sulfite, thiosulfate, and zero-valent sulfur in the pore water, and (i) zero-valent sulfur in the sediment from the summit (St. 1).**

S(II) and polysulfides were below the detection limit in the pore water of the summit (Fig. 3f). However, during the same campaign close to the sampled area up to 500 µmol $L^{-1}$ sulfide ($H_2S+HS^-$) was detected in the upper 10 cm of the sediment by in situ microsensor measurements (Lichtschlag et al., subm.). Despite the absence of S(II) in the sediment sulfite and thiosulfate were found with maximum concentrations of 11 µmol $L^{-1}$ respectively 4 µmol $L^{-1}$, and sulfite always prevailed over thiosulfate (Fig. 3g); concentrations of both sulfur intermediates decreased sharply at the point where sulfate was depleted. Concentrations of zero-valent sulfur in the pore water (Fig. 3h) and in the sediment (Fig. 3i) were constant with depth. Polythionates were not observed at any depth in the pore waters here and at any other DMV sampling site.

### 3.3. Geographical Center (St. 2)

At the geographical center sulfate was depleted at 5 cm depth (Fig. 4a) and the chloride gradient was less steep than at the summit (Fig. 4c). This is caused by reduced fluid upflow and higher sulfate turnover (Lichtschlag et al., subm.). Some dissolved iron was measured in the pore water (Fig. 4b), but might be an artifact caused by nanoparticular FeS passing through the 100 nm pore size Rhizon samplers. Extractions of solid phase iron exhibited lower concentrations than at the summit (maximally 10-15 µmol Fe $g^{-1}$), but the amount of $Fe_{Asc}$ and $Fe_{Dith}$ (Fig. 4d) was still significantly higher than at the site north of DMV site (St. 9). In contrast CRS and AVS concentrations were similar as in the summit sediments (Fig. 4e).

At the geographical center a wide range of sulfur species was detected. Different than at the summit S(II) was found in the pore waters; S(II) reached a peak of 1 mmol $L^{-1}$ at 6 cm bsf, but fluid upflow limited penetration (Fig. 4f) (Lichtschlag et al. subm.). Thiosulfate and sulfite were present in concentrations of 22 µmol $L^{-1}$ and 5 µmol $L^{-1}$ (Fig. 4h). Three polysulfide species ($S_4^{2-}$, $S_5^{2-}$, $S_6^{2-}$) were detected (Fig. 5g) and the abundance of the polysulfide species decreased with the increase in the sulfur chain length ($[S_4^{2-}] > [S_5^{2-}] > [S_6^{2-}]$).

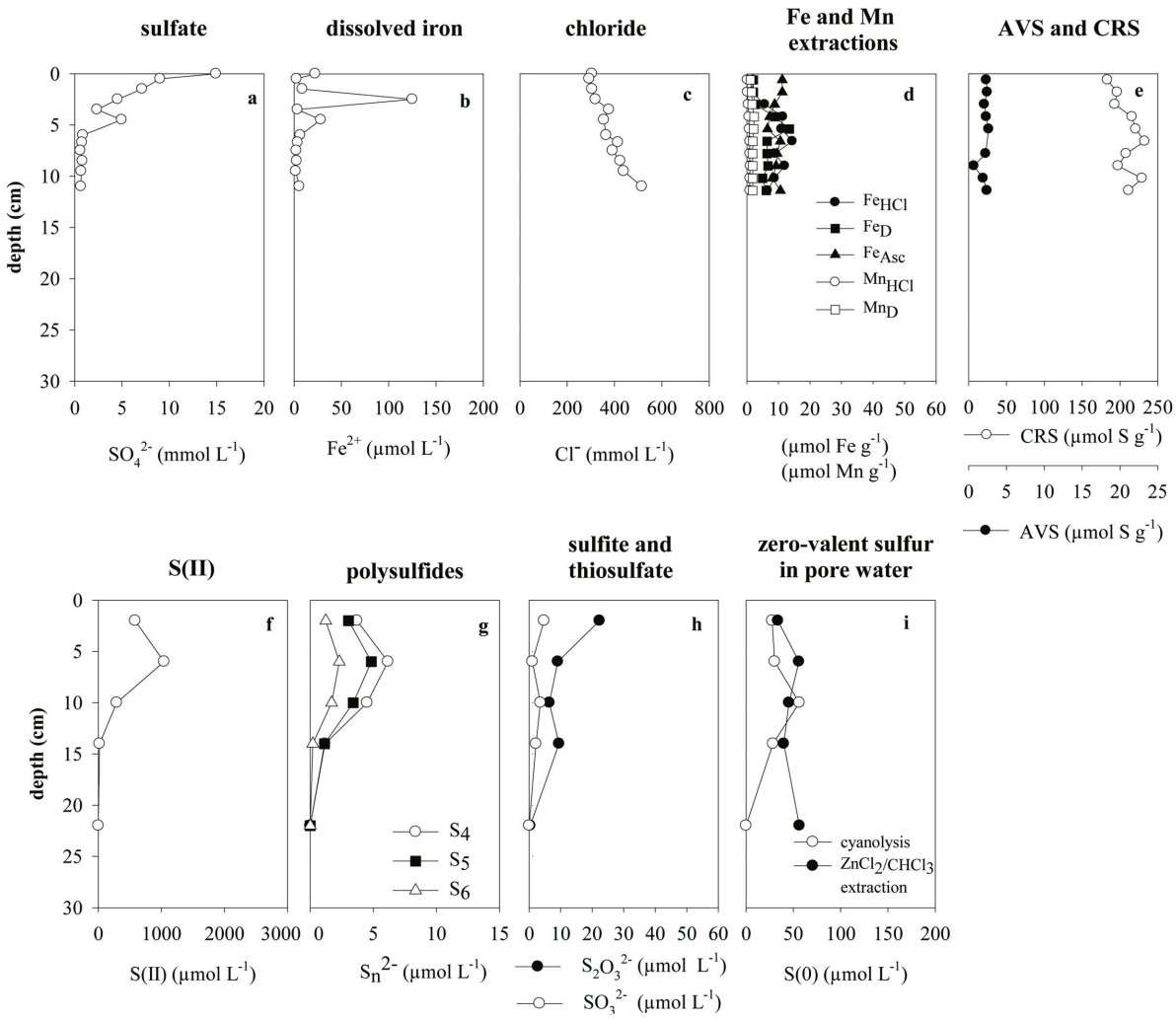


**Fig. 4: Distribution of (a-c) solutes, (d) extractable iron and manganese, (e) AVS and CRS, (f-i) S(II), polysulfide species, sulfite, thiosulfate, and zero-valent sulfur in the pore water from the geographical center site (St. 2).**

### 3.4. Western Edge (St. 8)

At the western edge the decrease of sulfate with depth was less pronounced than at the other DMV stations and sulfate was still detectable 13 cm bsf (Fig. 5a). However, chloride clearly increased with depth (Fig. 5c), ostensibly also due to rising mud volcano fluids. Dissolved iron was overall below the detection limit (Fig. 5b) and the vertical profile of all solid phase iron extractions showed low and constant concentrations. This is the only site, where concentrations of solid phase manganese ($Mn_D$, $Mn_{HCl}$) were in the same range as those of the solid phase iron (Fig. 5d), and slightly elevated compared to the other sampling sites. AVS and CRS concentrations steadily increased with depth (Fig. 5e).

At this most peripheral station of the DMV most sulfur species were observed. Of all sampling stations highest S(II) concentrations were measured at the western edge (Fig. 5f) and in parallel the highest number of polysulfide species was detected (Fig. 5g). As in the geographical center the abundance of polysulfide species decreased with the increase in the sulfur chain length, except for

trisulfide ($[S_4^{2-}] > [S_5^{2-}] > [S_6^{2-}] > [S_7^{2-}] > [S_3^{2-}]$). Thiosulfate and sulfite were present at all sampled depth intervals (Fig. 5h). Zero-valent sulfur concentrations in the pore water reached maximum values of 150 µmol $L^{-1}$ (Fig. 5i). The concentrations of elemental sulfur in the wet sediment (Fig. 5j) were slightly increased (maximally 0.3 µmol $g^{-1}$ wet sed.) compared to the summit but still lower than north of DMV (St. 9). Of the sedimentary zero-valent sulfur up to 64% passed through 100 nm pores of Rhizon samplers.

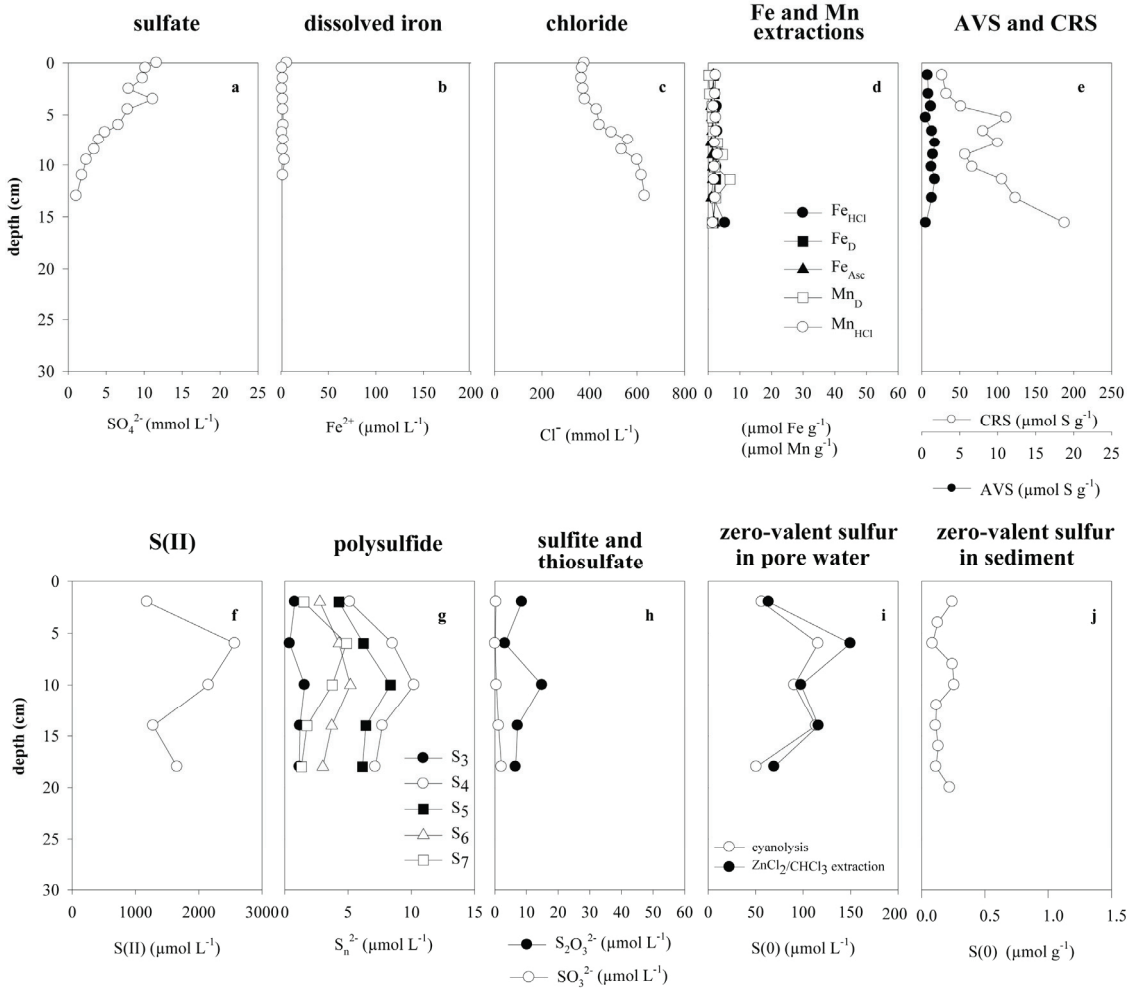


**Fig. 5: Distribution of (a-c) solutes, (d) extractable iron and manganese, (e) AVS and CRS, (f-i) sulfur intermediates in pore water, and (j) zero-valent sulfur in the wet sediment from the western edge (St. 8).**

### 3.5. South of the DMV (St. 10)

This station sampled south of the DMV was thought to represent another site outside the DMV, similar as 'north of the DMV'. Interestingly, pore water data from gravity cores (GC 306, data not shown) were obviously different from data from the reference north of the DMV (St. 9, GC 314, data not shown). The geochemistry indicated that this site might also be influenced by the mud volcano, however, with our set of data this unfortunately can not be proven. Nevertheless, it should be mentioned that at this station thiosulfate concentrations in the pore water and elemental sulfur concentrations in the sediment exceeded those of other mud volcano stations in some depth intervals (data not shown).

# 4. DISCUSSION

## 4.1. Sulfide Oxidation Intermediates in Dvurechenskii Mud Volcano Sediments

At the DMV, as in other well-studied submarine mud volcanoes, tectonically-mobilized, methane-rich fluid muds breach the surface and mix with surface mud and deep water. The main difference to other mud volcanoes is that these methane-rich fluid DMV muds come into contact with the sulfidic deep waters of the Black Sea, rather than with oxygen-rich sediment. The deep Black Sea moreover contains copious amounts of sulfate, and it is the down-mixing of sulfate with the upward flowing methane-rich mud that drives bacterial sulfate reduction coupled to anaerobic oxidation of methane within the first surface centimeters of the DMV (Wallmann et al., 2006, Lichtschlag et al., subm.). As expected, sulfate dependent methane oxidation leads to the production of hydrogen sulfide. In the absence of any oxidant, which initially one would expect for the deep Black Sea, no intermediate products should form. However, our results show that hydrogen sulfide oxidation products with intermediate oxidation state such as elemental sulfur, polysulfides, sulfite, and thiosulfate were present in the sediments of the DMV. Concentrations of sulfur intermediates in the DMV sediments far exceed those found in sites within the Black Sea studies. For example, typical concentrations of thiosulfate observed by Zopfi et al. (2004) were less than 3 μmol $L^{-1}$ in the deep sulfidic zone of the Black Sea. In the DMV sediments thiosulfate concentrations ranged up to over 20 μmol $L^{-1}$. The distribution of intermediate sulfur species indicates that non-equilibrium oxidation processes are occurring within the surface sediments of the DMV.

Formation of dissolved sulfur intermediates can, of course, occur due to the inadvertent introduction of oxidants, including oxygen, during sample handling. Retrieval of sediments from deep-sea mud volcanoes like the DMV may cause mixing of pore water and sea water during expansion of methane upon depressurization and formation of gas bubbles. However, we can exclude sulfur intermediate formation by this artifact, as the Black Sea water is depleted of possible oxidants for hydrogen sulfide. Therefore, mixing only would dilute the concentrations of the sulfur intermediates and not induce their formation. Furthermore, the cores were tightly sealed during sediment recovery. Shortly before the transport of the sediment cores into the anoxic glove-box the push core heads were replaced with gas-tight stoppers. Pore water extraction occurred immediately after sediment retrieval. The other possible source of oxidative artifact, the Rhizon sampling of the pore waters, is also considered to be negligible. Our tests of the Rhizon samplers, as described in the *Methods* section, strongly suggest that the Rhizon sampling should not cause oxidation artifacts. Thus formation of sulfur intermediates by the sediment retrieval and handling can be excluded.

### 4.2. A Deep Source of Oxidizing Power?

The source of oxidizing power in the euxinic depths of the Black Sea is not at first obvious. Hydrogen sulfide can be oxidized by oxygen and nitrate, and oxidized forms of iron or manganese. Oxidation of hydrogen sulfide with iron(III)- or manganese(IV)-oxides is often incomplete and leads to the formation of sulfur intermediates, such as elemental sulfur, sulfite or thiosulfate (Pyzik and Sommer, 1981; Burdige and Nealson, 1986; dos Santos Afonso and Stumm, 1992; Yao and Millero, 1993, 1996; Zopfi et al., 2004). However, oxygen and nitrate are absent in deep waters of the Black Sea, and highly reactive sedimentary iron- and manganese-oxides should become depleted while sinking through the anoxic seawater below the pycnocline (Muramoto et al., 1991). Nevertheless, Zopfi et al. (2004) attributed the presence of sulfur intermediates in Black Sea pore waters to the deposition and burial of iron(III)- or manganese(IV)-oxides that have a decreased reactivity towards hydrogen sulfide.

When we examined the iron mineral composition in our sediment samples, we found iron phases potentially reactive towards sulfide in most near-surface sediments of the mud volcano. The highest content was measured in the summit of the DMV with concentrations that exceeded five ($Fe_{HCl}$) to ten ($Fe_D$, $Fe_{Asc}$) times that from the non-mud volcano sediments north of DMV. The amount of the extractable iron-phases decreased from the summit site to the geographical center, and an even lower content was measured at the western edge. This progressive decrease in amounts of reactive iron-minerals from the active summit to the outer edges and beyond, suggests that the source for this metal-oxide oxidative power must come from the mud volcano itself and not from sedimentary input.

During the same sampling campaign a fresh mud flow was detected at the summit of the DMV (Lichtschlag et al., subm.), and our results indicate that thus reactive iron-minerals are transported with the muds from the deep subsurface. The dynamics of mud volcano activities and the frequency and extent of mud eruptions are unknown. However, fresh mud flows and hot spots of mud volcano activity close to our summit, but also at other areas of the DMV were reported from an earlier study in 2002 (Bohrmann et al., 2003). Whatever the location, the reactive iron-mineral has reached also the peripheral areas. As sulfur intermediates were detected in all sampled mud volcano locations, the oxidative power of the iron-minerals must have been sufficient for hydrogen sulfide oxidation even in the peripheral areas of the mud volcano.

After a mud eruption the microbial consortia will start to establish AOM in the fresh, reactive iron-rich mud, the occurring dissolved sulfide will first be stripped from solution. Sulfide concentrations will remain low as long as the rate of sulfide production does not exceed the kinetics or sulfide oxidation via reactive iron phases. Subsequently, sulfide concentrations build-up and the equilibrium reactions between sulfide and sulfur ensue, producing polysulfides (Eq. 3). Processes that remove these polysulfides include removal by diffusion or advection, and chemical reactions. Consumption of polysulfides can proceed through a variety of pathways, such as pyrite formation (Luther, 1991;

Thamdrup et al., 1993) and reaction with organic matter through cross-linking of organic polymers with polysulfide bonds (Kohnen et al., 1989; Amrani and Aizenshtat, 2004). However, the persistence of the oxidative power within the mud volcano will depend on the exposure time of the sediment to hydrogen sulfide, the hydrogen sulfide concentration, and the reactivity of the particular iron-mineral present. As the applied extraction methods were developed for common marine sediments with an intense cycling between reduced and oxidized forms of iron, the same conclusions as to iron reactivity of certain extracts may not be applied to sediments in mud volcanoes. The methods might extract a higher amount of iron from silicates respectively clay minerals than previously thought, as these compounds will be a main constituent of the mud volcano sediments. However, also silicate bound iron reacts with hydrogen sulfide (Canfield, 1989; Canfield et al., 1992; Raiswell and Canfield, 1996), but much slower than iron-minerals.

The hydrogen sulfide content of the sediments varies with the lateral changes in the fluid flow. Pore water chloride profiles provide an indication of the intensity of mixing between the deep fluids and the Black Sea water column. The steepest $Cl^-$ profile is that at the summit station, as shown in Figure 3. Recent and rapid mixing of upwardly transported mud at this site is consistent with the lack of dissolved sulfide and high dissolved ferrous iron concentrations. Sulfate penetration is constrained to the upper few centimeters of the sediment due to the high fluid upflow (Fig. 3a). Sulfate reduction rates at this site are low (1 - 2 nmol $cm^{-3}$ $d^{-1}$) and mainly restricted to the first 1 - 2 cm of the surface sediments (Lichtschlag et al., subm.). Little or no hydrogen sulfide is produced by sulfate reduction, and diffusion of hydrogen sulfide into the sediment is limited. Hence, in high fluid flow areas reactive iron-minerals persist at the surface. In areas with decreased fluid upflow sulfate penetrates deeper. Higher depth integrated rates of sulfide production prevail and the reactive iron-minerals are scavenged more rapidly.

Interestingly, the reactive iron-minerals rise from an ancient source together with a very reduced mud volcano fluid that is enriched in methane and ammonium. These observations directly contradict recent experimental findings of metal-oxide dependent anaerobic oxidation of methane (Beal et al., 2009). Thus, although thermodynamically in disequilibrium, methane and ammonium appear not be oxidized chemically or biologically by reactive iron. Paradoxically, reactive iron is preserved due to the absence of sulfate in the mud fluid. Only when methane is oxidized by AOM and sulfide is formed, the reactive iron can be reduced. Ammonium is probably not reactive at all under anaerobic conditions and will be processed further upon reaching the chemocline.

### 4.3. Polysulfide Equilibria

The major dissolved zero-valent sulfur pool consisted of polysulfides, when sulfide was present. Polysulfides may form in equilibrium reactions between elemental sulfur and dissolved hydrogen sulfide, as shown in Equation 3, and presence of polysulfides in the pore waters of the surface sediments of the DMV is consistent with the observation of solid elemental sulfur in the solid phase.

$$HS^- + \frac{(n-1)}{8}S_8 = H^+ + S_n^{2-} \qquad \text{(Eq. 3)}$$

Information on the state of equilibrium between polysulfides and solid phase elemental sulfur can be obtained by comparing the total measured polysulfide zero-valent sulfur content to the polysulfide zero-valent sulfur content that would be present at sulfur saturation conditions. With a set of thermodynamic constants (Kamyshny et al., 2006) the relative saturation level (RSL) of elemental sulfur can be compared to the actually detected individual concentrations. The RSL is calculated from the concentrations of the three most abundant and most reliably detected polysulfide dianions ($S_4^{2-}$, $S_5^{2-}$, $S_6^{2-}$) (Kamyshny et al., 2004). Values of RSL lower than one indicate that the polysulfides are not in equilibrium with the particulate sulfur. Log (RSL) is the slope of the linear plot of $\mathrm{Log}\left[\{S_n^{2-}\}/\{S_n^{2-}\}_s\right]$ *vs.* $(n-5)$, where

$$\mathrm{Log}\left[\{S_n^{2-}\}/\{S_n^{2-}\}_s\right] = \mathrm{Log}\left[\{S_5^{2-}\}/\{S_5^{2-}\}_s\right] + (n-5)\mathrm{Log(RSL)} \qquad \text{(Eq. 4)}$$

where $\{S_n\}$ is the measured activity of the polysulfide with 'n' sulfur atoms and $\{S_n^{2-}\}_s$ is the activity of the same polysulfide at equilibrium with hydrogen sulfide and particulate elemental sulfur. Derivation of Equation 4 can be found elsewhere (Kamyshny et al., 2008).

Likewise, the distribution pattern of measured polysulfide species can be compared to the pattern that would be present if the solution is in equilibrium with solid sulfur. The polysulfide distribution pattern is derived from the calculation of the average polysulfide chain length (APCL) based on all detected polysulfide species.

$$\mathrm{APCL} = \frac{\sum_{n=\text{shortest detected}}^{n=\text{longest detected}} n\left[S_n^{2-}\right]}{\sum_{n=\text{shortest detected}}^{n=\text{longest detected}} \left[S_n^{2-}\right]} \qquad \text{(Eq. 5)}$$

where 'n' is polysulfide chain length and $n \geq 2$. Under equilibrium conditions the APCL is 4.9. This value is calculated from the concentrations of the polysulfide species $S_3^{2-}$- $S_7^{2-}$ at in situ conditions (9 ºC, pH = 8, 20‰) (Kamyshny et al., 2006). APCL values lower than 4.9 indicate that polysulfides are not in equilibrium with particulate sulfur.

Calculations of polysulfide speciation at sulfur saturation revealed that not detected species accounted only for a minor part of polysulfidic zero-valent sulfur (Fig. 6a, d). Calculations of RSL

(Fig. 6b, e) and APCL (Fig. 6c, f) show that polysulfides and particulate sulfur are not in equilibrium. In the upper 10 cm of the geographical center sediments RSL does not change (0.65-0.70), but drops to 0.48 below. APCL has the same trend and is in the range between 4.61-4.71. In the western edge RSL and APCL show that the system is closer to equilibrium than the geometrical center, but again the deeper samples a further from equilibrium than the shallower ones.

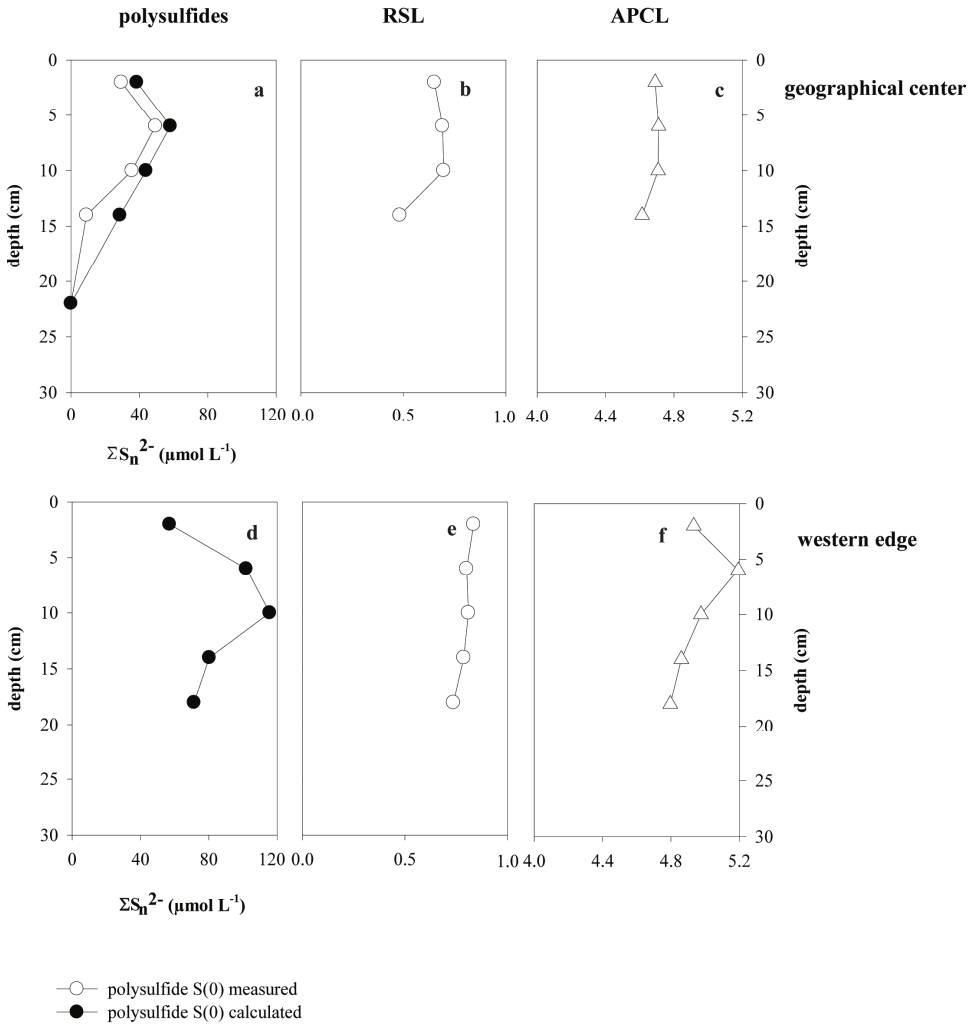


**Fig. 6: Comparison of measured vs. calculated polysulfide sulfur (a, d), in panel d) the measured polysulfide concentrations equal the calculated concentrations; RSL (relative saturation level: b, e) and APCL (average polysulfide chain length, c, f) from the geographical center and the western edge. Similar calculations were not possible for the active center as here no polysulfides were detected.**

In the DMV, the observation that the concentration of the three most abundant polysulfides $[S_4^{2-}] > [S_5^{2-}] > [S_6^{2-}]$ (Fig. 5g) deviate from concentrations in equilibrium with elemental sulfur ($[S_5^{2-}] > [S_4^{2-}] > [S_6^{2-}]$) (Kamyshny et al., 2004; Kamyshny et al., 2007) demonstrates that the system is not in equilibrium. Calculations of RSL and APCL show that though polysulfides are not in the equilibrium with particulate elemental sulfur the system is much closer to equilibrium in the western edge

sediments than at the geographical center of the DMV (Fig. 6). The lack of dissolved sulfide at the summit site precludes formation of polysulfides and making these equilibrium calculations.

Overall, deeper samples also tend to be further from equilibrium than shallower ones. If the system is in a steady state the production is balanced by consumption and diffusional or advectional losses from the sediment. As the dissolved products are removed by transport, but the solid elemental sulfur is not transported by the fluid, and the forward dissolution reaction is not instantaneous, the system moves away from equilibrium. The equilibrium calculations showed that the sulfur system at the edge is closer to equilibrium than at the geographical center, possibly because transport losses are smaller as the advection here is patchy (Lichtschlag et al., subm.). This is concurrent with the decreased iron-mineral availability and the higher concentrations of zero-valent sulfur in the pore water. The polysulfide system gets closer to equilibrium the less oxidative power is present, and if the sum of consumption and transport losses are smaller. Also the slow kinetics of solid elemental sulfur dissolution may cause the deviation from equilibrium as indicated both by the relative saturation level and the average polysulfide chain length. Generally, it is thought that the sulfide-polysulfide-dissolved elemental sulfur system comes into equilibrium within minutes seconds (Kamyshny et al., 2003), the sulfide-polysulfide-colloidal elemental sulfur system within minutes (Fossing and Jørgensen, 1990), and the sulfide-polysulfide-solid elemental sulfur system within hours or more (Boulegue and Michard, 1977). However, in natural aquatic systems even equilibration in the sulfide-polysulfide-solid elemental sulfur system appears to takes hours to days (Kamyshny and Ferdelman, subm.), and thus the equilibration time may be coupled to the concentration of hydrogen sulfide. For example the increase of deviation from equilibrium with depth may be due to the lower concentration of hydrogen sulfide, which has the effect of decreasing the forward rate of the polysulfide equilibrium reaction (Eq. 3) (Kamyshny and Ferdelman, subm.). Whatever the pathway, the presence of polysulfides suggests that zero-valent sulfur, as elemental sulfur in the solid phase and polysulfide sulfur in the aqueous phase, is a key oxidation product in the surface sediments of the DMV.

## 5. CONCLUSIONS

The Dvurechenskii mud volcano with its fresh mud flows and its high spatial variability in fluid flow is a remarkable site for sulfur and iron chemistry as it has a hidden oxidative potential. The extensive pore fluid and solid phase Fe and S chemical analyses showed that the surface sediments of the DMV react to form a unique oxidative environment in the midst of one of the most reduced environments in the deep ocean. In particular, deep upwardly advecting muds and fluids contain high concentrations of methane and reactive metal-minerals. Only at the surface where sulfate as an oxidant is present, the methane is consumed by anaerobic methane oxidation. Subsequently sulfide is produced and reacts at the surface of the AOM-zone with upward flowing reactive metal-oxides, thus sulfur intermediates form despite the permanent anoxic surrounding. The formation of sulfur intermediates such as elemental sulfur, polysulfide, thiosulfate, and sulfite can be attributed to purely abiotic reactions between sulfide and metal-minerals. Polysulfides and elemental sulfur are the dominant sulfide oxidation intermediates. Their concentrations do not come into chemical equilibrium, either due to the high consumption to production rates ratio or as the fluid flow continuously transports the sulfur intermediates away from their site of production, forcing new formation by the immobile elemental sulfur.

## REFERENCES


Aloisi, G., Drews, M., Wallmann, K., Bohrmann, G., 2004. Fluid expulsion from the Dvurechenskii mud volcano (Black Sea) - Part I. Fluid sources and relevance to Li, B, Sr, I and dissolved inorganic nitrogen cycles. *Earth Planet. Sci. Lett.* **225**, 347-363.

Amrani, A., Aizenshtat, Z., 2004. Reaction of polysulfide anions with α, β unsaturated isoprenoid aldehydes in aquatic media: simulation of oceanic conditions. *Org. Geochem.* **35**, 909-921.

Barnes, R.O., Goldberg, E. D., 1976. Methane production and consumption in anoxic marine sediments. *Geology* **4** , 297-300.

Beal, E. J., House, C. H., Orphan, V. J., 2009. Manganese- and iron-dependent marine methane oxidation. *Science* **325**, 184-187.

Boetius, A., Ravenschlag, K., Schubert, C. J., Rickert, D., Widdel, F., Gieseke, A., Amann, R., Jørgensen, B. B., Witte, U., Pfannkuche, O., 2000. A marine microbial consortium apparently mediating anaerobic oxidation of methane. *Nature* **407**, 623-626.

Bohrmann, G., Ivanov, M., Foucher, J. P., Spiess, V., Bialas, J., Greinert, J., Weinrebe, W., Abegg, F., Aloisi, G., Artemov, Y., Blinova, V., Drews, M., Heidersdorf, F., Krabbenhoft, A., Klaucke, I., Krastel, S., Leder, T., Polikarpov, I., Saburova, M., Schmale, O., Seifert, R., Volkonskaya, A., Zillmer, M., 2003. Mud volcanoes and gas hydrates in the Black Sea: new data from Dvurechenskii and Odessa mud volcanoes. *Geo-Mar. Lett.* **23**, 239-249.

Boulegue, J., Michard, G., 1977. Dissolving of elementary sulfur in aqueous solutions - dilutions of hydrogen sulfide. *Comptes Rendus De L'Academie Des Sciences Serie* **284**, 713-716.

Boulegue, J., Michard, G., 1978. Constantes de formation des ions polysulfures $S_6^{2-}$, $S_5^{2-}$ et $S_4^{2-}$ en phase aqueuese. *J. Français d'Hydrologie* **9**, 27-33.

Burdige, D. J., Nealson, K. H., 1986. Chemical and microbiological studies of sulfide-mediated manganese reduction. *Geomicrobiol. J.* **4**, 361-387.

Canfield, D. E., 1989. Reactive iron in marine sediments. *Geochim. Cosmochim. Acta* **53**, 619-632.

Canfield, D. E., Raiswell, R., Bottrell, S., 1992. The reactivity of sedimentary iron minerals toward sulfide. *Am. J. Sci.* **292**, 659-683.

Cline, J. D., 1969. Spectrophotometric determination of hydrogen sulfide in natural waters. *Limnol. Oceanogr.* **14**, 454-458.

de Beer, D., Sauter, E., Niemann, H., Kaul, N., Foucher, J.-P., Witte, U., Schlüter, M., Boetius, A., 2006. In situ fluxes and zonation of microbial activity in surface sediments of the Håkon Mosby Mud Volcano. *Limnol. Oceanogr.* **51**, 1315-1331.

dos Santos Afonso, M., Stumm, W., 1992. Reductive dissolution of iron(III) (hydr)oxides by hydrogen sulfide. *Langmuir* **8**, 1671-1675.

Fahey, R. C., Newton, G. L., 1987. Determination of low-weight thiols using monobromobimane fluoescent labeling and high-performance liquid chromatography. *Methods Enzymol.* **143**, 85-96.

Ferdelman, T. G., Church, T. M., Luther, G. W., 1991. Sulfur enrichment of humic substances in a Delaware salt marsh sediment core. *Geochim. Cosmochim. Acta* **55**, 979-988.

Feseker, T., Pape, T., Wallmann, K., Klapp, S. A., Schmidt-Schierhorn, F., Bohrmann, G., The thermal structure of the Dvurechenskii mud volcano and its implications for gas hydrate stability and eruption dynamics. *Mar. Petrol. Geol.* In Press, Corrected Proof.

Fossing, H., Jørgensen, B. B., 1989. Measurement of bacterial sulfate reduction in sediments: evaluation of a single-step chromium reduction method. *Biogeochemistry* **8**, 205-222.

Fossing, H., Jørgensen, B. B., 1990. Isotope exchange reactions with radiolabeled sulfur compounds in anoxic seawater. *Biogeochemistry* **9**, 223-245.

Haese, R. R., Meile, C., Van Cappellen, P., de Lange, G. J., 2003. Carbon geochemistry of cold seeps: Methane fluxes and transformation in sediments from Kazan mud volcano, eastern Mediterranean Sea. *Earth Planet. Sci. Lett.* **212**, 361-375.

Jørgensen, B. B., Böttcher, M. E., Lüschen, H., Neretin, L. N., Volkov, I. I., 2004. Anaerobic methane oxidation and a deep $H_2S$ sink generate isotopically heavy sulfides in Black Sea sediments. *Geochim. Cosmochim. Acta* **68**, 2095-2118.

Joye, S. B., Boetius, A., Orcutt, B. N., Montoya, J. P., Schulz, H. N., Erickson, M. J., Lugo, S. K., 2004. The anaerobic oxidation of methane and sulfate reduction in sediments from Gulf of Mexico cold seeps. *Chem. Geol.* **205**, 219-238.

Kamyshny, Jr., A., Solubility of cyclooctasulfur in pure water and sea water at different temperatures. *Geochim. Cosmochim. Acta* In Press, Corrected Proof.

Kamyshny, Jr., A., 2009. Improved cyanolysis protocol for detection of zero-valent sulfur in natural aquatic systems. *Limnol. Oceanogr.: Methods* **7**, 442-448.

Kamyshny, Jr., A., Borkenstein, C. G., Ferdelman, T. G., 2009. Protocol for quantitative detection of elemental sulfur and polysulfide zero-valent sulfur distribution in natural aquatic samples. *Geostand. Geoanal. Res.*

Kamyshny, Jr., A., Ekeltchik, I., Gun, J., Lev, O., 2006. Method for the determination of inorganic polysulfide distribution in aquatic systems. *Anal. Chem.* **78**, 2631-2639.

Kamyshny, Jr., A., Goifman, A., Gun, J., Rizkov, D., Lev, O., 2004. Equilibrium distribution of polysulfide ions in aqueous solutions at 25 °C: A new approach for the study of polysulfides equilibria. *Environ. Sci. Technol.* **38**, 6633-6644.

Kamyshny, Jr., A., Goifman, A., Rizkov, D., Lev, O., 2003. Kinetics of disproportionation of inorganic polysulfides in undersaturated aqueous solutions at environmentally relevant conditions. *Aquat. Geochem.* **9**, 291-304.

Kamyshny, Jr., A., Gun, J., Rizkov, D., Voitsekovski, T., Lev, O., 2007. Equilibrium distribution of polysulfide ions in aqueous solutions at different temperatures by rapid single phase derivatization. *Environ. Sci. Technol.* **41**, 2395-2400.

Kamyshny, Jr., A., Zilberbrand, M., Ekeltchik, I., Voitsekovski, T., Gun, J., Lev, O., 2008. Speciation of polysulfides and zerovalent sulfur in sulfide-rich water wells in southern and central Israel. *Aquat. Geochem.* **14**, 171-192.

Kohnen, M. E. L., Damste, J. S. S., ten Haven, H. L., de Leeuw, J. W., 1989. Early incorporation of polysulfides in sedimentary organic matter. *Nature* **341**, 640-641.

Kostka, J. E., Luther, G. W., 1994. Partitioning and speciation of solid phase iron in saltmarsh sediments. *Geochim. Cosmochim. Acta* **58**, 1701-1710.

Krastel, S., Spiess, V., Ivanov, M., Weinrebe, W., Bohrmann, G., Shashkin, P., Heidersdorf, F., 2003. Acoustic investigations of mud volcanoes in the Sorokin Trough, Black Sea. *Geo-Mar. Lett.* **23**, 230-238.

Luther, G. W., 1991. Pyrite synthesis via polysulfide compounds. *Geochim. Cosmochim. Acta* **55**, 2839-2849.

Maronny, G., 1959. Constantes de dissotiation de l`hydrogene sulfure. *Electrochimica Acta* **1**, 58-69.

Martens, C. S., Berner, R. A., 1974. Methane production in the interstitial waters of sulfate-depleted marine sediments. *Science* **185**, 1167-1169.

Mau, S., Sahling, H., Rehder, G., Suess, E., Linke, P., Soeding, E., 2006. Estimates of methane output from mud extrusions at the erosive convergent margin off Costa Rica. *Mar. Geol.* **225**, 129-144.

Michaelis, W., Seifert, R., Nauhaus, K., Treude, T., Thiel, V., Blumenberg, M., Knittel, K., Gieseke, A., Peterknecht, K., Pape, T., Boetius, A., Amann, R., Jørgensen, B. B., Widdel, F., Peckmann, J. R., Pimenov, N. V., Gulin, M. B., 2002. Microbial reefs in the Black Sea fueled by anaerobic oxidation of methane. *Science* **297**, 1013-1015.

Muramoto, J. A., Honjo, S., Fry, B., Hay, B. J., Howarth, R. W., Cisne, J. L., 1991. Sulfur, iron and organic carbon fluxes in the Black Sea: sulfur isotopic evidence for origin of sulfur fluxes. *Deep-Sea Res. Pt. I* **38 Suppl. 2**, 1151–1187.

Neretin, L. N., Volkov, I. I., Böttcher, M. E., Grinenko, V.A., 2001. A sulfur budget for the Black Sea anoxic zone. *Deep-Sea Res. Pt. I* **48**, 2569-2593.

Niemann, H., Elvert, M., Hovland, M., Orcutt, B., Judd, A., Suck, I., Gutt, J., Joye, S., Damm, E., Finster, K., Boetius, A., 2005. Methane emission and consumption at a North Sea gas seep (Tommeliten area). *Biogeosciences* **2**, 335-351.

Niemann, H., Lösekann, T., de Beer, D., Elvert, M., Nadalig, T., Knittel, K., Amann, R., Sauter, E.J., Schlüter, M., Klages, M., Foucher, J.-P., Boetius, A., 2006. Novel microbial communities of the Haakon Mosby mud volcano and their role as a methane sink. *Nature* **443**, 854-858.

Olu-Le Roy, K., Sibuet, M., Fiala-Medioni, A., Gofas, S., Salas, C., Mariotti, A., Foucher, J.P., Woodside, J., 2004. Cold seep communities in the deep eastern Mediterranean Sea: composition, symbiosis and spatial distribution on mud volcanoes. *Deep-Sea Res. Pt. I* **51**, 1915-1936.

Olu, K., Lance, S., Sibuet, M., Henry, P., Fiala-Medioni, A., Dinet, A., 1997. Cold seep communities as indicators of fluid expulsion patterns through mud volcanoes seaward of the Barbados accretionary prism. *Deep-Sea Res. Pt. I* **44**, 811-819

Podgorsek, L., Imhoff, J. F., 1999. Tetrathionate production by sulfur oxidizing bacteria and the role of tetrathionate in the sulfur cycle of Baltic Sea sediments. *Aquat. Microb. Ecol.* **17**, 255-265.

Pyzik, A. J., Sommer, S. E., 1981. Sedimentary iron monosulfides - kinetics and mechanism of formation. *Geochim. Cosmochim. Acta* **45**, 687-698.

Raiswell, R., Canfield, D. E., 1996. Rates of reaction between silicate iron and dissolved sulfide in Peru Margin sediments. *Geochim. Cosmochim. Acta* **60**, 2777-2787.

Rong, L., Lim, L. W., Takeuchi, T., 2005. Determination of iodide and thiocyanate in seawater by liquid chromatography with poly(ethylene glycol) stationary phase. *Chromatographia* **61**, 371-374.

Sauter, E. J., Muyakshin, S. I., Charlou, J. L., Schlüter, M., Boetius, A., Jerosch, K., Damm, E., Foucher, J.-P., Klages, M., 2006. Methane discharge from a deep-sea submarine mud volcano into the upper water column by gas hydrate-coated methane bubbles. *Earth Planet. Sci. Lett.* **243**, 354-365.

Stookey, L. L., 1970. Ferrozine - a new spectrophotometric reagent for iron. *Anal. Chem.* **42**, 779-781.

Thamdrup, B., Finster, K., Hansen, J. W., Bak, F., 1993. Bacterial disproportionation of elemental sulfur coupled to chemical reduction of iron or manganese. *Appl. Environ. Microbiol.* **59**, 101-108.

Treude, T., Krüger, M., Boetius, A., Jørgensen, B. B., 2005. Environmental control on anaerobic oxidation of methane in the gassy sediments of Eckernförde Bay (German Baltic). *Limnol. Oceanogr.* **50**, 1771-1786.

Troelsen, H., Jørgensen, B. B., 1982. Seasonal dynamics of elemental sulfur in two coastal sediments. *Estuarine Coastal Shelf Sci.* **15**, 255-266.

Tugolesov, D. A., Gorshkov, A. S., Meysner, L. B., Solovyev, V. V., Khakhalev, Y. M., 1985. *Tectonics of Mezo-Kainozoic deposits of the Black Sea basin*. Nedra, Moscow.

Wallmann, K., Drews, M., Aloisi, G., Bohrmann, G., 2006. Methane discharge into the Black Sea and the global ocean via fluid flow through submarine mud volcanoes. *Earth Planet. Sci. Lett.* **248**, 545-560.

Yao, W., Millero, F.J., 1993. The rate of sulfide oxidation by $\delta MnO_2$ in seawater. *Geochim. Cosmochim. Acta* **57**, 3359-3365.

Zhang, J.-Z., Millero, F.J., 1993. The products from the oxidation of $H_2S$ in seawater. *Geochim. Cosmochim. Acta* **57**, 1705-1718.

Zopfi, J., Ferdelman T. G., Jørgensen, B. B., Teske A., B., T., 2001. Influence of water column dynamics on sulfide oxidation and other major biogeochemical processes in the chemocline of Mariager Fjord (Denmark). *Mar. Chem.* **74**, 29-51.

Zopfi, J., Ferdelman, T. G., Fossing, H., 2004. Distribution and fate of sulfur intermediates – sulfite, tetrathionate, thiosulfate, and elemental sulfur – in marine sediments. *Sulfur biogeochemistry.* Geological Society of America Special Paper pp. 97-116.

Chapter 6

# The $H_2S$ microsensor & the dissociation constant $pK_1$: problems & solutions

Miriam Weber [1,2], Anna Lichtschlag[1], Stefan Jansen[1], Dirk de Beer[1]

[1]Max-Planck-Institute for Marine Microbiology, Celsiusstrasse 1, 28359 Bremen, Germany

[2]HYDRA Institute for Marine Sciences, Via del Forno 80, I-57034 Campo nell'Elba (LI), Italy

## INTRODUCTION

For the calculation of the total sulfide content ($S^{2-}_{tot}$) from hydrogen sulfide microsensor signal, the dissociation constant $pK_1$ is needed. Also for the calibration of the $H_2S$ microsensor in a medium with a pH >4 the $pK_1$ is necessary for $H_2S$ concentration calculations. Hence, its accuracy is important for a precise determination of S(II)-species with a microsensor. Here we describe and discuss the $pK_1$ problems and suggest a new calibration protocol.

Hydrogen sulfide is one component of the sulfide equilibrium system:

$$\left[S^{2-}_{tot}\right] = \left[H_2S\right] + \left[HS^-\right] + \left[S^{2-}\right] \qquad (Eq.\,1)$$

Presence and concentration of the S(II)-species depend on the dissociation constants $K_1$ $\left(H_2S \xleftrightarrow{H_2O} HS^- + H^+\right)$ and $K_2$ $\left(HS^- \xleftrightarrow{H_2O} S^{2-} + H^+\right)$. The equilibrium is influenced by pH, ionic strength and temperature of the medium (Kühl and Steuckart, 2000) (Fig. 1). The pK is the negative logarithm of this dissociation constant K.

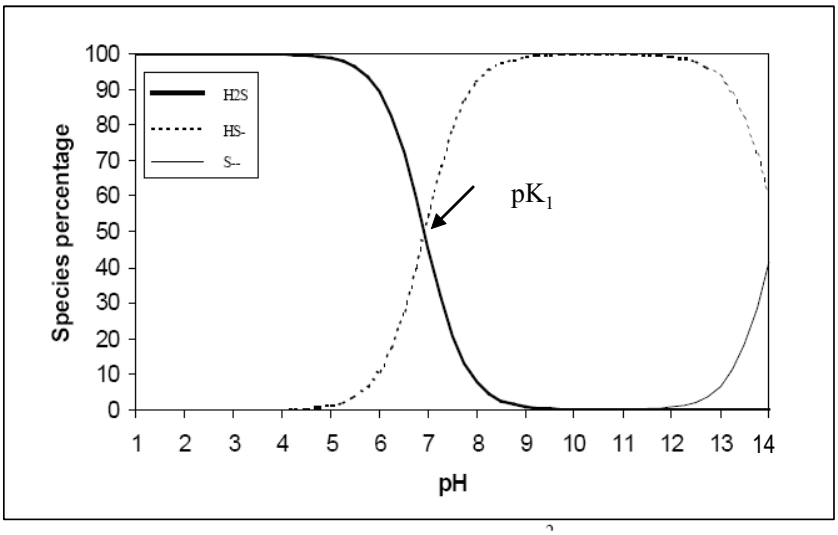


**Fig. 1: S(II)-species percentage as a function of pH at given ionic strength and temperature with the dissociation constant $pK_1$ for the $H_2S/HS^-$ equilibrium (Kühl and Steuckart, 2000; Unisense manual).**

The $H_2S$ concentration at a given total S(II) concentration ($S_{tot}^{2-}$) can be calculated as

$$\left[H_2S\right] = \left[S^{2-}_{tot}\right] \Big/ \left(1 + \frac{K_1}{\left[H_3O^+\right]} + \frac{K_1K_2}{\left[H_3O^+\right]^2}\right) \qquad K_1 = 10^{-pK_1},\ K_2 = 10^{-pK_2} \quad (Eq.\,2)$$

For pH <9, as is the case in most natural aquatic systems, the dissociation of $HS^-$ to $S^{2-}$ is negligible and the equation can be simplified to:

$$[H_2S] = [S^{2-}_{tot}] / \left(1 + \frac{K_1}{[H_3O^+]}\right) \qquad \text{(Eq. 3)}$$

In solutions with pH <4, also the dissociation of $H_2S$ to $HS^-$ is negligible and the equation can further be simplified to:

$$[H_2S] = [S^{2-}_{tot}] \qquad \text{(Eq. 4)}$$

For the calculation of Equation (3) the $pK_1$ and the pH (=-log $[H_3O^+]$) need to be known. The pH can be measured and the $pK_1$ can be calculated according to Millero et al. (1988) using the following equation:

$$pK_1 = -98.080 + 5765.4/T + 15.0455 \times \ln(T) + \left(-0.157 \times \left(S^{0.5}\right)\right) + (0.0135 \times S) \qquad \text{(Eq. 5)}$$

where T is the temperature in Kelvin and S is the salinity. It is very important to note that this equation is only valid for seawater! For media with another ionic composition (more precise: ionic strength), refer to further literature and *see* Chapter 3. Therein the problems of the correct $pK_1$-determination are elucidated and solutions are presented. Examples for $pK_1$-values at different salinities and temperatures are given in Figure 2.

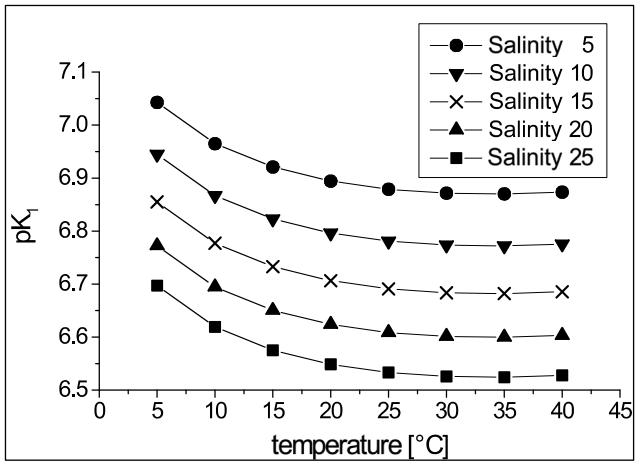


**Fig. 2: $pK_1$-values for the dissociation of $H_2S$ in seawater at certain temperatures and salinities using the equation from Millero et al. (1988).**

The hydrogen sulfide microsensor is an amperometric-type miniaturised sensor (Jeroschewski et al., 1996, Kühl et al., 1998) measuring $H_2S$ partial pressure: $H_2S$ gas penetrates the silicon membrane of the sensor tip and is converted to $HS^-$-ions in an alkaline electrolyte. Ferricyanide oxidizes this $HS^-$ to sulfur and ferrocyanide is formed. The ferrocyanide is re-oxidized at the anode of the sensor tip. The resulting current corresponds to the $H_2S$ concentration.

The electrolyte is photosensitive, mainly to UV and blue light (www.unisense.com). The detection limit of a new sensor is about 0.1 µM. The sensor signal is linear in a concentration range between 0-300 µM $H_2S$ and becomes non-linear at higher concentrations. In the linear range a 2-3 point calibration of the microsensor is sufficient, whereas in the non-linear range a more precise calibration is recommended.

According to literature and the Unisense manual of July 2003 (the reader should know that the current (2007) Unisense manual is modified), it was suggested to calibrate the $H_2S$ sensor in a 100-200 mM phosphate buffer (pH 7-7.5). Increments of a stock solution (100-500 mM $S^{2-}_{tot}$) should be added to a known volume of degassed buffer. Subsamples should be taken and fixed in 2% ZnAc after each calibration step. $S^{2-}_{tot}$ is determined photometrically (Cline, 1969, Budd and Bewick, 1952) and the $H_2S$ concentration is calculated using Equation (3). In publication using similar calibration protocols usually a $pK_1$ of 7.05 was used (Wieland & Kühl, 2000, Kühl & Jørgensen, 1992). Doing so for our studies, we discovered a discrepancy between the $S^{2-}_{tot}$ concentrations measured with $H_2S$ microsensors and the $S^{2-}_{tot}$ concentration measured in the pore water with analytical methods.

As a consequence we decided to determine the precise $pK_1$ for the phosphate buffer we had used for the calibration of the microsensor using the newly developed '2-way-calibration-method' (Chapter 3). When we compared results obtained using the defined $pK_1$ of 6.9 (see $^{**}$in Table 1 and Chapter 3) with those of the previously used $pK_1$ of 7.05 (see $^{*}$in Table 1) we obtained up to ± 30% deviance in the final $H_2S$ concentration. We saw that a $pK_1$-offset of 0.05 leads to over- or underestimation of 8.9% and an offset of 0.1 $pK_1$ units to over- or underestimation of 17% (Table 1) of the measured $H_2S$ concentration.

**Table 1: Effect of over-/underestimated $pK_1$ values on the final $H_2S$ concentration during $H_2S$ microsensor calibration in a phosphate buffer (pH 7.5).**

| mean value | | | $pK_1$ deviance | 0.05 unit | | 0.1 unit | |
|---|---|---|---|---|---|---|---|
| $pK_1$ | $H_2S$ [mM] | $H_2S$ difference [%] | $H_2S$ difference | [mM] | % | [mM] | % |
| 7.10 | 0.52 | 140.5 | | 0.04 | 7.69 | 0.08 | 15.38 |
| **7.05** | **0.48** | **129.7*** | | 0.04 | 8.33 | | |
| 7.00 | 0.44 | 118.9 | | 0.03 | 6.82 | 0.07 | 15.91 |
| 6.95 | 0.41 | 110.8 | | 0.04 | 9.76 | | |
| **6.90** | **0.37** | **100.0**** | | 0.03 | 8.11 | 0.06 | 16.22 |
| 6.85 | 0.34 | 91.9 | | 0.03 | 8.82 | | |
| 6.80 | 0.31 | 83.8 | | 0.03 | 9.68 | 0.06 | 19.35 |
| 6.75 | 0.28 | 75.7 | | 0.03 | 10.71 | | |
| 6.70 | 0.25 | 67.6 | | 0.02 | 8.00 | 0.04 | 16.00 |
| 6.65 | 0.23 | 62.2 | | 0.02 | 8.70 | | |
| 6.60 | 0.21 | 56.8 | | 0.02 | 9.52 | 0.04 | 19.05 |
| 6.55 | 0.19 | 51.4 | | 0.02 | 10.53 | | |
| 6.50 | 0.17 | 45.9 | **Mean value** | | **8.89** | | **16.99** |
| | | | **Standard deviation** | | **1.18** | | **1.74** |

$^{*}$ $pK_1$ literature value for phosphate buffer calibration

$^{**}$ $pK_1$ determined '2-way-calibration-method'

To solve this problem we describe in the following section:

**Chapter 1**: The new $H_2S$ microsensor calibration protocol, which we suggest to use from now on.

**Chapter 2:** Data showing the effect of 2.1.) degassing; 2.2.) salinity/ionic strength; 2.3.) temperature; 2.4.) pH; 2.5.a) temperature and salinity on the $pK_1$ using Equation (5) and 2.5. b) pH on the $H_2S$ concentration using Equation (3) on $H_2S$ microsensor sensitivity and/or measuring accuracy.

**Chapter 3**: The '2-way-calibration-method' for the $pK_1$-determination of any given solution.

## MATERIAL, METHODS, RESULTS

### Chapter 1: Calibration Protocol

*We suggest performing the calibration of a $H_2S$ microsensor in a subsample of the solution where the measurements will be carried out in (further referred to as calibration solution (e.g. seawater with a salinity of 36). To circumvent the problems described above the calibration solution is acidified to pH <4 and no $pK_1$ is needed for the calibration.*

1. Get a $H_2S$ microsensor started (*see* www.unisense.com).
2. The calibration should always be performed under in situ conditions, i.e. in the calibration solution the same temperature and salinity (more precise: ionic strength) should be maintained as will prevail during your measurements (*see* Chapter 2.2. and Fig. 3).
3. The calibration solution is acidified (e.g. with HCl) to a pH <4; as it is most probably not a buffered medium and you will add a base as stock solution ($Na_2S$) we suggest to acidify to a pH <2.
4. A defined volume (e.g. 100 mL) of the calibration solution is put on a stirrer (degassing is not necessary, *see* Chapter 2.1. and Fig. 3), the sensor inserted, and the signal measured.
5. 2-4 times increments (e.g. 50 µL) of a $Na_2S$ stock solution (e.g. 100 mM) are added, shortly and gently (!) stirred (no teflon stirrer) for mixing, and subsamples and sensor readings are taken between each stock solution addition. Consider that at pH <4 all S(II) is in form of $H_2S$ gas and can easily be flushed out by vigorous stirring! A subsample of the calibration solution is fixed in 2% ZnAc so that an end concentration of 20-50 µM is reached. Subsamples can be stored in the dark and cold (4 °C) for several weeks.
6. Check the pH in the medium after the calibration! It maximally should be at 3.9; this is important because only in this case $S^{2-}_{tot}=H_2S$.
7. The $S^{2-}_{tot}$ concentration of the subsamples is measured photometrically (Cline, 1969; Budd and Bewick, 1952). Results correspond directly to the $H_2S$ signal measured with the $H_2S$ microsensor (*see* Equation (4)).

**Chapter 2: Data on the $H_2S$ Sensor Sensitivity and Measurement Accuracy**

*2.1. We tested if the calibration solution needs to be anoxic. For that a calibration according to the new calibration protocol (see Chapter 1) with degassed ($N_2$-flushed) and air-saturated seawater (salinity 36, pH 2.5) was done.*

As the sensor signal was the same in the air-saturated and degassed solution during the calibration, degassing of the calibration solution is not needed (Fig. 3). Half lifetime of $H_2S$ in an oxic medium depends on pH, temperature, ionic strength, and the presence of catalysts, and is usually several hours in air saturated seawater (Millero et al., 1987).

*2.2. We tested if the new $H_2S$ microsensor calibration is salinity (respectively ionic strength) sensitive. For that a calibration was carried out in 100 mL (pH 2.5) of a) deionised water (salinity = 0), b) seawater (salinity = 36), c) deionised water + 15 g NaCl (NaCl was added to simulate a hypersaline medium, salinity = 150) and d) seawater + 15 g NaCl (salinity = 186).*

In our tests the microsensor signal in the calibration solutions with salinity 150 and 186 was strongly affected (Fig. 3). Furthermore our data showed that the ionic strength difference from e.g. deionised water compared to e.g. phthalate buffer (phthalate buffer = 0.1 M potassium hydrogen phthalate solution adjusted to a pH 2.2 - 4 by HCl addition) is also reflected in the sensor signal (Fig. 4).

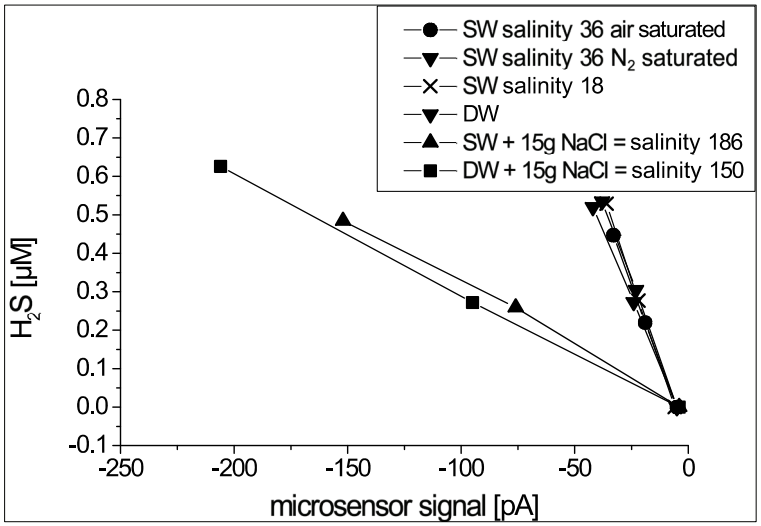


**Fig. 3: $H_2S$ microsensor calibrations at 21 °C in seawater (SW) and deionised water (DW) with various salinities, air-and $N_2$-flushed.**

*2.3. We tested if the new $H_2S$ microsensor calibration is temperature sensitive. For this a calibration at two different temperatures (15 and 23 °C) was carried out in: a) phosphate buffer (pH = 7.5), b) phthalate buffer (pH <4) and c) 10 mM HCl.*

As stated in the original reference (Jeroschewski et al., 1996), we confirmed that the $H_2S$ microsensor is temperature sensitive. Thus it is important to perform the calibration at in situ temperature (Fig. 4).

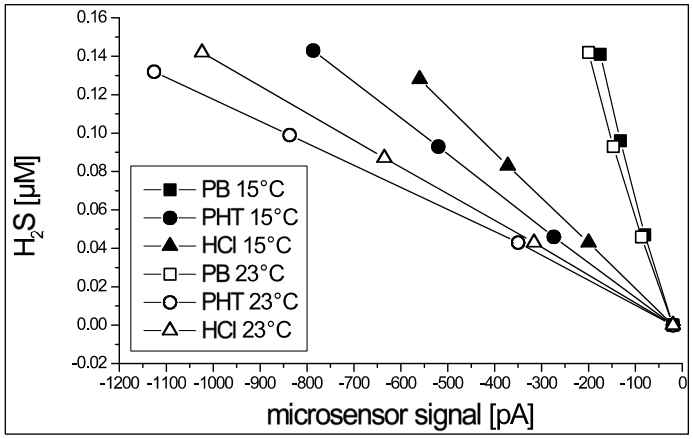


**Fig. 4: $H_2S$ microsensor calibrations at two different temperatures (15 and 23 °C) with a) 200 mM phosphate buffer pH = 7.5 (PB), b) phthalate buffer pH 3.8 (PHT) and c) 10 mM HCl as calibration solutions.**

*2.4. We tested if the new $H_2S$ microsensor calibration is pH sensitive. For that a stepwise acidification of the calibration solution (seawater salinity 36) from pH 3.9 to pH 1 was done.*

The microsensor signal stayed constant; the calibration of the sensor is not influenced by the decreasing pH (data not shown).

*2.5. We calculated a) the p$K_1$-deviance of imprecise temperature and salinity measurements when using Equation (5) and b) the $H_2S$ concentration deviance of imprecise pH measurements using Equation (3).*

a) A temperature offset ±1 °C affects the p$K_1$ in the first decimal. The effect of salinity is strongest at low salinities. An offset between salinity 5 and 18 changes the p$K_1$ in the first decimal, but at salinity values >18 in the second and >33 in the third decimal only (Table 2). Even though the effect is little, using Equation (5) it should be aimed to measure temperature and salinity with an accuracy of ±1 units. As shown in the introduction and Table 1 a p$K_1$ deviance in the second decimal already can have a severe effect on the $H_2S$ concentration.

b) A pH offset of ±0.05 units at e.g. pH 7.5 leads to an over-/underestimation of 8.9-9.5% (*see* *in Table 3) and an offset of ± 0.1pH unit to 17.1-19.7% (see **Table 3) deviance of the measured $H_2S$ concentration. The deviance decreases with higher pH. However, using Equation (3) pH measurements should be aimed at best accuracy possible. Because of this we suggest to use the calibration protocol described in Chapter 1.

**Table 2: $pK_1$-deviance caused by imprecise temperature and salinity measurements using Equation (5) (Millero et al., 1988). Note that the equation is valid for seawater salinity 5 - 40 at 5 - 25 °C only!**

| | Temp (°C) | Salinity | $pK_1$ (Millero et al., 1988) |
|---|---|---|---|
| brackish water | 23 | 5 | 6.7265 |
| brackish water | 23 | 18 | 6.5870 |
| brackish water | 23 | 19 | 6.5822 |
| brackish water | 23 | 20 | 6.5779 |
| seawater | 23 | 33 | 6.5537 |
| seawater | 23 | 34 | 6.5536 |
| seawater | 23 | 35 | 6.5537 |
| seawater | 24 | 35 | 6.5389 |
| seawater | 23 | 35 | 6.5537 |
| seawater | 22 | 35 | 6.5688 |
| seawater | 16 | 35 | 6.6651 |
| seawater | 15 | 35 | 6.6822 |
| seawater | 14 | 35 | 6.6996 |
| seawater | 6 | 35 | 6.8499 |
| seawater | 5 | 35 | 6.8701 |

**Table 3: $H_2S$ concentration deviance caused by imprecise pH measurements using Equation (3) from Jeroschewski et al. (1996).**

| Calibration solution | $pK_1$ | pH | $H_2S$ [mM] | $H_2S$ difference [mM] | % |
|---|---|---|---|---|---|
| Phosphate buffer 200 mM | 6.9 | 7.00 | 0.48 | 0.26 | 120.5 |
| | 6.9 | 7.05 | 0.45 | 0.23 | 106.5 |
| | 6.9 | 7.10 | 0.42 | 0.20 | 92.7 |
| | 6.9 | 7.15 | 0.39 | 0.17 | 79.3 |
| | 6.9 | 7.20 | 0.36 | 0.14 | 66.3 |
| | 6.9 | 7.25 | 0.33 | 0.12 | 53.8 |
| | 6.9 | 7.30 | 0.31 | 0.09 | 41.8 |
| | 6.9 | 7.35 | 0.28 | 0.07 | 30.4 |
| | 6.9 | 7.40 | 0.26 | 0.04 | **19.7**** |
| | 6.9 | 7.45 | 0.24 | 0.02 | **9.5*** |
| | **6.9** | **7.50** | **0.22** | **0.00** | **0.0** |
| | 6.9 | 7.55 | 0.20 | 0.02 | **8.9*** |
| | 6.9 | 7.60 | 0.18 | 0.04 | **17.1**** |
| | 6.9 | 7.65 | 0.16 | 0.05 | 24.8 |
| | 6.9 | 7.70 | 0.15 | 0.07 | 31.9 |
| | 6.9 | 7.75 | 0.13 | 0.08 | 38.3 |
| | 6.9 | 7.80 | 0.12 | 0.10 | 44.3 |
| | 6.9 | 7.85 | 0.11 | 0.11 | 49.7 |
| | 6.9 | 7.90 | 0.10 | 0.12 | 54.7 |
| | 6.9 | 7.95 | 0.09 | 0.13 | 59.2 |
| | 6.9 | 8.00 | 0.08 | 0.14 | 63.3 |

* Resulting $H_2S$ concentration deviance with an offset of 0.05 pH unit offset

** Resulting $H_2S$ concentration deviance with an offset of 0.1 pH unit offset

**Chapter 3: Determination of the $pK_1$ Using the '2-Way-Calibration-Method'**

*In case you used a phosphate buffer or another solution with pH >4 for the calibration of your $H_2S$ sensor, and you are unsure about the correct $pK_1$, we suggest determining the $pK_1$ afterwards using the following protocol:*

Theory: Two calibrations in two different calibration solutions (*hereafter*: calibration solution I and II) are carried out with the same microsensor. From the results the $pK_1$ of the solution you formerly used can be calculated. For this the calibration solution I must have the same properties (salinity/ionic strength, pH, temperature) as the solution you formerly calibrated in. In calibration solution I S(II) exists as $H_2S$ + $HS^-$. Calibration solution II must be prepared as suggested in the new calibration protocol (salinity, ionic strength and temperature as in the solution you have measured in, acidified to pH <4) and then all S(II) is in the form of $H_2S$ (*see* Fig. 1); by adding exactly the same concentration of stock solution in both calibration solutions, the sensor signal that is corresponding to the $HS^-$ concentrations in solution I can be calculated. The sensor signal corresponding to the $H_2S$ concentration is known from the calibration in solution II, because the $S^{2-}_{tot}$ corresponding to this sensor signal can be determined photometrically. The relation of the amount of $H_2S/HS^-$ determines the $pK_1$ and can be calculated by combining the calibration I and II (*see* Table 4).

Practical application:

1. Get a fresh $H_2S$ microsensor started (www.unisense.com).
2. Take 100 mL of the formerly used calibration solution (in this example calibration solution I = 200 mM phosphate buffer, pH 7.5) and measure the pH as precise as possible (check the temperature settings and calibrate the pH probe!).
3. Perform a 3-4 point calibration, fixate subsamples for later $S^{2-}_{tot}$ determination (see Chapter 1) and check the pH again.
4. Take 100 mL of the calibration solution II with equal ionic strength as the medium you have measured in (in this example seawater salinity 36) and acidify it with HCl to pH <2 (the pH has to stay <4 for the whole calibration procedure, thus, to assure a pH <4 also after the addition of the $Na_2S$ stock a pH of <2 is recommended).
5. Perform a 3-4 point calibration (with the same microsensor and at the same temperature as in calibration solution I!), take subsamples for later $S^{2-}_{tot}$ determination, and check the pH again.
6. To make both calibrations comparable you now have to calculate how much $S^{2-}_{tot}$ would be present in the different calibration solutions if the sensor signals in both calibrations would be identical (Table 4). For this (i) calculate the regression of calibration solution I (in this example phosphate buffer) and then (ii) calculate the $S^{2-}_{tot}$ at the corresponding sensor signals from calibration solution II.

7. Now you can use Equation (3) with $pK_1$ as the only unknown variable: the $S^{2-}_{tot}$ and pH you have measured, and the $pK_1$ needs to be fitted until the value for $S^{2-}_{tot}$ matches the value you measure in your calibration solution I.

Note: usually the pH cannot be measured more accurately than the first decimal (*see* Chapter 2.4.). Thus we suggest using a $pK_1$ value with the accuracy of one decimal only!

**Table 4: The $pK_1$-determination of a given solution using the '2-way-calibration-method'.**

| | | | | |
|---|---|---|---|---|
| I | Calibration | y = -11,396x + 0,0331 | | |
| Calibration solution I | | sensor signal | Stot = $H_2S$+$HS^-$ | |
| Phosphatebuffer | | 0.00 | 0.0 | |
| pH 7.5 | | -0.02 | 0.3 | |
| 23°C | | -0.04 | 0.5 | |
| II | Using | y = -11,396x + 0,0331 | | In calibration solution I |
| Calibration solution II | | sensor signal | $S_{tot}$ = $H_2S$ | $S_{tot}$ = $H_2S$ would be |
| seawater salinity 36 | | 0.00 | 0.0 | *0.0* |
| pH < 4 | | -0.12 | 0.3 | *1.4* |
| 23°C | | -0.24 | 0.5 | *2.7* |
| III | Using formula (3): | $[H_2S] = [S^{2-}_{tot}] / \left(1 + \frac{K_1}{[H_3O^+]}\right)$ | | |
| | | | | In calibration solution I |
| | | | $H_2S$ uM | $S_{tot}$ = $H_2S$ would be |
| | pH | *7.50* | 0.0 | *0.0* |
| | $Pk_1$ | *6.90* | 0.7 | *1.4* |
| | | | 1.4 | *2.7* |

Further possibilities for $pK_1$ determination were suggested and used:

- Titration (de Beer and Lichtschlag)
- Calibration with phosphate buffers at different pH and the common intercept corresponds to the $pK_1$ (Jansen and Weber)

## CONCLUSIONS & RECOMMENDATION

When doing your measurements/experiments always measure pH, temperature and ionic strength/salinity as precise as possible. Be aware of the potential over-/underestimation caused by imprecise temperature, salinity and/or pH measurements, when

a) determining the $pK_1$ with the Equation (5) of Millero et al. (1988).
b) doing the $H_2S$ calibration with a solution pH >4 (not recommended by the authors!) using Equation (3).
c) calculating $S^{2-}_{tot}$ concentration using Equation (3) .

Precise pH measurements can usually be done accurately to the first decimal. That is why $pK_1$-values should be used with one decimal only. After all we suggest avoiding calibration in solutions with pH >4 as then the $pK_1$ can be neglected for the calibration. Anyhow, always consider to measure $pK_1$ directly, if you are unsure about the calculations and literature.

Also measuring salinity needs to be thought through carefully. The most accurate measurement method is conductivity. However when working with seawater salinities 5 - 40 we consider a refractometer, calibrated against normal seawater, as sufficient. Other solutions than seawater need further investigations and are not covered within this study.

Take care using $H_2S$ microsensors under 'abnormal' conditions like hypersaline, hyperbaric, or very high temperature, and check the sensor for its sensitivity if uncertain. Researchers interested in measuring under high pressure should consult the literature of e.g. Carroll & Mather (1989). If you work with hypersaline media, check Gamsjäger and Schindler (1969), Wieland and Kühl (2000), and for high temperature check Hershey et al. (1988), Millero (1986), and Millero and Hershey (1989). In order to determine the threshold at which salinity and/or ionic strength values affect the microsensor signal, further tests are needed. However we strongly recommend calibrating in the same solution/medium, as where the measurements will be done.

Further, all $H_2S$ microsensor users should consider mentioning the potential percentage deviance of the $H_2S$ concentration of their results. We suggest that this provides all of us with a better understanding on the difficulties of $H_2S$ microsensor measurements, but also on the absolute and relative values of the published $H_2S$ data.

## REFERENCES

Budd, M.S. and Bewick, H.A., 1952. Photometric determination of hydrogen sulfide and reducible sulfur in alkalines. *Anal. Chem*. **24:** 1536-1540.

Carroll, J.J. and Mather, E., 1989. The solubility of hydrogen sulphide in water from 0 and 90 °C and pressures to 1 MPa. *Geochim. Cosmochim. Acta* **53:**1163-1170.

Cline, J., 1969. Spectrophotometric determination of hydrogen sulfide in natural waters. Limnol. Oceanogr. **14:** 454-458.

Gamsjäger, H., and P. Schindler, 1969. Solubility and activity coefficients of $H_2S$ in electrolyte mixtures. *Helvetica Chimica Acta* **52:**1395-1402.

Hershey, J. P., T. Plese, and F. J. Millero, 1988. The $pK_1^*$ for the dissociation of $H_2S$ in various ionic media. *Geochim. Cosmochim. Acta* **52:**2047-2051.

Jeroschewski, P., C. Steuckart, and M. Kühl, 1996. An amperometric microsensor for the determination of $H_2S$ in aquatic environments. *Anal. Chem*. **68:**4351-4357.

Kühl and Jørgensen, 1992. Microsensor measurements of sulfate reduction and sulfide oxidation in compact microbial communities of aerobic biofilms. *Appl. Environ. Microbiol*. **58:**1164-1174.

Kühl and Steukart, 2000. Sensors for in situ analysis of sulfide in aquatic systems. In: *In situ monitoring of aquatic systems: chemical analysis and speciation.* Eds: Buffle, J. and Horvai, G. pp 121-159.

Kühl, M., C. Steuckart, G. Eickert, and P. Jeroschewski, 1998. A $H_2S$ microsensor for profiling biofilms and sediments: application in an acidic lake sediment. *Aquat. Microb. Ecol*. **15(2):** 201-209.

Millero, F. J., 1986. The thermodynamics and kinetics of the hydrogen sulfide system in natural waters. *Mar. Chem*. **18:**121-147.

Millero, F. J., and J. P. Hershey, 1989. Thermodynamics and kinetics of hydrogen sulfide in natural waters. *Acs Symposium Series* **393:**282-313.

Millero, F. J., T. Plese, and M. Fernandez, 1988. The dissociation of hydrogen sulfide in seawater. *Limnol. Oceanogr.* **33:**269-274.

Millero, F., S. Hubinger, M. Fernandez, and S. Garnett, 1987. Oxidation of $H_2S$ in seawater as a function of temperature, pH, and ionic strength. *Environ. Sci. Technol.* **21:**439-443.

Truper, H. G., and H. G. Schlegel, 1964. Sulphur metabolism in Thiorhodaceae 1. Quantitative measurements on growing cells of *chromatium okenii*. *Antonie Van Leeuwenhoek* **30:**225-238.

Wieland, A., and M. Kühl, 2000. Short-term temperature effects on oxygen and sulfide cycling in a hypersaline cyanobacterial mat (Solar Lake, Egypt). *Mar. Ecol. Prog. Ser.* **196:**87-102.

www.unisense.com/Files/Filer/Manuals/Sulfide_manual_A5_www.pdf

Chapter 7

# Conclusions and perspectives

# CONCLUSIONS AND PERSPECTIVES

In this thesis the interaction between microbiology and geochemistry, and the physical driving forces for the biogeochemical cycles in near-surface sediments of different cold seeps were investigated. Ecologically and environmentally important processes, such as methane export from the sediment to the water column, methane oxidation with concurrent sulfide production, and sulfide consumption were studied in different habitats of different cold seeps. Particular emphasis was given to the sedimentary iron and sulfur chemistry, the area where chemical redox reactions compete with the biological counterparts. The presented study contributes to the small record currently existing on cold seep spatial and temporal heterogeneities. The work was closely integrated with microbial rate and community studies, which will mainly be reported elsewhere (summarized in Chapter 1.5.3). With this dataset we describe both, the heterogeneity within a cold seep structure, and the variability between different cold seep sites. We finally report about the physico-chemical drivers on ecologically and environmentally relevant cold seep processes.

## 1.1. The Sulfur Cycle in Cold Seep Sediments

One major objective of this work was to study the intensity of the sulfide production and the pathway for sulfide turnover in oxic and anoxic cold seep surface sediments, and whether microbial sulfide consumption can compete with geochemical oxidation in cold seeps. Sulfidic sediments are often populated by members of the genus *Beggiatoa,* interesting and typical inhabitants of cold seeps that are conspicuous due to their large size. Their physiology, their habit to glide between oxic and anoxic sediment zones, and their ability to consume sulfide with nitrate were already largely studied in the laboratory, making it much easier to look for similar traits in the environment.

One surprising outcome of this study was that removal of sulfide from cold seep sediments can be controlled by both, geochemical and microbial processes. In geochemical removal electrons are directly accepted by reactive oxidized iron, biological oxidation is via microbes using nitrate or oxygen as electron-acceptor. The essential ecological difference is that microbes fix inorganic carbon into biomass and geochemistry does not. To distinguish between the two processes is not easy, and detailed investigations are needed to assess the dominant pathway of sulfide removal by methods as we used in studies on the Håkon Mosby Mud Volcano and Eckernförde Bay (Chapter 2, 3). Key players in sulfide removal at the Håkon Mosby Mud Volcano were thiotrophic bacteria, in particular *Beggiatoa.* With their high internal nitrate and elemental sulfur content the *Beggiatoa* sustained their metabolism while gliding between the oxic and the anoxic sediment zones. They were able to consume the total sulfide flux before it reached the oxic zone, producing a gap of around 4 mm between the sulfidic and oxic zone and a complex shape of the pH profile by sequential sulfide oxidation in different zones. Overall, the sulfide fluxes varied over one order of magnitude in the thiotrophic mat

habitats of the Håkon Mosby Mud Volcano, but the fluxes of oxygen and nitrate were always sufficient for a complete microbial consumption of the sulfide. Chemical sulfide oxidation or precipitation with iron was not important as the iron minerals contained in the mud volcano sediment seemed rather recalcitrant towards sulfide. The upward flowing pore fluid and the consumption in microbial turnover processes limited the penetration of oxygen and nitrate for re-oxidation of iron-sulfides. An active iron-sulfur cycle was not developed due to absence of bioturbation, thus oxidized iron was not mixed down. From the geochemical and microbiological characteristics the Eckernförde Bay site looked similar at first, with a pH profile resembling that of the Håkon Mosby sediments, and a suboxic zone, where neither oxygen nor free sulfide was detectable but most nitrate-storing *Beggiatoa* filaments were present. However, despite a similarly high biomass and internal nitrate and sulfur content as those in the Håkon Mosby Mud Volcano, *Beggiatoa* accounted only for a small fraction of the sulfide removal in this seep site. Most of the sulfide flux was removed by chemical processes, mainly by precipitation with $Fe^{2+}$ and oxidation by iron-oxides, which is coupled to a pH increase. The free $Fe^{2+}$ diffusing upwards was oxidized chemically by Mn(IV), resulting in a strong pH decrease. The shapes of the pH profiles at Eckernförde Bay and the Håkon Mosby Mud Volcano *Beggiatoa* habitat were similar, but driven by different processes. The two studies showed that generally, if reactive iron is present it will react first and the microbes will have to live on the leftovers. The differences in the sulfide oxidation pathway between the sites are due to the availability of reactive iron: at Eckernförde Bay there is a regular mixing of reduced and oxidized sediments by storm-events, wave-action and bioturbation, oxidizing the iron-sulfides and refreshing the subsurface iron-oxide pool. The freshly precipitated iron-oxides will have a much higher reactivity towards sulfide than the iron-oxides rising in the Håkon Mosby Mud Volcano, which are rather inefficient in sulfide removal as this study showed. A similar active iron cycle in mud volcano sediments could only be stimulate by regular vigorous seep eruptions with suspension of sediments in the water column and this is only possible at fluid flow orders of magnitude higher. However, such a high upflow would totally block sulfate penetration, inhibit AOM, and thus block the sulfur-cycle (de Beer et al. 2006). Another major difference between the two sites is the dimension of the suboxic zone the *Beggiatoa* filaments have to cross for the access to both, electron-acceptor and -donor: at the Håkon Mosby Mud Volcano sulfide is present close to the sediment surface (suboxic zone: 4 mm), while at Eckernförde Bay the gap can extend to several centimeter.

To better define the boundary conditions for the competition between geochemical and microbial sulfide oxidation, experiments with iron minerals with different reactivity towards sulfide and defined amounts of *Beggiatoa* biomass could be performed. Another interesting finding and task for further environmental studies was that there were areas in the thiotrophic mat habitats of the Håkon Mosby mud volcano where no mat was formed, and here the sulfide fluxes were similar as those beneath the thiotrophic mats in Eckernförde Bay. Thus, the tendency to form thiotrophic mats seems to depend not only on the sulfide flux but also on other factors. Further studies of sulfide oxidation pathways would

also be highly interesting at the outer edge of the Håkon Mosby Mud Volcano, where dense populations of siboglinid tubeworms are found in the sediments. Siboglinid tubeworms pump seawater downwards and induce AOM-related sulfide production with the contained sulfate at several decimeters depth (de Beer et al., 2006). This sulfide nourishes the thiotrophic tubeworm symbionts, however, whether the bioirrigation by the tubeworms also induces geochemical sulfide consumption is not known and would be a fascinating topic for further investigation. For the ecological importance of the tubeworms, the total amount of oxidants transferred into the sediment needs to be determined, and the geochemical characteristics of the sediments needs to be investigated.

An exciting finding concerning sulfide oxidation in seep sediments was made at the Dvurechenskii mud volcano, a mud volcano in the permanent anoxia of the Black Sea (Chapter 5). Although the mud volcano sediments could not scavenge all sulfide formed at the surface by AOM, they still contained oxidative potential towards sulfide. Intermediate sulfur species, such as elemental sulfur, polysulfides, thiosulfate, and sulfite were detected in the sediment and the presence of such sulfur intermediates is a sign of active sulfide oxidation. During the extensive pore fluid and solid phase iron and sulfur chemical analyses at the Dvurechenskii mud volcano elevated concentrations of reactive iron-minerals (reactive = reactive towards sulfide) were detected in the fresh mud flows. In the AOM-zone sulfide is formed and the iron minerals are slowly reacting with the sulfide, inducing the sulfur intermediate formation. Thus, reactive iron was retained during millions of years in a highly reduced environment, enriched in methane. We concluded that the outcome of this 'natural experiment' excludes the possibility of microbial oxidation of methane by Fe(III) in cold seeps. An important finding and further searches towards such a mechanism seem futile. As the constituents of the fluid and the sediment composition is highly variable, redox reactions in the sediments will differ per site. We have to search in other cold seep sites for sulfur intermediates, and return to the Dvurechenskii mud volcano to perform controlled laboratory experiments with fresh sediments, in particular determining the degree of the oxidative power of the iron minerals and the rates of sulfide turnover and sulfur intermediate production.

In conclusion, this thesis shows that there is no single sulfide oxidation pathways in cold seeps but both, geochemical reactions or microbial sulfide oxidation by *Beggiatoa* can dominate. An extended suboxic zone and a large amount of reactive iron will reduce the potential of the *Beggiatoa*, as they are not fast enough to outcompete geochemical reactions. Sulfide oxidation depends on the availability of reactive iron, and thus on the degree of sediment disturbances by bioturbation, storm events, fluid upflow or frequency of eruptions, and the content of the fluids and sediments rising in the seeps. Important from an environmental point of view, in cold seeps in oxygenated environments both pathways - geochemical and microbiological oxidation - do efficiently prevent the environmentally harmful sulfide from being released into the hydrosphere. However, although unexpectedly some sulfide oxidation occurs, in the permanently anoxia of the Black Sea most sulfide is released from the sediments into the water column. I believe that for more reliable statements on iron reactivity the

methodology urgently needs improvement. The current methods for extraction of 'reactive' or 'unreactive' iron minerals are based on laboratory experiments (Poulton et al., 2004) or sediments from very specific geochemical environments like salt marshes and coastal areas (Canfield, 1989; Ferdelman et al., 1991; Kostka and Luther, 1994), and for samples from environments with a different geochemical record it sometimes is uncertain which minerals were extracted, and how their reactivity towards sulfide will be. Further investigations on the actual oxidative potential of the cold seep sediments should be determined by experiments.

**1.2. Controlling Factor for Seep Biogeochemistry and Primary Production**

Previous studies suggested that in cold seeps the intensity of the fluid flow might be one of the main driving forces for habitat development, causing a concentric-zonal distribution of the habitats (Lance et al., 1998; Sibuet and Olu, 1998; Ginsburg et al., 1999; Treude et al., 2003; de Beer et al., 2006). In this study this hypothesis was tested in detail for different cold seeps and the chemosynthetic and geochemical zones therein. One interesting finding was that although at mud volcanoes the shape of the habitats often displays a roughly concentric-zonal distribution, and temperature gradients, fluid flow, and geochemical turnover processes are related with each other, there is no gradual ecological zonation from the center to the edges. The fluid flow rates may not differ a lot between the center and the periphery. Also in the periphery confined areas with increased fluid flow can be found, indicating secondary feeder channels and patchiness in upflow. Small scale patchiness in fluid flow and substrate supply (size-scale of centimeter to 100 m) were visible from sulfide fluxes and oxygen penetration depth varying up to one order of magnitude, and indicated by the presence and absence of thiotrophic mats. It should be realized for further habitat characterization that this thiotrophic community has a high biomass turnover in the order of days, as shown for the *Beggiatoa* habitat of the Håkon Mosby Mud Volcano (Chapter 2), and thus is only indicative of the actual fluid flow, not accounting for temporal variances in substrate supply. This is important as seeps are often only identified from the presence of a specific community. However, the high biomass turnover together with results from Paull et al. (2005), who showed that a chemosynthetic community can also establish due to exposure of methane and sulfide by sediment erosions, shows that this should be done with care. Probably, gray mats are the result of such erosions as indeed no evidence for seepage was found here.

The results confirmed that the rate of methane oxidation and sulfide production can be controlled by fluid flow. Both methane and sulfate need to be supplied for AOM to proceed. Upflow is needed to bring methane from large depth to the surface, but at a modest flow velocity, else sulfate cannot diffuse downward from the seawater. AOM has a very low yield, but it is essential as it supplies the habitat with sulfide that allows abundant chemoautotrophy. At medium upflow (*Beggiatoa* habitat, Håkon Mosby Mud Volcano) thiotrophic bacteria were the main primary producers as sufficient sulfate was available to sustain high methane turnover and sulfide production. Aerobic methane

consumption and AOM together contributed <20% of the biomass. As discussed above, the pathways of sulfide oxidation rather depends on the availability of iron-oxides than on fluid flow.

A different situation is present above methane hydrates. These grow from methane supply from the conduit and dissolve near the seafloor forming a methane conveyor. The hydrates are usually covered by rather thick layers of sediment, and AOM would have been limited by sulfate diffusion to the hydrates. However, siboglinid tubeworms bring sulfate downwards by pumping, thereby enhancing AOM, and harvesting the produced sulfide for symbiotic growth. The primary production in this area is unknown, but might well be very high. Rather often, the hydrates near the surface dissolve and erode, probably by local warm conduits. Then methane can come in direct contact with sulfate and the hole is strongly enriched in sulfide, up to 17 mmol $L^{-1}$. On these probably rather short living sulfidic holes thiotrophic mats develop (gray mat site, Håkon Mosby Mud Volcano), which are interesting for their diversity.

At the Dvurechenskii mud volcano, however, the distribution of seep organisms could not be used as indicator for different fluid flow, since thiotrophic communities are simply absent. Chemoautotrophy and thus biomass production is very low as sulfide can not be oxidized due to absence of oxygen or nitrate. Also here decreased fluid flow was correlating with an increase in sulfate penetration, allowing high sulfate and methane consumption and significantly reducing the total methane flux. The lack of oxygen has no large effect on methane oxidation rates, as these depend largely on sulfate. The maximal areal methane consumption with oxygen at mud volcanoes in oxic environments (Niemann et al., 2006) is only about 5% of the anoxic methane turnover at the Dvurechenskii mud volcano.

However, high methane export from the mud volcano to the hydrosphere from small areas of mud volcanoes can also be associated with other phenomena than fluid flow. Clearly, in both mud volcanoes fluid upflow >1 m $yr^{-1}$ might have prevented deep sulfate penetration and thus reduced the potential for methane oxidation. Alternatively, also fresh mud flow can have disturbed the AOM community and the slowly growing consortia might have had not time to re-establish the AOM process. This can clearly be true for the Dvurechenskii mud volcano, where the highest methane export was correlated with seemingly fresh muds that were microbe-depleted. Reports from 2002 about fresh mud flow in the central part of the Dvurechenskii mud volcano, but also in more peripheral areas (Meteor cruise M 52/1, Bohrmann et al., 2003), let us suggest that this active mud volcano has frequent outbursts leading to disturbances of the upper sediment layer and of its microbial community. Also the center site of the Håkon Mosby Mud is subjected to disturbances. As high resolution topographic maps recorded three years apart show clear changes in the surface topography of the inner zone of the mud volcano (Foucher et al., 2009, Ifremer, unpublished data), also here fresh mud flow might have disturbed the AOM community and the center was not yet re-colonized by the slowly growing AOM community. The most active area is rather small, with a diameter of 50-100 m, and a very irregular surface indicating strong disturbances. Directly outside of this area the sediments are

smooth and featureless, and thus probably less influenced by eruptions. The variable sulfide concentration in and especially near the active center site measured in different years (de Beer et al., 2006, Chapter 2, introduction Fig. 13) can be a consequence of this disturbance but also of the high patchiness in fluid flow.

In conclusion, medium to low fluid upflow allows high sulfate and methane turnover and thus reduces the methane release from the seep. In this case thiotrophic microbes contribute most to the primary production. High fluid upflow of >1 m $yr^{-1}$, as already shown by modeling of geochemical gradients (Luff et al., 2004), but also the disturbance of the AOM community by outflow of fresh, microbe-depleted mud can significantly reduce methane oxidation and lead to high methane export. Reduced AOM leads to lower primary production via thiotrophy. Environmentally important for the Black Sea hydrosphere is that mud volcano emissions do not play a large role in the methane and sulfide budget of the Black Sea. Instead, gas vents as frequently found on shelves and slopes, supply most of the methane present in the Black Sea and sulfate reduction in non-seep sediments and in the water column is responsible for the high sulfide content below the chemocline.

These research outcomes were achieved by combining visual observations with remotely operated vehicles (ROVs) with the in situ quantification of geochemical fluxes (oxygen, sulfide), pH, and temperature gradients, and ex situ geochemical analyses. With the application of high resolution in situ methods, more reliable calculations of the individual processes were possible. In situ instruments like the microprofiler are definitively the method of choice for sediment studies on cold seeps and further deployments of such instruments will be very useful to assess the controlling factors for seep processes, and the interaction between geochemistry and microbiology. For extended in situ work, technical improvements like battery power, and reduction of instrument size and -weight would be of large importance, allowing longer bottom time. However, improvements most desperately needed are microsensors for nitrate, sulfate, and methane applicable for in situ work. With these we would overcome the remaining problems we have with the sampling artifacts.

From the few ‘longer’-term monitoring studies at cold seeps (Tryon and Brown, 2004; Tryon et al., 1999), and observations of methane eruptions in shallow water (Leifer et al., 2006), it is known that the efflux from seeps can be highly variable with time. We and others obtained clear indications that the Håkon Mosby and the Dvurechenskii mud volcano are highly dynamic. The next challenge in cold seep work will be to document the temporal variability of seeps, in particular the frequency and the magnitude of eruptive events, and the degree of fluid flow variability. We have to learn about the mechanisms of such eruptions, which might be external cycling forces such as tides, interaction between gases and sediments, changes in methane generation or refill of reservoirs, and changes of gas hydrate stability. This will help to estimate the amount of gas released and the consequences for geochemistry and local communities as well as for seafloor stability. First projects for such work have started, e.g. the LOOME project, a long-term autonomous observatory at the Håkon Mosby Mud Volcano with an ocean bottom seismometer, a piezometer, cameras, and a temperature-lance that will

document physico-chemical phenomena before, during, and after an eruption. It will be retrieved in one year from now and when proven successful, will hopefully be the first of many such observatories. A next step is the use of cabled networks that supply power and data transfer to instruments near or on cold seeps.

### 1.3. Overall Ecological and Environmental Relevance of Cold Seeps

Cold seeps are extraordinary players in the marine realm. They are oases of life where primary production can proceed - and supposedly already did in the geological past - also if large disturbances in the sunlight-depended biosphere happen such as 'snowball earth events'. Fascinating from a biogeochemical point of view, diagenetic reactions, which e.g. in deep see sediments are distributed over hundreds of meters sediment depth, are condensed to a couple of centimeters in cold seeps. Thus the interaction of processes is much more intense and easier accessible. Inevitable, but also most interesting, good research at cold seeps can only be done with an interdisciplinary approach. Essential disciplines needed for cold seep research are seismics (for the detection of seeps, subsurface gas, and gas hydrates), geology (to find the source of the advected sediments, their origin, and the driving force for the seep formation), geochemistry (to see what constituents are present in cold seep sediments and how they react with each other), and biology (as seeps are oases of life with many highly specialized organisms). In this work the distribution and the limits of the biogeochemical reactions have been investigated for different seep habitats at various cold seep sites. Our observations clearly show that cold seeps are no steady state systems, temporarily highly dynamic and just as well spatially variable. Temporal changes in fluid upflow and fresh mud eruptions will produce spatial irregularities at mud volcanoes and lead to a new organization of zones of methane oxidation and sulfide production. When studying cold seeps it should be carefully considered, if the sampled spot is representative for the whole seep habitat and for the whole seep structure, and if the investigated process is in (or close to) steady state or if the seeping activity is too variable to draw robust conclusions.
This thesis contributes to the overall knowledge about the ecological and environmental relevance of cold seeps. Key statements that can be drawn from this work are:

- Most primary production at cold seeps proceeds not directly by methane oxidation, but is linked to anaerobic methane oxidation via sulfide production and consumption of this sulfide by thiotrophic bacteria.
- Sulfide is quite efficiently removed in cold seeps in oxic environments, either geochemically or by thiotrophic bacteria.
- In anoxic environments like the Black Sea, the sulfide flux from a mud volcano to the water column is high. Nevertheless, organoclastic sulfate reduction in non-seep related sediments

and the water column are the main source for sulfide in the Black Sea and mud volcanoes play no significant role.

- Gas vents contribute much more to the methane release into the hydrosphere of the Black Sea than mud volcanoes.
- The hot spot of fluid flow and methane release is not necessarily in the middle of the seep structure.
- The small scale heterogeneity in cold seeps is controlled by fluid flow and by temporal changes in fluid flow, dictating the nature of the geochemical gradients and thus the cold seep community.
- As thiotrophic bacteria have a high biomass turnover they are only indicative for the actual fluid flow.
- Unexpectedly, sediments rising in mud volcanoes can contain oxidized iron that is reactive towards sulfide. Although these minerals are not sufficiently reactive to be important in sulfide scavenging, they induce a highly interesting sulfur geochemistry and the formation of sulfur intermediates.
- Oxidized iron can not be an electron-acceptor for microbial methane oxidation in mud volcano sediments.

## REFERENCES

Bohrmann, G., Ivanov, M., Foucher, J. P., Spiess, V., Bialas, J., Greinert, J., Weinrebe, W., Abegg, F., Aloisi, G., Artemov, Y., Blinova, V., Drews, M., Heidersdorf, F., Krabbenhoft, A., Klaucke, I., Krastel, S., Leder, T., Polikarpov, I., Saburova, M., Schmale, O., Seifert, R., Volkonskaya, A., and Zillmer, M., 2003. Mud volcanoes and gas hydrates in the Black Sea: new data from Dvurechenskii and Odessa mud volcanoes. *Geo-Mar. Lett.* **23**, 239-249.

Canfield, D. E., 1989. Reactive iron in marine sediments. *Geochim. Cosmochim. Acta* **53**, 619-632.

de Beer, D., Sauter, E., Niemann, H., Kaul, N., Foucher, J.-P., Witte, U., Schlüter, M., and Boetius, A., 2006. In situ fluxes and zonation of microbial activity in surface sediments of the Håkon Mosby Mud Volcano. *Limnol. Oceanogr.* **51**, 1315-1331.

Ferdelman, T. G., Church, T. M., and Luther, G. W., 1991. Sulfur enrichment of humic substances in a Delaware salt marsh sediment core. *Geochim. Cosmochim. Acta* **55**, 979-988.

Foucher, J. P., Westbrook, G. K., Boetius, A., Ceramicola, S., Dupre, S., Mascle, J., Mienert, J., Pfannkuche, O., Pierre, C., and Praeg, D., 2009. Structure and drivers of cold seep ecosystems. *Oceanography* **22**, 92-109.

Ginsburg, G. D., Milkov, A. V., Soloviev, V. A., Egorov, A. V., Cherkashev, G. A., Vogt, P. R., Crane, K., Lorenson, T. D., and Khutorskoy, M. D., 1999. Gas hydrate accumulation at the Hakon Mosby Mud Volcano. *Geo-Mar. Lett.* **19**, 57-67.

Kostka, J. E. and Luther, G. W., 1994. Partitioning and speciation of solid phase iron in saltmarsh sediments. *Geochim. Cosmochim. Acta* **58**, 1701-1710.

Lance, S., Henry, P., Le Pichon, X., Lallemant, S., Chamley, H., Rostek, F., Faugères, J.-C., Gonthier, E., and Olu, K., 1998. Submersible study of mud volcanoes seaward of the Barbados accretionary wedge: sedimentology, structure and rheology. *Mar. Geol.* **145**, 255-292.

Leifer, I., Luyendyk, B. P., Boles, J., and Clark, J. F., 2006. Natural marine seepage blowout: Contribution to atmospheric methane. *Glob. Biogeochem. Cycles* **20**.

Luff, R., Wallmann, K., and Aloisi, G., 2004. Numerical modeling of carbonate crust formation at cold vent sites: significance for fluid and methane budgets and chemosynthetic biological communities. *Earth Planet. Sci. Lett.* **221**, 337-353.

Niemann, H., Lösekann, T., de Beer, D., Elvert, M., Nadalig, T., Knittel, K., Amann, R., Sauter, E. J., Schlüter, M., Klages, M., Foucher, J.-P., and Boetius, A., 2006. Novel microbial communities of the Haakon Mosby mud volcano and their role as a methane sink. *Nature* **443**, 854-858.

Paull, C. K., Ussler, W., Greene, H. G., Barry, J., and Keaten, R., 2005. Bioerosion by chemosynthetic biological communities on Holocene submarine slide scars. *Geo-Mar. Lett.* **25**, 11-19.

Poulton, S. W., Krom, M. D., and Raiswell, R., 2004. A revised scheme for the reactivity of iron (oxyhydr)oxide minerals towards dissolved sulfide. *Geochim. Cosmochim. Acta* **68**, 3703-3715.

Sibuet, M. and Olu, K., 1998. Biogeography, biodiversity and fluid dependence of deep-sea cold-seep communities at active and passive margins. *Deep-Sea Res. Pt. II* **45**, 517-567.

Treude, T., Boetius, A., Knittel, K., Wallmann, K., and Jørgensen, B. B., 2003. Anaerobic oxidation of methane above gas hydrates at Hydrate Ridge, NE Pacific Ocean. *Mar. Ecol. Prog. Ser.* **264**, 1-14.

Tryon, M. D. and Brown, K. M., 2004. Fluid and chemical cycling at Bush Hill: Implications for gas- and hydrate-rich environments. *Geochem. Geophys. Geosys.* **5**.

Tryon, M. D., Brown, K. M., Torres, M. E., Trehu, A. M., McManus, J., and Collier, R. W., 1999. Measurements of transience and downward fluid flow near episodic methane gas vents, Hydrate Ridge, Cascadia.

## DANKSAGUNG

An dieser Stelle möchte ich allen danken, die zum Fortgang und Gelingen dieser Arbeit beigetragen haben. Es waren sehr spannende Jahre und vor allem die Möglichkeit auf Forschungsschiffen zu arbeiten und Einblicke in die sonst unzugänglichen Regionen des Meeres zu erhalten, aber auch das interdisziplinäre Arbeiten habe ich sehr genossen.

Besonders danke ich Prof. Dr. Bo Barker Jørgensen, der als Betreuer immer wieder großes Interesse an meiner Arbeit gezeigt hat. Ein großes Dankeschön geht auch an Dr. Dirk de Beer, vor allem für die Einführung in die Geheimnisse der Kniffe und Tricks der Mikrosensormessungen, und die Unterstützung beim Schreiben der Manuskripte durch sein weit gefächertes Wissen und seinen so scharfen wissenschaftlichen Verstand. Ein besonderer Dank geht auch an Prof. Dr. Antje Boetius, die eine große Unterstützung beim Verfassen der Manuskripte war; es war sehr spannenden mit ihr zusammenzuarbeiten und zu lernen, wie man sich und andere gut organisiert und immer eine große Freude, mit ihr die Wochen auf dem Schiff zu teilen. Ich danke Priv. Doz. Matthias Zabel für die Übernahme des zweiten Gutachten, sowie den Mitgliedern des Prüfungskomitees, Prof. Dr. Gerhard Bohrmann, Dr. Dirk de Beer, Matthias Kellermann und Friedrich Schröder.

Die Erstellung der Arbeit war auch nur möglich durch die Hilfsbereitschaft und technische Unterstützung im Labor und auf den Schiffen. Hier möchte ich vor allem den Mikrosensor TA's Gaby Eickert, Ines Schröder, Karin Hohmann, Cäcilia Wiegand, Anja Niclas, Ingrid Dohrmann und Vera Hübner für das Anfertigen der exzellenten Sensoren danken. Vielen Dank auch an die Technikerinnen der Biogeochemie Gruppe und der Habitat Gruppe zu denen ich auch jederzeit kommen konnte und immer Hilfe erhalten habe; hier möchte ich speziell Andrea Schippers, Martina Meyer, Viola Baier und Martina Alisch danken. Natürlich wäre die Arbeit auch nicht möglich gewesen ohne die Unterstützung des Teams aus der Landerhalle, das mit seiner großen Fachkenntnis noch jedes Gerät zum Laufen gebracht hat. Bernd Stickford auch vielen Dank für Gastfreundschaft in der Bibliothek.

Wem ich besonders danken möchte ist Janine Felden, die mich privat und in der Arbeit immer unterstützt hat, auf die ich mich jederzeit verlassen konnte und die mit mir zusammen durch die Höhen und Tiefen der letzten Jahre gegangen ist. Natürlich möchte ich mich auch bei den übrigen Leuten meiner Mittagsessen-Gruppe, Jan Fischer, Gunther Wegener und Simone Böer für die vielen fachlichen und ebenso die weniger fachlichen Diskussionen während des Kaffeetrinkens bedanken. Und natürlich darf ich meine Büro-Mädels Miriam Weber, Friederike Hoffmann, Susanne Borgwardt und Anna Behrendt nicht vergessen! Viele lehrreiche und effiziente Diskussionen hatte ich auch mit Frank Wenzhöfer, Hans Røy, Felix Janssen, Peter Stief, Jochen Nüster, Katharina Kohl, Stefanie Grünke, und Anja Kamp. Ein besonderer Dank geht an Tim Ferdelman für die anregenden und motivierenden Diskussionen. Dann natürlich auch großen Dank für die Unterstützung aus beiden Gruppen, von denen ich ein Teil war, die Mikrosensor und die Habitat Gruppe. Nicht zuletzt möchte ich meiner Familie und meinen Freunden für ihre Unterstützung und ihr Vertrauen danken.

# CRUISE PARTITIONING

**Eckernförde Bay** "Littorina", 7. June 2005, MUMM[II]

**Håkon Mosby Mud Volcano,** *ATL05/02-3* October 2005, R/V L'Atalante, AWI, Ifremer

**Håkon Mosby Mud Volcano,** *Viking cruise*, May/June 2006, R/V Pourquoi Pas?, HERMES, MUMM[II]

**Eastern Mediterranean,** *Bionil cruise*, M70/2a, M702/b, Eastern Mediterranean Sea – Nile Deep Sea Fan, October/November 2006, R/V Meteor, MUMM[II], Euromargin

**Black Sea,** *Microhab cruise*, M72/2, February/March 2007, R/V Meteor MUMM[II], HERMES

## POSTER AND ORAL PRESENTATIONS

A. Lichtschlag, H. Røy, H. Niemann, A. Boetius, M. Klages, D. de Beer, (2006),
*Microbial turnover of sulfide in combination with iron precipitation at the Håkon Mosby Mud Volcano,*
EGU General Assembly, Vienna, Austria,
poster

A. Lichtschlag, G. Wegener, A. Boetius, M. Schlüter, D. de Beer, (2007),
*The impact of methane on biogeochemical processes at the Håkon Mosby Mud Volcano,*
EGU General Assembly,Vienna, Austria,
oral presentation

A. Lichtschlag, J. Felden, F. Wenzhöfer, S. Grünke, G. Wegener, A. Boetius, J.-P. Foucher, D. de Beer, (2007),
*Biogeochemical processes associated with microbial mats of the Nile Deep Sea Fan pockmark area,*
EGU General Assembly, Vienna, Austria,
oral presentation

A. Lichtschlag, J. Felden, F. Wenzhöfer, T. Mohr, T. Feseker, A. Boetius, D. de Beer, (2007),
*Methane fluxes and turnover in permanent anoxia: in situ studies of the Dvurechenskii mud volcano (Black Sea),*
Goldschmidt 2007 - "Atoms to Planets", Cologne, Germany,
poster

A. Lichtschlag, J. Felden, F. Wenzhöfer, S. Grünke, G. Wegener, A. Boetius, J.-P. Foucher, D. de Beer, (2007),
*In situ fluxes and turnover rates of microbial mats of the Nile Deep Sea Fan,*
International Conference and 97th Annual Meeting of the Geologische Vereinigung e.V., Bremen, Germany,
poster

A. Lichtschlag, J. Felden, F. Wenzhöfer, T. Mohr, T. Feseker, A. Boetius, D. de Beer, (2007),
*In situ studies at the Dvurechenskii mud volcano (Black Sea): methane-driven geochemical processes in permanent anoxia,*
International Conference and 97th Annual Meeting of the Geologische Vereinigung e.V. Bremen, Germany,
oral presentation

A. Lichtschlag, J. Felden, S. Grünke, F. Wenzhöfer, D. de Beer, A. Boetius, (2008),
*Methane, sulfide and oxygen fluxes at methane and brine seeps of the Nile Deep Sea Fan (Eastern Mediterranean)*,
AOM-meeting, Aselage, Germany,
poster

A. Lichtschlag, J. Felden , F. Wenzhöfer, S. Grünke, A. Boetius, D. de Beer, (2008),
*Thiotrophic mats and their association with methane discharge- comparison of different cold seep sites,*
9. International Conference on Gas in Marine Sediments, Bremen, Germany,
oral presentation

# Erklärung

Hiermit versichere ich, dass ich

1. die Arbeit ohne unerlaubte fremde Hilfe angefertigt habe,

2. keine anderen als die von mir angegebenen Quellen und Hilfsmittel benutzt habe und

3. die den benutzten Werken wörtlich oder inhaltlich entnommenen Stellen als solche kenntlich gemacht habe.